Lecture Notes in Nuclear Structure Physics

B. Alex Brown

November 2005

National Superconducting Cyclotron Laboratory
and Department of Physics and Astronomy
Michigan State University, E. Lansing, MI 48824

Contents

1 Nuclear masses

1.1 Masses and binding energies

A basic quantity which can be measured for the ground states of nuclei is the atomic mass $M(N,Z)$ of the neutral atom with atomic mass number A and charge Z. Atomic masses are usually tabulated in terms of the mass excess defined by

$$\Delta(N,Z) \equiv M(N,Z) - uA, \tag{1.1}$$

where u is the Atomic Mass Unit defined by $u = M(^{12}\mathrm{C})/12 = 931.49386\,\mathrm{MeV}/c^2$. [1] I will use the data from the 2003 compilation of Audi, Wapstra and Thibault [1]. Fig. (1.1) shows the position on the nuclear chart for these measured masses together with the experimental error. There are 2127 nuclei measured with an accuracy of 0.2 MeV or better and 101 nuclei measured with an accuracy of greater than 0.2 MeV. For heavy nuclei one observes several chains of nuclei with a constant $N - Z$ value whose masses are obtained from the alpha-decay Q values.

Nuclear binding energy is defined as the energy required to break up a given nucleus into its constituent parts of N neutrons and Z protons. In terms of the atomic masses $M(N,Z)$ the binding energy $B(N,Z)$ [2] is defined by:

$$B(N,Z) = ZM_H c^2 + NM_n c^2 - M(N,Z)c^2, \tag{1.2}$$

where M_H is the mass of the hydrogen atom and M_n is the mass of the neutron.[3] In terms of the mass excess the binding energy is given by:

$$B(N,Z) = Z\Delta_H c^2 + N\Delta_n c^2 - \Delta(N,Z)c^2, \tag{1.3}$$

where $\Delta_H c^2 = 7.2890$ MeV and $\Delta_n c^2 = 8.0713$ MeV.

How do we know that nuclei are made up of protons and neutrons? In the 1920's when it was observed that nuclei decay by the emission of alpha particles, protons and electrons one tried to make nuclear models out of constituent protons and electrons. [4] However, after the discovery of the neutron in 1932, it was observed that the

[1] This and other constants can be found on the website:
http://physics.nist.gov/cuu/Constants/index.html

[2] The binding energy will also be denoted by BE.

[3] This binding energy also includes contribution from the Coulomb interaction between electrons which is approximately given by $-1.43\text{x}10^{-5}\ \mathrm{Z}^{2.39}$ MeV. On the scale of nuclear binding this can usually be ignored. It is most important for heavy nuclei where, for example, for $Z = 120$ the electronic contribution is -1.34 MeV.

[4] "Just because barks come out of dogs does not mean that dogs are made of barks." (Denys Wilkinson).

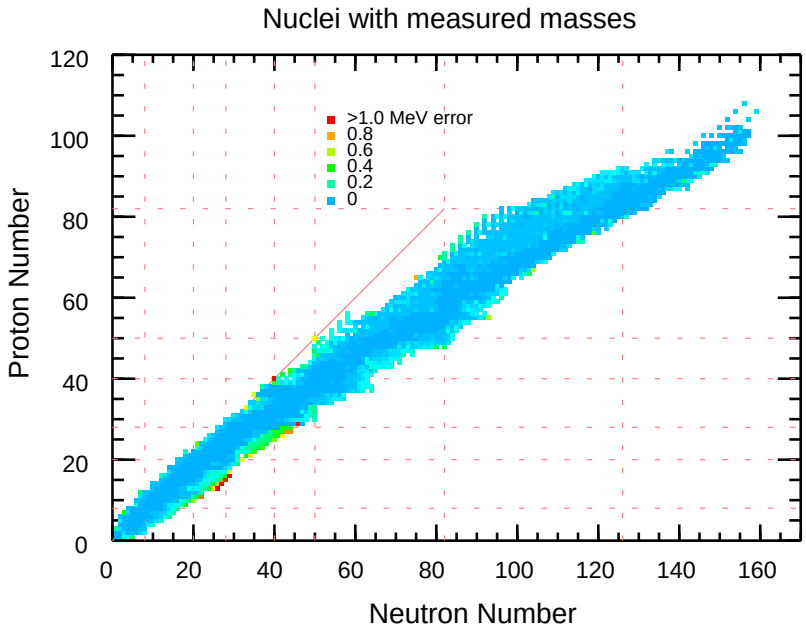

Figure 1: Nuclei with measured masses. The solid line is for $N = Z$. The dashed lines indicate the locations of the magic numbers 8, 20, 28, 40, 50, 82 and 126

atomic masses can be qualitatively understood by the contribution of the masses of the individual protons and neutrons which make up the nucleus. To emphasize this point the ratio

$$\frac{M(N,Z) - [ZM_H + NM_n]}{[ZM_H + NM_n]}$$

is plotted in Fig. (1.2) as a function of mass. The largest deviation is found near $A = 60$ where the total mass is only about one percent smaller than expected from the sum of nucleon masses. The intrinsic properties of neutrons and protons inside the nucleus are essentially the same as those of the free nucleons. Nuclear properties are a result of these nucleons interacting with each other through the exchange of mesons. At some level we will need to include small admixtures of other baryons.

We are interested in understanding the binding energy as a function of N and Z. The total BE are shown in Fig. (1.3) as a function of A. One observes an overall linear increase with A reaching a maximum value of about 2 GeV for the heaviest nuclei. One can bring out more detail by plotting BE/A as in Figs. (1.4) and (1.5) [Note that Fig. (1.4) is the inverse Fig. (1.2)]. The maximum as a function of A in Fig. (1.4) are shown separately in the bottom of Fig. (1.6). These represent the nuclei which are most stable and the most abundant in nature. An expanded portion for the experimental for light nuclei is shown in Fig. (1.7). These are the nuclei at the

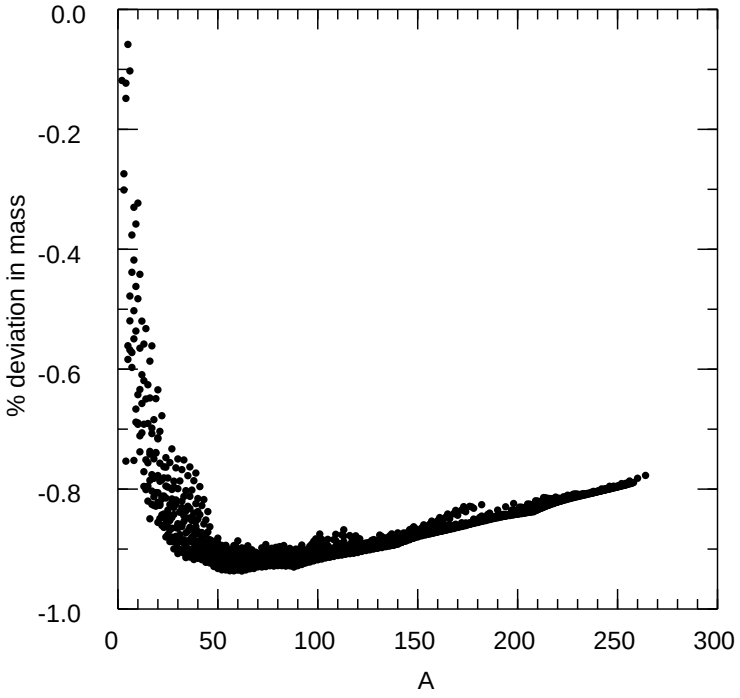

Figure 2: Deviation of the atomic masses from that expected from the sum of proton and neutron masses.

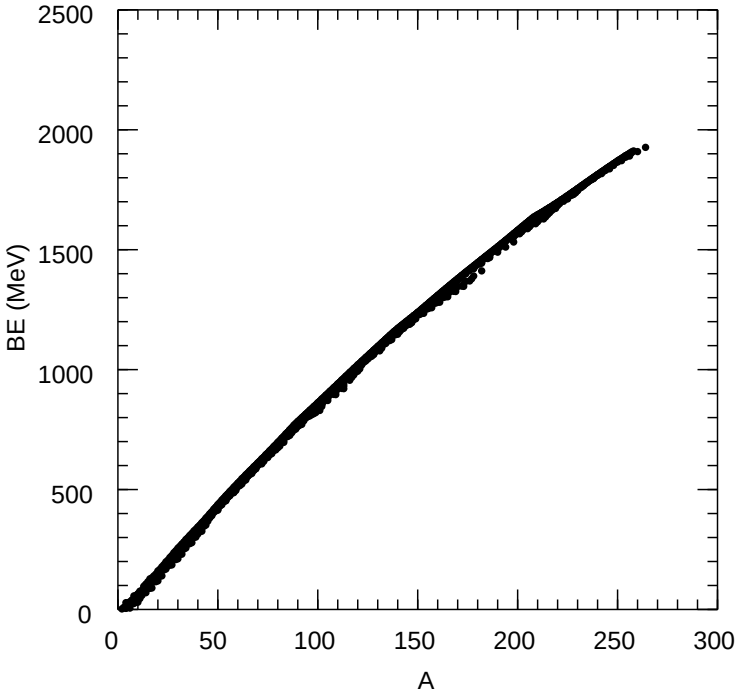

Figure 3: Binding energy as a function of A.

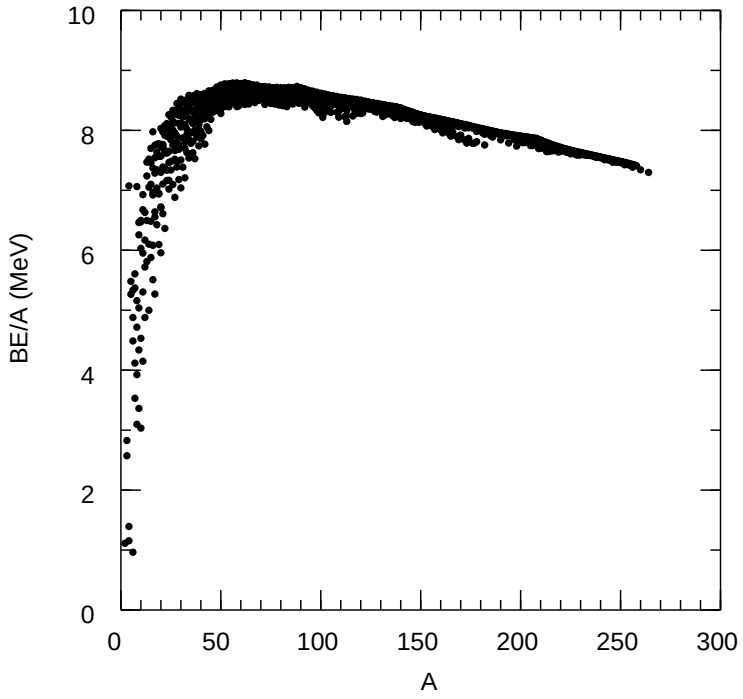

Figure 4: BE/A as a function of A.

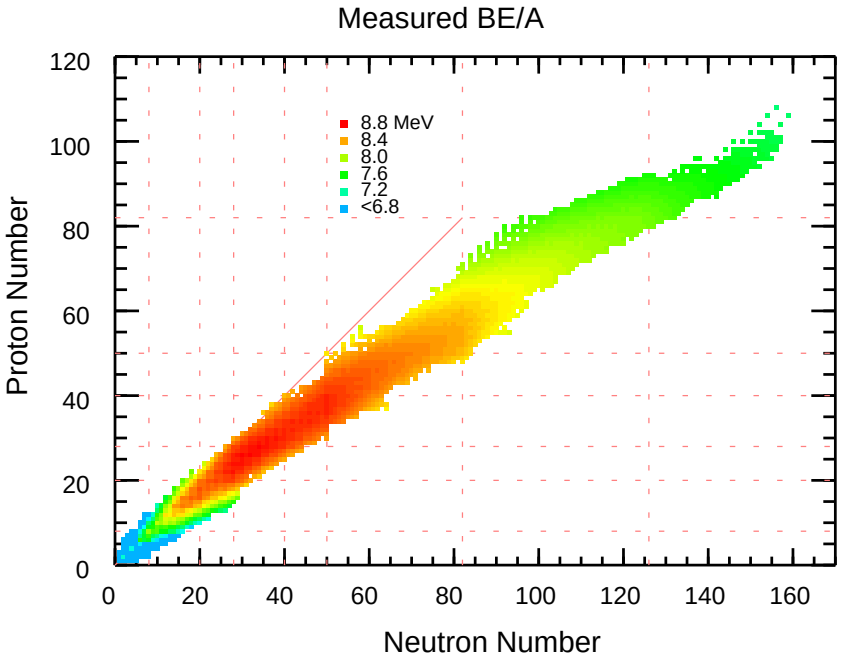

Figure 5: BE/A as a function of N and Z.

top of the "ridge-of-stability" in binding energy or those at the bottom of the "valley-of-stability" in mass. For a fixed A value nuclei away from the valley of stability beta decay until they reach the bottom of the valley. Nuclear structure models are used to understand the overall features of these data as well as the deviations from the averge.

The maximum in the binding energy per nucleon occurs for ^{58}Fe. ^{58}Fe represents the most bound (lowest energy) state for nucleons. Thus fusion of two light nuclei with a combined mass of $A < 58$ usually results in energy release. The fusion of deuterium and tritium is the main reaction being investigated for controlled fusion reactors. Other fusion processes are important for solar energy and for the creation of elements up to $A = 58$ in stellar environments. The falloff in binding energy per nucleon above $A = 58$ implies that most of these nuclei can spontaneously decay into lighter products. The most common of these decay processes are alpha decay, where a ^{4}He is emitted, and fission, where the nucleus breaks up into two roughly equal mass fragments. The fission products are usually accompanied by neutrons. Intermediate decay modes, where light fragments such as ^{14}C are emitted, are also possible and have also been observed, but their decay rate relative to alpha decay is extremely small. Although most heavy nuclei have a positive Q value for spontaneous decay, many of them have lifetimes on the order of the age of the universe and thus exist in nature, due to the hindrance of tunneling through the Coulomb barrier.

1.2 Q values and separation energies

In this section we consider energy conservation for nuclear transformations that include, for example, the fussion of two nuclei a and b into the combined system c

$$[N, Z]_a + [N, Z]_b \rightarrow [N, Z]_c \tag{1.4}$$

or the decay of nucleus a into two other nuclei b and c

$$[N, Z]_a \rightarrow [N, Z]_b + [N, Z]_c \tag{1.5}$$

In general we consider the combinations

$$\sum_i [N, Z]_i \rightarrow \sum_f [N, Z]_f \tag{1.6}$$

where N and Z are conserved.

$$\sum_i N_i = \sum_f N_f \text{ and } \sum_i Z_i = \sum_f Z_f \tag{1.7}$$

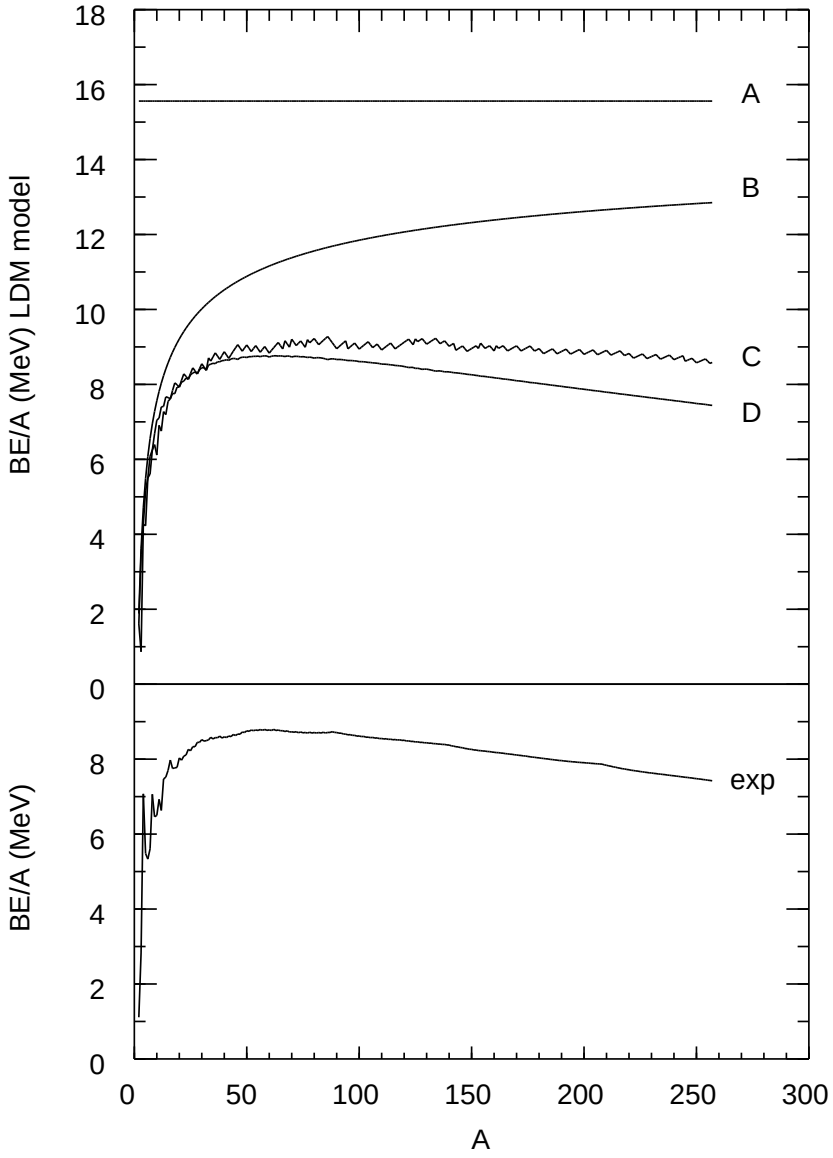

Figure 6: Bottom panel: Experimental values for the BE/A as a function of A for the most stable nuclei. Top panel: Liquid-drop model for BE/A (curve D) and shown in terms its components the volume term (A), the volume plus surface terms (B), the volume plus surface plus Coulomb terms (C).

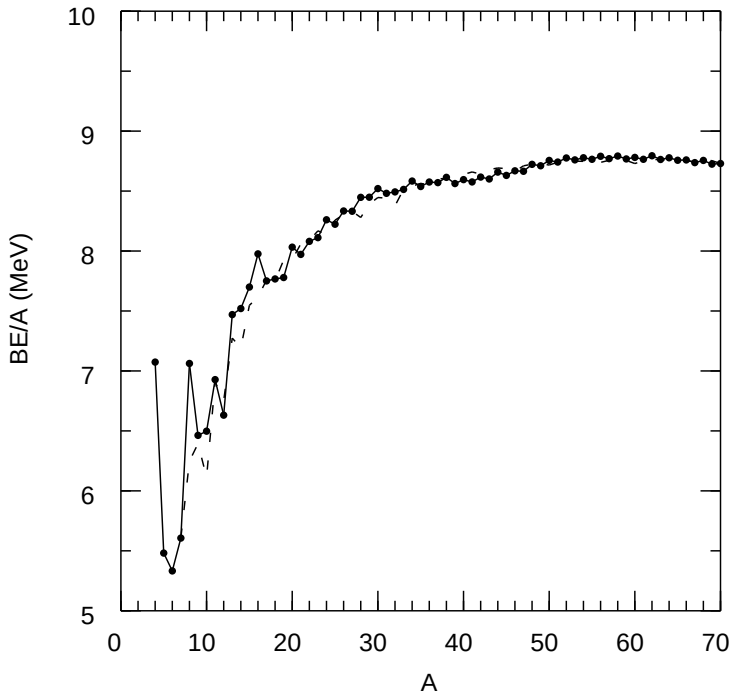

Figure 7: An expanded portion of the experimental values for BE/A (points connected by a line). The liquid-drop model is shown by the dashed line.

This process is characterized by the Q value:

$$Q = \sum_i M(N_i, Z_i)c^2 - \sum_f M(N_f, Z_f)c^2 = \sum_f B(N_f, Z_f) - \sum_i B(N_i, Z_i). \qquad (1.8)$$

Spontaneous decay involves a single initial nuclear state and is allowed if $Q > 0$. In the decay, energy is released in the form of the kinetic energy of the final products. Reactions involving two initial nuclei and are endothermic (a net loss of energy) if $Q < 0$; the reactions are exothermic (a net release of energy) if $Q > 0$.

We can consider the Q values associated with the removal of one or two nucleons from a nucleus. These are conventionally defined in terms of the one-nucleon and two-nucleon separation energies, S:

$$S_n = -Q_n = B(N, Z) - B(N-1, Z), \qquad (1.9)$$

$$S_p = -Q_p = B(N, Z) - B(N, Z-1), \qquad (1.10)$$

$$S_{2n} = -Q_{2n} = B(N, Z) - B(N-2, Z), \qquad (1.11)$$

and

$$S_{2p} = -Q_{2p} = B(N, Z) - B(N, Z-2). \qquad (1.12)$$

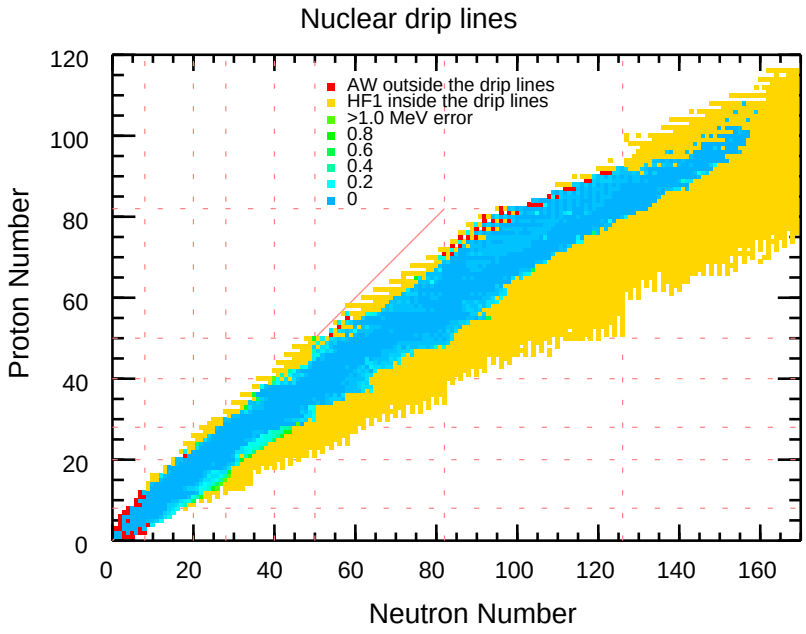

Figure 8: Nuclei in the Audi-Wapstra-Thibault mass compilation together with the HF1 prediction for nuclei out to the neutron and proton drip lines. Observed nuclei outside the drip lines are indicated.

A negative value for one of these quantities means that the nucleus can spontaneously decay by the emission of neutrons or protons. The boundary between positive and negative values of S is called the drip line. Nuclei inside the drip lines are stable to the spontaneous emission of nucleons, whereas those outside the drip line can spontaneously decay by emission of one and/or two nucleons. The neutron drip line represents a sharp boundary between those nuclei just inside drip line that beta decay with a lifetime on the order of ms, and those outside the drip line that have lifetimes on the order of 10^{-20}s associated with the strong interaction decay widths of MeV. For heavy nuclei, the Coulomb barrier can greatly hinder the proton decay, and the the lifetimes for the one or two proton decay of nuclei just outside the proton-drip line can be comparable to or even longer than the lifetimes for beta decay. Fig. (1.8) shows the nuclear chart for nuclei whose masses have been measured together with those that are predicted to lie within the neutron and proton drip lines from a microscopic nuclear model called HF1 [2]. An expanded version of this figure for light nuclei is shown in Fig. (1.9). HF1 is a Hartree-Fock(*) [5] calculation where on the order of 10 parameters of the Hamiltonian are fitted to the experimental binding energies. These figures also show nuclei with measured masses which lie outside the drip lines. For light nuclei, the masses given in the Audi-Wapstra-Thibault compilation are usually

[5]The (*) indicates an idea or topic that will be covered latter in the book.

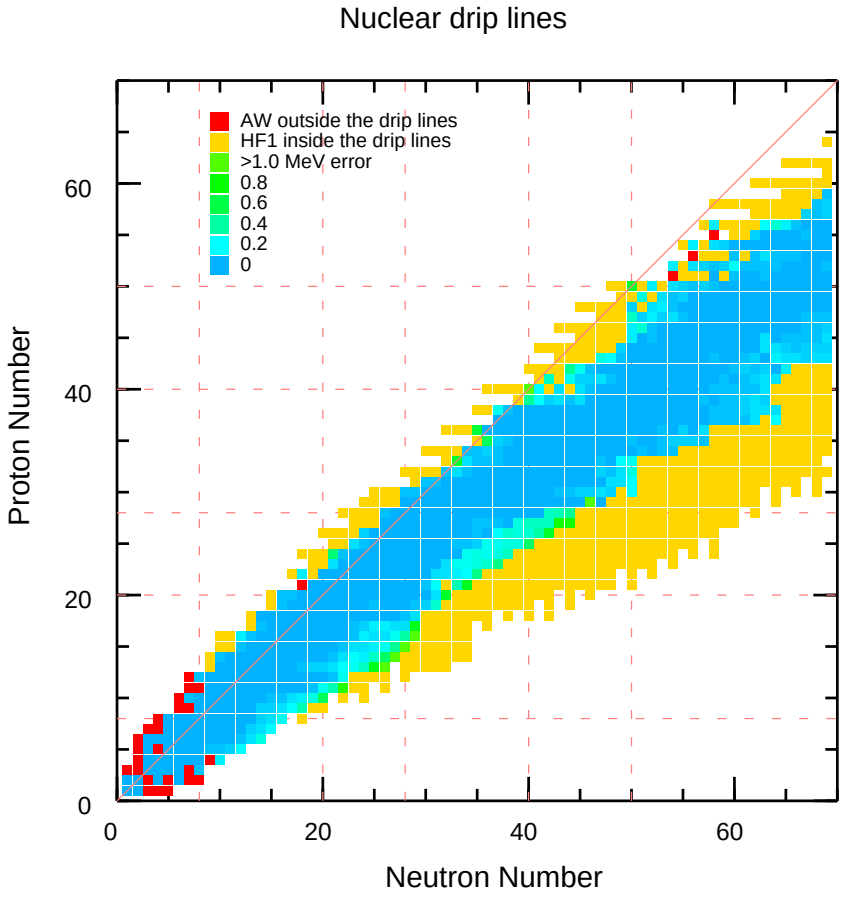

Figure 9: An expanded version of Fig. (1.8) for light nuclei.

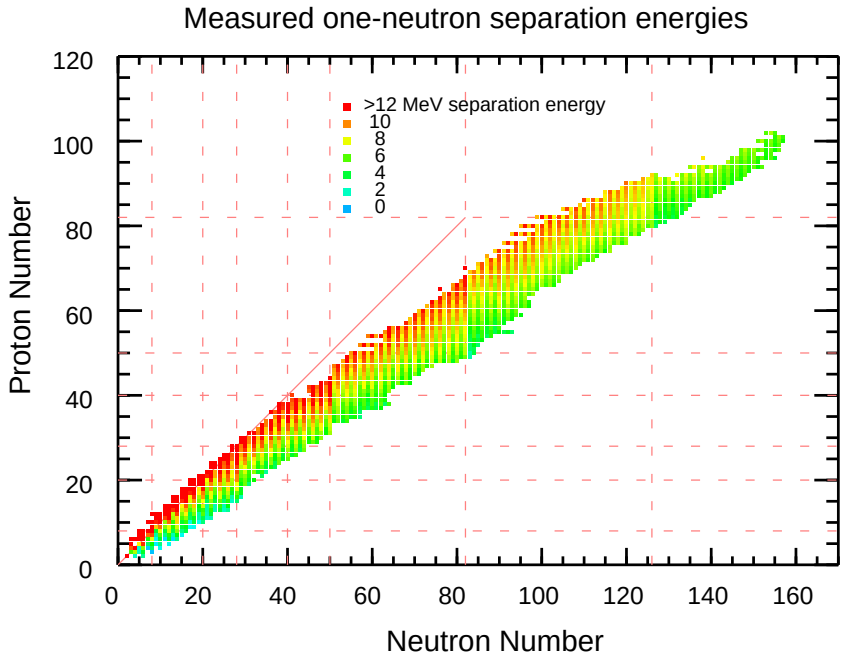

Figure 10: Measured one-neutron separation energies.

obtained from the observation of resonances in nuclear reactions. As such, it would be better to call these quantities resonance energies rather than masses or binding energies. In addition, there are several light nuclei not shown in Fig. (1.9) whose non-observation in experimental studies implies that they lie outside of the drip lines [3]. For light nuclei the proton and neutron drip lines are experimentally established only up to about $A = 24$. For heavier nuclei the proton-drip line is observed in a few regions from the observation of proton decays with relatively long lifetimes. The HF1 model gives a prediction for the neutron and proton drip lines. Between $A = 40$ and $A = 200$ nearly half of the nuclei expected to be inside the drip lines have not yet been observed in experiments. The properties for many of these unobserved nuclei are critical for the understanding of nuclear models as well as the astrophysical processes in element production. New generations of accelerators such are RIA (the Rare Isotope Accelerator project in the US) are being planned to produce and study these nuclei.

The systematics of the one-neutron separation energies, S_n, are shown in Fig. (1.10) for experiment and in Fig. (1.11) for the HF1 model. As one moves from the proton to the neutron drip lines, the one-neutron separation energies decrease. This decrease is not smooth but shows odd-even oscillations associated with the two-body pairing nature of the strong interaction between neutrons(*).

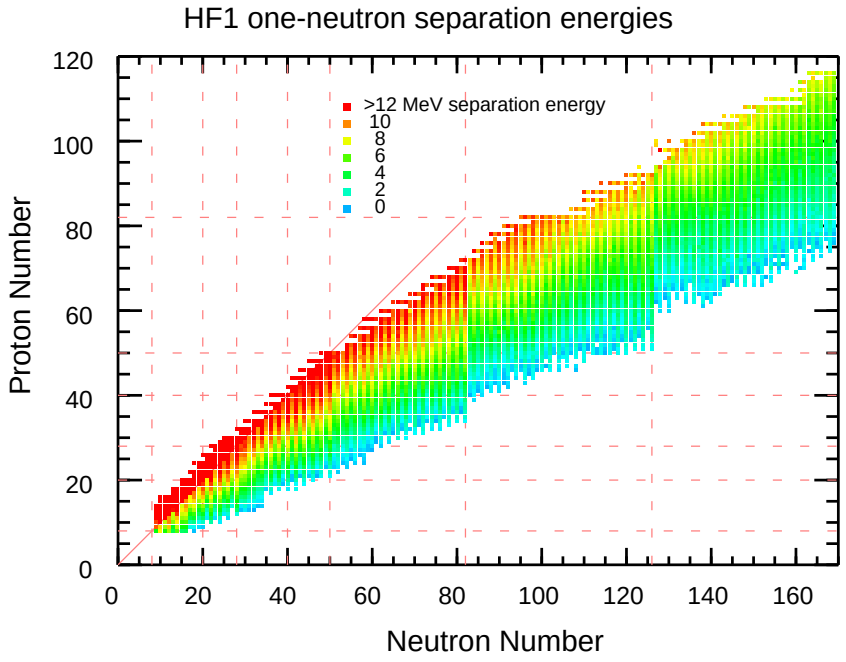

Figure 11: HF1 results for the one-neutron separation energies.

The S_n values vs neutron number for the even-even nuclei with $N > Z$ are shown in Fig. (1.12). Just after the magic numbers 28, 50, 82 and 126 there is sudden decrease in the separation energy due to the fact that neutrons go into valence shells which are loosely bound compared to those which have just been filled at the magic numbers(*).

This jump at the magic numbers can be emphasized by taking the differences in one-neutron separation energy:

$$\Delta S_n = B(N,Z) - B(N-1,Z) - [B(N+1,Z) - B(N,Z)]$$
$$= 2B(N,Z) - B(N-1,Z) - B(N+1,Z). \quad (1.13)$$

The values of $\Delta \mathrm{S}_n$ for the even-even nuclei (N, Z) are shown in the bottom panel of Fig. (1.12). One observes clear peaks at the magic numbers 50, 82 and 126. The magic numbers 8, 20 and 28 also appear as peaks, but the peak for 20 goes away for $Z = 10$ and 12. The value of peak height is related to the size of the shell gaps(*). Similar results are found for the proton separation energies.

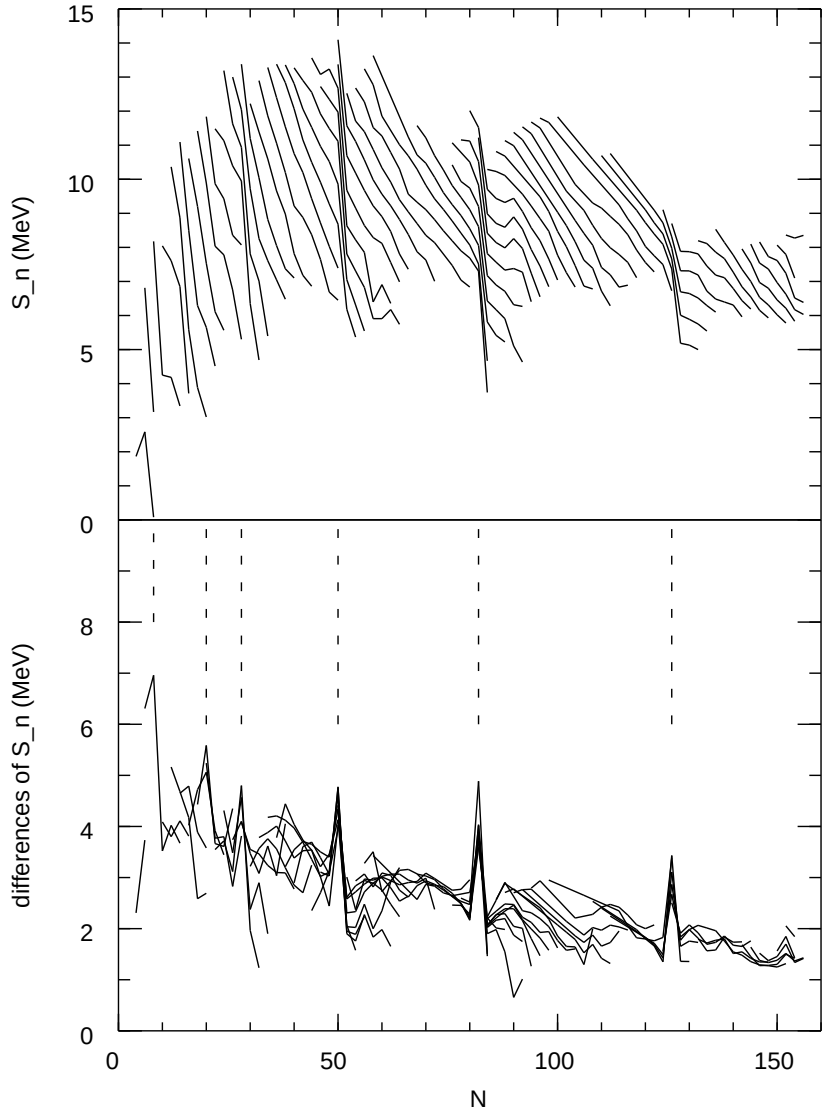

Figure 12: The top panel shows the one-neutron separation energies as a function of neutron number for even-even nuclei with $N > Z$. The lines connect nuclei with the same Z value. The bottom panel shows the differences between one-neutron separation energies for the same set of even-even nuclei. The dashed lines show the magic numbers 8, 20, 28, 50, 82 and 126.

1.3 The liquid-drop model

Nuclei are bound due to the overall attractive strong interactions between nucleons. The strong interaction arises from the exchange of mesons. The interactions are short ranged and occur mainly between neighboring nucleons. In addition, the nuclear interaction saturates, resulting in a nearly constant interior nucleon density and a surface radius approximately equal to $1.2\,A^{1/3}$. The analogy of this situation with a droplet of liquid, results in the liquid-drop model for the nuclear binding energies in which the binding energy is expressed in the form:

$$B(N,Z) = \alpha_1 A - \alpha_2 A^{2/3} - \alpha_3 \frac{Z^2}{A^{1/3}} - \alpha_4 \frac{(N-Z)^2}{A}. \tag{1.14}$$

The four terms on the right-hand side are referred to as the volume, surface, Coulomb and symmetry energy terms, respectively. The first term represents the nearest neighbor attractive interaction between nucleons, and the second term represents the correction due to the fact that the nucleons on the surface only interact with those in the interior. The third term is due to the Coulomb repulsion between protons. The fourth term called the symmetry energy arises because the proton-neutron strong interaction is on the average more attractive than the proton-proton or neutron-neutron strong interactions and because the total kinetic energy is minimized when $N = Z$. The constant α_3=0.697 MeV is fixed by the Coulomb interaction and the nuclear size. Typical values of the liquid-drop constants that reproduce the average trends in the experimental data are given by $\alpha_1 = 15.49$ MeV, $\alpha_2 = 17.23$ MeV and $\alpha_4 = 22.6$ MeV.

The comparison of the liquid-drop model for the most stable nuclei is shown in Fig. (1.6). The total is shown with by the line (D). Combinations of individual terms are also shown: the volume term (A), the volume plus surface terms (B), the volume plus surface plus Coulomb terms (C). The term "symmetric nuclear matter" refers to extrapolation of properties of nuclei with $N = Z$ and with no Coulomb interaction to infinite sized nuclei where the surface can be ignored. Thus the symmetric nuclear matter extrapolation of the liquid-drop model used for this example gives BE/A= -15.5 MeV.

The size of the symmetry energy term determines how the binding energy decreases as we move away from stability. To isolate this term we can examine the chain of nuclei for a fixed A value as a function of Z. Experimental values $B(N,Z)/A$ vs Z are shown in Fig. (1.13) for $A = 100$. The form of this curve for $A = 100$ is similar to those for other A values. The binding energy has a maximum at $Z_{\max} = 44$. Without the Coulomb interaction between protons, the maximum would occur at $N = Z$ due to the symmetry energy (the α_4 term). When the Coulomb interaction between protons (the α_3 term) is added, the peak is shifted to more neutron-rich nuclei. The

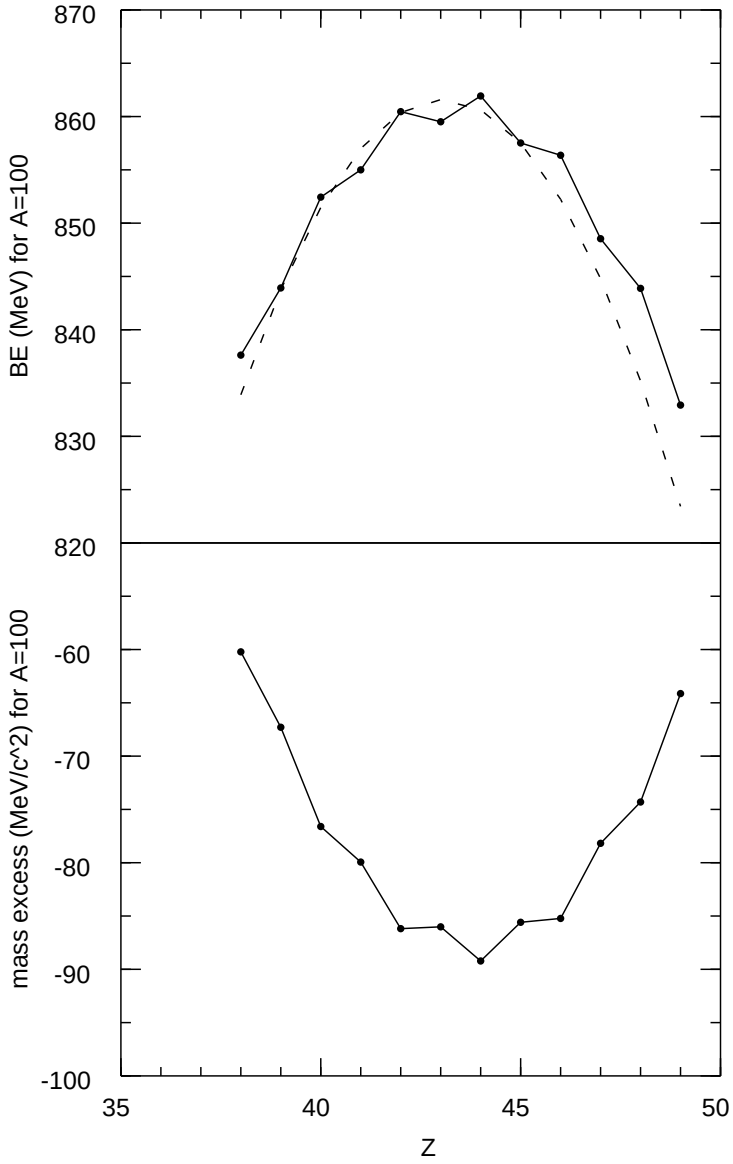

Figure 13: Binding energy per nucleon, BE/A, and the mass excess, Δ, for $A = 100$ as a function of Z. The points connected by a line are the experimental values and the liquid-drop model for the binding energy is shown by the dashed line.

oscillation in the binding energy curve in Fig. (1.13) is due to nuclear pairing interaction(*), which gives rise to the fact that nuclei with even numbers of protons or neutrons are more bound than their neighboring (odd) nuclei. The droplet model would predict that $Z = 43$ has the highest binding, but the pairing changes this to $Z = 44$.

The stability of nuclei to beta decay is determined by the differences in the mass excess shown in this example for $A = 100$ in the bottom panel of Fig. (1.13). From Eq. (1.2), the differences in the mass excesses are related to differences in the binding energies by $[\Delta(N,Z) - \Delta(N,Z \pm 1)]c^2 = -[B(N,Z) - B(N,Z \pm 1)] \pm [\Delta_n - \Delta_H]c^2$ where $[\Delta(n) - \Delta(H)]c^2 = 0.782$ MeV. Thus, for example, for $A = 100$ we find two stable isotopes in nature, ^{100}Mo and ^{100}Ru. If we consider the very weak double-beta decay process, ^{100}Mo will eventually decay into ^{100}Ru. This occurs with a lifetime which is greater than the age of the universe, but such rare decay modes have been detected in experiments.

To go further, we are interested in the deviations between the experimental and liquid-drop models for the binding energies, and in understanding these deviations in terms of microscopic models. The difference between the experimental and liquid-drop model binding energies are Fig. (1.14). The difference between the HF1 model and the liquid-drop model is shown in Fig. (1.15). In light nuclei the deviations are largest near the neutron drip line. This deviation for light nuclei can be improved by adding another term to Eq. (1.14) related to the "surface symmetry" energy [4]. In Fig. (1.14) there are two strong peaks at $A = 132$ and $A = 208$ which are the "doubly closed shell" nuclei ^{132}Sn and ^{208}Pb. There is also a hint of a peak forming near ^{100}Sn.

The values for the difference between experiment and the liquid-drop model plotted vs N and Z are shown in Figs. (1.16) and (1.17), respectively. One observes several types of deviations. When the differences are plotted vs proton number Z as in Fig. (1.16), one observes that the nuclei with Z=28, 50 and 82 are more bound than average. These are the shell-model magic numbers for the closed-shell configurations at these Z values. For neutrons, Fig. (1.17), the same magic numbers are observed with the addition of $N = 126$. The small oscillations observed in these figures is due to nuclear pairing(*). This can be removed by plotting the results for only the even-even nuclei as shown in Figs. (1.18) and (1.19).

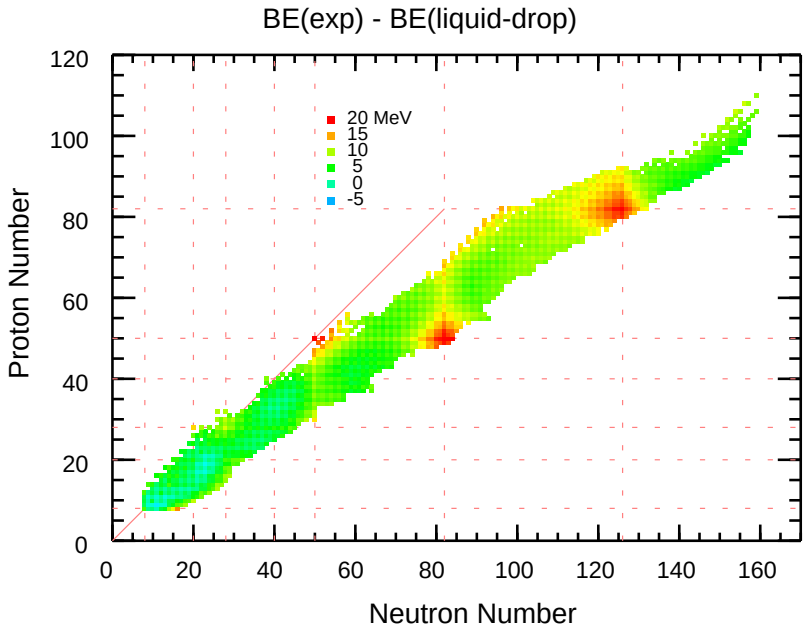

Figure 14: The difference between the experimental and liquid-drop binding energies as a function of N and Z.

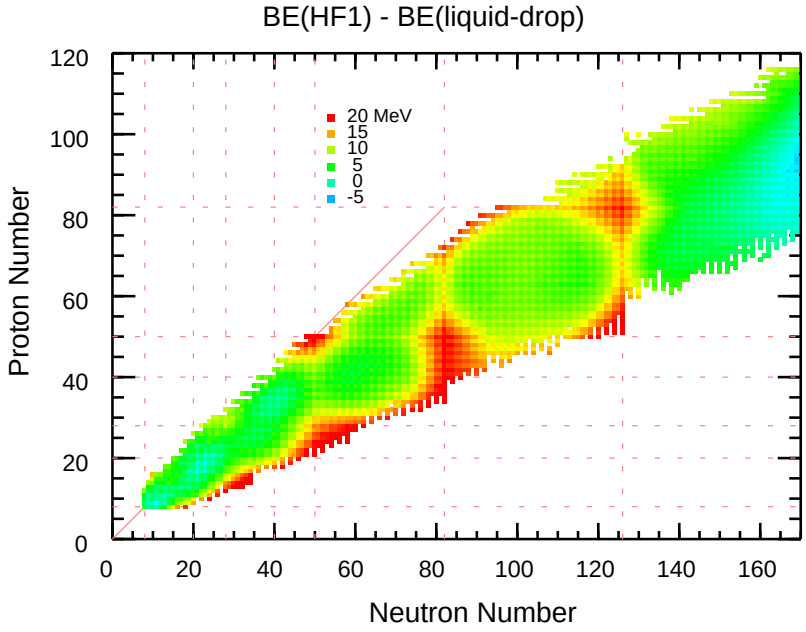

Figure 15: The difference between the HF1 and liquid-drop binding energies as a function of N and Z.

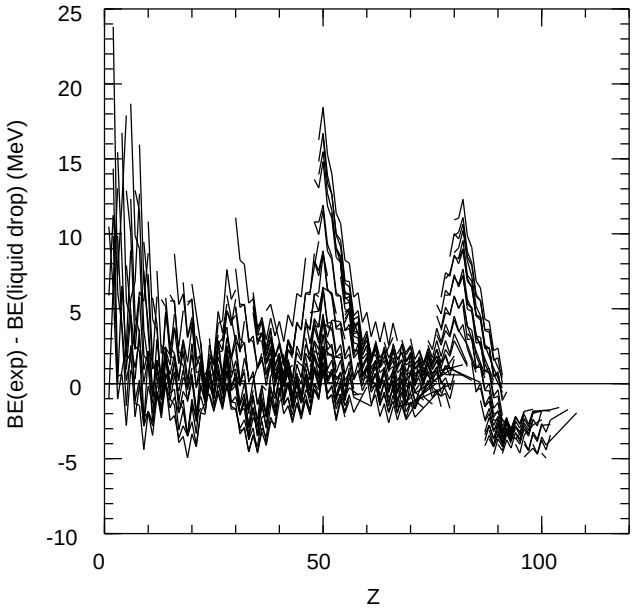

Figure 16: The difference between the experimental and liquid-drop binding energies as a function of Z. The dashed lines show the magic numbers 28, 50 and 82.

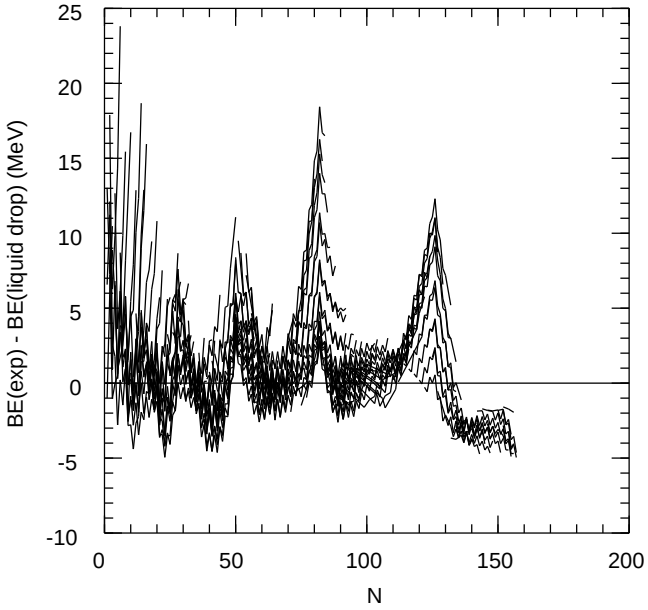

Figure 17: The difference between the experimental and liquid-drop binding energies as a function of N. The dashed lines show the magic numbers 28, 50, 82 and 126.

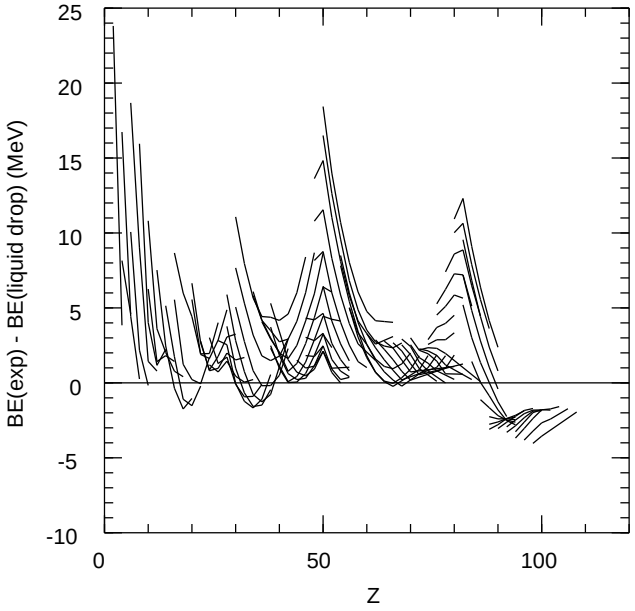

Figure 18: Same as in Fig. (1.16) but only for even-even nuclei.

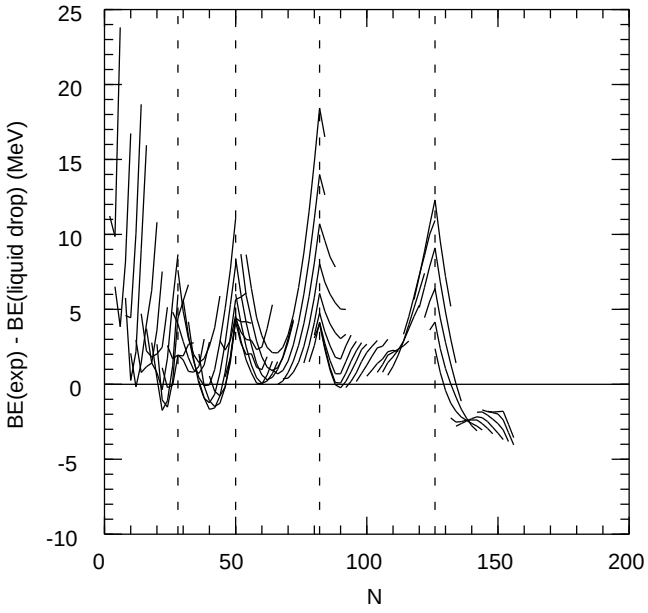

Figure 19: Same as in Fig. (1.17) but only for even-even nuclei.

References

[1] The Ame2003 atomic mass evaluation (II), G. Audi, A. H. Wapstra and C. Thibault Nuclear Physics A **729**, 337 (2003).

[2] F. Tondeur, S. Goriely and J. M. Pearson, Phys. Rev. C **62**, 024308 (2000); S. Goriely, J. M. Pearson and F. Tondeur, At. Data and Nucl. Data Tables **77**, 311 (2001).

[3] M. Thoennessen, Rep. Prog. Phys., to be published.

[4] P. Danielewicz, Nucl. Phys. A **727**, 233 (2003).

2 Rms charge radii

The root-mean-square (rms) charge radius has been measured for the ground states of many nuclei. For a spherical charge density, $\rho(r)$, the mean-square radius is defined by:

$$< \bar{r^2} > = \frac{\int \rho(r) r^2 \, d\tau}{\int \rho(r) \, d\tau}, \tag{2.1}$$

and the rms radius is the square root of this quantity. Experimental values have been compiled in [1]. The rms charge radii for the 687 nuclei shown in Fig. (2.1) are plotted vs A in Fig. (2.2). This selection of nuclei is a result of the variety of ways in which the charge radii have been measured. The radii for most stable nuclei (those on the solid line in Fig. (2.1)) have been deduced from electron scattering form factors and/or from the x-ray transition energies of muonic atoms. The relative radii for a series of isotopes can be extracted from the isotope shifts atomic x-ray transitions.

The charge density of the nucleus, ρ_{ch}, with rms radius $\bar{R}_{ch}$ is given by the point proton density in the nucleus, ρ_p, with rms radius $\bar{R}_p$,convoluted with the charge density of the proton, $\bar{R}_o$, with rms radius $\bar{R}_o = 0.88$ fm. Thus we have

$$\bar{R}_{ch} = \sqrt{\bar{R}_p^2 + \bar{R}_o^2}. \tag{2.2}$$

and

$$\bar{R}_p = \sqrt{\bar{R}_{ch}^2 - \bar{R}_o^2}. \tag{2.3}$$

This last equation is used to obtain the rms radii for point protons shown in Fig. (2.3).

In the spherical liquid-drop model the density is given by:

$$\rho(r) = \rho_o, \text{ for } r < R = r_o A^{1/3}, \text{and}$$

$$\rho(r) = 0, \text{ for } r > R. \tag{2.4}$$

The rms radius for this sharp-surface distribution is given by

$$\bar{R}_d = \sqrt{\frac{3}{5}} R = \sqrt{\frac{3}{5}} (r_o A^{1/3}). \tag{2.5}$$

The liquid-drop model with $r_o = 1.185$ fm is shown by the dashed line in Fig. (2.3). The value of $r_o = 1.185$ fm is chosen so that the line passes through the lower values of the rms radii for heavy nuclei. (For the charge radii in Fig. (2.2) one needs $r_o = 1.20$ fm.) It is observed that the data follow the liquid-drop line rather closely except for light nuclei and some regions of heavy nuclei where the data is higher than the model.

The distribution of neutrons is not known so well but we will start out by assuming that the rms radius for neutrons is the same as that for protons. In the liquid-drop model the density for nucleons in the interior of the nucleus saturates to a value ρ_o.

We improve the sharp-surface model if we allow the surface to be diffuse. The typical way to introduce the diffuseness is with the Fermi function shape:

$$\rho(r) = \frac{\rho_o}{1 + \exp[(r - R)/a]}. \tag{2.6}$$

The rms radius is given by:

$$\bar{R}_f = \sqrt{\frac{3}{5}}\sqrt{R^2 + \frac{7}{3}\pi^2 a^2} \tag{2.7}$$

The fit to the data obtained with $r_o = 1.15$ fm and $a = 0.35$ fm is shown by the solid line in Fig. (2.3). This is a better overall fit to light and heavy nuclei, but the data still fluctuate around the curve. In the Fermi distribution model for A nucleons the interior density is given by

$$\rho_o = \frac{A}{\frac{4\pi}{3}R^3(1 + \frac{\pi^2 a^2}{R^2})}. \tag{2.8}$$

For large A we can neglect the $\frac{\pi^2 a^2}{R^2}$ term, and if we assume that the rms radius for neutrons is the same as that for the protons then $R^3 = r_o^3 A$ and $\rho_o = \frac{3}{4\pi r_o^3} = 0.16$ nucleons/fm^3 with $r_o = 1.15$ fm. This is approximately the saturation density of symmetric nuclear matter. The assumption of equal rms radii for protons and neutrons means that the interior density will be divided between protons and neutrons in the ratio Z/N. So, for example, in ^{208}Pb, the interior nucleon density of 0.16 nucleons/fm^3 will be divided into $(82/208)0.16 = 0.06$ protons/fm^3 and $(126/208)0.16 = 0.10$ neutrons/fm^3.

In order to bring out the differences in the rms radii I show the experimental values plotted vs neutron number in Fig. (2.4) and the difference $\bar{R}_{exp} - \bar{R}_f$ in Fig. (2.5). One observes that the experimental rms radii are relatively small at the magic numbers. This means that the nuclei associated with the magic numbers are more compact than those away from the magic numbers. This increase in rms radii away from the magic numbers is qualitatively related to nuclear deformation(*).

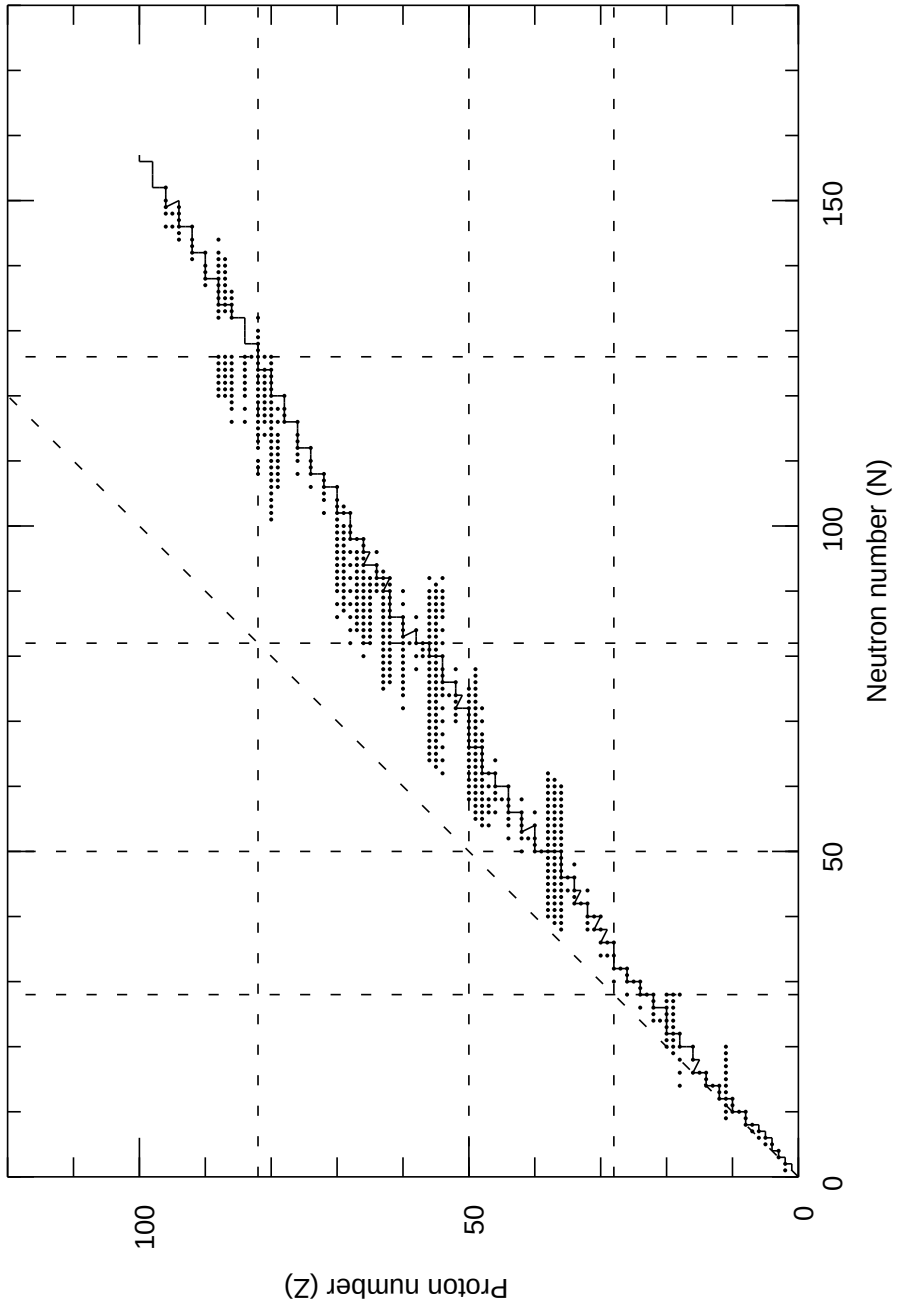

Figure 1: Nuclei with measured rms charge radii. There are a total of 687. The dashed lines are for $N = Z$, and the magic numbers 28, 50, 82 and 126. the solid line is drawn through those nuclei with the largest binding energy for a given A value (the most stable nuclei).

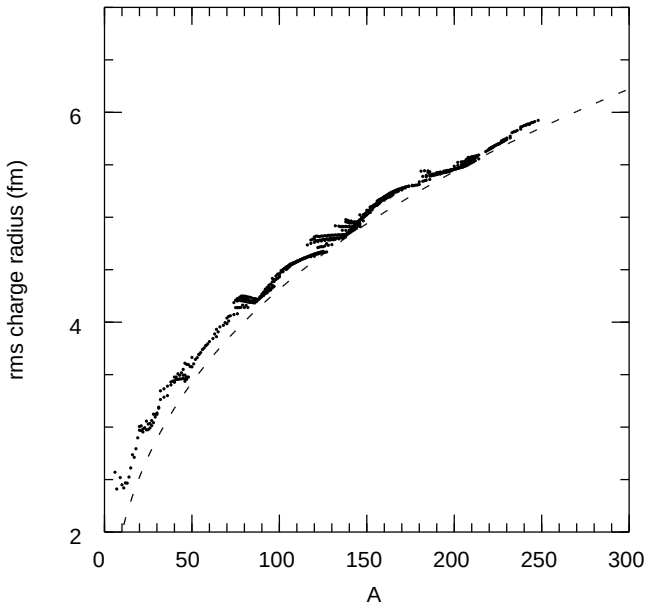

Figure 2: The rms charge radii for 687 nuclei plotted as a function of the atomic number A. The dashed line is the liquid-drop model with a sharp surface $R = r_o A^{1/3}$ with $r_o = 1.20$ fm.

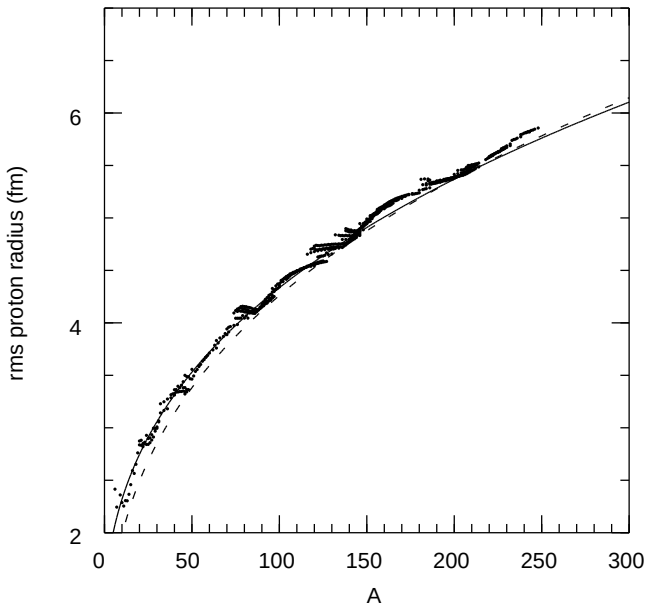

Figure 3: The rms proton radii for 687 nuclei plotted as a function of the atomic number A. The dashed line is the liquid-drop model with a sharp surface $R = r_o A^{1/3}$ with $r_o = 1.185$ fm. The solid line uses the form of Eq. (2.7) which takes into account the diffuseness.

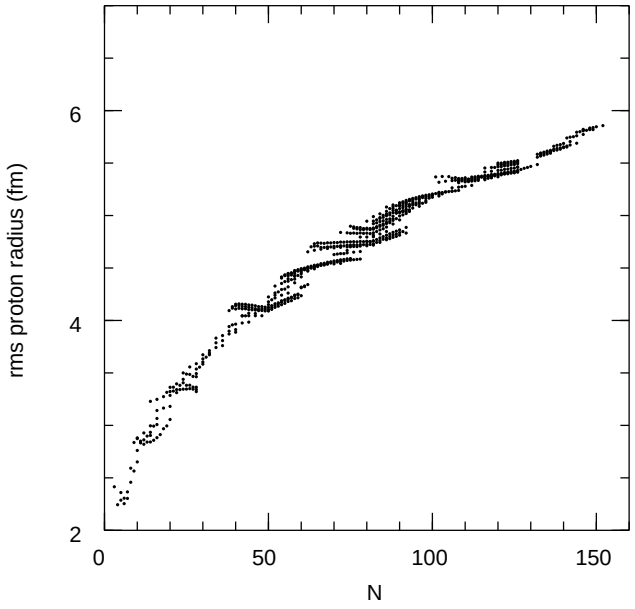

Figure 4: The rms proton radii for 687 nuclei plotted as a function of the neutron number N.

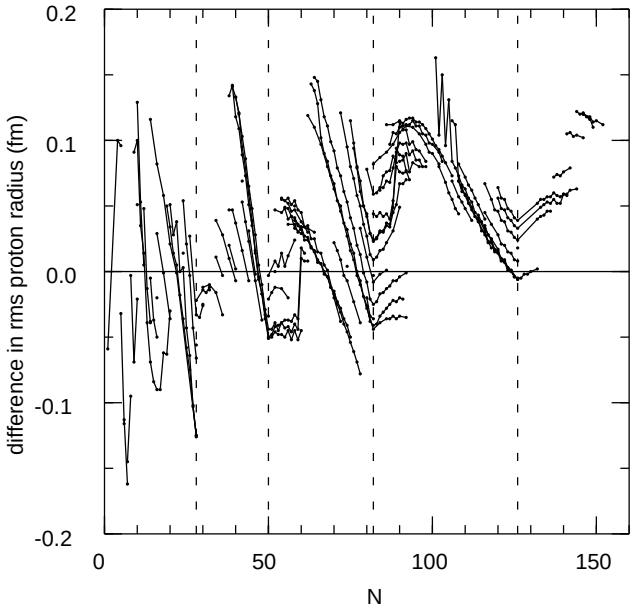

Figure 5: The rms proton radii for 687 nuclei with the diffuse liquid-drop model values of Eq. (2.7) subtracted. The magic numbers 28, 50, 82 and 126 are indicated by the dashed lines.

References

[1] H. de Vries, C. W. de Jager and C. de Vries, At. Data and Nucl. Data Tables **36**, 495 (1987); G. Fricke, C. Bernhardt, K. Heilig, L. A. Schaller, L. Shellenberg, E. B. Shera and C. W. de Jager, At. Data and Nucl. Data Sheets **60**, 177 (1995).

3 Charge densities and form factors

Elastic electron scattering from nuclei has provided a great resource of experimental data with which to test models for nuclear ground states. It evolved from the early determinations of rms charge radii, to much more precise measurements in the 70's and 80's which have provided nearly model-independent determinations of the charge-density distributions of many nuclei. In these density distributions one can observe oscillations in the interior density which represent the quantum "waves" in the nucleus.

The charge-density normalization is given by:

$$\int \rho(r)_{ch}\, d\tau = 4\pi \int \rho(r)_{ch} r^2 dr = Z, \tag{3.1}$$

where Z is the number of protons in the nucleus. The charge probability density,

$$P(r)_{ch} = 4\pi r^2 \rho(r)_{ch}, \tag{3.2}$$

represents the probability to find Z protons at a given radius r from the center of the nucleus.

As an example, the charge density measured for ^{208}Pb is shown in Fig. (3.1). The charge density is shown it the top panel and the probabilitly density in the lower panel. If one were to put the 208 nucleons of ^{208}Pb into a simple cubic lattice, a density of 0.16 nucleons/fm^2 corresponds to a lattice spacing of 1.85 fm. I have respresented this situation in the upper panel of Fig. (3.1) by drawing Gaussian distributions for several nucleons each of which has an rms radius of 0.88 fm and which are spaced a distance of 1.85 fm. One observes in this situation that the overlap between nucleons is small. (In nuclear models the nucleons are not confined to lattice sites but are described by wave functions spread over the whole nuclear volume. Nucleons confined to lattice sites would have zero-point kinetic energies that are an order of magnitude larger than those allowed to spread over the nuclear volume.)

The ratio of the electron scattering cross section to the Rutherford cross section (scattering from a point) as a function of momentum transfer, q, is related to the plane-wave Fourier transform of the charge density:

$$F(q) = \frac{1}{Z} \int \rho(r)_{ch}\; e^{i\vec{q}\,\vec{r}}\, d\tau = \frac{4\pi}{Z} \int \rho(r)_{ch}\; j_o(qr)\; r^2 dr, \tag{3.3}$$

where

$$j_o(qr) = \frac{\sin(qr)}{qr}. \tag{3.4}$$

The normalization in Eq. (3.3) is chosen to given $F(q = 0) = 1$. For light nuclei the electron energy distortion is small, and the cross section is closely proportional to the

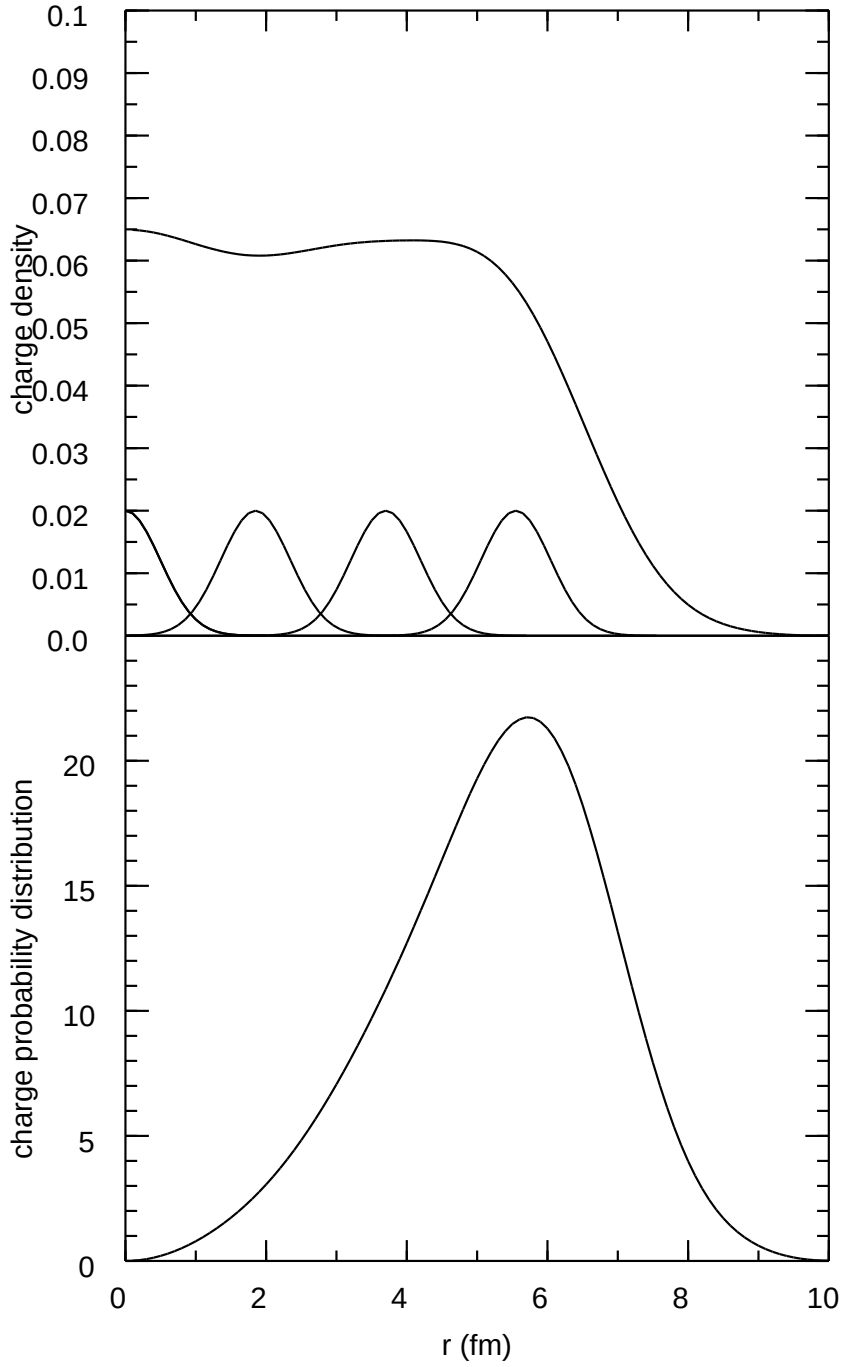

Figure 1: Experimental charge-density profile (upper panel) and probability profile (lower panel) for ^{208}Pb. The upper panel also shows the density profiles for some individual nucleons with an rms radius of 0.88 fm and spaced a distance of 1.85 fm.

form factor $\mid F(q) \mid^2$ which has minima corresponding to the zeros of $F(q)$. For heavy nuclei the electron energy distortion is larger, and the minima in the cross sections are washed out. From a DWBA analysis of the electron scattering cross section one can extract $F(q)$ with good precision over the range of momentum transfers measured.

From the measured form factors one can obtain the charge-density with the inverse of Eq. (3.3):

$$\rho(r)_{ch} = \frac{Z}{2\pi^2} \int F(q)\ j_o(qr)\ q^2 dq. \tag{3.5}$$

Since the form factor data are only determined up to some q_{max}, the resulting charge-density has some "error band" which depends upon the assumptions made about $F(q)$ for $q > q_{max}$.

A common method for extracting the charge density from the electron scattering form factors is to make a Fourier-Bessel expansion fit [1] to the data. The Fourier-Bessel expansion is given by:

$$\rho(r)_{ch} = \sum_{\nu=1}^{n_{max}} a_\nu j_o(\nu\pi r/R), \tag{3.6}$$

for $r \leq R$ and $\rho(r)_{ch} = 0$ for $r > R$, with the associated plane-wave transform:

$$F(q) = \frac{4\pi}{Z} \frac{(qR)^2}{\nu q^3} \sum_{\nu=1}^{n_{max}} \alpha_\nu [j_o(\nu\pi - qR) - j_o(\nu\pi + qR)]. \tag{3.7}$$

The parameters a_ν, ν_{max} and R for a wide range of nuclei are given in Refs. [2] and [3].

In order to obtain a qualitative understanding of how the form factors depend upon the properties of the charge density, I show in Figs. (3.2) and (3.3) some results for ^{208}Pb ($Z = 82$) based upon the Fermi distribution:

$$\rho(r)_{ch} = \frac{\rho_o}{1 + \exp[(r - R)/a]} \tag{3.8}$$

The densities are shown in the upper panels and the associated form factors $\mid F(q) \mid^2$ are shown in the lower panels.

In Fig. (3.2) I have fixed the diffuseness to be $a = 0.4$ fm and then varied R to make the rms charge radius 5.30 fm (solid line), 5.50 fm (dashed line) and 5.70 fm (crosses). In Fig. (3.3) I have varied the diffuseness from a=0.4 (solid line), 0.5 (dashed line) and 0.6 (crosses) but with R chosen to give a fixed rms of 5.50 fm.

Note that an increase in the diffuseness is associated with an increase in the interior density and a large decrease in the form factor maxima at large q values. The

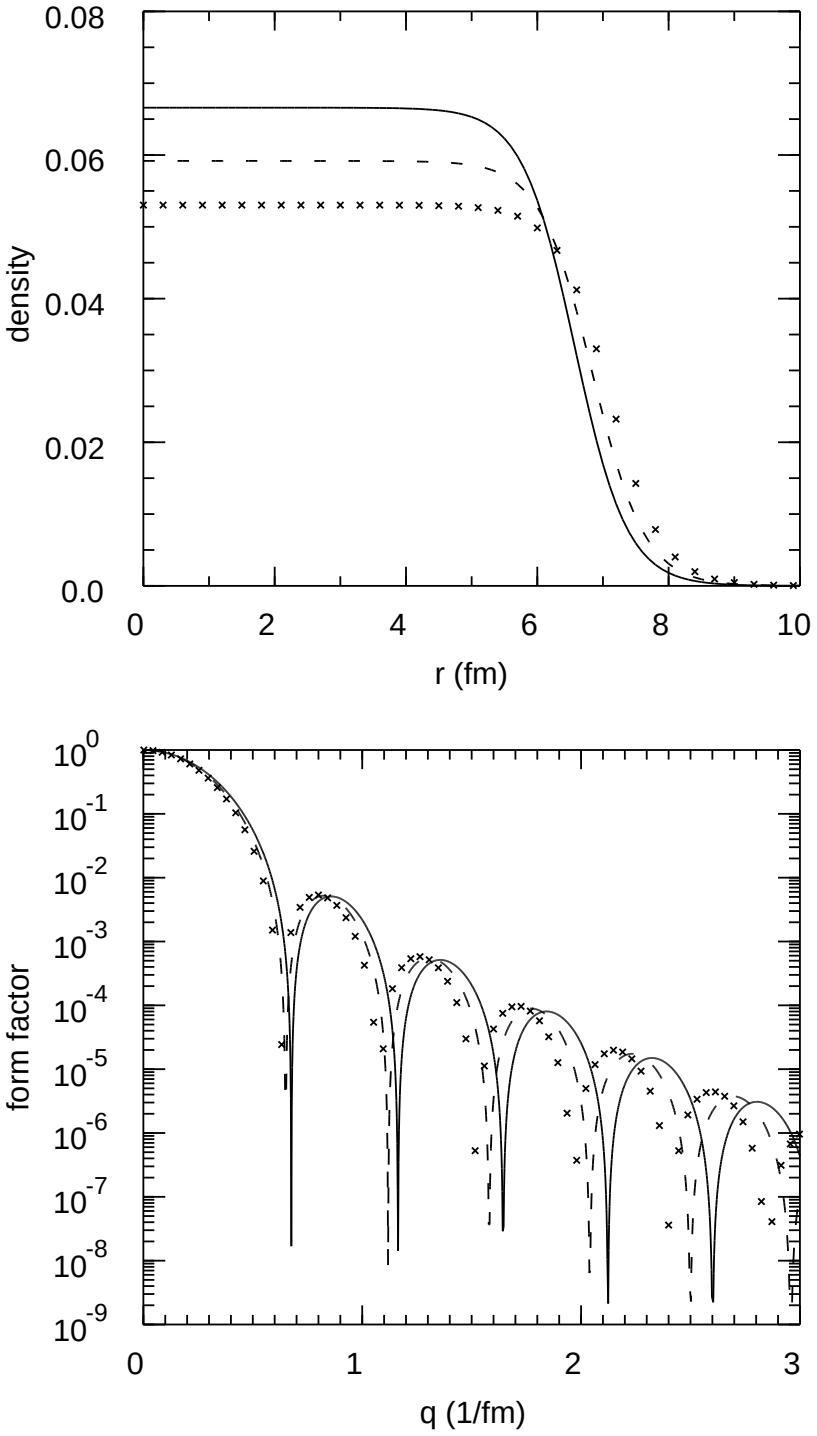

Figure 2: Features of the fermi-function densities and the associated form factors when the diffuseness is constrained to $a = 0.4$ fm and the R is used to vary the rms radius to be 5.30 fm (solid line), 5.50 (dashed line) fm and 5.70 fm (crosses).

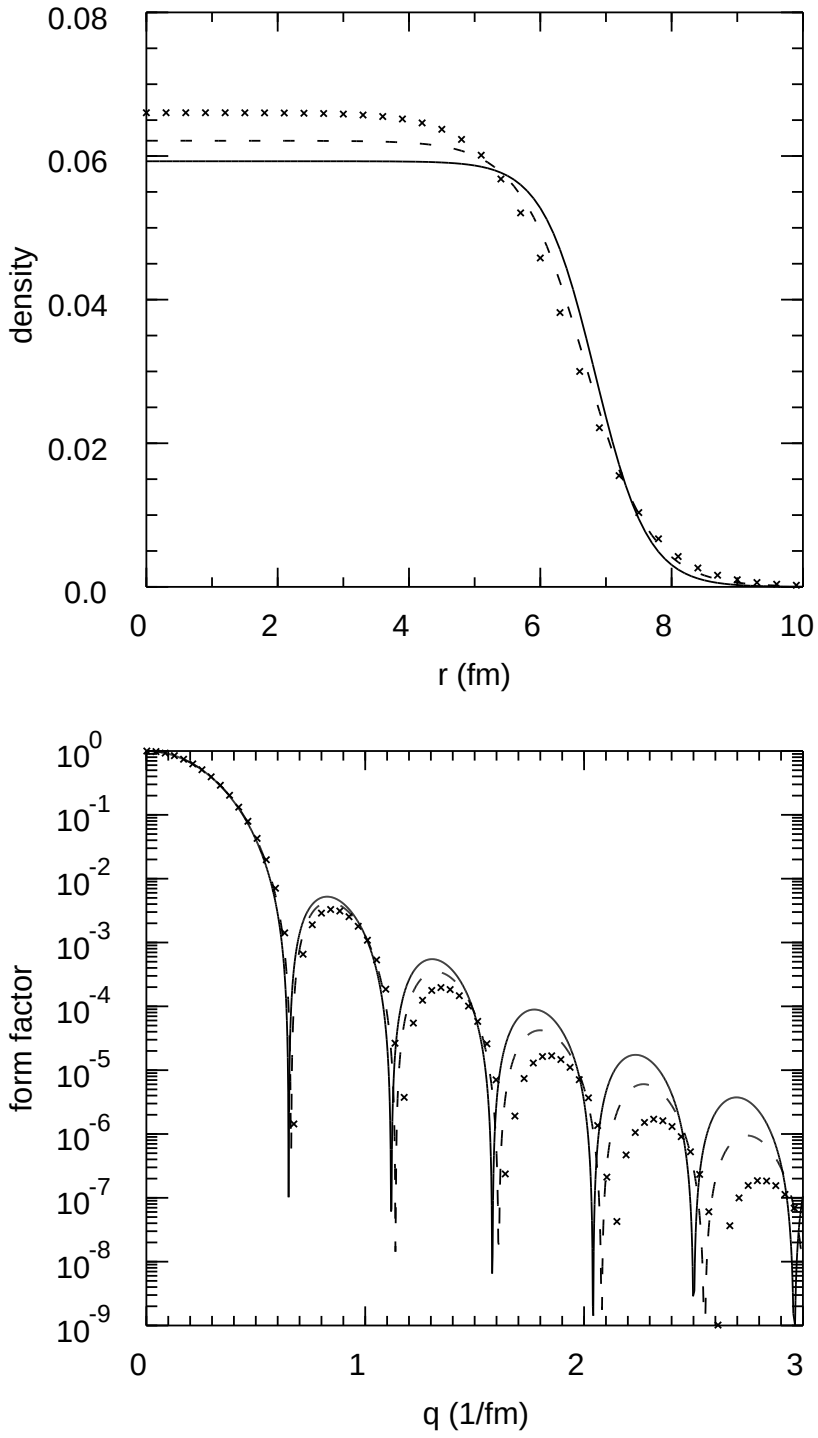

Figure 3: Features of the fermi-function densities and the associated form factors when the rms radius is constrained to be 5.5 fm. The results are given for diffuseness values $a = 0.4$ fm (solid line), 0.5 fm (dashed line) and 0.6 fm (crosses).

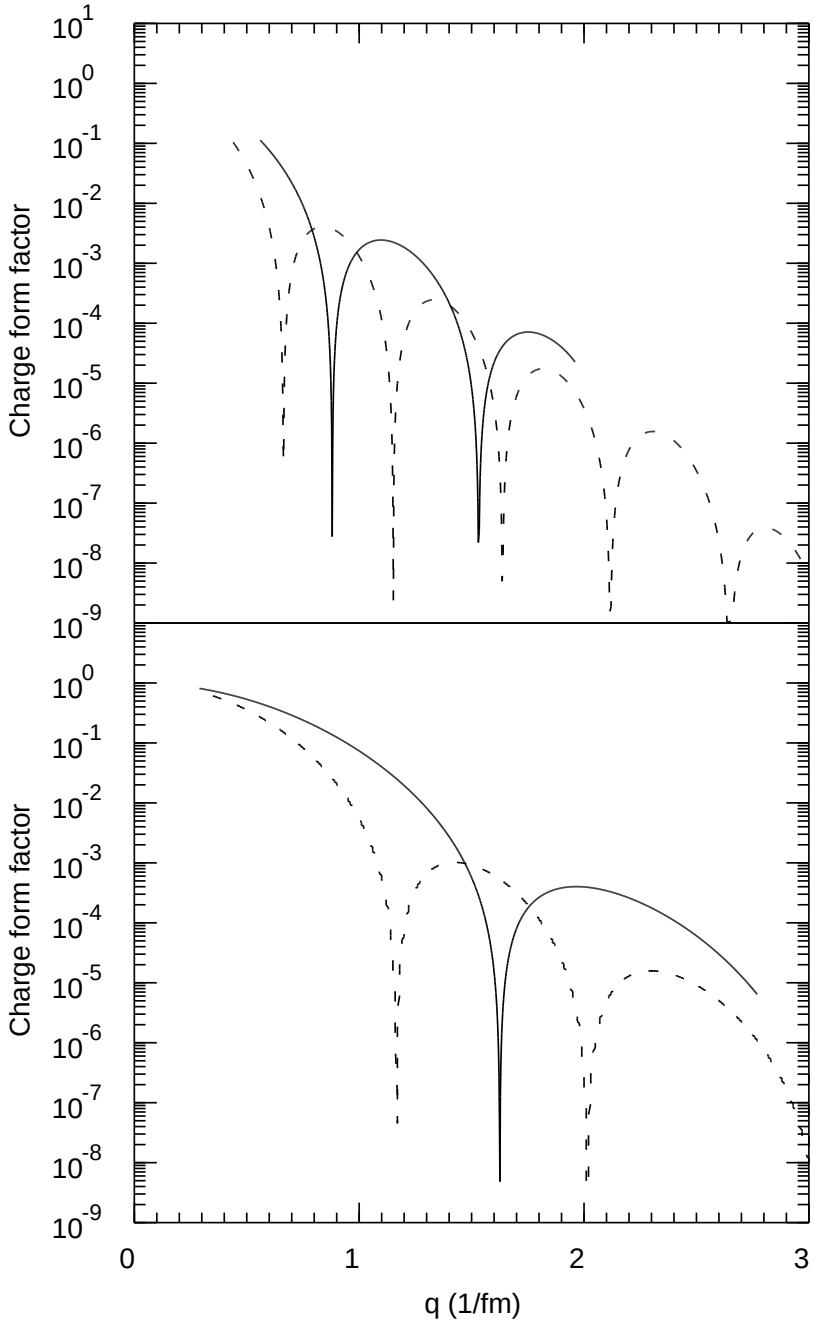

Figure 4: Experimental form factors for ^{16}O (solid line in the lower panel), ^{40}Ca (dashed line in the lower panel), ^{92}Mo (solid line in the upper panel) and ^{208}Pb (dashed line in the upper panel). The lines are plotted over the range of q values measured.

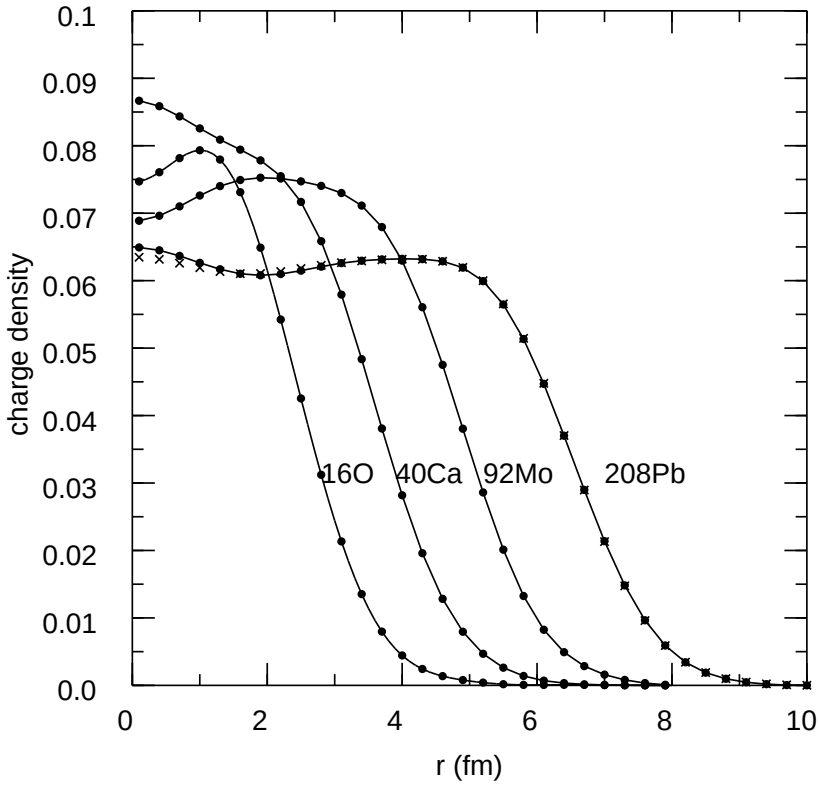

Figure 5: Experimental charge-density distributions for ^{16}O, ^{40}Ca, ^{92}Mo and ^{208}Pb. The results for the analysis of two different data sets for ^{208}Pb are shown by the circles and crosses.

qualitative effects of oscillations in the densities on the form factors are discussed in Ref. [4].

The form factors which have been measured for ^{16}O, ^{40}Ca, ^{92}Mo and ^{208}Pb are shown in (3.4). The charge densities which have been extracted from these data are shown in (3.5). One observes various oscillations in the charge density which is related to the shell structure of nuclei. The surface gradually extends out for heavier nuclei but the diffuseness is rather constant as assumed in the Fermi distribution model.

The experimental errors are not given in Refs. [2] and [3], and I do not attempt to show an experimental "error band" for the charge densities, the size of which is strongly correlated with q_{max}. For ^{208}Pb in Fig. (3.5) the density extracted from two difference sets of set are used to give an indication of the error. General aspects of the statistical and model-dependent errors in these Fourier-Bessel fits are discussed by Dreher et al., [1] and those related to specific experiments are discussed in the original experimental papers. Generally the width of the error band increases toward the center of the distribution (where the number of protons is small). For example for ^{92}Mo [5] the statistical and model-dependent error is 1.5% at $r = 2$ fm and goes down to 0.6% (about the size of the circles used to represent the experimental data in the figures to be discussed below) for $r = 4$ fm.

References

[1] B. Dreher, J. Friedrich, K. Merle, H. Rothhaas and G. Luhrs, Nucl. Phys. **A235**, 219 (1974).

[2] H. de Vries, C. W. de Jager and C. de Vries, At. Data and Nucl. Data Tables **36**, 495 (1987).

[3] G. Fricke, C. Bernhardt, K. Heilig, L. A. Schaller, L. Shellenberg, E. B. Shera and C. W. de Jager, At. Data and Nucl. Data Sheets **60**, 177 (1995).

[4] P. G. Reinhard, J. Friedrich and N. Voegler, Z. Phys. A **316**, 207 (1984).

[5] B. Dreher, Phys. Rev. Lett **35**, 716 (1975)

4 Overview of nuclear decays

In 1896 Antoine Henri Becquerel found radiations which were spontaneously emitted from uranium salts. In 1898 Maria and Pierre Curie found new elements latter called Polonium and Radium that also spontaneously emitted radiations. These radiations were observed to be bent by magnetic field, and were named alpha (α) and beta (β) by Ernest Rutherford in 1899 after the observations that one was easily absorbed (alpha) and one was more penetrating (beta). In 1900, Villard identified a third form of penetrating radiation which could not be bent by a magnetic field, and these were called gamma (γ) radiations.

In 1909, Ernest Rutherford and Thomas Royds established that alpha particles were the nuclei of helium atoms and have atomic mass number $A = 4$ and nuclear charge number $Z = 2$. Antoine Henri Becquerel (1899) and Walter Kaufmann (1902) identified the beta radiation with the electron by its deflection in electric and magnetic fields. The basic theory for beta decay was constructed by Enrico Fermi in 1934 after Wolfgang Pauli's suggestion in the same year about the existence of the neutrino.

Gamma radiation was soon realized to be a high-energy form of the electromagnetic radiation described by Maxwell's equations. Today "gamma" radiation generally refers to the high-energy region of the electromagnetic-radiation spectrum associated with the decay of particles and nuclei. Gamma-ray energies range from a few keV (where their energy range overlaps with those of X rays that are emitted in the decay of atoms and molecules) up to 10^2 TeV (10^{14} eV) for those found in cosmic rays. The gamma ray, like the X ray, consists of photons that have no mass and no charge.

A group led by Lise Meitner and including Otto Hahn and Fritz Strassmann began studying the products formed when uranium is bombarded by neutrons in the 1930's which led to the discovery of fission in 1938-39. Fission is the induced or spontaneous breakup of a heavy nucleus into two nuclei each of which has about one half of the mass of the parent. The breakup is usually accompanied by the emission of one or more neutrons.

Other forms of ground-state radioactivity we may consider are proton decay discovered in 1981 [1], light cluster emission, $^{223}\mathrm{Ra} \rightarrow {}^{209}\mathrm{Bi} + {}^{14}\mathrm{C}$ discovered in 1984 [2], two-neutrino double-beta decay discovered in 1987 [3], and two-proton decay discovered in 2002 [4].

Since 1981 a many more cases of one-proton emission have been observed [5]. Also several other cases of light cluster emission have been observed including the emission of ^{20}O, ^{24}Ne, ^{26}Ne, ^{28}Mg, ^{30}Mg, ^{32}Si and ^{34}Si [6].

Nuclear decays are characterized by their Q value and half-life. The lifetimes we consider vary over an extremely wide range of magnitudes. In terms of $x = \mathrm{Log}_{10}[T_{1/2}(\mathrm{sec})]$ it is useful to keep in mind the values of $x \approx 37$ for the proton lifetime limit, $x \approx 17$ for the age of the universe (10 billion years), $x \approx 5$ for one day, $x \approx -7$ (100 nsec) for the typical time it take to analyze a secondary beam from the cyclotron, and $x \approx -21$ for the lifetime corresponding to a resonance width of 1 MeV.

4.1 Decay widths and lifetimes

The decay of an emsemble of quantum states is descibed by the rate equation for the number of nuclei present at time t.

$$\frac{dN}{dt} = -WN(t), \tag{4.1}$$

where W is the transition rate or decay constant. The solution of this equation is the exponential decay law

$$N(t) = N_o e^{-Wt}. \tag{4.2}$$

The time at which the number is reduced by half is the half-life

$$T_{1/2} = \frac{\ln 2}{W} = \frac{0.693}{W}. \tag{4.3}$$

The mean-lifetime τ is the average amount of time it takes to decay

$$\tau = \frac{\int te^{-Wt}dt}{\int e^{-Wt}dt} = \frac{1}{W} = \frac{T_{1/2}}{ln2} = \frac{T_{1/2}}{0.693}. \tag{4.4}$$

The time dependence of a decaying wavefunction involves both real and imaginary parts

$$\psi(t) = e^{-i\omega t - Wt/2}. \tag{4.5}$$

where the average anergy is $E_o = \hbar\omega$. The square of the Fourier transform of Eq. (4.5) gives the probability to find the state in energy E

$$P(E) = \frac{1}{4\pi^2}\frac{1}{(E-E_o)^2 + (\hbar W/2)^2}. \tag{4.6}$$

The value of $E - E_o$ at which $P(E)$ falls by a factor of two is $E - E_o = \hbar W/2$. Thus the full-width at half maximum denoted by Γ is

$$\Gamma = \hbar W = \hbar/\tau. \tag{4.7}$$

The Heisenberg uncertainty relation in terms of Γ and τ is

$$\Gamma\tau = \hbar = 6.58 \times 10^{-22} \text{ MeV s} = 6.58 \times 10^{-4} \text{ eV ps}. \tag{4.8}$$

In nuclear physics we may describe the decay of a state in terms of its lifetime in units of s, ms (10^{-3}), μs (10^{-6}), ns (10^{-9}), ps (10^{-12}) or fs (10^{-15}), or alternatively with Eq. (4.8) in terms of its width in MeV. Hitorically one usually the mean lifetime τ for gamma decay of excited-state lifetimes and the half-life $T_{1/2} = \ln(2)\ \tau$ for ground-state lifetimes for beta decay and alpha decay. (Note that the Table of Isotopes by Firestone et al. uses $T_{1/2}$ for excited states.)

A given initial state may decay to several final states. The total transition rate is:

$$W = \sum_f W_{i,f}, \tag{4.9}$$

where $W_{i,f}$ is the partial decay rate to the particular final state f. The branching fraction to this state is: [6]

$$b(i \to f) = \frac{W_{i,f}}{W}. \tag{4.10}$$

When the total lifetime and the branching fraction for a given decay are known, we can find the partial lifetime τ_p related to that specific decay channel by:

$$\tau_p = \tau / b. \tag{4.11}$$

4.2 Alpha and cluster decay

Alpha decay occurs when a parent nucleus (A, Z) with atomic mass number A and nuclear charge number Z spontaneously emits an alpha particle leaving a residual (daughter) nucleus $(A-4, Z-2)$:

$$^{A}Z \to {}^{(A-4)}(Z-2) + {}^{4}\text{He}. \tag{4.12}$$

Alpha decay usually occurs from the nuclear ground state, but decay from excited states may also occur. The alpha decay of a given parent nucleus often leads to daughter nuclei that are themselves alpha or beta radioactive, thus giving rise to a disintegration series. By 1935 the detailed decay schemes for three naturally occurring series that started with ^{238}U (Z=92), ^{235}U, and ^{232}Th (Z=90) had been discovered. The alpha particles observed for these naturally occurring decays have energies in the range of 5 to 10 MeV, and were used as a source of projectiles for nuclear reaction experiments until the use of particle accelerators took over in the 1940's.

[6] The branching fraction is often denoted by BR and is given in percent.

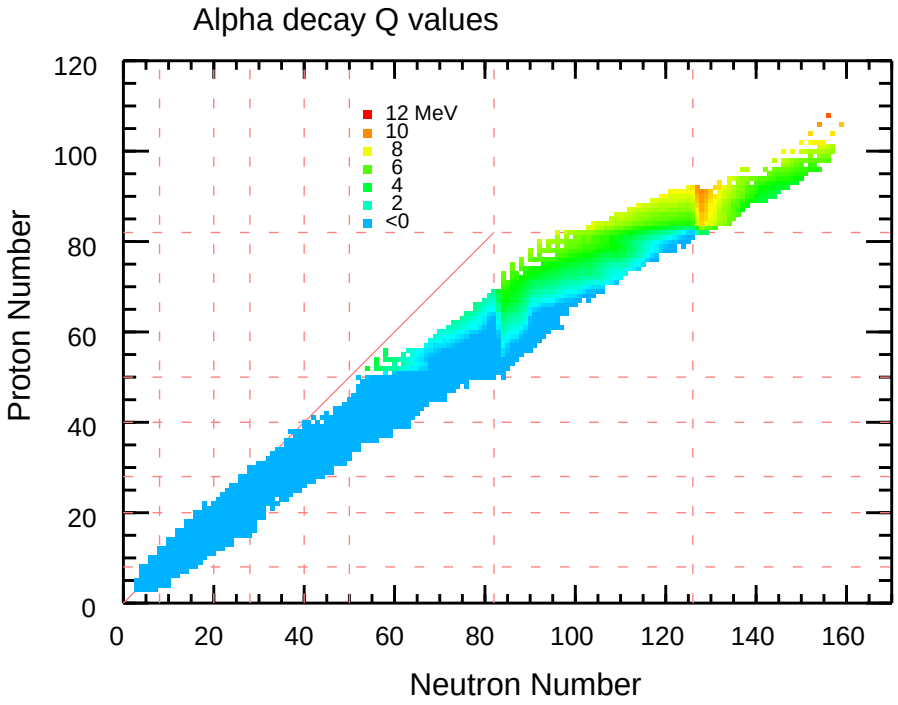

Figure 1: Experimental values for the alpha decay Q values.

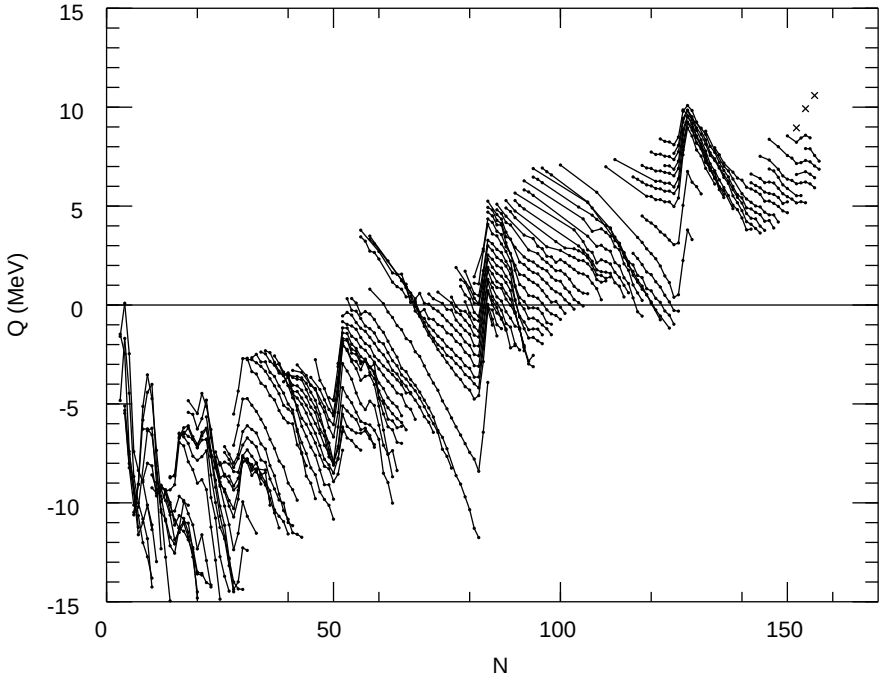

Figure 2: Experimental values for the alpha decay Q values.

Spontaneous alpha decay is allowed when the Q_α value for the decay is positive. The energy of the emitted alpha particle is given by

$$E_\alpha = Q_\alpha M_d/(M_d + M_\alpha), \tag{4.13}$$

where M_d and M_α are the masses of the daughter nucleus and alpha particle, respectively, and the Q_α is given in terms of binding energies B by:

$$Q_\alpha = B(N-2, Z-2) + B(2,2) - B(N,Z), \tag{4.14}$$

were $B(2,2) = 28.296$ MeV. The values obtained with the experimental binding energies are shown in Figs. (4.1) and (4.2). The alpha-decay Q_α value becomes positive above $Z \approx 50$ and, generally, for nuclei that are proton-rich compared to the most stable. (An exceptional case is that of ^{8}Be for which the Q_α value is positive for the decay into two alpha particles.) Alpha decay is more important than other light element emissions because of the relatively large binding energy of the alpha particle together with its small Z value. The alpha decay of nuclear ground states competes with beta decay and fission decay. The alpha decay of nuclear excited states competes, in addition, with gamma decay. Man-made heavy elements are often most easily identified by their characteristic alpha decay series. For example, the element with $Z = 110$ discovered in 1994 at GSI was identified from the detection of an alpha particles with an energy of 11.13 MeV and a half-life of about 400 μs in coincidence with the alpha particle from the decay of the $Z = 108$ daughter, whose properties had been studied in previous experiments.

The basic theory for alpha decay was developed by George Gamow and others in 1930. One postulates an alpha particle moving in the potential well of an attractive strong interaction. The potential energy diagram for the ^{238}U decay is shown in Fig. (4.3) The radius of the strong interaction potential, R_t, is determined by the distance between the centers when the surfaces of the alpha particle and the daughter nucleus touch. This is given approximately by $R_t = R_d + R_\alpha$, where $R_d = 1.2A^{1/3}$ fm is the radius the daughter nucleus and $R_\alpha = 2.15$ fm for the alpha particle. For illustrative purposes the magnitude of the potential inside R_t has been set to zero. The dashed line shows the Q_α value energy of 4.27 MeV. Beyond the distance R_t the interaction between the alpha particle and the daughter nucleus is determined by the repulsive Coulomb potential $V(r) = 2Z_d e^2/r$, where Z_d is the nuclear charge number of the daughter nucleus.

The semi-classical picture developed by Gamow envisions an alpha particle moving back and forth classically inside the radius R_t and hitting the potential barrier at R_t with a decay rate $W_c = v/(2R_t) = \sqrt{Q_\alpha/(2\mu R_t^2)}$ where μ is the reduced mass $M_d M_\alpha/(M_d + M_\alpha)$, and we estimate the velocity v by $Q_\alpha = \frac{1}{2}\mu v^2$. When the alpha particle hits the potential barrier it has a probability, P, in the theory of quantum

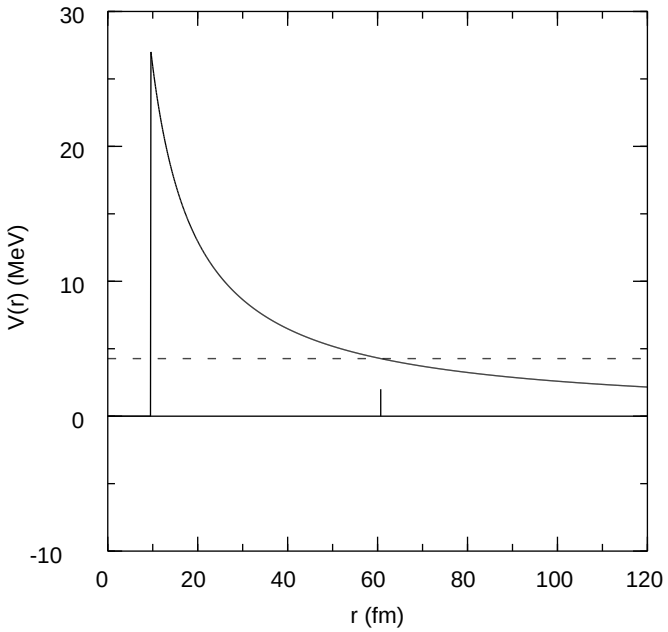

Figure 3: The potential energy diagram for the alpha decay of ^{238}U. The solid line is the Coulomb barrier to the radius R_t. the dashed line is the Q_α value.

mechanics to tunnel though the barrier given by:

$$P = \exp\{-2\int_{R_t}^{R_c} \sqrt{2\mu[V(r) - Q_\alpha]/\hbar^2}\, dr\}. \tag{4.15}$$

The radius, $R_c = 2Z_d e^2/Q_\alpha$, at which $V(r) = Q_\alpha$ is referred to as the classical turning radius, since classically an alpha particle approaching the daughter nucleus from a large radius cannot go beyond this point. Integration gives

$$P = \exp\{-4Z_d e^2\sqrt{2\mu/(Q_\alpha\hbar^2)}\,[\cos^{-1}(x) - x\sqrt{1-x^2}\,]\}, \tag{4.16}$$

where $x = \sqrt{R_t/R_c}$. The total alpha decay rate is $W = W_c P$ and the alpha-decay half-life is given by

$$T_{1/2} = \frac{\ln 2}{(W_c P)}. \tag{4.17}$$

The experimental half-lifes for the alpha decays of 119 (even-even) nuclei with ground state angular momenta of $J = 0$ are compared to the Gamow estimate in Fig. (4.4) One observes qualitative agreement with the Gamow estimate over 25 orders of magnitude in the half-life with a systematic trend for the experimental half-lifes to be about 10-100 times longer than predicted. This hindrance can be qualitatively interpreted as the probability that the actual many-body wave function

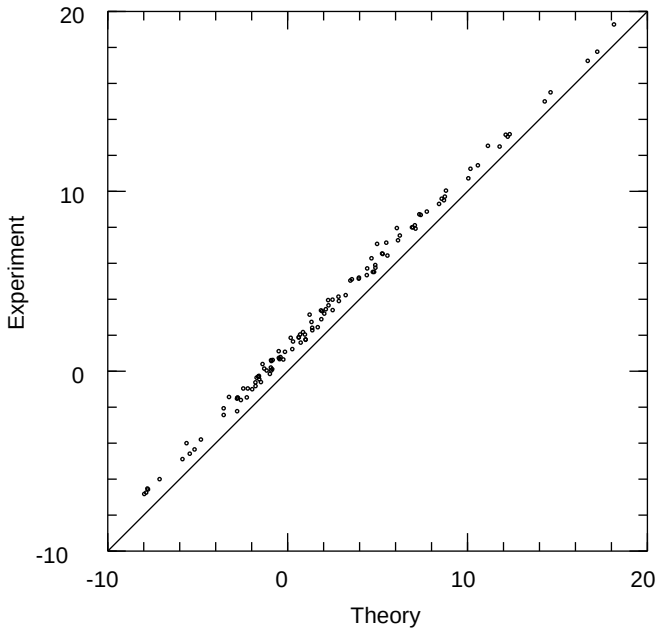

Figure 4: Comparison of experimental and theoretical values for $\log_{10}[T_{1/2}(\mathrm{sec})]$.

of the parent nucleus has an overlap with the wave function representing the alpha particle plus daughter nucleus. The structure dependence in this hindrance factor can be seen in Fig. (4.5), where the ratio of the experimental to theoretical decay rates are shown. One observes a reduction in the experimental rate as one approaches the magic number 126 and then a sudden jump up.

From the form of Eq. (4.16) one obtains with some approximations the Gieger-Nuttall relation for alpha decay, $\mathrm{Log}_{10}[T_{1/2}] \sim Z_d/\sqrt{Q_\alpha}$. However a more accurate empirical relation [7] which is able to reproduce the alpha decay half-lifes to within about a factor of three is

$$\log_{10}[T_{1/2}(\mathrm{sec})] = -51.37 + 9.54 Z_d^{0.6}/\sqrt{Q_\alpha}\,. \tag{4.18}$$

where Z_d is the charge of the daughter nucleus and Q_α is in units of MeV. Generally equation (4.18) has the same accuracy as Eq. (4.17), and neither equation contains the structure dependence observed in Fig. (4.5).

Eq. (4.18) has been used to calculate the alpha-decay half-life for those nuclei in Fig. (4.1). The results for all nuclei are shown in Fig. (4.6). Results based on the HF1 model are shown (4.7). One observes that alpha decay is responsible for the instability of nuclei above ^{208}Pb except for a small region of nuclei around ^{232}Th and $^{234-238}$U.

The Gamow model can be extended to the decay of non-zero spin nuclei by

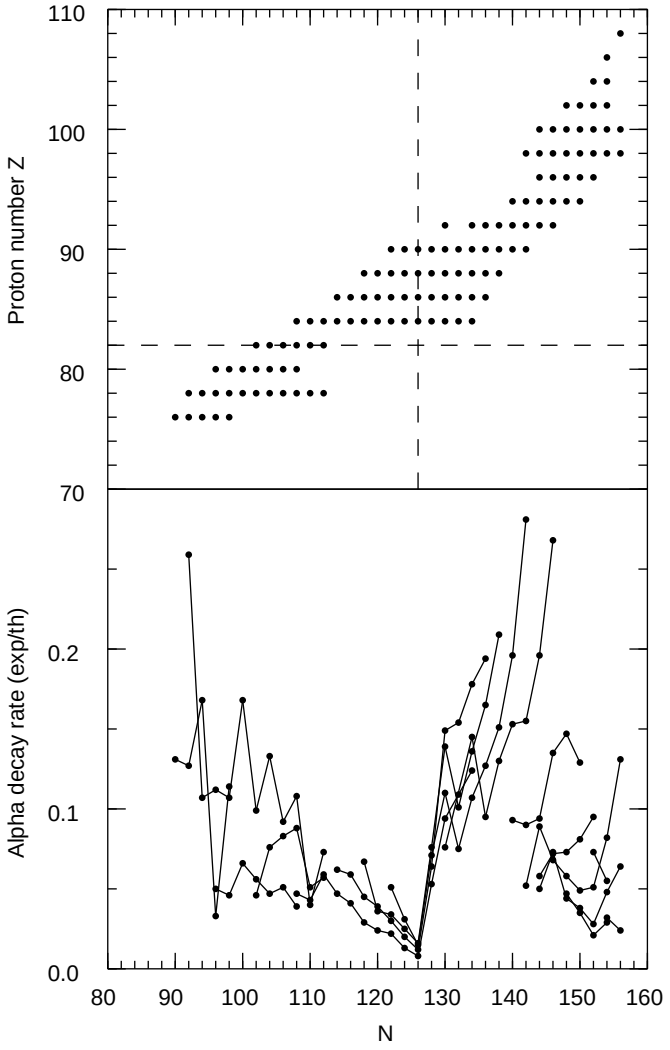

Figure 5: Ratio of the experimental to theoretical alpha decay rates (W) plotted as a function of neutron number. The top part of the figure shows the nuclei which are considered in the bottom part with the magic numbers $Z = 82$ and $N = 126$ shown by the dashed lines.

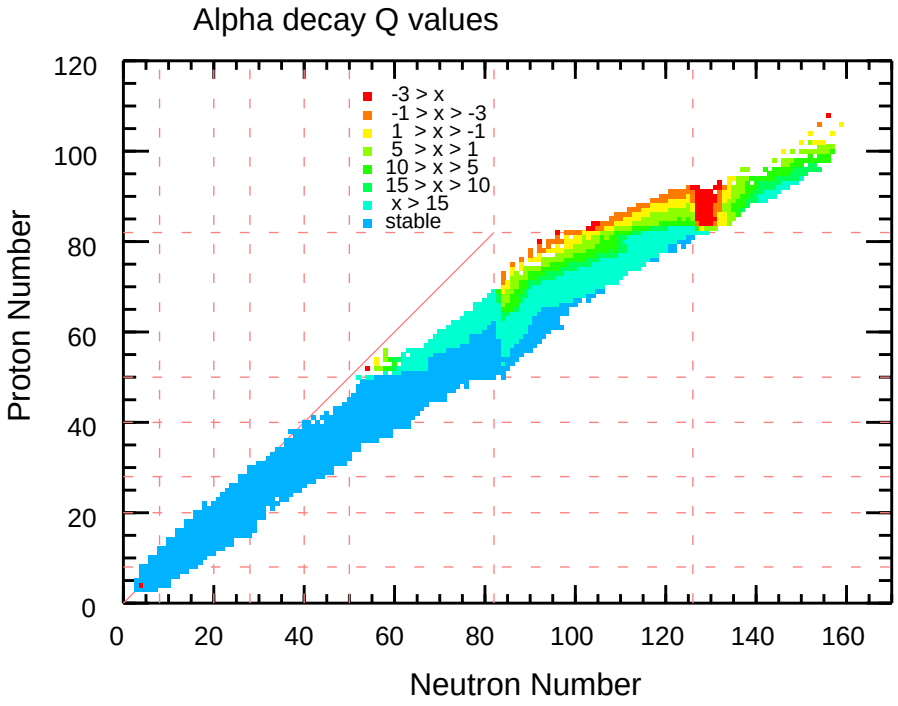

Figure 6: Nuclei that are unstable to alpha decay. The symbols represent different ranges of $x = \log_{10}[T_{1/2}(\text{sec})]$ as calculated with equation (4.18) with the experimental Q_α values.

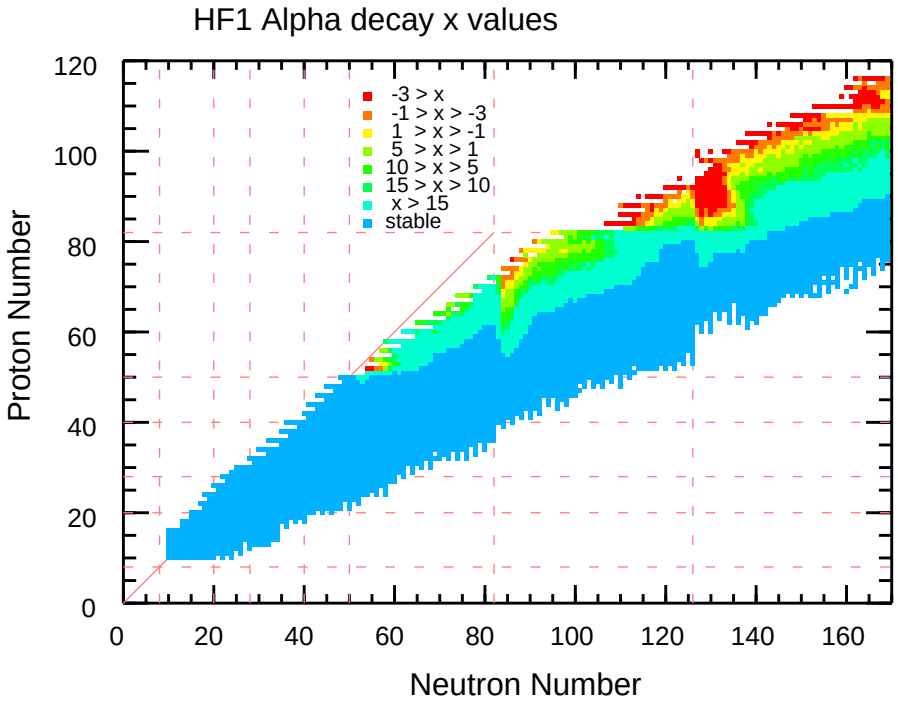

Figure 7: Nuclei that are unstable to alpha decay. The symbols represent different ranges of $x = \log_{10}[T_{1/2}(\text{sec})]$ as calculated with equation (4.18) with the HF1 Q_α values.

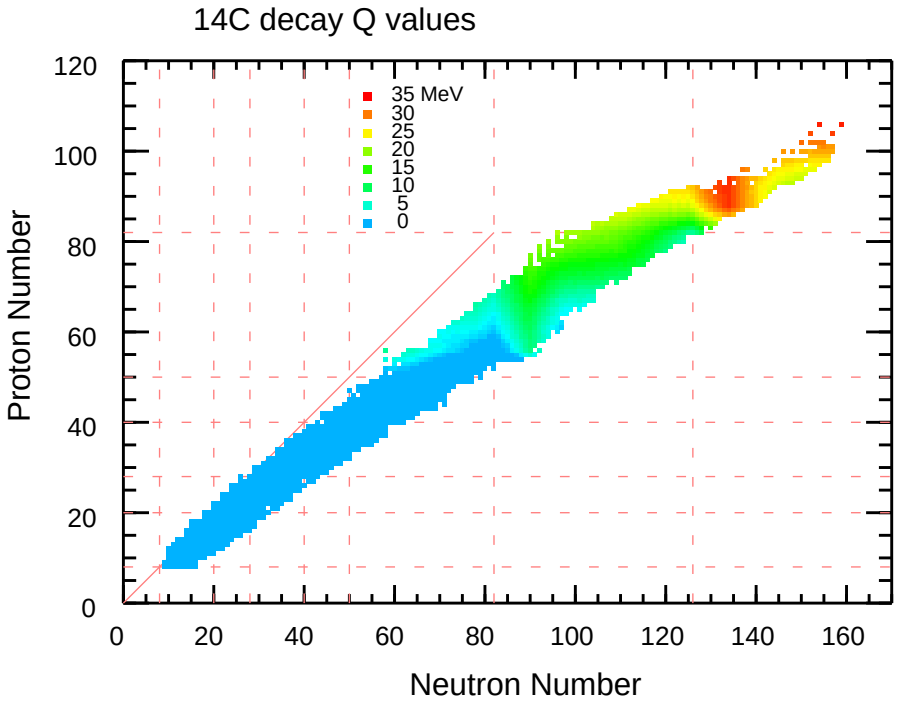

Figure 8: Experimental values for ^{14}C decay Q values.

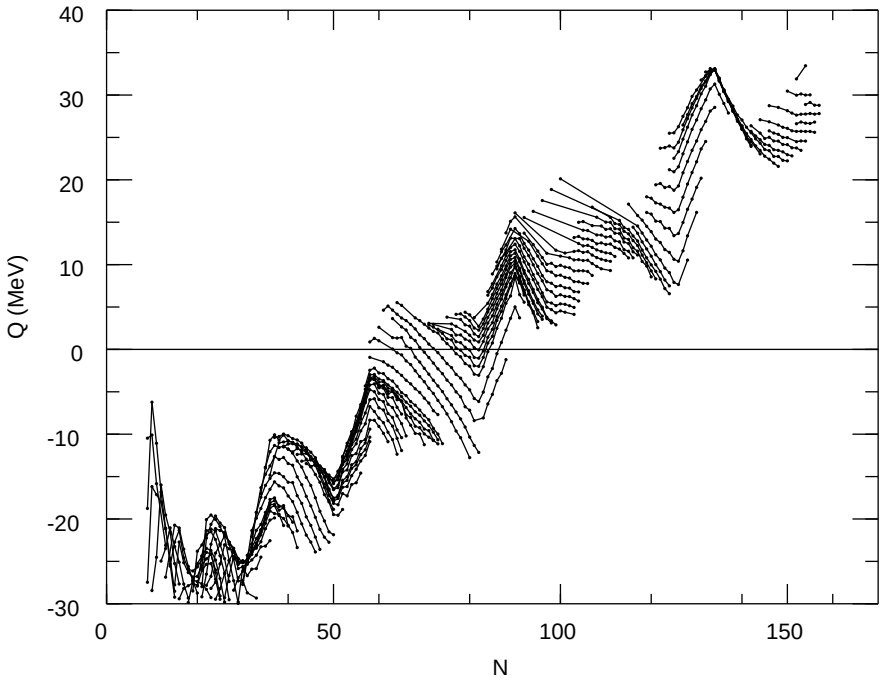

Figure 9: Experimental values for ^{14}C decay Q values.

adding a centrifugal barrier to the potential $V(r)$ corresponding to the relative angular momentum L between the daughter nucleus and the emitted nucleus:

$$V_L = \frac{L(L+1)\hbar^2}{2\mu r^2}$$

The model can be refined by considering a more realistic shape for the interior and surface region of the potential. A more quantitative understanding of alpha decay relies on using many-body wave functions for all three particles involved in the decay that incorporate the individual proton and neutron degrees of freedom. The experimental data as well as the microscopic calculations indicate deviations from the Gamow model that are related to change in shape and change in shell-structure between nuclei. The basic idea behind the Gamow model can also be used to calculate lifetimes for proton and cluster decay [8]. The Q value systematics is the essential ingredient which determined the existence and half-lives of these charged particle decay. For example I show in Figs. (4.8) and (4.9) the Q values for ^{14}C decay. The large peak in the Q values just above ^{208}Pb is what determines the the region of nuclei which have been observed to have a ^{14}C decay branch, although even in the most likely case cluster emission is extremely small ($\approx 10^{-12}$ or less) compared to alpha decay.

4.3 Beta decay

The most elementary form of nuclear beta decay is that of the neutron into a proton, an electron, and an electron antineutrino:

$$n \rightarrow p + e^- + \bar{\nu}_e. \tag{4.19}$$

Nuclei are composed of protons and neutrons bound together by the strong interaction. In the beta decay of nuclei, a given initial nuclear state $^{A_i}Z_i$ is converted into the ground state or an excited state of the final nucleus $^{A_f}Z_f$, where $Z_f = Z_i \pm 1$. The transition rate for nuclear beta decay is determined by the Q_β value or energy release and the structure of the initial and final nuclear states.

Beta decays with the fastest rates occur when the leptons carry away ℓ=0 angular momentum and are referred to as "allowed" transitions. Decays with $\ell > 0$ for the leptions are referred to as "forbidden" transitions. The dependence upon the energy release can usually be calculated to a precision of about 0.1 percent, and beta decay thus provides a precise test of the strength of the weak interaction, as well as of the internal structure of particles and nuclei. In the limit when Z is small and Q_β is large, the transition rate for "allowed" beta transitions is proportional to Q_β^5.

In 1956 Tsung Dao Lee and Chen Ning Yang suggested that beta decay should violate the principle of parity nonconservation, and they proposed an experiment to

test this idea. In 1957 parity nonconservation was confirmed by experiments carried out by Wu, Ambler, Hayward, Hoppes and Hudson on the beta decay of ^{60}Co.

The modern theory of beta decay is based upon the Standard Model which unifies the weak and electromagnetic interactions. The Standard Model of beta decay involves the $W^{\pm}$ bosons at an intermediate stage of the decay process. The most elementary of these processes involved in nuclear beta decays are:

$$d \rightarrow u + W^- \rightarrow u + e^- + \bar{\nu}_e, \tag{4.20}$$

and

$$u \rightarrow d + W^+ \rightarrow d + e^+ + \nu_e, \tag{4.21}$$

where u and d are the "up" and "down" quarks, respectively. These transformations are examples of a larger class of transformations that involve all quarks and leptons. Each step in the elementary decay process is proportional to the weak-interaction coupling constant g. The Standard Model relates the value of g to the mass of the W boson and value of the electric charge e. Also in the standard model, beta decay is unified with a larger class of weak interaction processes that involve the Z boson as an intermediate particle.

4.3.1 Beta decay Q values

Beta minus, β^-, decay involves the emission of an electron and electron antineutrino:

$${}^A Z \rightarrow {}^A(Z+1) + e^- + \bar{\nu}_e. \tag{4.22}$$

The Q value for β^- decay is given in terms of nuclear masses M and nuclear binding energies BV by

$$\begin{aligned} Q(\beta^-) &= [M(A,Z) - M_{-1}(A,Z+1) - m_e]c^2 = [M(A,Z) - M(A,Z+1)]c^2 \\ &= B(A,Z+1) - B(N,Z) + \delta_{nH}, \end{aligned} \tag{4.23}$$

where $m_e c^2 = 0.511$ MeV is the mass of the electron,

$$M_{-1}(A,Z+1) = M(A,Z+1) - m_e \tag{4.24}$$

is the mass of the final nucleus with one electron missing, and

$$\delta_{nH} = \Delta_n c^2 - \Delta_H c^2 = 0.782 \text{ MeV} \tag{4.25}$$

comes from the mass difference between the neutron and the Hydrogen atom. In these expressions we assume that the mass of the neutrino is zero and we ignore the electronic binding energy.

Beta plus, β^+, decay involves emission of a positron and electron neutrino:

$$^A Z \rightarrow {}^A(Z-1) + e^+ + \nu_e, \tag{4.26}$$

The Q value for β^+ decay is given by

$$Q(\beta^+) = [M(A,Z) - M_{+1}(A,Z-1) - m_e]c^2 = [M(A,Z) - M(A,Z-1) - 2m_e]c^2$$
$$= B(A,Z-1) - B(A,Z) - 2m_e c^2 - \delta_{nH}. \tag{4.27}$$

where

$$M_{+1}(A,Z-1) = M(A,Z-1) + m_e \tag{4.28}$$

is the mass of the final nucleus with one extra electron.

Another form of beta decay that competes with β^+ decay is electron capture (EC) in which one of the atomic electrons is captured by the nucleus and an electron-neutrino is emitted:

$$e^- + {}^A Z \rightarrow {}^A(Z-1) + \nu_e. \tag{4.29}$$

The Q value for electron capture decay is given by

$$Q(EC) = [M(A,Z) - M(A,Z-1)]c^2 = B(A,Z-1) - B(A,Z) - \delta_{nH}. \tag{4.30}$$

The experimental beta decay Q values are shown in Fig. (4.10) and those for the HF1 predictions are shown in (4.11). The energy released in β^- or β^+ decay is shared between the recoiling nucleus, the electron and the neutrino. Since the nucleus is heavy compared to the electron and neutrino, most of the energy is shared between the electron and the neutrino with a probability distribution for each that can be be accurately calculated. Usually only the electron or positron is detected, and it has a range of kinetic energies ranging from zero up to Q_β (the end-point energy), assuming that the mass of the neutrino is zero. If the neutrino has a mass, the end-point energy of the electron would be reduced. The end-point energy of the tritium beta decay has been used to set a limit of about $m_\nu < 9$ eV/c^2 for the mass of the electron antineutrino. In the electron-capture process is all of the energy goes into that of the neutrino. An experimental signature of electron capture is the X ray emitted when the vacancy left by the inner electron that was absorbed by the nucleus is filled by one of outer electrons.

4.3.2 Allowed beta decay

The allowed beta decay rate W between a specific set of initial and final states is given by:

$$W_{i,f} = (f/K_o)\left[g_V^2\ B_{i,f}(F_\pm) + g_A^2\ B_{i,f}(GT_\pm)\right], \tag{4.31}$$

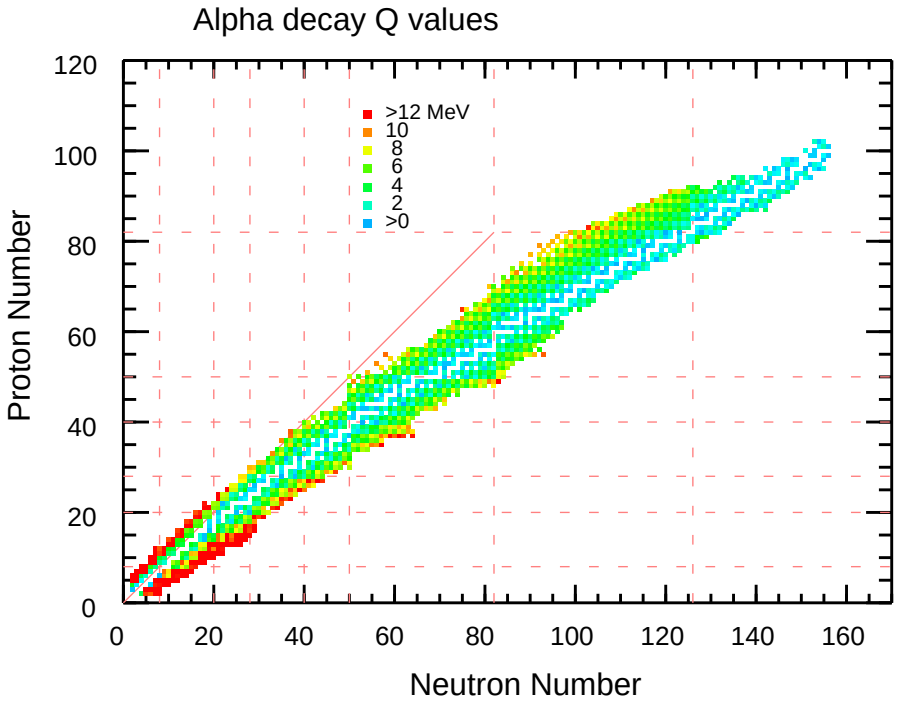

Figure 10: Experimental beta decay Q values.

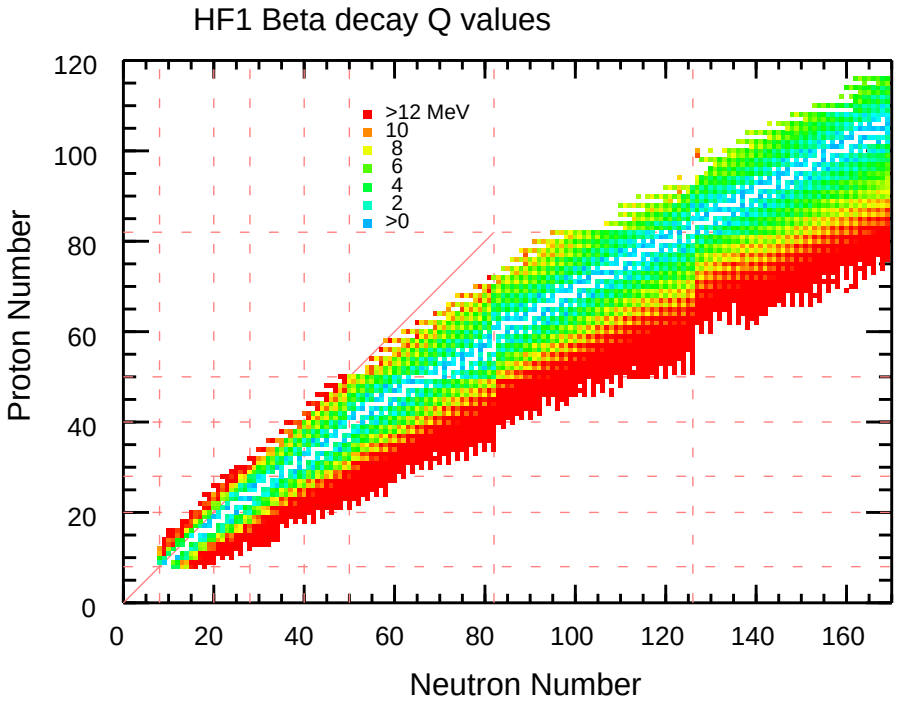

Figure 11: HF1 beta decay Q values.

where f is dimensionless three-body phase-space factor which depends upon the beta-decay Q value, and K_o is a specific combination of fundamental constants:

$$K_o = \frac{2\pi^3\hbar^7}{m_e^5 c^4} = 1.8844 \times 10^{-94} \text{ erg}^2 \text{ cm}^6 \text{ s}. \tag{4.32}$$

The $\pm$ refer to $\beta_\pm$ decay of nucleus (A_i, Z_i) into nucleus $(A_i, Z_i \mp 1)$. The weak-interaction vector (V) and axial-vector (A) coupling constants for the decay of neutron into a proton are denoted by g_V and g_A, respectively.

The operators for Fermi and Gamow-Teller beta decay in terms of sums over nucleons are:

$$\mathcal{O}(F_\pm) = \sum_k t_{k\pm}, \tag{4.33}$$

and

$$\mathcal{O}(GT_\pm) = \sum_k \sigma_k t_{k\pm}. \tag{4.34}$$

In terms of these operators the reduced matrix elements(*) in Eq. (4.31) are:

$$B_{i,f}(F_\pm) = \frac{|< f||\mathcal{O}(F_\pm)||i >|^2}{(2J_i+1)}, \tag{4.35}$$

and

$$B_{i,f}(GT_\pm) = \frac{|< f||\mathcal{O}(GT_\pm)||i >|^2}{(2J_i+1)} = \frac{[M_{i,f}(GT_\pm)]^2}{(2J_i+1)}, \tag{4.36}$$

where

$$M_{i,f}(GT_\pm) = < f||\mathcal{O}(GT_\pm)||i > \tag{4.37}$$

The matrix elements are reduced in orbital space and the $(2J_i+1)$ factor comes from the average over initial M_i states. The magnitude of reduced matrix element $M(GT)$ does not depend on the direction of the transition, i.e.,

$$\mid M(GT, a \to b) \mid = \mid M(GT, b \to a) \mid \tag{4.38}$$

whereas

$$B(GT, a \to b) = \frac{(2J_b+1)}{(2J_a+1)} B(GT, b \to a). \tag{4.39}$$

The matrix elements obey the triangle conditions(*) $J_f = J_i$ $(\Delta J = 0)$ for Fermi and $\Delta(J_i, j_i, 1)$ $(\Delta J = 1)$ for Gamow-Teller.

Historically one combines the partial half-life for a particular decay with the calculated phase-space factor f to obtain from Eq. (4.31) an "ft" value given by:

$$ft_{1/2} = \frac{C}{[B(F) + (g_A/g_V)^2 B(GT)]} \tag{4.40}$$

where

$$C = \frac{\ln(2)\, K_o}{(g_V)^2} \tag{4.41}$$

One often compiles the allowed beta decay rates in terms of a "logft" which stands for $\log_{10}$ of the $ft_{1/2}$ value.

4.3.3 Phase-space for allowed beta decay

The phase-space factors f are given by Wilkinson and collaborators [9], [10], [11]. The starting point is the analytic result for a nucleus of $Z = 0$ given by

$$f_{Z=0} = \frac{1}{60}(2W_o^4 - 9W_o^2 - 8)p_o + \frac{1}{4}W_o \ln(W_o + p_o) \tag{4.42}$$

In this expression W_o is the total electron (positron) endpoint energy in units of $m_e c^2$

$$W_o = \frac{E_o}{m_e c^2} + 1, \tag{4.43}$$

and

$$p_o = \sqrt{(W_o^2 - 1)}\,. \tag{4.44}$$

The end point energy of the electron in units of MeV is

$$E_o = (Q + E_i) - E_f \text{ for } \beta_-, \tag{4.45}$$

and

$$E_o = (Q + E_i) - E_f - 2m_e c^2 \text{ for } \beta_+, \tag{4.46}$$

where Q is the beta decay Q value, and E_i and E_f are the excitation energies of the initial and final states.

In the limit when $E_o >> m_e c^2$:

$$f_{Z=0} \rightarrow \frac{1}{30}W_o^5, \tag{4.47}$$

which can be used as a qualitative estimate of the phase space factor and its dependence on the decay energy.

To to higher level of accuracy one must take into account the distortion of the electron energy due to the nuclear Coulomb field and the effects of nuclear finite size as well as other smaller corrections [10]. The finite size corrections are slightly different for the Fermi and Gamow-Teller decays [10] and thus at this more precise

level one introduced two factors $f = f_A$ for the axial vector matrix element and f_V for the vector matrix element. Eq. (4.40) written in terms of the "ft" value is:

$$ft_{1/2} = \frac{C}{\left[\left(\frac{f_V}{f}\right) B(F) + \left(\frac{g_A}{g_V}\right)^2 B(GT)\right]} \tag{4.48}$$

Several correction factors are applied to Eq. (4.42) to obtain f, the relation being expressed in as:

$$f = \delta_D \delta_R \delta_{WM} f_{Z=0}. \tag{4.49}$$

The most important of these correction factors is δ_{WM} which takes into account the electron distortion factors. The values are tabulated by Wilkinson and Macefield [10] in the form

$$\delta_{WM} = \exp[\sum_{n=0,3} a_n (lnE_o)^n], \tag{4.50}$$

The calculation of δ_{WM} uses electron wave functions for an atom generated from a uniform spherical nuclear charge distribution whose radius is adjusted to fit the appropriate electron scattering and muonic x-ray data and which is corrected for the screening of the atomic electrons. Also included in the values of δ_{WM} are the effects of the energy-dependent "outer" radiative correction to order α and of the finite mass of the nucleus. The parametrization of the values of δ_{WM} by Eq. (4.50) is accurate to better than 0.1% throughout [10].

The factor δ_R incorporates the effects of the "outer" radiative correction to orders $Z\alpha^2$ and $Z^2\alpha^3$ and is given [9], [10] by

$$\delta_R = 1 + 3.67 \times 10^{-4} \mid Z \mid + 3.60 \times 10^{-6} Z^2. \tag{4.51}$$

where Z is the proton number of the daughter nucleus. The factor δ_D incorporates the effects of the diffuseness of the actual nuclear charge distribution [11]

$$\delta_D = 1 + 1.8 \times 10^{-5} \mid Z \mid^{1.36} - 1.2 \times 10^{-6} \mid Z \mid W_o. \tag{4.52}$$

The Fermi phase-space factor f_V is related [10] to the factor f by

$$f_V = \delta_V f, \tag{4.53}$$

where

$$\delta_V = 1 \pm (2/15) W_o R \alpha Z - (4/105)(W_o R)^2 \tag{4.54}$$

for beta $\pm$ decay, where $\alpha = 1/137$ and where we have used

$$R = 1.35 A^{1/3} \text{fm} \tag{4.55}$$

The process of electron capture is combined with that of β_+ decay in terms of a total phase space factor:

$$f_+ = f(\beta_+) + f(ec). \tag{4.56}$$

Electron-capture phase-space factors are given in the tables of Behrens and Janecke [12].

4.3.4 Weak-interaction coupling constants

The values of the coupling constants for Fermi decay, g_V, and Gamow-Teller decay, g_A, in the combinations in which they appear in Eq. (4.48) are obtained as follows.

For a $0^+ \rightarrow 0^+$ nuclear transition $B(GT) = 0$, and for a transition between $T = 1$ analogue states with $B(F) = 2$ Eq. (4.48) reduces to

$$C = 2t_{1/2}f_V. \tag{4.57}$$

The partial half-lives and Q values for several $0^+ \rightarrow 0^+$ analogue transitions have been measured to an accuracy of about one part in 10000. One obtains [11]:

$$C = 6170(4) \tag{4.58}$$

This result, which together with the value of K_o in Eq. (4.32), can be used with Eq. (4.41) to obtain g_V.

At the quark level $g_V = -g_A$. But for nuclear structure we use the value obtained from the neutron to proton beta decay [13]:

$$\mid g_A/g_V \mid = 1.261(8). \tag{4.59}$$

4.3.5 Double beta decay

Nuclear double-beta decay takes place in situations where a nucleus is energetically stable to single-beta decay but unstable to the simultaneous emission of two electrons (or two positrons). For example, for the nuclei with atomic mass number A=100, ^{100}Mo $\rightarrow$ ^{100}Ru double-beta decay may occur. The Q values for double-beta decay for those nuclei with single-beta decay Q values of 0.3 MeV or less is shown in Fig. (4.12).

There are two types of double-beta decay: the standard $(2e, 2\nu)$ type in which two neutrinos are emitted:

$$^AZ \rightarrow {}^A(Z+2) + 2e^- + 2\bar{\nu}_e, \tag{4.60}$$

or

$$^AZ \rightarrow {}^A(Z-2) + 2e^+ + 2\nu_e, \tag{4.61}$$

and the $(2e, 0\nu)$ type in which no neutrinos are emitted:

$$^AZ \rightarrow {}^A(Z+2) + 2e^-, \tag{4.62}$$

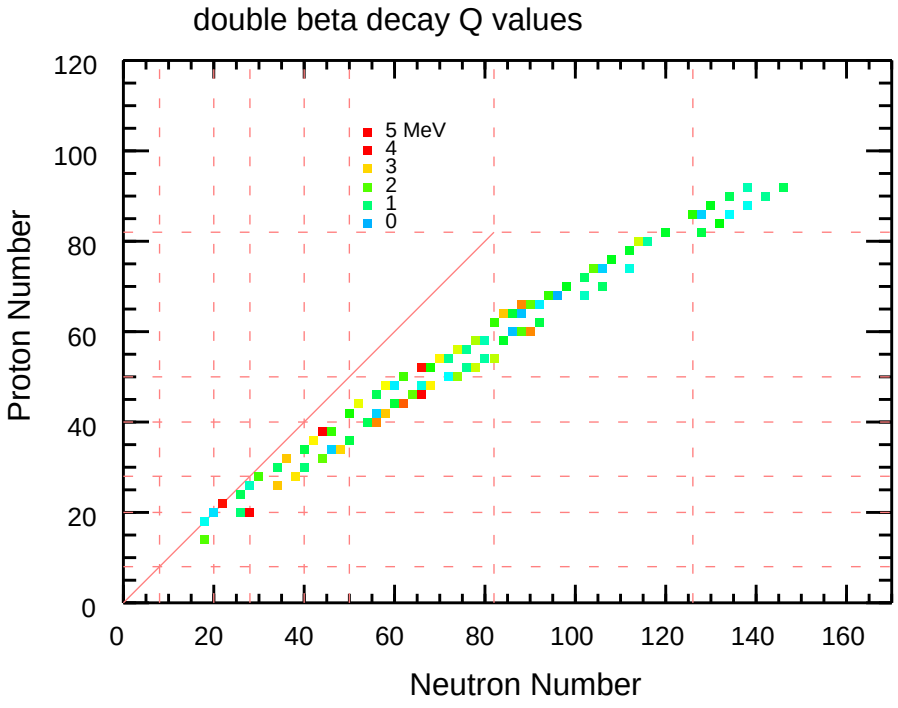

Figure 12: Experimental double-beta decay Q values.

or

$$^{A}Z \rightarrow {}^{A}(Z-2) + 2e^{+}. \tag{4.63}$$

The $(2e, 2\nu)$ double-beta decay mode has been observed in recent experiments. The $(2e, 0\nu)$ double-beta decay mode has the unique signature that the total energy of the two electrons (or positrons) must add up to the $Q_{\beta\beta}$ value. The $(2e, 0\nu)$ decay mode is being searched for experimentally, but has not yet been observed. The $(2e, 0\nu)$ decay mode is possible only if the neutrinos have a finite mass, and the nonobservation of this decay allows one to set an upper limit on the neutrino mass of about one eV/c^2.

4.4 Gamma decay

For an electromagnetic transition from an initial nuclear state i (where the nucleus is at rest) to nuclear state f, the momentum of the nucleus in state f (after the transition) and the emitted gamma ray are equal and opposite. The nucleus recoils with a kinetic energy $T_f = (\Delta E)^2/(2m_f c^2)$ and the gamma ray has an energy $E_\gamma = \Delta E - T_f$, where $\Delta E = E_i - E_f$ (the transition energy) is the rest-mass energy difference between initial and final nuclear states. T_f is much smaller than ΔE and thus to a good approximation $E_\gamma = \Delta E$. The energy and angular frequency ω of the photon are related by $E_\gamma = \hbar\omega$. The wavelength is $\lambda = hc/E_\gamma = 1237$ MeV-fm$/E_\gamma$.

The electromagnetic transition between them can take place only if the emitted gamma ray carries away an amount of angular momentum $\vec{\ell}$ such that $\vec{J}_f = \vec{J}_i + \vec{\ell}$ which means that $\mid J_i - J_f \mid \leq \ell \leq J_i + J_f$ where $J = \mid \vec{J} \mid$. Since the photon has an intrinsic spin of one, transitions with ℓ=0 are forbidden, and hence gamma transitions with $J_i = 0 \rightarrow J_f = 0$ are not allowed. A specific ℓ value determines the multipolarity of the gamma radiation; ℓ=1 is called dipole, ℓ=2 is called quadrupole, etc. In addition, when states can be labeled with a definite parity π_i=$\pm$1 and π_f=$\pm$1, the transitions between them are restricted to the "electric" type of radiation when $\pi_i\pi_f$(-1)$^\ell$ is even and the "magnetic" type of radiation when $\pi_i\pi_f$(-1)$^\ell$ is odd.

The gamma transition rate is determined by the transition energy ΔE, the multipolarity, and a factor that depends upon the details of the internal nuclear structure. For example, the power for electric-dipole radiation (E1) from classical electromagnetism is given by $P = \omega^4 e^2 d^2/(3c^3)$ where d is the average distance between the positive and negative charge, $\omega = 2\pi f$, f is the frequency of the vibration in the distance between the positive and negative charge, and c is the speed of light. The E1 transition rate $W(E1)$ (the number of gamma rays per second) is the power divided by the energy per gamma ray ($E_\gamma = \hbar\omega$): $W = P/E_\gamma = \omega^3 e^2 d^2/(3\hbar c^3) = 2.9\text{x}10^{15} E_\gamma^3 d^2$ MeV^{-3} fm^{-2}. The quantity d^2 depends upon the internal structure of the nuclear states. An estimate for the lifetime associated with electric dipole radiation can be

obtained by taking a typical nuclear transition energy of $E_\gamma = 1$ MeV and a typical nuclear size scale of $d^2 = 1$ fm^2 which gives a mean lifetime of $\tau = 1/W \approx 0.3\text{x}10^{-15}$ s.

The lowest allowed multipolarity in the decay rate dominates over the next higher one (when more than one is allowed) by several orders of magnitude. The most common types of transitions are electric dipole (E1), magnetic dipole (M1), and electric quadrupole (E2). Electromagnetic transition rates provide one of the most unambiguous tests for models of nuclear structure. The strong interaction conserves parity, and to the extent that the protons and neutrons are held together in the nucleus by the strong interaction, their states can be labeled by a definite parity. Since the weak interaction does not conserve parity, the weak interaction between protons and neutrons leads to nuclear states that have a slightly mixed parity. The electromagnetic decay between nuclear states that have a mixed parity gives rise to "mixed" transitions (such as E1 plus M1), which produce circularly polarized gamma rays (gamma rays in which the electric field vector rotates around the axis of propagation). Recent observations of circular polarized gamma rays have provided a test of the weak interaction between protons and neutrons in the nucleus.

4.4.1 Reduced transition probabilities for gamma decay

The interaction of the electromagnetic field with the nucleons can be expressed in terms of a sum of electic and magnetic multipole operators with tensor rank(*) λ

$$\mathcal{O} = \sum_{\lambda,\mu} [\mathcal{O}(E\lambda)_\mu + \mathcal{O}(M\lambda)_\mu]. \tag{4.64}$$

For a given E or M operator of rank λ the electromagnetic transition rate $W_{M_i,M_f,\mu}$ for the transition between specific M states(*) is given by:

$$W_{M_i,M_f,\mu} = \left(\frac{8\pi(\lambda+1)}{\lambda[(2\lambda+1)!!]^2}\right)\left(\frac{k^{2\lambda+1}}{\hbar}\right) |< J_f M_f \mid \mathcal{O}(\lambda)_\mu \mid J_i M_i >|^2 . \tag{4.65}$$

In this expression k is the wave-number for the electromagnetic transition of energy E_γ given by:

$$k = \frac{E_\gamma}{\hbar c} = \frac{E_\gamma}{197 \text{ MeV fm}}. \tag{4.66}$$

W is explicitly labeled by the M values but depends implicitly on the wavefunctions and operator.

The electric transition operator given by:

$$O(E\lambda) = r^\lambda \, Y^\lambda_\mu(\hat{r}) \, e_{t_z} e, \tag{4.67}$$

were Y_μ^λ are the spherical harmonics. Gamma transitions with λ=0 are forbidden because the photon must carry off at least one unit of angular momentum. The e_{t_z} are the electric charges for the proton and neutron in units of e. For the free-nucleon charge we would take $e_p = 1$ and $e_n = 0$, for the proton and neutron, respectively.

The magnetic transition operator is given by:

$$O(M\lambda) = \left[\vec{\ell}\,\frac{2g^\ell_{t_z}}{(\lambda+1)} + \vec{s}\,g^s_{t_z}\right]\,\vec{\nabla}[r^\lambda Y^\lambda_\mu(\hat{r})]\,\mu_N$$

$$= \sqrt{\lambda(2\lambda+1)}\,\left[[Y^{\lambda-1}\otimes\vec{\ell}]^\lambda_\mu\,\frac{2g^\ell_{t_z}}{(\lambda+1)} + [Y^{\lambda-1}\otimes\vec{s}]^\lambda_\mu\,g^s_{t_z}\right] r^{\lambda-1}\,\mu_N, \tag{4.68}$$

where μ_N is the nuclear magneton,

$$\mu_N = \frac{e\hbar}{2m_pc} = 0.105\ e\text{fm}, \tag{4.69}$$

and where m_p is the mass of the proton. The g-factors $g^\ell_{t_z}$ and $g^s_{t_z}$ are the orbital and spin g-factors for the proton and neutron, respectively. The free-nucleon values for the g-factors are $g^\ell_p = 1$, $g^\ell_n = 0$, $g^s_p = 5.586$ and $g^s_n = -3.826$.

The total rate for a specific set of states and a given operator is obtained my averaging over the M_i states and summing over M_f and μ:

$$W_{i,f,\lambda} = \frac{1}{(2J_i+1)}\sum_{M_f,M_f,\mu} W_{M_i,M_f,\mu}$$

$$= \left(\frac{8\pi(\lambda+1)}{\lambda[(2\lambda+1)!!]^2}\right)\left(\frac{k^{2\lambda+1}}{\hbar}\right)\frac{|<J_f||\mathcal{O}(\lambda)||J_i>|^2}{(2J_i+1)}. \tag{4.70}$$

The last factor in this equation is referred to as a "reduced transition probability" B defined by:

$$B(i\to f) = \frac{|<J_f||\mathcal{O}(\lambda)||J_i>|^2}{(2J_i+1)}. \tag{4.71}$$

B depends upon the direction of the transition. For electromagnetic transitions J_i is the higher-energy initial state. But in Coulomb excitation the initial state is the lower state, and one often uses the notation $B(\uparrow)$ for this situation. If J_a is the lower state, J_b is the higher state, and $B(\uparrow)$ is given, then the value use for the electromagnetic transitions $J_b \to J_a$ is:

$$B(b\to a) = \frac{(2J_a+1)}{(2J_b+1)}B(\uparrow a\to b). \tag{4.72}$$

In general, a level may gamma decay by several multipoles to a given final state:

$$W_{i,f} = \sum_\lambda [W_{i,f}(E\lambda) + W_{i,f}(M\lambda)]. \tag{4.73}$$

One observes from the factors in Eq. (4.70) (with $E_\gamma \approx 1$ MeV) that the rate for electric (magnetic) transitions with $\lambda + 2$ about seven orders of magnitude smaller than those electric (magnetic) transitions for λ. Thus in most cases only the lowest multipole for a given type of transition is important. Comparing rates for electric and magnetic transitions we observe that the lowest allowed multipole may be equally important. Thus (if allowed by the triangle condition) we need to consider mixed transitions of the form ($E1$ and $M2$); ($M1$ and $E2$); .... For these mixed transition we detine a mixing ratio δ by:

$$\delta^2(M2/E1) = \frac{W(M2)}{W(E1)}, \tag{4.74}$$

and

$$\delta^2(E2/M1) = \frac{W(E2)}{W(M1)}. \tag{4.75}$$

The convention is that the rate for the higher λ value is on top. By convention the sign of the mixing ratio is taken as:

$$\text{sign}[\delta(M2/E1)] = \text{sign}\frac{< J_f||O(M2)||J_i >}{< J_f||O(E1)||J_i >}, \tag{4.76}$$

and

$$\text{sign}[\delta(E2/M1)] = -\text{sign}\frac{< J_f||O(E2)||J_i >}{< J_f||O(M1)||J_i >}. \tag{4.77}$$

These mixing ratios can be measured from the angular distribution of the gamma rays when the initial state is aligned (e.g. the M_i state population is not uniform). For a mixed transition the branching fraction, b, for a given type of transition is related to δ. For example for a mixed $M1$ and $E2$ transition, the $E2$ branching fraction is:

$$b(E2) = \frac{W(E2)}{W(M1) + W(E2)} = \frac{\delta^2}{1 + \delta^2}, \tag{4.78}$$

and the $M1$ branching fraction is:

$$b(M1) = \frac{W(M1)}{W(M1) + W(E2)} = \frac{1}{1 + \delta^2}. \tag{4.79}$$

By convention the electric transition matrix elements are usually taken to be in units of e fm$^\lambda$. The values of the magnetic matrix elements are usually taken to be in units μ_N fm$^{\lambda-1}$, where

$$\mu_N = \frac{e\hbar}{2m_p c} = 0.105e\,\text{fm} \tag{4.80}$$

is the nuclear magneton. It is convenient to make an explicit list of the factors which relate the partial mean lifetime τ_p and reduced transition probability B for the most common types of transitions. For electric transitions:

$$B(E1) = \frac{0.629}{E_\gamma^3\ \tau_p} e^2\mathrm{fm}^2\mathrm{MeV}^3\mathrm{fs}) \tag{4.81}$$

$$B(E2) = \frac{816}{E_\gamma^5\ \tau_p} e^2\mathrm{fm}^4\mathrm{MeV}^5\mathrm{ps}) \tag{4.82}$$

$$B(E3) = \frac{1760}{E_\gamma^7\ \tau_p} e^2\mathrm{fm}^6\mathrm{MeV}^7\mu\mathrm{s}) \tag{4.83}$$

$$B(E4) = \frac{5882}{E_\gamma^9\ \tau_p} e^2\mathrm{fm}^8\mathrm{MeV}^9\mathrm{s}) \tag{4.84}$$

$$B(E5) = \frac{2.89 \times\ 10^{10}}{E_\gamma^{11}\ \tau_p} e^2\mathrm{fm}^{10}\mathrm{MeV}^{11}\mathrm{s}) \tag{4.85}$$

$$B(E6) = \frac{1.95 \times\ 10^{17}}{E_\gamma^{13}\ \tau_p} e^2\mathrm{fm}^{12}\mathrm{MeV}^{13}\mathrm{s}) \tag{4.86}$$

and for magnetic transitions:

$$B(M1) = \frac{56.8}{E_\gamma^3\ \tau_p} \mu_N^2\mathrm{MeV}^3\mathrm{fs} \tag{4.87}$$

$$B(M2) = \frac{74.1}{E_\gamma^5\ \tau_p} \mu_N^2\mathrm{fm}^2\mathrm{MeV}^5\mathrm{ns}) \tag{4.88}$$

$$B(M3) = \frac{0.1585}{E_\gamma^7\ \tau_p} \mu_N^2\mathrm{fm}^4\mathrm{MeV}^7\mathrm{s}) \tag{4.89}$$

$$B(M4) = \frac{0.533 \times\ 10^6}{E_\gamma^9\ \tau_p} \mu_N^2\mathrm{fm}^6\mathrm{MeV}^3\mathrm{s}) \tag{4.90}$$

4.4.2 Weisskopf units for gamma decay

In order to judge whether a transition is relatively weak or strong, one often gives the B value in "single-particle" or Weisskopf units. This Weisskopf unit is an estimate of the B value for a single-particle (proton or neutron) and how it depends upon mass. By convention it is defined by:

$$B_W(E\lambda) = \left(\frac{1}{4\pi}\right)\left[\frac{3}{(3+\lambda)}\right]^2 (1.2A^{1/3})^{2\lambda}\ e^2\ \mathrm{fm}^{2\lambda}, \tag{4.91}$$

and

$$B_W(M\lambda) = \left(\frac{10}{\pi}\right)\left[\frac{3}{(3+\lambda)}\right]^2 (1.2A^{1/3})^{2\lambda-2}\ \mu_N^2\ \mathrm{fm}^{2\lambda-2}. \tag{4.92}$$

The most commonly used are:

$$B_W(E1) = 0.0645\ A^{2/3}\ e^2\ \mathrm{fm}^2, \tag{4.93}$$

$$B_W(E2) = 0.0594\ A^{4/3}\ e^2\ \mathrm{fm}^4, \tag{4.94}$$

and

$$B_W(M1) = 1.790\ \mu_N^2. \tag{4.95}$$

Weisskopf units for the decay widths are:

$$\Gamma_W(E2)(\mathrm{eV}) = 4.9 \times\ 10^{-8}\ A^{4/3}\ [E_\gamma(\mathrm{MeV})]^5 \tag{4.96}$$

$$\Gamma_W(M1)(\mathrm{eV}) = 2.1 \times\ 10^{-2}\ [E_\gamma(\mathrm{MeV})]^3 \tag{4.97}$$

References

[1] S. Hofmann et al., Z. Phys. A **305**, 111 (1982); O. Klepper et al., Z. Phys. A **305**, 125 (1982).

[2] H. J. Rose and G. A. Jones, Nature **307**, 345 (1984); D. V. Aleksandov et al., JEPT Lett. **40**, 909 (1984).

[3] S. R. Elliott, A. A. Hahn and M. K. Moe, Phys. Rev. Lett. **59**, 2020 (1987).

[4] M. Pfutzner et al., Eur. Phys. J. **A14**, 279 (2002); J. Giovinazzo et al., Phys. Rev. Lett. **89**, 102501 (2002).

[5] P. Woods and C. Davids, Annu. Rev. Nucl. Part. Sci. **47**, 541 (1997).

[6] G. Ardisson and M. Hussonnois, Radiochim. Acta. **70/71**, 123 (1995); A. A. Oglobin et al., Phys. Rev. C **61**, 034301 (2000).

[7] B. A. Brown, Phys. Rev. Lett. **69**, 1034 (1992).

[8] S. B. Duarte et al., Atomic Data Nucl. Data Tables **80**, 235 (2002).

[9] D. H. Wilkinson, Nucl Phys. A209, 470 (1973)

[10] D. H. Wilkinson and B. E. F. Macefield, Nucl. Phys. A232, 58 (1974)

[11] D. H. Wilkinson, A. Gallman and D. E. Alburger, Phys. Rev. C18, 401 (1978)

[12] H. Behrens and J. Janecke, in Landolt-Bornstein, Numerical Data dn Functional Relationships in Science and Technology, New Series, editor in cheif K. -H. Hellwege, Group I: Nuclear Physics and Technology, Vol 4, ed. by H. Schopper (Springer-Verlag) 1969.

[13] D. H. Wilkinson, Nucl. Phys. A377, 474 (1982)

5 The Fermi gas model

The fermi-gas model is used to obtain an approximate distribution for the kinetic energy of nucleons confined to a volume V with density $\rho = A/V$. It is evaluated for the conditions present in nuclear matter and will give an approximate result for the kinetic energy distribution in heavy nuclei. One assumes the lowest energy state allowed by the Pauli exclusion principle. We will start with symmetric nuclear matter ($N = Z$) with A nucleons confined to a box of length L on each side. The interaction between nucleons enters indirectly in determining the saturation density and the size of the box. The normalized wave function for a nucleon is given by:

$$\phi(\vec{r}) = \left(\frac{2}{L}\right)^{3/2} \sin(k_x x)\sin(k_y y)\sin(k_z z). \tag{5.1}$$

The condition that the wave functions vanish on the boundary L means that:

$$k_x = \frac{\pi n_x}{L} \tag{5.2}$$

with $n_x = 1, 2, 3 \ldots$. with similar conditions for k_y and k_z. Each state is represented by a set of quantum numbers (n_x, n_y, n_z) with energy:

$$\epsilon_i = \frac{\hbar^2 k^2}{2m} = \frac{\hbar^2}{2m}\left(\frac{\pi}{L}\right)^2 (n_x^2 + n_y^2 + n_z^2), \tag{5.3}$$

and wave number

$$k_i = \frac{\pi}{L}\sqrt{(n_x^2 + n_y^2 + n_z^2)}\,. \tag{5.4}$$

From to the Pauli principle each state can be occupied by at most one identical fermion. For nucleons we have protons and neutrons each of which can have spin up or down, so the state degeneracy is $g = 4$. To get the lowest energy state we would consider all states filled up to some radius:

$$n = \sqrt{(n_x^2 + n_y^2 + n_z^2)} = \frac{Lk}{\pi}. \tag{5.5}$$

The total number of states inside the radius n is equal to 1/8 of the volume of the sphere:

$$N = \left(\frac{g}{8}\right)\left(\frac{4}{3}\pi n^3\right) = \frac{gL^3k^3}{6\pi^2}, \tag{5.6}$$

and the number of states inside the ring dk is:

$$dN = \frac{gL^3k^2\,dk}{2\pi^2}. \tag{5.7}$$

The maximum value for the wave number is called k_f with the associated Fermi energy:

$$\epsilon_f = \frac{\hbar^2 k_f^2}{2m}. \tag{5.8}$$

The total number of states up to k_f is the number of nucleons A:

$$A = \int_0^{k_f} dN = \int_0^{k_f} \frac{gL^3 k^2\, dk}{2\pi^2} = \frac{gL^3 k_f^3}{6\pi^2}. \tag{5.9}$$

The total kinetic energy up to k_f:

$$< T >= \int_0^{k_f} \frac{\hbar^2 k^2}{2m} dN = \int_0^{k_f} \frac{\hbar^2 k^2}{2m} \frac{gL^3 k^2\, dk}{2\pi^2} = \left(\frac{1}{5}\right)\left(\frac{\hbar^2}{2m}\right)\frac{gL^3 k_f^5}{2\pi^2}. \tag{5.10}$$

With Eq. (5.9) for A and Eq. (5.8) for ϵ_f we have for the total kinetic energy:

$$< T >= \frac{3}{5} A \epsilon_f, \tag{5.11}$$

and for the average kinetic energy:

$$\frac{< T >}{A} = \frac{3}{5}\epsilon_f. \tag{5.12}$$

These results can be evaluated in terms of the density for symmetric nuclear matter with Eq. (5.6):

$$\rho_o = \frac{A}{L^3} = \frac{g}{6\pi^2} k_f^3, \tag{5.13}$$

with $\rho_o = 0.16$ nucleons/fm^3 to obtain:

$$k_f = \left(\frac{6\pi^2 \rho_o}{g}\right)^{1/3} = 1.33\,\mathrm{fm}^{-1}, \tag{5.14}$$

$$\epsilon_f = \frac{\hbar^2 k_f^2}{2m} = 36.7\,\mathrm{MeV}, \tag{5.15}$$

and for the average kinetic energy:

$$\frac{< T >}{A} = \frac{3}{5}\epsilon_f = 22.0\,\mathrm{MeV}. \tag{5.16}$$

For unequal numbers of protons and neutrons we take two overlapping Fermi gases in the same size box with densities for protos and neutrons given by

$$\rho_{op} = \frac{Z}{A}\rho_o, \tag{5.17}$$

and

$$\rho_{on} = \frac{N}{A}\rho_o, \tag{5.18}$$

With the spin degeneracy for one kind of nucleon of $g' = 2$ we obtain for protons

$$k_{fp} = \left(\frac{6\pi^2}{g'}\rho_{op}\right)^{1/3} = \left(\frac{6\pi^2}{g'}\frac{Z}{A}\rho_o\right)^{1/3} = \left(\frac{g}{g'}\frac{Z}{A}\right)^{1/3} k_f = \left(\frac{2Z}{A}\right)^{1/3} k_f, \tag{5.19}$$

$$\epsilon_{fp} = \frac{\hbar^2 k_{fp}^2}{2m} = \left(\frac{2Z}{A}\right)^{2/3} \epsilon_f, \tag{5.20}$$

and for the average kinetic energy:

$$\frac{< T >_p}{Z} = \frac{3}{5}\epsilon_{fp}. \tag{5.21}$$

Likewise for the neutrons:

$$k_{fn} = \left(\frac{2N}{A}\right)^{1/3} k_f, \tag{5.22}$$

$$\epsilon_{fn} = \left(\frac{2N}{A}\right)^{2/3} \epsilon_f, \tag{5.23}$$

and for the average energy:

$$\frac{< T >_n}{N} = \frac{3}{5}\epsilon_{fn}. \tag{5.24}$$

The total kinetic energy is thus given by

$$< T > = < T >_p + < T >_n = \frac{3}{5}\left[Z\left(\frac{2Z}{A}\right)^{2/3} + N\left(\frac{2N}{A}\right)^{2/3}\right]\epsilon_f. \tag{5.25}$$

The numerical values for ^{208}Pb with $Z = 82$ and $N = 126$ are $\epsilon_{fp} = 31.6$ MeV, $\epsilon_{fn} = 42.0$ MeV, $< T > = 4700$ MeV and $\frac{<T>}{A} = 22.8$ MeV. The average kinetic energy is larger than the value of 22.0 MeV obtained for $N = Z$ (Eq. (5.16)).

One can expand Eq. (5.25) to first order in $[\frac{(N-Z)}{A}]^2$ to obtain:

$$< T > = \frac{3}{5}A\epsilon_f + \frac{2}{5}\epsilon_f\frac{(N-Z)^2}{A} = 22\,A + 15\,\frac{(N-Z)^2}{A}\,\text{MeV}. \tag{5.26}$$

Comparing this with the total energy obtained empirically with the liquid drop model ($E = -BE$):

$$E = < T > + < V > = -16\,A + 23\,\frac{(N-Z)^2}{A}\,\text{MeV}, \tag{5.27}$$

we would deduce for the interaction energy:

$$< V > = -38\,A + 8\,\frac{(N-Z)^2}{A}\,\text{MeV}. \tag{5.28}$$

6 Overview of the nuclear shell model

Nuclei are made up of protons and neutrons (nucleons) held together by the strong interaction inside of a volume with a radius of a few Fermis (fm), (1 fm $=10^{-15}$m). One might expect that the motions of these nucleons in this closely packed system should be very complex because of the large number of frequent collisions. Niels Bohr made the analogy of the nucleus to a table of billiard balls [1] and said that an analogy with the motion of electrons in a one-body potential "loses any validity" for nucleons in the nucleus [2]. But the data on nuclear properties increased rapidly, see Table I, and by 1948 Maria G. Mayer was able to summarize the experimental data which indicated that nuclei with 20, 50, 82 or 126 neutrons or protons were particularly stable [3]. In 1949 the key role of the spin-orbit splitting in the one-body potential was proposed by Maria Goeppert Mayer [4] and Otto Haxel, J. Hans D. Jensen and Hans Suess [5]. This one-body potential model is the starting point for the nuclear shell model. A short history of Mayer's contributions is given in [6].

Table of Isotopes

Edition	Year	Authors	Pages
1st	1940	Livingood and Seaborg	17
2nd	1944	Seaborg	32
3rd	1948	Seaborg and Perlman	82
4th	1953	Hollander, Perlman and Seaborg	182
5th	1958	Strominger, Hollander and Seaborg	320
6th	1967	Lederer, Hollander and Perlman	556
7th	1978	Lederer et al.	1523
8th	1996	Firestone et al.	2877

In the shell model, the quantum mechanical problem for the motion of one nucleon in a nucleus is similar to that for the motion of an electron in the hydrogen atom, except that overall scale is determined by the size of the nucleus (10^{-15} m) rather than the size of the atom (10^{-10} m). Another important difference between the atomic and nuclear potentials is that the dependence of the potential on the relative orientation of the intrinsic nucleon (electron) spin and its orbital angular momentum is much stronger and opposite in sign for the nucleon compared to that for the electron.

The single-particle potential has eigenstates that are characterized by their single-particle energies and their quantum numbers. The properties of a nucleus with a given number of protons and neutrons are determined by the filling of the lowest energy single-particle levels allowed by the Pauli exclusion principle which must be obeyed in a system of identical Fermions (the nucleons in this case). The Pauli exclusion principle allows only one proton or neutron to occupy a state with a given

set of quantum numbers. The average nuclear potential arises from the short-ranged attractive nucleon-nucleon interaction and is determined by the shape of the nuclear density distribution.

Evidence for the validity of the nuclear shell model comes from the observation of shell effects in experimental observables such as binding energy, size, spin, and level density. In particular, the nuclear binding energy is not a smooth function of proton and neutron number, but exhibits small fluctuations. The deviation of the experimental binding energies from the liquid-drop model was shown in Sec. 1. The liquid-drop model binding energy is a smooth function of proton and neutron number. When the liquid-drop values for the binding energies are subtracted from the experimental values, the differences show peaks at the magic numbers: N_m=28, 50, 82 and 126. The peak indicates that the nuclei with these magic number are more tightly bound than average. Those nuclei that are magic with respect to both neutron and proton numbers are referred to as doubly-magic; an example is the nucleus ^{208}Pb with $N = 126$ and $Z = 82$. Although not so obvious from the binding energy data $N_m = 2$, 6, 8, 14, 16, 20 and 32 are also magic numbers for some nuclei. In addition $N_m = 34$ has recently been proposed as a magic number for ^{54}Ca [7]. The occurrence of magic numbers in nuclei is analogous to that observed for the properties of electrons in atoms. However, for electrons the magic numbers are 2, 10, 18, 54, and 86.

The calculated single-particle energy levels appropriate for the neutrons in ^{208}Pb are shown in Fig. (6.1). The potential arises from the average interaction of one neutron with the 207 other nucleons. Since the nuclear force is short-ranged, the shape of potential is similar to the nucleon density in ^{208}Pb which is experimentally known to be close to the Fermi- or Woods-Saxon shape of

$$V(r) = \frac{V_o}{[1 + \exp(r - R)/a]}, \tag{6.1}$$

where $R \approx 1.2A^{1/3}$ fm and $a \approx 0.60$ fm. The single-particle energy levels for a potential of approximately this shape and with a central depth of about $V_o = -50$ MeV are shown in the middle of Fig. (6.1). The number of neutrons that are allowed by the Pauli principle to occupy one of these levels, the occupation number, is given by the number in square brackets. In addition, each level is labeled by its cumulative occupation number (the total number of neutrons needed to fill up to the given level) and its $n\ell$ value. n is the radial quantum number (the number of times the radial wave function changes sign) and ℓ is the angular momentum quantum number represented in the spectroscopic notations s, p, d, f, g, h, i and j for ℓ=0, 1, 2, 3, 4, 5, 6 and 7, respectively. Each ℓ value can have 2ℓ+1 m states and each m state can contain a proton or neutron with spin up and spin down (s_z=$\pm$1/2). The occupation number given by the Pauli principle is thus $N_o = 2(2\ell + 1)$.

The Woods-Saxon results are compared to the levels of an harmonic oscillator

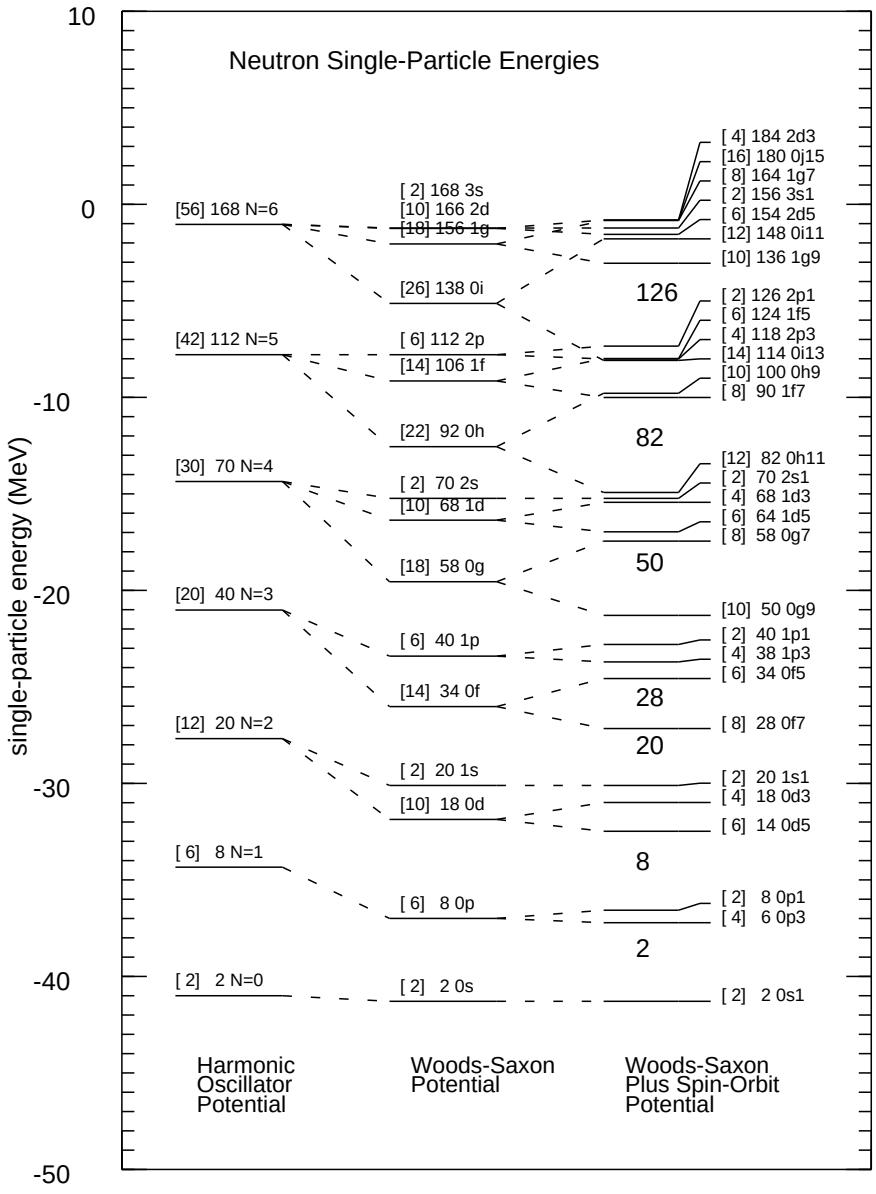

Figure 1: Neutron single-particle states in ^{208}Pb with three potential models, harmonic oscillator (left), Woods-Saxon without spin-orbit (middle) and Woods-Saxon with spin orbit (right). The numbers in square brackets are the maximum number of neutrons in that each level can contain, the following number is a running sum of the total. In addition the harmonic oscillator is labeled by the major quantum number $N = 2n + \ell$, the Woods Saxon is labeled by n, ℓ and the Woods-Saxon with spin-orbit is labeled by $n, \ell, 2j$.

potential on the left-hand side of Fig. (6.1). Note that the ℓ degeneracy present in the oscillator is broken in the Woods-Saxon potential with levels of larger ℓ coming lower in energy.

The relative spacing of the neutron and proton levels for all nuclei are qualitatively similar to those shown in Fig. (6.1). (The overall spacing between levels goes approximately as $A^{-1/3}$.) According to the Pauli principle, as neutrons are added to nuclei they go into the lowest energy level not already occupied. When a nucleon is added to a nucleus in which the neutron number is equal to one of the cumulative occupation numbers, the neutron must be placed into a relatively higher-energy (more loosely bound) state. Thus the nuclei with the highest relative binding energy are those for which the proton or neutron number is equal to one of the cumulative occupation numbers. A magic number occurs when there is a relatively large energy gap above one of the cumulative numbers. The magic numbers are thus related to the bunching of energy levels. The Woods-Saxon potential gives the correct magic numbers for $N_m = 2$, 8 and 20 but is incorrect for the higher values.

In 1949 Goeppert-Mayer and Haxel, Jensen and Suess postulated the existence of an additional strong spin-orbit potential that could account for the observed magic numbers. The spin-orbit potential has the form, $V_{so}(r)\vec{\ell}\cdot\vec{s}$, where $\vec{\ell}$ is the orbital angular momentum and $\vec{s}$ is the intrinsic spin angular momentum of the nucleon. With the spin-orbit potential, m and s_z are no longer good quantum numbers. The orbital and spin angular momentum must be coupled to a definite total angular momentum, $\vec{j} = \vec{\ell} + \vec{s}$. Eigenstates of the spin-orbit potential are determined by the total angular momentum quantum number $j = \ell \pm 1/2$ (except $j = 1/2$ for ℓ=0) and the quantum number m_j associated with the z component of j. The expectation value of $\vec{\ell}\cdot\vec{s}$ can be obtained from the operator

$$j^2 = (\vec{\ell} + \vec{s})^2 = \ell^2 + s^2 + 2\vec{\ell}\cdot\vec{s}. \tag{6.2}$$

Hence,

$$-\vec{\ell}\cdot\vec{s} \mid \psi_j > = -\frac{1}{2}(j^2 - \ell^2 - s^2) \mid \psi_j > = -\frac{1}{2}[j(j+1) - \ell(\ell+1) - s(s+1)] \mid \psi_j > \tag{6.3}$$

(the minus sign takes into account the observed sign of the $< V_{so}(r) >$) which gives

$$< \psi_{j=\ell+1/2} \mid -\vec{\ell}\cdot\vec{s} \mid \psi_{j=\ell+1/2} > = -\frac{\ell}{2} \tag{6.4}$$

and

$$< \psi_{j=\ell-1/2} \mid -\vec{\ell}\cdot\vec{s} \mid \psi_{j=\ell-1/2} > = +\frac{\ell+1}{2} \tag{6.5}$$

Each j has $2j+1$ m_j values and hence each j orbit can contain up $N_o = 2j+1$ protons or neutrons. The energy levels obtained when the spin-orbit potential is

added to the Woods-Saxon potential are shown on the right-hand side of Fig. (6.1). The dashed lines that connect to the middle of Fig. (6.1) indicate the effect of the spin-orbit potential in splitting the states of a given ℓ value. The overall strength of the spin-orbit potential has been determined empirically. Each level is labeled by the occupation number (in square brackets), the cumulative occupation number, and the values for $n, \ell, 2j$ ($2j$ is twice the angular momentum quantum number j). The values of the neutron number for which there are large gaps in the cumulative occupation number now reproduce all of the observed magic numbers (as emphasized by the numbers shown in the energy gaps on the right-hand side).

The average nuclear potential can be calculated microscopically from the nucleon-nucleon interaction by using Hartree-Fock theory together with the Breuckner theory for taking into account the repulsion at very short distances between the nucleons. The strength of the spin-orbit potential for nucleons is much larger and opposite in sign to spin-orbit potential for electrons atoms. The radial part of the spin-orbit potential, $V_{so}(r)$, is largest at the nuclear surface and is often taken to be proportional to the derivative of the Woods-Saxon form.

The essential physics behind the shell model is that the many-nucleon collisions that might be expected are greatly suppressed in the nuclear ground states and low-lying nuclear levels because the nucleons would be scattered into states which are forbidden by the Pauli principle. At higher excitation energy the number of allowed states becomes much greater and the nuclear properties indeed become complex and chaotic.

The shell model in its simplest form is able to successfully predict the properties of nuclei which are one nucleon removed or added to the one of the magic number. The shell model can also be extended to include the more complex configurations that arise for the nuclei with nucleon numbers that are in between the magic numbers. For many applications these complex configurations can be taken into account exactly by the diagonalization of a Hamiltonian matrix. In other cases approximations must be used; these include the use of a deformed intrinsic single-particle potential, and the use of group theory to classify the configurations. Current theoretical investigations using the shell model focus on these complex configurations.

References

[1] Niels Bohr, Science **86**, 161 (1937).

[2] Niels Bohr, Nature, February, 1936.

[3] Maria G. Mayer, Phys. Rev. **74**, 235 (1948).

[4] M. G. Mayer, Phys. Rev. **75**, 1969 (1949).

[5] O. Haxel, J. H. D. Jensen and H. E. Suess, Phys. Rev. **75**, 1766 (1949).

[6] K. E. Johnson, "Maria Goeppert Mayer: Atoms, molecules and nuclear shells", Physics Today **39**, 44 (1986).

[7] M. Honma, T. Otsuka, B. A. Brown and T. Mizusaki, Phys. Rev. C **65**, 061301 (2002).

7 The one-body potential

7.1 General properties

The Schroedinger equation for a particle of mass m in a spin-independent central potential, U_o, is

$$H_o \mid \alpha\rangle = (T + U_o) \mid \alpha\rangle = \epsilon_\alpha \mid \alpha\rangle, \tag{7.1}$$

where T is the kinetic energy operator given in coordinate space by

$$T = -\frac{\hbar^2}{2m}\nabla^2 = -\frac{\hbar^2}{2m}\left\{\frac{1}{r}\frac{d^2}{dr^2}r - \frac{\vec{\ell}^2}{r^2}\right\}, \tag{7.2}$$

the ket $\mid \alpha\rangle$ is the single-particle wave function, and ϵ_α is the eigenvalue. The coordinate space solution of this equation has the form

$$\phi_\alpha(\vec{r}) = \frac{R_\alpha(r)}{r}Y^\ell_{m_\ell}(\hat{r}), \tag{7.3}$$

where $Y^\ell_{m_\ell}$ are the spherical harmonics. The subscript α stands for the set of quantum numbers (n_r, ℓ, m_ℓ), with n_r being the radial quantum number. We will use the quantum numbers $n_r = 0, 1, 2, \ldots$ which indicate the number of times the radial wave functions crosses the r axis. (Some other books use the convention which starts at one, $n_r = 1, 2, 3, \ldots$). The spherical harmonics are eigenfunctions of the ℓ^2 and ℓ_z operators

$$\ell^2 Y^\ell_{m_\ell}(\hat{r}) = \ell(\ell+1)Y^\ell_{m_\ell}(\hat{r}), \tag{7.4}$$

and

$$\ell_z Y^\ell_{m_\ell}(\hat{r}) = m_\ell Y^\ell_{m_\ell}(\hat{r}), \tag{7.5}$$

and are orthonormal functions

$$\int Y^\ell_{m_\ell}(\hat{r})\, Y^{\ell'}_{m'_\ell}(\hat{r})\, d\Omega = \delta_{\ell\ell'}\delta_{m_\ell m'_\ell}. \tag{7.6}$$

The radial wave function $R_\alpha(r)$ is a solution of the one-dimensional radial equation

$$-\frac{\hbar^2}{2m}R''_\alpha(r) + \frac{\hbar^2}{2m}\frac{\ell(\ell+1)}{r^2}R_\alpha(r) + U_o(r)R_\alpha(r) = \epsilon_\alpha R_\alpha(r), \tag{7.7}$$

where $R''(r)$ indicates the second derivative of $R(r)$ with respect to r. The solution to Eq. (7.7) is independent of m_ℓ.

For a particle with an intrinsic spin, $\vec{s}$, the central potential may also contain a spin-orbit term of the form

$$U_{so}(r) = f_{so}(r)\,\vec{\ell}\cdot\vec{\sigma}, \tag{7.8}$$

where $\vec{\sigma} = 2\vec{s}$. The total angular momentum, $\vec{j} = \vec{\ell} + \vec{s}$, is conserved and the wave function takes the form

$$\phi_{k,m}(\vec{r}) = \frac{R_k(r)}{r}[Y^\ell \otimes \chi^s]^j_m, \tag{7.9}$$

where χ^s is the intrinsic-spin wave function, k stands for the set of quantum numbers (n_r, ℓ, s, j), and the cross symbol $\otimes$ denotes the Clebsch-Gordan product

$$[Y^\ell \otimes \chi^s]^j_m = \sum_{m_\ell, m_s} \langle \ell, m_\ell, s, m_s \mid j, m\rangle \, Y^\ell_{m_\ell}(\hat{r}) \, \chi^s_{m_s}. \tag{7.10}$$

This equation defines the ordering and phase convention associated with spin-orbit coupling used in this book. The intrinsic-spin wave functions are also assumed to be orthonormal

$$\langle \chi^s_{m_s} \mid \chi^{s'}_{m'_s} \rangle = \delta_{ss'}\delta_{m_s m'_s}. \tag{7.11}$$

The operation of $\vec{\ell}\cdot\vec{\sigma}$ on $\phi_{k,m}(\vec{r})$ gives

$$(\vec{\ell}\cdot\vec{\sigma})\phi_{k,m}(\vec{r}) = [j(j+1) - \ell(\ell+1) - s(s+1)]\,\phi_{k,m}(\vec{r}) = a_{so}\phi_{k,m}(\vec{r}). \tag{7.12}$$

Taking $s = \frac{1}{2}$ and $j = \ell \pm \frac{1}{2}$,

$$a_{so} = -(\ell+1) \text{ for } j = \ell - \frac{1}{2},$$

and

$$a_{so} = \ell \text{ for } j = \ell + \frac{1}{2}.$$

Thus $R_k(r)$ satisfies the equation

$$-\frac{\hbar^2}{2m}R''_k(r) + \frac{\hbar^2}{2m}\frac{\ell(\ell+1)}{r^2}R_k(r) + [U_o(r) + a_{so}f_{so}(r)]R_k(r) = \epsilon_k R_k(r). \tag{7.13}$$

Eq. (7.13) has discrete solutions for bound states with $\epsilon < 0$ as well as continuum solutions for $\epsilon > 0$. The normalization convention for bound states is

$$\int \mid \phi_{k,m}(\vec{r}) \mid^2 \, d\tau = \sum_{\substack{m_\ell, m_s \\ m'_\ell, m'_s}} \langle \ell, m_\ell, s, m_s \mid j, m\rangle\langle \ell, m'_\ell, s, m'_s \mid j, m\rangle$$

$$\times \int \mid R_k(r) \mid^2 dr \int Y^\ell_{m_\ell}(\hat{r})Y^\ell_{m'_\ell}(\hat{r}) \, d\Omega \, \langle \chi^s_{m_s} \mid \chi^s_{m'_s}\rangle. \tag{7.14}$$

The spherical harmonics and intrinsic-spin wave functions are orthonormal and thus

$$\int \mid \phi_{k,m}(\vec{r}) \mid^2 \, d\tau = \int \mid R_k(r) \mid^2 dr = 1. \tag{7.15}$$

Eq. (7.15) defines the normalization of the radial wave functions. In addition, the radial wave functions will be chosen to be real and positive at the origin. Observables are, of course, independent of this phase convention, however, it is important to keep the phase convention consistent throughout intermediate steps of a calculations which involve $R(r)$ or matrix elements of $R(r)$. The quantity $\mid R_k(r)/r|^2$ is the radial profile function – the density observed for a thin slice at $z = 0$ in the xy plane. The quantity $P(r) = \mid R_k(r) \mid^2$ is the radial probability distribution – the probability of finding the particle at a distance r from the origin. The $\ell = 0$ states are the only ones with a nonvanishing radial-profile at the origin.

There are a variety of numerical methods [1] for solving the radial differential equation for the eigenvalues and the eigenfunctions. As a function of increasing n_r for a fixed ℓ-value, the excitation energy relative to the ground state (gs) $\epsilon_\alpha - \epsilon_{\rm gs}$ usually increases and the root-mean-square radius of the radial probability distribution increases. Other properties will depend upon the details of the potential. For example, the Coulomb potential with $U_o(r) = 1/r$ has energies proportional to $-1/n_p^2$, where $n_p = n_r + \ell + 1$ is the "principal" quantum number. In the following subsections, some results for the harmonic-oscillator and Woods-Saxon forms for the central potential, which are commonly used in nuclear physics, are presented.

7.2 The harmonic-oscillator potential

A very useful form for $U_o(r)$ used in nuclear physics is the harmonic-oscillator (HO) potential given by

$$U_o^{\rm HO}(r) = \frac{1}{2} m\omega^2 r^2, \tag{7.16}$$

where m is the nucleon mass and ω is a parameter. This potential has nice analytical properties, the most important of which is that the many-body HO Hamiltonian can be exactly separated into a sum of intrinsic and center-of-mass terms. This will be discussed in the next section. The single-particle energy levels are given by

$$\epsilon_\alpha = (N + 3/2)\hbar\omega, \tag{7.17}$$

where N is the major-shell HO quantum number given by

$$N = 2n_r + \ell. \tag{7.18}$$

The radial wave functions are given by

$$R_\alpha(r) = \sqrt{\frac{2^{\ell - n_r + 2}\,(2\ell + 2n_r + 1)!}{\sqrt{\pi}\;(n_r)!\,b^{2\ell+3}\,[(2\ell+1)!!]^2}}\; r^{\ell+1} e^{-r^2/2b^2}$$

$$\times \sum_{k=0}^{n_r} \frac{(-1)^k\, 2^k (n_r)!\, (2\ell+1)!!}{k!\, (n_r-k)!\, (2\ell+2k+1)!!}\, (r/b)^{2k}, \tag{7.19}$$

where

$$b = \sqrt{\frac{\hbar}{m\omega}}, \tag{7.20}$$

is the HO length parameter. Taking $\hbar c = 197$ MeV-fm and $mc^2 = 938$ MeV

$$b^2 = \frac{(\hbar c)^2}{(mc^2)(\hbar\omega)} = \frac{41.4\,\mathrm{MeV\,fm}^2}{\hbar\omega}. \tag{7.21}$$

The diagonal matrix element of r^2 can be obtained by using the virial theorem for the HO potential,

$$\langle \phi_\alpha \mid U_o^{\mathrm{HO}} \mid \phi_\alpha \rangle = \frac{1}{2} m\omega^2 \langle \phi_\alpha | r^2 \mid \phi_\alpha \rangle = \langle \phi_\alpha \mid T \mid \phi_\alpha \rangle,$$

together with

$$\langle \phi_\alpha \mid U_o^{\mathrm{HO}} \mid \phi_\alpha \rangle + \langle \phi_\alpha \mid T \mid \phi_\alpha \rangle = (N + 3/2)\hbar\omega$$

to give

$$\langle \phi_\alpha | r^2 \mid \phi_\alpha \rangle = \langle N | r^2 \mid N \rangle = (N + 3/2)\, b^2. \tag{7.22}$$

and

$$\langle \phi_\alpha \mid T \mid \phi_\alpha \rangle = \frac{\hbar\omega}{2}(N + 3/2) \tag{7.23}$$

An analytic expression for the general matrix elements of r^λ can be found in [2] and [3], and Fortran programs are given in [2] and [4].

The maximum number of spin $\frac{1}{2}$ fermions which can occupy a given N value is given by

$$D_N = (N+1)(N+2). \tag{7.24}$$

The total number of states which can be occupied up to $N_{\max}$ is given by

$$\sum_{N=0}^{N=N_{\max}} D_N = \frac{1}{3}(N_{\max}+1)(N_{\max}+2)(N_{\max}+3). \tag{7.25}$$

The harmonic oscillator parameter ω is conventionally chosen to reproduce the observed mean-square charge radius. This is related to the mean-square radius for protons given nucleus whose harmonic oscillator levels are filled up to $N_{\max}$

$$\langle r^2 \rangle_p = \frac{\displaystyle\sum_{N=0}^{N=N_{\max}} D_N \langle N | r^2 \mid N \rangle}{\displaystyle\sum_{N=0}^{N=N_{\max}} D_N} = \frac{3}{4}(N_{\max}+2) b^2. \tag{7.26}$$

A common way of choosing the appropriate value of $\hbar\omega$ is to compare Eq. (7.26) to the observed proton mean-square radius as obtained from measured charge mean-square radius by

$$\langle r^2\rangle_p = \langle r^2\rangle_{ch} - \langle r^2\rangle_o. \tag{7.27}$$

where $\langle r^2\rangle_o = 0.77$ fm^2 is the mean-square charge radius of the proton. For example, for the nucleus ^{16}O, where the eight protons fill the $N = 0$ and $N = 1$ major shells, $N_{\max} = 1$ and $\langle r^2\rangle_p(^{16}\mathrm{O}) = (9/4)b^2$. The experimental root-mean-square (rms) charge radius for ^{16}O is [5] $\sqrt{\langle r^2\rangle_{ch}}$= 2.71 fm, and hence $\langle r^2\rangle_p = 6.57$ fm^2, $b^2 = 2.92$ fm^2 and $\hbar\omega = 14.2$ MeV for the point protons. Since there are equal numbers of neutrons and protons in ^{16}O and since they should have about the same rms radii, it is a good approximation to use the same oscillator parameter for the neutrons as was obtained for protons.

For heavy nuclei, one can use the large $N_{\max}$ approximation for the sum in Eq. (7.25), $Z \approx (N_{\max} + 2)^3/3$, to obtain from (7.26)

$$\langle r^2\rangle_p \approx \frac{3}{4}(3Z)^{1/3}b^2. \tag{7.28}$$

For example, for ^{208}Pb (Z=82) the experimental rms charge radius is [5] 5.50 fm, giving $\langle r^2\rangle_p = 29.4$ fm^2, $b^2 = 6.27$ fm^2 and $\hbar\omega_p = 6.6$ MeV for the point protons. It is observed experimentally that the proton and neutron rms radii in ^{208}Pb are about equal [6]: $\langle r^2\rangle_n \approx \langle \mathrm{r}^2\rangle_p$. The oscillator parameter for neutrons in ^{208}Pb, obtained by using an rms radius of 5.5 fm and Eq. (7.28) with N in place of Z, is $\hbar\omega_n = 7.6$ MeV.

Along the valley of stability the rms proton radii are approximately given by $1.08A^{1/3}$. Rewriting Eq. (7.28) in terms of $A \approx 2.5Z$, one obtains for heavy nuclei $\hbar\omega_p \approx 39A^{-1/3}$ MeV. A better smooth approximation for the proton oscillator parameter in both light and heavy nuclei is [7]

$$\hbar\omega_p \approx 45A^{-1/3} - 25A^{-2/3}. \tag{7.29}$$

7.3 Separation of intrinsic and center-of-mass motion

7.3.1 The kinetic energy

The many-body nuclear Hamiltonian for A nucleons with two-body interactions has the form

$$H = \frac{1}{2m}\sum_i^A p_i^2 + \sum_{i<j}^A V(|\,\vec{r}_i - \vec{r}_j\,|). \tag{7.30}$$

The coordinates refer to a fixed point in space. For the internal structure of a given nucleus we are not interested in the center-of-mass motion, and we would like to rewrite the Hamiltonian as a sum of an intrinsic part H_{int} and a center-of-mass part H_{cm}

$$H = H_{int} + H_{cm}. \tag{7.31}$$

The center-of-mass Hamiltonian depends only on the center-of-mass position $\vec{R}$ and momentum $\vec{Q}$:

$$\vec{R} = \frac{1}{A}\sum_{i}^{A} \vec{r}_i, \tag{7.32}$$

and

$$\vec{Q} = \sum_{i}^{A} \vec{p}_i. \tag{7.33}$$

The intrinsic Hamiltonian depends upon the coordinates relative to the the center-of-mass:

$$\vec{\rho}_i = \vec{r}_i - \vec{R}, \tag{7.34}$$

and

$$\vec{q}_i = \vec{p}_i - \frac{1}{A}\vec{Q}. \tag{7.35}$$

The two-body interaction is explicitly a function of the center-of-mass coordinates $\vec{\rho}_i - \vec{\rho}_j = \vec{r}_i - \vec{r}_j$. The kinetic energy part of H can be rewritten as

$$T = T_{int} + T_{cm}, \tag{7.36}$$

where

$$T_{int} = \frac{1}{2m}\sum_{i}^{A} q_i^2 = \frac{2}{Am}\sum_{i<j}^{A} (\vec{p}_{ij})^2, \tag{7.37}$$

and

$$T_{cm} = \frac{1}{2mA}Q^2, \tag{7.38}$$

where $\vec{p}_{ij}$ = ($\vec{p}_i$-$\vec{p}_j$)/2. Thus H separates into

$$H = H_{int} + H_{cm},$$

with

$$H_{int} = \frac{1}{2m}\sum_{i}^{A} q_i^2 + \sum_{i<j}^{A} V(\mid \vec{\rho}_i - \vec{\rho}_j \mid) \tag{7.39}$$

and

$$H_{cm} = T_{cm} = \frac{1}{2mA}Q^2. \tag{7.40}$$

The solution to

$$H\Psi = (H_{int} + H_{cm})\Psi = E\Psi \tag{7.41}$$

has the form

$$\Psi = \Psi_{int}\,\Psi_{cm}, \tag{7.42}$$

with

$$H_{int}\Psi_{int} = E_{int}\Psi_{int}, \tag{7.43}$$

$$H_{cm}\Psi_{cm} = E_{cm}\Psi_{cm}, \tag{7.44}$$

and

$$E = E_{int} + E_{cm}. \tag{7.45}$$

The coordinates $\vec{\rho}_i$ are not independent and therefore the equation for the intrinsic Hamiltonian Eq. (7.43) is in general more difficult to solve than that for the full Hamiltonian Eq. (7.41). Thus, one usually solves the full problem constrained is a way which guarantees that the center-of-mass is in a known state, such as a plane wave or the ground state of a harmonic oscillator. The intrinsic wave function is then obtained by dividing Ψ by Ψ_{cm} and the intrinsic energy is obtained by subtracting E_{cm} from E.

7.3.2 The harmonic-oscillator

In the nuclear many-body problem one divides the hamiltonian into a mean-field (single-particle) potential U plus a residual interaction W:

$$H' = \frac{1}{2m}\sum_i^A p_i^2 + \sum_i^A U(r_i) + \sum_{i<j}^A W(\mid \vec{r}_i - \vec{r}_j \mid). \tag{7.46}$$

In general $U(r_i)$ does not easily separate into an intrinsic and center-of-mass part. However, in the special case of the harmonic-oscillator potential the separation can be made analytically:

$$\sum_i^A U^{HO}(r_i) = \frac{1}{2}m\omega^2\sum_i^A r_i^2 = \frac{1}{2}m\omega^2\sum_i^A \rho_i^2 + \frac{1}{2}A\omega^2 mR^2. \tag{7.47}$$

Thus H' separates into

$$H' = H'_{int} + H'_{cm}, \tag{7.48}$$

with

$$H'_{int} = \frac{1}{2m}\sum_i^A q_i^2 + \frac{1}{2}M\omega^2\sum_i^A \rho_i^2 + \sum_{i<j}^A W(\mid \vec{\rho}_i - \vec{\rho}_j \mid) \tag{7.49}$$

and

$$H'_{cm} = \frac{1}{2mA}Q^2 + \frac{1}{2}Am\omega^2 R^2, \tag{7.50}$$

Thus, if one solves Eq. (7.46) such a way that the center-of-mass is guaranteed to be in a $0s$ oscillator state, the intrinsic wave function and energy can be obtained.

When the single-particle levels of the oscillator potential are filled in their lowest energy state the center of mass must also be in its lowest energy energy state of $0s$ for the nucleus with mass Am in the potential $\frac{1}{2}Am\omega^2R^2$, with a center of mass energy of

$$\langle \Psi \mid H'_{cm} \mid \Psi \rangle = \frac{3}{2}\hbar\omega, \tag{7.51}$$

Many-body states for which the center-of-mass is in the $0s$ ground state are referred to as nonspurious states.

Excitations of nucleons across across major shells or from a filled major shell to partially filled major shells are characterized by a single-particle energy change $\Delta E_{sp} = \Delta N\hbar\omega$, where

$$H_{sp} = \frac{1}{2m}\sum_i^A p_i^2 + \sum_i^A U^{HO}(r_i). \tag{7.52}$$

This energy change may occur all in the intrinsic motion, all in the center-of-mass motion, or partly in each.

Spurious states are formed when the center-of-mass is excited from its $0s$ ground state into its excited states. These states can be explicitly constructed by operating with $\vec{R}$ on one of the nonspurious states in which the center-of-mass is in the $0s$ ground state. The complete set of spurious states can be obtained from the angular momentum coupling of all such spurious states with all of the nonspurious states. For example, if one starts with the ^{16}O ground state, the $1\hbar\omega$ excitations lead to negative parity states. One of these states with $J^\pi{=}1^-$ (and T=0) is spurious.

For the special situations where the excited configuration cannot be connected to the original nonspurious configuration by the $(\vec{R})^n$ operator, these states are also nonspurious. The pure $0p_{1/2}$ to $0d_{5/2}$ excitation, for example, is completely nonspurious. There are also special SU(3) configurations which are nonspurious [8].

In order to carry out the transformation of Ψ into Ψ_{int} and Ψ_{cm} one must be sure that the basis states Ψ are complete with respect to all center-of-mass modes of a given ΔE_{sp}. The center-of-mass wave functions can then be explicitly constructed within the Ψ basis and projected out. Alternatively one can add a fictitious Hamiltonian which acts only on the center-of-mass:

$$H''_{cm} = \beta\left\{\frac{Q^2}{2Am} + \frac{1}{2}Am\omega^2R^2 - \frac{3}{2}\hbar\omega\right\}. \tag{7.53}$$

The center-of-mass for the full Hamiltonian $H + H''_{cm}$ will be in the $0s$ ground state if the constant β is made large enough so that the excitation energies of the center-of-mass are larger than all of the intrinsic excitation energies of interest. Subtraction of the constant $\frac{3}{2}\hbar\omega$ means that $E''_{cm} = 0$ when the center-of-mass is in the 0s ground state. Thus, the Hamiltonian

$$H' + H''_{cm} \tag{7.54}$$

with H' given by Eq. (7.46) and H''_{cm} given by Eq. (7.53) can be used to solve the nuclear many-body problem in terms of the fixed space coordinates $\vec{r}_i$. This is the method employed by the OXBASH shell-mode code [4] If one is starting with the original Hamiltonian of Eq. (7.30), one can construct a Hamiltonian which generates nonspurious states and is also corrected for the kinetic energy of the center-of-mass by

$$H - H_{cm} + H''_{cm}, \tag{7.55}$$

where H_{cm} is given by Eq. (7.40).

References

[1] J. R. Cash, A. D. Raptis and T. E. Simos, Jour. of Comput. Phys. 91, 413 (1990).

[2] K. L. G. Heyde, *The Nuclear Shell Model*, (Springer-Verlag, 1994)

[3] R. D. Lawson, *Theory of the Nuclear Shell Model*, (Clarendon Press, 1980).

[4] B. A. Brown, et al., the computer code OXBASH.

[5] B. A. Brown, C. R. Bronk and P. E. Hodgson, J. Phys. G10, 1683 (1984) and references therin.

[6] B. A. Brown, S. E. Massen, J. I. Escudero, P. E. Hodgson, G. Madurga and J. Vinas, J. Phys. G9, 423 (1983).

[7] J. Blomqvist and A. Molinari, Nucl. Phys. A106, 545 (1968).

[8] J. Millener et al., private communication.

8 The Woods-Saxon potential

8.1 General form

The Woods-Saxon potential is a convenient phenomenological choice for the one-body potential. It provides a model for the properties of bound-state and continuum single-particle wavefunctions. The Woods-Saxon potential (or any other one-body potential) cannot be used for the total binding energy since it is not based upon a specific two-body interaction. The parameters of the Woods-Saxon are chosen for a best fit of nuclear single-particle energies and nuclear radii. The Woods-Saxon potential is based upon the sum of a spin-independent central potential, a spin-orbit potential, and the Coulomb potential:

$$V(r) = V_o(r) + V_{so}(r)\ \vec{\ell}\cdot\vec{s} + V_c(r), \tag{8.1}$$

where $V_o(r)$ is the spin-independent central potential:

$$V_o(r) = V_o\ f_o(r), \tag{8.2}$$

with a fermi shape

$$f_o(r) = \frac{1}{1+[\exp(r-R_o)/a_o]}, \tag{8.3}$$

$V_{so}(r)$ is the spin-orbit potential:

$$V_{so}(r) = V_{so}\frac{1}{r}\frac{df_{so}(r)}{dr}, \tag{8.4}$$

with

$$f_{so}(r) = \frac{1}{1+[\exp(r-R_{so})/a_{so}]}, \tag{8.5}$$

and $V_c(r)$ is the Coulomb potential for protons based upon the Coulomb potential for a sphere of radius R_c:

$$V_c(r) = \frac{Ze^2}{r} \ \text{ for } \ r \geq R_c$$

and

$$V_c(r) = \frac{Ze^2}{R_c}\left[\frac{3}{2} - \frac{r^2}{2R_c^2}\right] \ \text{ for } \ r \leq R_c. \tag{8.6}$$

The radii R_o, R_{so} and R_c are usually expressed as:

$$R_i = r_i A^{1/3}. \tag{8.7}$$

For nuclei with a neutron excess the protons will feel a stronger potential than the neutrons, since the average proton-neutron potential is stronger than the average neutron-neutron (or proton-proton) potential. Thus we take:

$$V_{op} = V_0 + \frac{(N-Z)}{A} V_1 \text{ for protons} \tag{8.8}$$

and

$$V_{on} = V_0 - \frac{(N-Z)}{A} V_1 \text{ for neutrons} \tag{8.9}$$

In principle, r_o and a_o could also be a little difference for proton and neutrons in a nucleus with $N \neq Z$. Thus the spin-indepedent potential could have six parameters (and even more is any of them are allowed to take some additional mass dependence). The values of these parameters are chosen to give an overall accounting of the observed single-particle energies, the rms charge radii, and the electron scattering form factors.

The form of the spin-orbit interaction was originally taken from the form of the spin-orbit interaction used for electrons in atoms which was derived from the Dirac theory by Thomas and Frenkel [1]. For nuclear physics the spin-orbit interaction ultimately comes from the nucleon-nucleon interaction, but there is still some debate over whether or not relativistic effects are very important. The spin-orbit interaction for nucleons in the nucleus has the opposite sign and is much larger than for electrons in the atom. In the nuclear interior a nucleon sees an equal number of spin-up and spin-down nucleons on both sides and the spin-orbit interaction must vanish. Thus, the spin-orbit potential is peaked at the nuclear surface as in Eq. (8.4), and the particular form of this equation gives a good overall description of the ℓ and mass dependence observed experimentally. In analogy to the spin-independent potential, one could introduce up to six parameters for the spin-orbit interaction. The strength of the spin-orbit interaction is chosen to reproduce spin-orbit splittings (especially for large ℓ). For $N \neq Z$ the strength V_{so} could be different for protons and neutrons, but it practice they are nearly the same. For the geometry one usually takes $r_{so} = r_o$ and $a_{so} = a_o$. Thus, the introduction of one parameter in the spin-orbit interaction V_{so} gives a good overall accounting of the data.

A typical set of parameters for the Woods-Saxon potential is $V_0 = -53$ MeV, $V_1 = -30$ MeV and $V_{so} = 22$ MeV for the strengths, and $r_o = r_{so} = 1.25$ fm and $a_o = a_{so} = 0.65$ fm for the geometry. For the Coulomb term the radius is a little smaller with $r_c = 1.20$ fm. One can find in the literature many other sets of parameters which are better for specific nuclei or mass regions.

The figure on the next page from page 239 of Bohr and Mottelson Vol I [2] shows the neutron single-particle energies for nuclei near the valley of stability obtained with a set of Woods-Saxon parameters similar to those given above (note that the radial quantum numbers in this figure start with one rather than with our convention of zero). One observed that as A increases more single-particle states become bound so that the energy of the most loosely bound filled orbit is aways around -8 MeV.

Figure from BM

8.2 Computer program for the Woods-Saxon potential

The program WSPOT.FOR can be used to obtain the single-particle energies and single-particle radial wavefunctions for the bound states of the Woods-Saxon potential with quantum numbers n_r, ℓ and j. (It could also be used for other potentials if the program is modified.) If can also be used to calculate the nucleon scattering cross sections for a given ℓ and j. values. The program is initialized with a typical set of Woods-Saxon parameters:

$V_0 = -53$ MeV,
$V_1 = -30$ MeV,
$V_{so} = 22$ MeV,
$r_o = r_{so} = 1.25$ fm,
$a_o = a_{so} = 0.65$ fm and
$r_c = 1.20$ fm.

Some parameters can be modified in the input files. Other parameters can be changed internally to the program and then program can be recompiled.

The inputs are given in the x.dai files. Run the pot.bat file by typing

pot x

This will leaves the output in the file x.dao. The pot.bat does the following:

```
del x.dai
copy x.dai pot.dai
wspot
rename pot.dao x.dao
del pot.dai
```

In the following I provide some sample inputs for calculating nucleon bound state and scattering cross sections Some output is given in the screen and a more detailed output is given in the file x.dao.

8.2.1 Example for bound states

To obtain the bound states for neutrons in ^{40}Ca the input is:

```
40 20 1 0
0. 0. 0. 0.
0 0 1 0. 0. 0.
0 1 3 0. 0. 0.
0 1 1 0. 0. 0.
1 0 1 0. 0. 0.
0 2 5 0. 0. 0.
0 2 3 0. 0. 0.
0 0 0 0. 0. 0.
```

The first line is (A, Z) of the nucleus and (a, z) of the nucleon. So a proton would be $(a, z) = (1,1)$. After the blank line the next lines are a list of $n_r, \ell, 2j$ with a 0 in the last line. The output will give

n$_r$, ℓ, 2j, spe, k, kt, rms, rmst

for each orbit, where spe is the single-particle energy, k is the expectation value of the kinetic energy $< T >$, and rms is $\sqrt{< r^2 >}$. The program will indicate if the orbit is unbound. Kt means

$$\sum_i (2j_i + 1) < T >_i$$

where the sum runs over all orbits up to the current one, with the assumption that there are $(2j_i + 1)$ nucleons in orbit j_i. At the end this will tell you the total kinetic energy for neutrons (if the complete set is included in the input). Rmst is obtained from:

$$x_1 = \sum_i (2j_i + 1) < r^2 >_i$$

$$x_2 = \sum_i (2j_i + 1)$$

where the sum runs over all orbits up to the current one. Rmst $= \sqrt{(x_1/x_2)}$ is the total rms radius for all orbits up to the current one.

8.2.2 Changing the potential parameters

In order to change the parameters of the central spin-independent potential the input can be modified to be:

```
40 20 1 0
0. 0. 0. 0.
0 0 1 0.9 0.7 1.3
0 1 3 0. 0. 0.
0 1 1 0. 0. 0.
1 0 1 0. 0. 0.
0 2 5 0. 0. 0.
0 2 3 0. 0. 0.
0 0 0 0. 0. 0.
```

where $V_N = 0.9$ modifies the central potential strength to $V_o' = V_N V_o$, and a_o and r_o are changed to $a_o' = 0.7$ and $r_o' = 1.3$. These value are used for this and all following orbits. Other parameters can be changed by modifying the program.

8.2.3 Width of an unbound state resonance

For a given ℓ-j value the program calculates the phase shift $\delta(E)$ and the scattering cross section $\sigma(E)$ as a function of (positive) energy, where

$$\sigma(E) = \frac{4\pi(2\ell+1)}{k^2}[\sin(\delta)]^2$$

where $E = \hbar^2 k^2/2m$ (m is the mass of the nucleon).

As an example, the input for the $0d_{5/2}$ proton resonance in ^{13}N.

```
12 6 1 1
0.1 10.0 0. 0.
0 2 5 0. 0. 0.
0 0 0 0. 0. 0.
```

The first line is (A, Z) of the "core" nucleus and (a, z) of the nucleon. The next line contains emin, emax for the energy interval over which to look for a resonance. The next line contains $n_r, \ell, 2j$, and this is followed by 0 which stops program.

If a resonance peak is found in that interval, the program iterates over a series of steps in which this energy interval is narrowed down until the full resonance curve is found. It outputs EI and G where EI is the resonance energy peak and G=Γ is the full width at half maximum of the resonance. This particular input gives EI=0.99 MeV and Γ=0.010 MeV. The output for the cross section vs E is given in the output file POT.DAO.

For the scattering n_r is not a quantum number and the value in the input has no effect on the output. The value given on the detailed output in POT.DAO indicates how often the wavefunction crosses zero. Usually the resonance is a quasi-bound state corresponding to a particular the n_r value of interest. One should check in the output that the correct n_r value is given. If not, the correct value may correspond to a different energy range (or to a difference value for V_N discussed in the next section).

A resonance width is useful is the resonance is reasonably sharp. Broad resonances will be asymmetry and the width itself is not a full measure of its nature. Rather one must look at the full function of σ vs E. The program is probably not accurate below about 0.1 MeV which is emin in the above input. Also narrow resonances (if they exist) are at an energy below the Coulomb plus centrifugal barrier. For these light nuclei this is not more than 10 MeV which is what determines emax in the input.

8.2.4 Width of an unbound state resonance at a fixed energy

Experimentally one observes a $5/2^+$ resonance at 3.547 MeV in ^{13}N with a one-proton resonance energy of 1.60 MeV (the neutron separation energy is -1.60 MeV). This is below the energy (0.99 MeV) obtained from the standard potential. We could ask – if the potential is slightly adjusted so that the resonance is exactly at 1.60 MeV then what is the width? We need to slightly reduce the potential in order to increase the resonance energy. We could so this by hand, for example:

```
12 6 1 1
0.1 6.0 0. 0.
0 2 5 0.96 0. 0.
0 0 0 0. 0. 0.
```

where the potential depth has been multiplied by 0.96 gives the resonance energy at 1.69 MeV (closer but not exactly the required value). We would then change V_N by trial and error until the resonance is at the correct position. However, the program will automatically search for the correct V_N by the following input:

```
12 6 1 1
1.60 1.60 0.8 1.2
0 2 5 0. 0. 0.
1. 2. 0. 0.
0 2 5 0. 0. 0.
0. 0. 0. 0.
```

The input 1.60,1.60,0.8,1.2 will search on V_N over the interval 0.8 to 1.2 to put the $0d_{5/2}$ resonance at exactly 1.6 MeV. Then the input 1.0,2.0 will search over the energy interval 1.0 to 2.0 MeV with the new value of V_N to find the width of the resonance at 1.6 MeV. The result is 64 keV which is not far from the observed width of 47(7) keV.

References

[1] Thomas, Nature **107**, 514 (1926); Frenkel, Zeits. fur Phys. **37**, 243 (1926).

[2] A. Bohr and B. R. Mottelson, *Nuclear Structure*, Vol. I, (W. A. Benjamin, 1969), *Nuclear Structure* Vol. II, (W. A. Benjamin, 1975).

9 The general many-body problem for fermions

The Schroedinger equation for a system of n particles each of mass m in a central potential, U_k, which interact via a two-body potential, V_{kl}, is

$$H \mid \Psi > = E \mid \Psi >, \tag{9.1}$$

with

$$H = \left\{ \sum_{k=1}^{n} (T_k + U_k) \right\} + \left\{ \sum_{k<l}^{n} V_{kl} \right\} \equiv H^{(0)} + W, \tag{9.2}$$

where T_k is the kinetic energy operator, $-(\hbar^2/2m)\nabla_k^2$, and Ψ is the n-particle wave function represented in coordinate space by $\Psi(\vec{r}_1 \ldots \vec{r}_n)$. In applications to atomic physics, U_k is the Coulomb potential between the nucleus and the electrons. In applications to nuclear physics one takes $U_k = 0$. The coordinate space forms of U_k and V_{kl} will be denoted by $U(r_k)$ and $V(\vec{r}_k \vec{r}_l)$, respectively

The standard technique for solving this equation involves first solving the simple problem

$$H^{(0)} \mid \Phi_a > = E_a^{(0)} \mid \Phi_a >, \tag{9.3}$$

which has the solution

$$\mid \Phi_a > = \prod_{k=1}^{n} \mid \alpha_k > = \phi_{\alpha_1}(\vec{r}_1)\ \phi_{\alpha_2}(\vec{r}_2)\ \phi_{\alpha_3}(\vec{r}_3) \ldots \phi_{\alpha_n}(\vec{r}_n), \tag{9.4}$$

with

$$E_a^{(0)} = \sum_{k=1}^{n} \epsilon_{\alpha_k}. \tag{9.5}$$

The $\mid \alpha >$ are solutions of the single-particle equation

$$(T + U) \mid \alpha > = \epsilon_\alpha \mid \alpha >, \tag{9.6}$$

and label a represents one particular choice for the set of quantum numbers α_k. There are infinitly many different sets a which can be ordered by their total energy $E_a^{(0)}$.

The states ϕ_α are assumed to form a complete orthonormal single-particle basis:

$$< \alpha_k \mid \alpha_l > = \delta_{kl}$$

The states Φ are assumed to form a complete orthonormal basis for the solution of Eq. (9.1). In a spherical basis α would represent the set of quantum numbers (n_r, ℓ, m_ℓ). If the spin coupling is included the quantum numbers would be (n_r, ℓ, j, m_j).

The full exact many-particle problem can then be reformulated in terms of the Φ basis by expanding Ψ over the basis,

$$\mid \Psi >= \sum_a c_a \mid \Phi_a >, \tag{9.7}$$

and then solving the matrix equation

$$\sum_a < \Phi_b \mid H \mid \Phi_a > c_a = E c_b. \tag{9.8}$$

Alternatively, solutions can be obtained with perturbation theory. Nondegenerate Rayleigh-Schroedinger perturbation theory gives

$$E_a = E_a^{(0)} + E_a^{(1)} + E_a^{(2)} \ldots \tag{9.9}$$

and

$$\mid \Psi_a >= \mid \Psi_a^{(0)} > + \mid \Psi_a^{(1)} > \ldots, \tag{9.10}$$

where

$$E_a^{(0)} = < \Phi_a \mid H^{(0)} \mid \Phi_a >, \tag{9.11}$$

$$E_a^{(1)} = < \Phi_a \mid W \mid \Phi_a >, \tag{9.12}$$

$$E_a^{(2)} = \sum_{b \neq a} \frac{< \Phi_a \mid W \mid \Phi_b >< \Phi_b \mid W \mid \Phi_a >}{E_a^{(0)} - E_b^{(0)}}, \tag{9.13}$$

and

$$\mid \Psi_a^{(0)} >= \mid \Phi_a >, \tag{9.14}$$

$$\mid \Psi_a^{(1)} >= \sum_{b \neq a} \frac{< \Phi_b \mid W \mid \Phi_a >}{E_a^{(0)} - E_b^{(0)}} \mid \Phi_b > . \tag{9.15}$$

By either method, the ingredients of the calculations are the matrix elements of one- and two-body operators between the many-body basis states.

These methods of solution are limited by the fact that in practice one must deal with finite matrices and/or that the perturbation series must converge. Improved solutions by the above methods can often be achieved by adding and subtracting single-particle potential in Eq. (9.2) to obtain

$$H = \left\{ \sum_{k=1}^{n} (T_k + U_k + U_k') \right\} + \left\{ \sum_{k<l}^{n} V_{kl} - \sum_{k=1}^{n} U_k' \right\} \equiv H^{(0)} + W. \tag{9.16}$$

U_k' is chosen in order to minimize the size of off-diagonal matrix elements of W in the Φ basis, thus providing a means of truncating the matrix and/or improving the convergence of the perturbation expansion. One systematic way of choosing U_k' is the Hartree-Fock method.

When the particles are identical fermions, the wave functions must be totally antisymmetric with respect to the interchange of the coordinates of any two particles. This is arranged by constructing Slater determinants within the Φ basis. For the two-particle system the Slater determinant is given by

$$\mid \Phi_a > = \mid \alpha\beta > = \frac{1}{\sqrt{2}} \begin{vmatrix} \phi_\alpha(1) & \phi_\alpha(2) \\ \phi_\beta(1) & \phi_\beta(2) \end{vmatrix}$$

$$= \frac{1}{\sqrt{2}} \left\{ \phi_\alpha(1)\phi_\beta(2) - \phi_\beta(1)\phi_\alpha(2) \right\}. \tag{9.17}$$

or, in Dirac notation, as

$$\mid \Phi_a > = \mid \alpha\beta > = \frac{1}{\sqrt{2}} \left\{ \mid \alpha\beta >_p - \mid \beta\alpha >_p \right\}, \tag{9.18}$$

where the subscript p denotes the product wave function given in coordinate space by Eq. (9.4). For the n-particle system there are $n!$ terms and the normalization is $1/\sqrt{n!}$. The Slater determinant enforces the Pauli principle - the fact that no two members of the set of quantum numbers α_k can be identical or the wave function will vanish.

The matrix elements of H between these Slater determinants are straightforward but tedious to evaluate. However, the diagonal matrix elements are particularly simple. The diagonal matrix element for the one-body operator $T_k + U_k$ is

$$< \Phi_a \mid \sum_{k=1}^{n} (T_k + U_k) \mid \Phi_a > = \sum_\alpha < \alpha \mid T + U \mid \alpha >, \tag{9.19}$$

where the sum over α runs over the set of n occupied single-particle states in Φ_a, and $< \alpha \mid T + U \mid \alpha >$ stands for the single-particle matrix element

$$\sum_\alpha \int \phi_\alpha^*(\vec{r}) \left[\frac{-\hbar^2}{2m} \nabla^2 + U(\vec{r}) \right] \phi_\alpha(\vec{r})\, d\tau. \tag{9.20}$$

The diagonal matrix element for the two-body operator V_{kl} is

$$< \Phi_a \mid \sum_{k<l} V_{kl} \mid \Phi_a > = \sum_{\alpha<\beta} < \alpha\beta \mid V \mid \alpha\beta >$$

$$= \frac{1}{2} \sum_{\alpha\neq\beta} < \alpha\beta \mid V \mid \alpha\beta > = \frac{1}{2} \sum_{\alpha\beta} < \alpha\beta \mid V \mid \alpha\beta > . \tag{9.21}$$

where the sums over α and β run over the set of n occupied single-particle states in Φ_a. The summation over $(\alpha \neq \beta)$ can be replaced by the unrestricted summation $(\alpha\beta)$ because the two-particle wave function automatically vanishes when $\alpha = \beta$.

The two-body matrix element is given by

$$\begin{aligned} < \alpha\beta \mid V \mid \alpha\beta > &= < \alpha\beta \mid V \mid \alpha\beta >_p - < \alpha\beta \mid V \mid \beta\alpha >_p \\ &= \int\int \phi^*_\alpha(\vec{r}_1)\ \phi^*_\beta(\vec{r}_2) V(\vec{r}_1\vec{r}_2) \phi_\alpha(\vec{r}_1)\ \phi_\beta(\vec{r}_2)\, d\tau_1\, d\tau_2 \\ &- \int\int \phi^*_\alpha(\vec{r}_1)\ \phi^*_\beta(\vec{r}_2) V(\vec{r}_1\vec{r}_2) \phi_\beta(\vec{r}_1)\ \phi_\alpha(\vec{r}_2)\, d\tau_1\, d\tau_2 \end{aligned} \tag{9.22}$$

where $V(\vec{r}_1\vec{r}_2) = V(\vec{r}_2\vec{r}_1)$ has been used, and the subscript p indicates that the product wave functions of Eq. (9.4) are used. The two terms in Eq. (9.22) are referred to as the direct and exchange terms, respectively. Evaluation of the most general case will be considered in the framework of the creation and destruction operators.

10 Conserved quantum numbers

10.1 Angular momentum

The hamiltonian is a scalar in the spacial coordinates - the expectation value does not depend on the orientation of the system. Thus the hamiltonian commutes with total angular momentum operators:

$$[H, \hat{J}^2] = 0, \tag{10.1}$$

$$[H, \hat{J}_z] = 0. \tag{10.2}$$

The many-body wave functions are eigenstates of $\hat{J}^2$ and $\hat{J}_z$ with:

$$\hat{J}^2 \mid \Psi >= J(J+1) \mid \Psi >, \tag{10.3}$$

$$\hat{J}_z \mid \Psi >= M \mid \Psi >, \tag{10.4}$$

where there are $(2J+1)$ values of M going from $M = -J$ up to $M = +J$ in integer steps. Thus one of our goals is to construct wave functions which have good J and J_z. One can construct basis states which have good J and J_z - this is called the J-scheme. Sometimes one constructs a basis which has only good J_z but not good J - this is called the M-scheme. If this M-scheme basis is complete with regard to rotations in the J-space, then the eigenstates will have good J and J_z. For nuclei the total angular momentum is sum of the orbital and spin angular momenta of all nucleons.

10.2 Parity

The strong and electromagnetic hamiltonians conserve parity. Thus the eigenstates can be broken down into two classes of states labeled by their parity π=+1 or π=-1, and the hamiltonian does not mix these two classes. For nuclear structure the total parity originates from the the intrinsic parity of the nucleon which is π_{int}=+1 and the parities associated with the orbital angular momenta $\pi_\ell = (-1)^\ell$. The total parity is the product over all nucleons

$$\pi = \Pi_i \; \pi_{int}(i) \; \pi_\ell(i) = \Pi_i \; (-1)^{\ell_i} \tag{10.5}$$

One usually constructs basis states and eigenstates which which have a definite parity.

The weak hamiltonian does not conserve parity. When considered as a perturbation the matrix elements of the weak hamiltonian are typically on the order of a few

eV or less. Thus, parity mixing can always be calculated in first-order perturbation theory.

The effects of parity nonconservation can be observed in several types of experiment in which the observable must be zero in the absence of parity nonconservation. For example, when parity is conserved a $\Delta L = 1$ electromagnetic transition must either be M1 if the two states do not change parity ($\pi_i\pi_f$=+1), or E1 if the two states change parity ($\pi_i\pi_f$=-1). The angular distribution of both E1 and M1 gamma rays is symmetric around the spin axis of the nucleus. When parity is not conserved then there can be interference between E1 and M1 which leads to an left-right asymmetry in the angular distribution.

10.3 Isospin

Since the spin of the proton and neutron are both 1/2 and the masses are nearly the same, it is useful to think of them as members of an isospin doublet of the nucleon. Thus they have isospin $t = 1/2$ and projection $t_z = -1/2$ and $t_z = +1/2$ for the proton and neutron, respectively. The isospin operator $\vec{t}$ for the isospin degrees of freedom is analogous to the spin operator $\vec{s}$ for the spin degrees of freedom. For many nucleons the total isospin and its z projection are given by

$$\vec{T} = \sum_i \vec{t}(i). \tag{10.6}$$

$$\hat{T}_z = \sum_i \hat{t}_z(i). \tag{10.7}$$

The strong interaction conserves isospin, that is, the expectation value of H_s does not depend on the orientation in isospin space. Thus H_s commutes with the total isospin operators:

$$[H_s, \hat{T}^2] = 0 \tag{10.8}$$

$$[H_s, \hat{T}_z] = 0 \tag{10.9}$$

The many-body wave functions are eigenstates of $\hat{T}^2$ and $\hat{T}_z$ with:

$$\hat{T}^2 \mid \Psi > = T(T+1) \mid \Psi >, \tag{10.10}$$

$$\hat{T}_z \mid \Psi > = T_z \mid \Psi >, \tag{10.11}$$

where there are $2T + 1$ values of T_z going from $T_z = -T$ up to $T_z = +T$ in integer steps. For a nucleus with Z protons and N neutrons, $T_z = (N - Z)/2$. The sign convention here is chosen so that the more common neutron-rich nuclei will have positive T_z (but other books may use a difference convention). For a given T_z value

the minimum value of T is $T_{min} = \mid T_z \mid$ and the maximum value is $T_{max} = A/2$. The lowest level in a nucleus usually has $T = T_z$ (there are a few exceptions for odd-odd nuclei with $N = Z$). This is related to the fact that the nuclear interaction in the $T = 0$ two-nucleon system is a stronger that in the $T = 1$ system (only the deuteron has a bound state).

The experimental evidence for isospin conservation comes from a comparison of the proton-proton, proton-neutron and neutron-neutron scattering lengths in their $T = 1$ state, and the observation that the energy levels of nuclei can be organized into T multiplets of $(2T + 1)$ nuclei with $T_z = -T$ up to $T_z = T$.

One of the special consequences of isospin conservation is mirror symmetry. The energy spectrum of a nucleus should be identical to that of another nucleus in which the protons and neutrons numbers are interchanged. These are called mirror nuclei. There are many examples of mirror nuclei whose spectra can be compared in this way. The deviation from mirror symmetry is attributed to the Coulomb interaction.

The Coulomb hamiltonian does not conserve isospin since it only enters into the interaction between protons. If the Coulomb interaction is treated as a perturbation, then its off-diagonal matrix elements are typically on the order of 100 keV or less. For many nuclear structure problems this is small (at least compared to the uncertainty in the strong interaction matrix elements) and we can start with basis states and eigenfunction which are constructed to have good isospin. Isospin non-conservation is often treated in first-order perturbation theory.

The diagonal matrix elements are relatively large. The diagonal energies can be estimated from liquid-drop (ld) model for the Coulomb interaction for Z protons in a sphere of radius $R = r_o A^{1/3}$:

$$E_c(ld) = \frac{3}{5}\frac{e^2 Z^2}{R} = \frac{3e^2}{5r_o}\frac{Z^2}{A^{1/3}}. \tag{10.12}$$

An isobaric mass multiplet for a state with isospin T are those $(2T + 1)$ states in different nuclei which have $T_z = -T$ up to $T_z = T$. The isobaric mass multiplet equation (IMME) is an expression for the masses of these levels in terms of an expansion in T_z. We can also write the IMME in terms of binding energies:

$$BE(T, T_z) = a + bT_z - cT_z^2. \tag{10.13}$$

where the signs are chosen so that a, b and c will be positive. The strong interaction does not depend on T_z, and only contributes to the first term in Eqs. (10.13). When the Coulomb interaction is treated in first order-perturbation theory one can show that its contribution to the binding energy does not have terms higher than T_z^2 (This

comes from the fact that the Coulomb interaction can be written in terms of isospin tensors of rank 0, 1 and 2. One then uses the Wigner-Eckart theorem to show T_z^2 is the highest power of T_z which is allowed.) The b coefficient of the IMME can be determined from the binding energy differences between mirror nuclei:

$$b = \frac{BE(T, T_z = T) - BE(T, T_z = -T)}{2T}. \tag{10.14}$$

The liquid-drop estimate for the Coulomb contribution to these terms comes from Eq. (10.12) with $Z = (A/2) - T_z$:

$$BE_c(ld) = -\frac{3e^2}{5R}\left[\frac{A^2}{4} - AT_z + T_z^2\right]. \tag{10.15}$$

Thus

$$b(ld) = \frac{3e^2 A}{5R} \text{ and } c(ld) = \frac{3e^2}{5R}. \tag{10.16}$$

The experimental masses (binding energies) have been used to obtain the coefficients a, b and c in Eq. (10.13) with results given in Ref. [1]. States with $T = 1/2$ are called isobaric doublets, and only the first two two terms in Eq. (10.13) are needed to fit the two binding energies. States with $T = 1$ are called isobaric triplets, and all three terms are needed. States with $T = 3/2$ are called isobaric quartets. For quartets, the most general expansion in terms of T_z would require a term of the form dT_z^3. However from the experimental binding energies the coefficient d is zero within experimental error, except for small values for $A = 9$ and $A = 13$ [1]. This fact is consistent with the treatment of the Coulomb interaction as a first-order correction to the energy.

The b coefficients obtained from the experimental binding energy are shown in Fig. (10.1). They are compared with the prediction of the liquid drop model. The liquid drop model is always higher than experiment. The reason is that the observed displacement energy is related to a change in proton-neutron occupancy of the orbits near the Fermi surface (the valence orbits that are the most loosely bound) which have an rms radius which is larger than the average rms radius implicit in the liquid drop model (R in the denominator of Eq. (10.16) is effectively larger). One can observe in Fig. 1 some small downward glitches in the data at $A = 16$ and $A = 40$ corresponding to the magic numbers 8 and 20, respectively. This is due to the increase in rms radius of the orbit at the Fermi surface going from the p to sd ($A = 16$) and sd to pf ($A = 40$) valence shells.

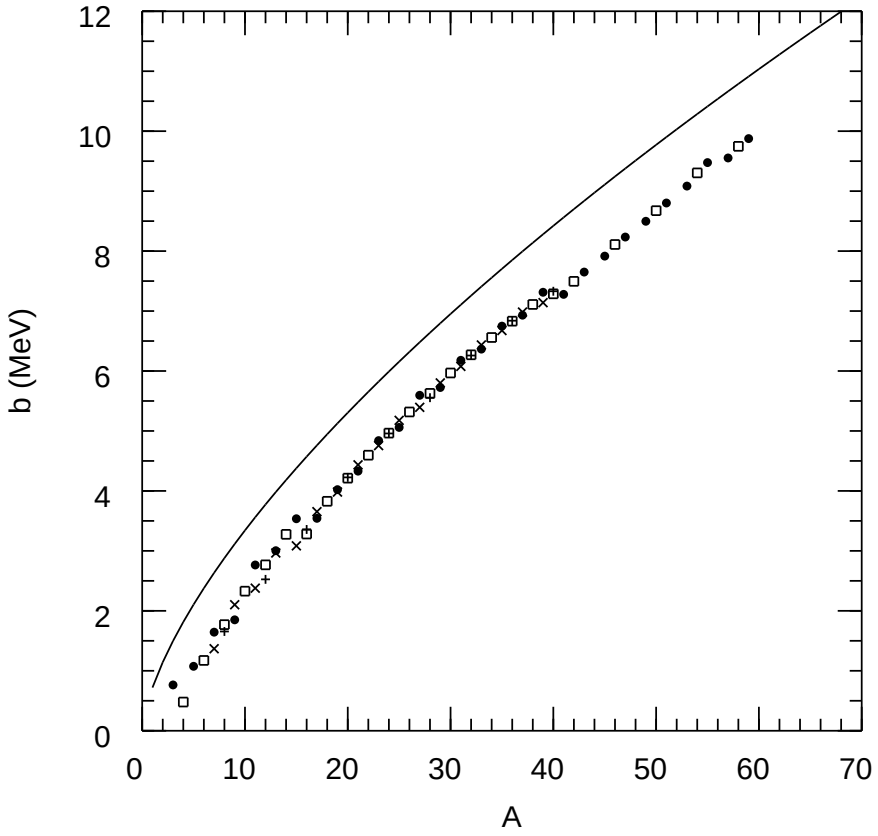

Figure 1: b-coefficients for the IMME. The symbols show the values obtained from experimental binding energies for $T = 1/2$ (29 filled circles), $T = 1$ (24 squares), $T = 3/2$ (17 crosses) and $T = 2$ (9 pluses). The line is the prediction of the liquid drop model.

References

[1] W. Benenson and E. Kashy, Rev. Mod. Phys. **51**, 527 (1979); M. S. Anthony, J. Britz, J. R. Bueb and A. Pape, At. Data Nucl. Data Tables **33**, 447 (1985).

11 Quantum numbers for the two nucleon system

11.1 Two neutrons or two protons

There are no bound states for two neutrons. However, there is a strong low-energy s-wave scattering resonance. First we will construct the antisymmetric wavefunction for two neutrons in the ℓ=0 state. The wavefunctions are a product of the space, spin and isospin parts:

$$f(r)\ Y_m^\ell(\hat{r})\ \phi(S)\ \chi(T). \tag{11.1}$$

Initially we will consider only the space and spin part. The parity associated with the change of phase of the spherical harmonics Y when $\vec{r}$ is replaced by $-\vec{r}$ is π=$(-1)^\ell$. For a two-particle system the symmetry under the interchange of the two particles P_{12} is related to the parity since

$$P_{12}\vec{r} = P_{12}[\vec{r}_1 - \vec{r}_2] = [\vec{r}_2 - \vec{r}_1] = -\vec{r}. \tag{11.2}$$

For $l = 0$, π=+1, and the spatial wave function is symmetric under the interchange of the two neutrons. In order to make the entire wavefunction antisymmetric the spin wave function must be antisymmetric. The spin wave functions

$$|\ \alpha > = |\ s = 1/2, s_z = 1/2 >, \tag{11.3}$$

$$|\ \beta > = |\ s = 1/2, s_z = -1/2 > . \tag{11.4}$$

The neutron spins can be coupled to make wavefuncitons $\phi(S, S_z)$ with total angular momentum S by using the Clebsch-Gordan coefficients $< 1/2, s_z, 1/2, s_z' \mid S, S_z >$

$$\phi(1,1) = |\ \alpha(1) > |\ \alpha(2) >, \tag{11.5}$$

$$\phi(1,0) = \sqrt{\frac{1}{2}}\ [|\ \alpha(1) > |\ \beta(2) > + |\ \beta(1) > |\ \alpha(2) >]\,, \tag{11.6}$$

$$\phi(1,-1) = |\ \beta(1) > |\ \beta(2) >, \tag{11.7}$$

$$\phi(0,0) = \sqrt{\frac{1}{2}}\ [|\ \alpha(1) > |\ \beta(2) > - |\ \beta(1) > |\ \alpha(2) >]\,, \tag{11.8}$$

where $\alpha(1)$ indicates that neutron "1" is in the state α. The $S = 1$ wavefunctions are symmetric under P_{12}, and $S = 0$ is antisymmetric. Thus the spin symmetry under P_{12} is $(-1)^{S+1}$. To make the entire ℓ=0 wavefunction antisymmetric we must take the $S = 0$ solution. Thus the quantum numbers for the $\ell = 0$ state of the two neutrons are:

$$^1S_0 :\ \text{nn},\ \ell = 0,\ S = 0,\ J = 0 \text{ and } \pi = +1. \tag{11.9}$$

A similar analysis for the scattering in the $l = 1$ state would give:

$$^3P_J : \text{ nn, } \ell = 1, \ S = 1, \ J = 0, 1, 2 \text{ and } \pi = -1, \tag{11.10}$$

where the first symbol in Eqs. (11.9) and (11.10) indicates $^{2S+1}\ell_J$, with $(2S + 1) = 1$ for the "singlet" state and $(2S + 1) = 3$ for the "triplet" state. The values of J are restricted by the triangle condition for the coupling of ℓ and S.

In general the total symmetry under P_{12} must be negative:

$$(-1)^{\ell+S+1} = -1, \tag{11.11}$$

which means that $\ell + S$ must be even for the two neutrons. If we add isospin to the two-neutron system there is nothing new since the two neutrons must be in the state

$$\chi(T = 1, T_z = 1) = \mid t = 1/2, t_z = 1/2 \ (1) > \mid t = 1/2, t_z = 1/2 \ (2) >, \tag{11.12}$$

which is symmetric under P_{12}. The same results apply to the proton-proton system.

11.2 Proton-neutron

If we consider a proton and neutron in an ℓ=0 state there is no antisymmetry requirement since these are not identical particle. Thus both S values are allowed. For ℓ=0:

$$^1S_0 : \text{ pn, } \ell = 0, \ S = 0, \ J = 0 \text{ and } \pi = +1. \tag{11.13}$$

$$^3S_1 : \text{ pn, } \ell = 0, \ S = 1, \ J = 1 \text{ and } \pi = +1. \tag{11.14}$$

The $J = 1$ wave function corresponds to the bound state of state of the deuteron which has $J^\pi = 1^+$. A similar set of states exist for higher ℓ values.

11.3 Two nucleons

When isospin is considered we also have to include the isospin coupling to $T = 0$ and 1 which in analogy with the spin coupling is:

$$\chi(1, 1) = \mid a(1) > \mid a(2) >, \tag{11.15}$$

$$\chi(1, 0) = \sqrt{\frac{1}{2}} \left[\mid a(1) > \mid b(2) > + \mid b(1) > \mid a(2) > \right], \tag{11.16}$$

$$\chi(1, -1) = \mid b(1) > \mid b(2) >, \tag{11.17}$$

$$\chi(0,0) = \sqrt{\frac{1}{2}}\,[\mid a(1) > \mid b(2) > - \mid b(1) > \mid a(2) >]\,, \tag{11.18}$$

where:

$$\mid a >= \mid t = 1/2, t_z = 1/2 >, \tag{11.19}$$

$$\mid b >= \mid t = 1/2, t_z = -1/2 > . \tag{11.20}$$

The symmetry under P_{12} is $(-1)^{T+1}$.

The total symmetry under P_{12} must be negative:

$$(-1)^{\ell+S+1+T+1} = (-1)^{\ell+S+T} = -1, \tag{11.21}$$

which means that $\ell + S + T$ must be odd. Thus with isospin the proton-neutron state with ℓ=0 and $S = 0$ must have $T = 1$ and it is the $T_z = 0$ member of the $T = 1$ triplet, the other two being the neutron-neutron and proton-proton states

$$^1S_0 :\ T = 1,\ \ell = 0,\ S = 0,\ J = 0 \text{ and } \pi = +1. \tag{11.22}$$

The state with ℓ=0 and $S = 1$ must have $T = 0$

$$^3S_1 :\ T = 0,\ \ell = 0,\ S = 1,\ J = 1 \text{ and } \pi = +1. \tag{11.23}$$

For ℓ=1 and ℓ=2 we have

$$^3P_J :\ T = 1,\ \ell = 1,\ S = 1,\ J = 0, 1, 2 \text{ and } \pi = -1. \tag{11.24}$$

$$^1P_1 :\ T = 0,\ \ell = 1,\ S = 0,\ J = 1 \text{ and } \pi = -1. \tag{11.25}$$

$$^1D_2 :\ T = 1,\ \ell = 2,\ S = 0,\ J = 2 \text{ and } \pi = +1. \tag{11.26}$$

$$^3D_J :\ T = 0,\ \ell = 2,\ S = 1,\ J = 1, 2, 3 \text{ and } \pi = +1. \tag{11.27}$$

In general only the total angular momentum J is a good quantum number. For $S = 0$, $J = \ell$ is unique. For $S = 1$, the wavefunction for a given J value can have $\ell = J - 1$ or $\ell = J + 1$. Thus bound state of the deuteron with $J^\pi = 1^+$ is in general a mixture of the ^{3}S$_1$ and ^{3}D$_1$ states. ℓ=0 is the dominant part of the wavefunction but there is some ℓ=2 (d-state) admixture.

12 The Hartree-Fock approximation

12.1 Properties of single Slater determinants

Before deriving the Hartree-Fock equations is it useful to give some special cases of some diagonal matrix elements. The eigenstates of $H^{(0)}$ can be ordered with respect to the total energy $E^{(0)}$, with the lowest energy state being the one in which all of the particles occupy the lowest energy set of single-particle states allowed by the Pauli principle. This lowest-energy state will be denoted by $\mid C >$. (This notation derives from the fact that it will be associated with the closed-shell configuration.) The n single-particle states occupied in $\mid C >$ will be labeled by $\alpha, \beta, \gamma \ldots$. The total energy $E(C)$ of the state $\mid C >$ is

$$E(C) = < C \mid H \mid C > = \sum_{\alpha} < \alpha \mid T \mid \alpha > + \frac{1}{2} \sum_{\alpha\beta} < \alpha\beta \mid V \mid \alpha\beta > . \tag{12.1}$$

I will use i and j to label specific states above or below the fermi surface which will be considered explicitly in the summations. The total energy of a system with the configuration $\mid C >$ plus one particle in the state i above the fermi surface (a state unoccupied in $\mid C >$) is

$$\begin{aligned} E(Ci) &= < Ci \mid H \mid Ci > \\ &= E(C) + < i \mid T \mid i > + \sum_{\alpha} < i\alpha \mid V \mid i\alpha > . \end{aligned} \tag{12.2}$$

The difference between $E(Ci)$ and $E(C)$ will be denoted by, ϵ(i), the single-particle energy:

$$\epsilon(i) = E(Ci) - E(C) = < i \mid T \mid i > + \sum_{\alpha} < i\alpha \mid V \mid i\alpha > . \tag{12.3}$$

The total energy of a system with the configuration $\mid C >$ plus particles in the states i and j above the fermi surface is

$$\begin{aligned} E(Cij) &= < Cij \mid H \mid Cij > \\ &= E(C) + < i \mid T \mid i > + \sum_{\alpha} < i\alpha \mid V \mid i\alpha > \\ &+ < j \mid T \mid j > + \sum_{\alpha} < j\alpha \mid V \mid j\alpha > + < ij \mid V \mid ij > \\ &= E(C) + \epsilon(i) + \epsilon(j) + < ij \mid V \mid ij > \end{aligned} \tag{12.4}$$

The total energy of a system with the configuration $\mid C >$ with one particle absent in the state i (normally occupied in $\mid C >$) is

$$E(Ci^{-1}) = < Ci^{-1} \mid H \mid Ci^{-1} >$$

$$= E(C) - < i \mid T \mid i > - \sum_{\alpha} < i\alpha \mid V \mid i\alpha > . \tag{12.5}$$

The difference between $E(Ci^{-1})$ and $E(C)$ will be denoted by, ϵ(i):

$$\epsilon(i) = E(C) - E(Ci^{-1}) =< i \mid T \mid i > + \sum_{\alpha} < i\alpha \mid V \mid i\alpha >, \tag{12.6}$$

which has the same form as the single-particle energy. Finally, the total energy of a system with the configuration $\mid C >$ plus particles absent in the states i and j is

$$\begin{aligned} E(Ci^{-1}j^{-1}) &=< Ci^{-1}j^{-1} \mid H \mid Ci^{-1}j^{-1} > \\ &= E(C) - \epsilon(i) - \epsilon(j) + < ij \mid V \mid ij > \end{aligned} \tag{12.7}$$

12.2 Derivation of the Hartree-Fock equations

In the Hartree-Fock approximation, $E(C)$ is minimized with respect to variation of the single-particle wave functions $\phi_i(\vec{r})$ [or equivalently with respect to $\phi_i{}^*(\vec{r})$]. With the coordinate space matrix elements of T and V, one obtains

$$\frac{\partial}{\partial \phi_i^*(\vec{r})} \left\{ E(C) - \sum_{\alpha} \lambda_\alpha \int \mid \phi_\alpha(\vec{r}_1) \mid^2 \, d\tau_1 \right\} = 0$$

$$\begin{aligned} &= T\phi_i(\vec{r}) - \lambda_i \phi_i(\vec{r}) + \frac{1}{2} \Big\{ \sum_{\beta} \int \phi_\beta^*(\vec{r}_2)\, V(\vec{r}\vec{r}_2)\, \phi_i(\vec{r})\, \phi_\beta(\vec{r}_2)\, d\tau_2 \\ &+ \sum_{\alpha} \int \phi_\alpha^*(\vec{r}_1)\, V(\vec{r}_1\vec{r})\, \phi_\alpha(\vec{r}_1)\phi_i(\vec{r})\, d\tau_1 - \sum_{\beta} \int \phi_\beta^*(\vec{r}_2)\, V(\vec{r}\vec{r}_2)\, \phi_\beta(\vec{r})\, \phi_i(\vec{r}_2)\, d\tau_2 \\ &- \sum_{\alpha} \int \phi_\alpha^*(\vec{r}_1)\, V(\vec{r}_1\vec{r})\, \phi_i(\vec{r}_1)\, \phi_\alpha(\vec{r})\, d\tau_1 \Big\}, \end{aligned} \tag{12.8}$$

where λ are Lagrange multipliers which are introduced to enforce the normalization. Using $V(\vec{r}_1\ \vec{r}_2) = V(\vec{r}_2\ \vec{r}_1)$, this reduces to

$$\begin{aligned} &T\phi_i(\vec{r}) + \left\{ \sum_{\alpha} \int \phi_\alpha^*(\vec{r}_1) V(\vec{r}\vec{r}_1) \phi_\alpha(\vec{r}_1)\, d\tau_1 \right\} \phi_i(\vec{r}) \\ &- \int \left\{ \sum_{\alpha} \phi_\alpha^*(\vec{r}_1) V(\vec{r}\vec{r}_1) \phi_\alpha(\vec{r}) \right\} \phi_i(\vec{r}_1)\, d\tau_1 = \lambda_i \phi_i(\vec{r}). \end{aligned} \tag{12.9}$$

This nonlocal differential equation can be used to solve for λ_i and $\phi_i(\vec{r})$. It can be solved in an iterative fashion: (i) choose some initial guess for $\phi_i(\vec{r})$ and calculate the integrals as a function of $\vec{r}$, (ii) solve the differential equation for λ_i and $\phi_i(\vec{r})$, (iii) recalculate the integrals, and (iv) iterate until the λ_i and $\phi_i(\vec{r})$ converge.

Multiplying Eq. (12.9) by $\phi_i^*(\vec{r})$ on both sides and integrating gives

$$< i \mid T \mid i > + \sum_\alpha < i\alpha \mid V \mid i\alpha > = \lambda_i = \epsilon(i), \tag{12.10}$$

where the Lagrange multiplier has been equated to the single-particle energy by comparison to Eqs. (12.3) and (12.6). The term $\sum_\alpha < i\alpha \mid V \mid i\alpha >$ can be identified as the expectation value of the mean-field potential U'.

$$< i \mid U' \mid i > = < i \mid U^{\rm HF} \mid i > = \sum_\alpha < i\alpha \mid V \mid i\alpha > . \tag{12.11}$$

Thus, the full Hartree-Fock hamiltonian is

$$H = H^{(0)} + W, \tag{12.12}$$

with

$$H^{(0)} = \sum_k (T + U^{\rm HF})_k, \tag{12.13}$$

and

$$W = \sum_{kl} V_{kl} - \sum_k U_k^{\rm HF}. \tag{12.14}$$

The state $\mid C >$ with the Hartree-Fock condition of Eq. (12.11) enforced will be denoted by $\mid \Phi_{\rm HF} >$. The zeroth-order and first-order matrix elements are

$$E_{\rm HF}^{(0)} = < \Phi_{\rm HF} \mid \sum_k (T + U^{\rm HF})_k \mid \Phi_{\rm HF} > = \sum_\alpha \epsilon(\alpha), \tag{12.15}$$

and

$$\begin{aligned} E_{\rm HF}^{(1)} &= < \Phi_{\rm HF} \mid W \mid \Phi_{\rm HF} > = < \Phi_{\rm HF} \mid \sum_{kl} V_{kl} - \sum_k (U^{\rm HF})_k \mid \Phi_{\rm HF} > \\ &= \frac{1}{2} \sum_{\alpha\beta} < \alpha\beta \mid V \mid \alpha\beta > - \sum_\alpha < \alpha \mid U^{\rm HF} \mid \alpha > \\ &= -\frac{1}{2} \sum_{\alpha\beta} < \alpha\beta \mid V \mid \alpha\beta > . \end{aligned} \tag{12.16}$$

The total unperturbed energy can thus be expressed in several ways:

$$E_{\rm HF}^{(0)} + E_{\rm HF}^{(1)} = \sum_\alpha \epsilon(\alpha) - \frac{1}{2} \sum_{\alpha\beta} < \alpha\beta \mid V \mid \alpha\beta >$$

$$= \sum_\alpha < \alpha \mid T \mid \alpha > + \frac{1}{2} \sum_{\alpha\beta} < \alpha\beta \mid V \mid \alpha\beta >$$

$$= \frac{1}{2}\left\{\sum_\alpha \epsilon(\alpha) + \sum_\alpha < \alpha \mid T \mid \alpha >\right\}. \tag{12.17}$$

It is to be noted that the Hartree-Fock condition does not make $E^{(1)}$ vanish. The advantage of the Hartree-Fock procedure is that an important class of matrix elements $< \Phi_{\rm HF} \mid W \mid \Phi >$ which enter into the second-order corrections vanish − namely, all of those for which Φ differs from $\Phi_{\rm HF}$ by the addition of one particle above the fermi surface and the removal of one particle below the fermi surface. These are called one-particle one-hole, 1p-1h, configurations. The most important corrections are those in which the Φ differs from $\Phi_{\rm HF}$ by addition of two-particle above the fermi surface and the removal of two particles below the fermi surface (2p-2h configurations).

12.3 Examples of single-particle energies

The Hartree-Fock model works best for those nuclei where there is a large gap at the fermi surface for both protons and neutrons. The total energies for the closed shell, one-particle and one-hole configurations are the interaction energies E measured for the respective, nuclei, where $BE = -E$. For example, if we take ^{16}O as a doubly closed shell nucleus, then energies obtained from the ground state binding energies are:

$$E(^{16}O) = E(C) = -127.619 \text{ MeV}$$

$$E(^{17}O) = E[C, 0d_{5/2} \text{ neutron}] = -131.763 \text{ MeV}$$

$$E(^{17}F) = E[C, 0d_{5/2} \text{ proton}] = -128.220 \text{ MeV}$$

$$E(^{15}O) = E[C, (0p_{1/2})^{-1} \text{ neutron}] = -111.956 \text{ MeV}$$

$$E(^{15}N) = E[C, (0p_{1/2})^{-1} \text{ proton}] = -115.492 \text{ MeV}$$

where the n, ℓ, j values are inferred from the spin-parity of the odd-even ground states. The experimental single-particle energies for these states are thus:

$$\epsilon(0d_{5/2} \text{ neutron}) = E(^{17}O) - E(^{16}O) = -4.144 \text{ MeV}$$

$$\epsilon(0d_{5/2} \text{ proton}) = E(^{17}F) - E(^{16}O) = -0.601 \text{ MeV}$$

$$\epsilon(0p_{1/2} \text{ neutron}) = E(^{16}O) - E(^{15}O) = -15.663 \text{ MeV}$$

$$\epsilon(0p_{1/2} \text{ proton}) = E(^{16}O) - E(^{15}N) = -12.127 \text{ MeV}$$

The single-particle energies for other states can be inferred form the energies E associated with excited states in the A=15 and A=17 nuclei.

It will be shown in a homework that Eq. (12.17) is in fact not satisfied by experimental data in nuclear physics, when the ϵ are taken from experiment and when

the kinetic energies are calculated. This means that higher-order corrections to the Hartree-Fock are important. If these corrections are taken into account by using an effective hamiltonian, this hamiltonian will need to include three-body and/or density dependent terms. An example is the Skyrme interaction which includes a density-dependent interaction.

12.4 Results with the Skyrme hamiltonian

The Skyrme approximation [1], [2] is an $s-$ and $p-$wave expansion of an effective two-body interaction together with an $s-$wave density dependent interaction:

$$V_{\rm Skyrme} = t_0(1+x_0P_\sigma)\delta + \frac{1}{2}t_1(1+x_1P_\sigma)\left(\mathbf{k'}^2\,\delta + \,\delta\,\mathbf{k}^2\right)$$

$$+t_2(1+x_2P_\sigma)\,\mathbf{k'}\,\cdot\delta\,\mathbf{k} + \frac{1}{6}t_3(1+x_3P_\sigma)\,\rho^\alpha(\mathbf{R})\,\delta$$

$$+iW_0(\sigma_i+\sigma_j)\cdot\mathbf{k}\times\delta\mathbf{k} + V^{Coul}, \tag{12.18}$$

where $\delta = \delta(\mathbf{r}_i - \mathbf{r}_j)$, $\mathbf{k} = (1/2i)(\nabla_i - \nabla_j)$ is the relative momentum operator acting on the wave function to the right and $\mathbf{k'}$ is the adjoint of $\mathbf{k}$. P_σ is the spin-exchange operator and $\mathbf{R} = (\mathbf{r}_i + \mathbf{r}_j)/2$. The form of the Skyrme interaction allows one to calculate the potentials analytically in terms of the densities which makes the self-consistent calculations fast.

The Skyrme interaction results in a non-local potential for protons ($q = p$) and neutrons ($q = n$) given by $U_q(r) + U'_q(r)$ with

$$U_q(r) = t_0\left(\left[1+\frac{x_0}{2}\right]\rho - \left[x_0+\frac{1}{2}\right]\rho_q\right)$$

$$+\frac{t_1}{8}\left(\left[1+\frac{x_1}{2}\right][2\tau - 3(\Delta\rho)] - \left[x_1+\frac{1}{2}\right][2\tau_q - 3(\Delta\rho_q)]\right)$$

$$+\frac{t_2}{2}\left(\left[1+\frac{x_2}{2}\right][2\tau + (\Delta\rho)] + \left[x_2+\frac{1}{2}\right][2\tau_q + (\Delta\rho_q)]\right)$$

$$+\frac{t_3}{6}\left(\left[1+\frac{x_3}{2}\right]\rho - \left[x_3+\frac{1}{2}\right]\rho_q\right)\rho^\alpha - \frac{W_0}{2}\nabla\cdot(\mathbf{J}+\mathbf{J}_q)$$

$$+U_q^{Coul}(r) + U_q^{so}(r)[\ell\cdot\sigma] \tag{12.19}$$

and

$$U'_q(r) = -\nabla\cdot\left\{\frac{t_1}{4}\left(\left[1+\frac{x_1}{2}\right]\rho - \left[x_1+\frac{1}{2}\right]\rho_q\right)\right.$$

$$\left.+\frac{t_2}{4}\left(\left[1+\frac{x_2}{2}\right]\rho + \left[x_2+\frac{1}{2}\right]\rho_q\right)\right\}\nabla, \tag{12.20}$$

where the spin-orbit potential is:

$$U_q^{so}(r) = \frac{1}{r}\left\{\frac{W_0}{2}\left[\frac{d}{dr}(\rho+\rho_q)\right] + \frac{1}{8}\left[(t_1-t_2)J_q\right] - \frac{1}{8}\left[t_1x_1 + t_2x_2\right]J\right\} \tag{12.21}$$

The U' term of Eq. (12.20) can be combined with the kinetic energy operator to write Eq. (12.9) in terms of the a Schroedinger-like equation with an effective mass:

$$\left\{-\nabla \cdot \frac{\hbar^2}{2m_q^*(r)}\nabla + U_q(r)\right\}\phi_{i,q}(\mathbf{r}) = \epsilon_{i,q}\ \phi_{i,q}(\mathbf{r}). \tag{12.22}$$

where the effective mass is defined by:

$$\frac{\hbar^2}{2m_q^*(r)} = \frac{\hbar^2}{2m} + \frac{t_1}{4}\left(\left[1+\frac{x_1}{2}\right]\rho - \left[x_1+\frac{1}{2}\right]\rho_q\right)$$
$$+\frac{t_2}{4}\left(\left[1+\frac{x_2}{2}\right]\rho + \left[x_2+\frac{1}{2}\right]\rho_q\right) \tag{12.23}$$

The densities in these equations are

$$\rho_q(r) = \sum_\alpha \mid \phi_{q\alpha}(r) \mid^2, \tag{12.24}$$

$$\tau_q(r) = \sum_\alpha \mid \nabla\phi_{q\alpha}(r) \mid^2 \tag{12.25}$$

$$\mathbf{J}_q(r) = i\sum_\alpha \phi^*_{q\alpha}(r)[\sigma \times \phi_{q\alpha}(\mathbf{r})], \tag{12.26}$$

$$\rho(r) = \rho_p(r) + \rho_n(r), \tag{12.27}$$

$$\tau(r) = \tau_p(r) + \tau_n(r), \tag{12.28}$$

$$\mathbf{J}(r) = \mathbf{J}_p(r) + \mathbf{J}_n(r), \tag{12.29}$$

and

$$(\Delta f) = \frac{1}{r}\left[\frac{d^2}{dr^2} r f(r)\right], \tag{12.30}$$

where the derivative operates only inside the brackets.

Eq. (12.22) can be rewrittin in terms of the Schroedinger equation with an energy-dependent potential [3]:

$$\left\{-\frac{\hbar^2}{2m_q}\nabla^2 + U_q^*(r,\epsilon)\right\}\phi_{i,q}(\mathbf{r}) = \epsilon_{i,q}\ \phi_{i,q}(\mathbf{r}), \tag{12.31}$$

where

$$U_q^*(r,\epsilon) = \frac{m_q^*(r)}{m}\Big[U_q(r) + \frac{1}{2}\left(\frac{d^2}{dr^2}\frac{\hbar^2}{2m_q^*(r)}\right)$$
$$-\frac{m_q^*(r)}{2\hbar^2}\left(\frac{d}{dr}\frac{\hbar^2}{2m_q^*(r)}\right)^2\Big] + \left[1-\frac{m_q^*(r)}{m}\right]\epsilon_{i,q} \tag{12.32}$$

Table 1: Values of the Skyrme parameters obtained with SKX .

Parameter	SKX	SKX error
α	0.5	
t_0	−1444.0	1.0
t_1	251.3	1.9
t_2	−131.4	1.2
t_3	12043.9	18.1
W_o	149.4	2.7
x_0	0.364	0.021
x_1	0.521	0.171
x_2	0.131	0.013
x_3	0.088	0.051

The goal of the Skyrme HF formulation is to write the HF equations in terms of a few parameters (the ten in Eq. (12.18)) that can be obtained from a least-squares fit to some selected set of experimental data. In principle one would like to derive the Skyrme parameters from the experimental nucleon-nucleon interaction. This involves understanding the effect of the trucation of the actual many-body wave function to the closed-shell structure assumed in the derivation. It also requires an understanding of the contributions of real three-body forces. There has not yet been a quantitative derivation of the Skyrme parameters from the first principles. The Skyrme formulation is a specific type of density-functional model which have been widely used in atomic, molecular and condensed matter physics. One can show that such functionals exist even if they cannot be explicitly derived [4], [5].

The have been many attemps to obtain the Skyrme parameters from various types of experimental data. In this book I will concentrate on two recent results. One is the SKX hamiltonian which is obtained by applying the above equations to the eleven closed-shell nuclei: ^{16}O, ^{34}Si, ^{40}Ca, ^{48}Ca, ^{48}Ni, ^{88}Sr, ^{100}Sn, ^{132}Sn and ^{208}Pb. The data include the binding energies of these nuclei, together with five rms charge radii and 65 single-particle energies. Ten parameters in Eq. (12.18) were varied (although only six linear-combinations are well determined). The SKX spin-orbit energy-density leaves out terms involving t_1, t_2, x_1 and x_2, and a generalized two-parameter spin-orbit force based upon the Hartree reduction was used [6]. SKX uses the Friedman-Pandharipande neutron matter equation of state [7] as a constraint (it has recently been shown that the neutron skin is sensitive to the properties of the neutron equation of state [8], [9]). SKX also introduces a new parameter which is needed to reproduce the mirror displacement energies by the addition of a charge symmetry breaking (CSB) interaction (SkXcsb [10]). The values of the Skyrme parameters for SKX are given in Table 1.

Goriely et al. [11] obtained the parameter set called MSk7. In addition to the formulation given above for closed-shell nuclei, the effect of nuclear pairing and deformation were also taken into account. The MSk7 parameters are based on a fit to the binding energies of 1772 nuclei (the radii or single-particle energies were not included). Of the ten parameters in Eq. (12.18), seven were varied (x_0 and x_1 were fixed at -0.5 and α was fixed at $1/3$). The spin-orbit energy density retains the terms involving t_1, t_2, x_1 and x_2, a four-parameters δ-function pairing force was added, and a two-parameter Wigner correction term was added. The MSk7 interaction was used to calculate the binding energies and shapes of 9200 nuclei [11]. The results were shown as the HF1 calculation in Chapter 1.

The relativistic mean-field is an alternative to the Skyrme HF. The relativistic description of nuclear systems uses a field theoretical approach (quantum hydrodynamics) where the interaction of nucleons is described by an exchange of mesons. [12] I will use the non-linear parameter set NL3 [13] which gives a good description of binding energies and radii.

12.4.1 Binding energies

The binding energies for the region of nuclei up to $A = 60$ vary by hundreds of MeV, yet we consider theoretical calculations which reproduce experiment to the level of several hundred keV to an MeV. The "coast to coast" situation for all nuclei between the drip lines is illustrated in Fig. (12.1) where the BE obtained with the MSk7 HF calculations [11] are shown for all nuclei between the proton and neutron drip lines centered on $Z = 20$ (left-hand side) and $N = 20$ (right-hand side) and compared to experiment where known.

The drip line is reached in each case when the derivative of the BE curve with respect to proton or neutron number goes to zero. One observes in the bottom panels of Fig. (12.1) an apparently featureless and smooth curve with the data in agreement with theory. However, we are interested in a much higher level of detail which is illustrated in the top panel by subtracting a smooth curve given by the liquid drop model (LDM) from theory and experiment. This top curve brings out the detail related the microscopic aspects of the nuclear shell model.

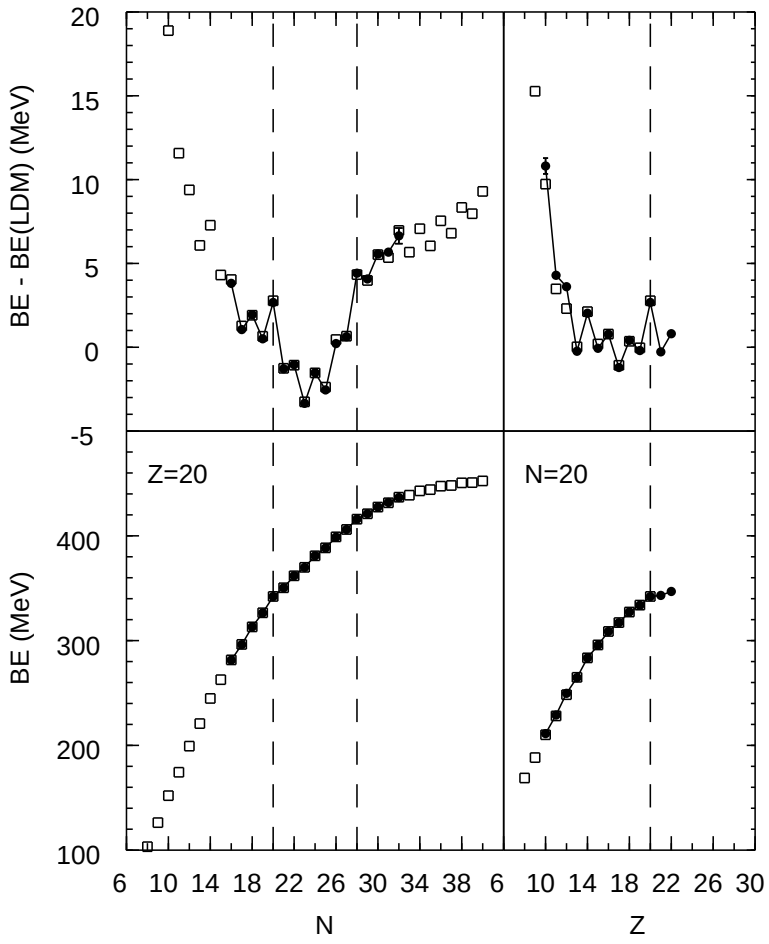

Figure 1: Theoretical (squares) and experimental (filled circles) binding energy for $Z = 20$ as a function of neutron number (left-hand side) and for $N = 20$ as a function of proton number (right-hand side). In the upper panels a smooth curve given by the liquid drop model is subtracted from theory and experiment. The magic numbers $N = 20$, $N = 28$ and $Z = 20$ are indicated by dashed lines.

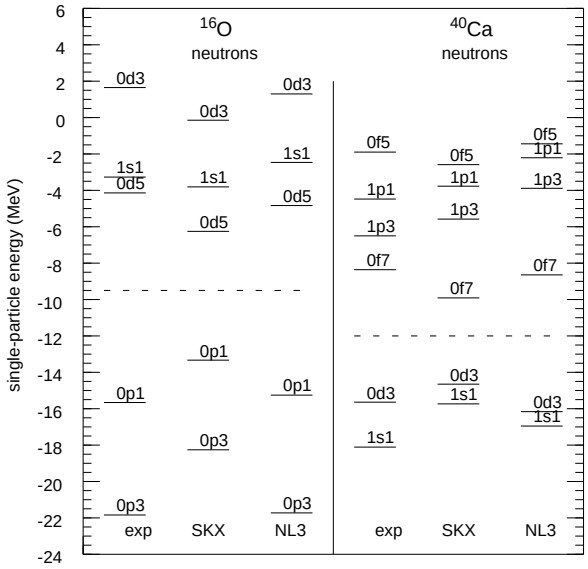

Figure 2: Experimental and theoretical neutron single-particle energies for ^{16}O and ^{40}Ca. The orbits are labeled by $(n, \ell, 2j)$, and the dashed line is the Fermi energy.

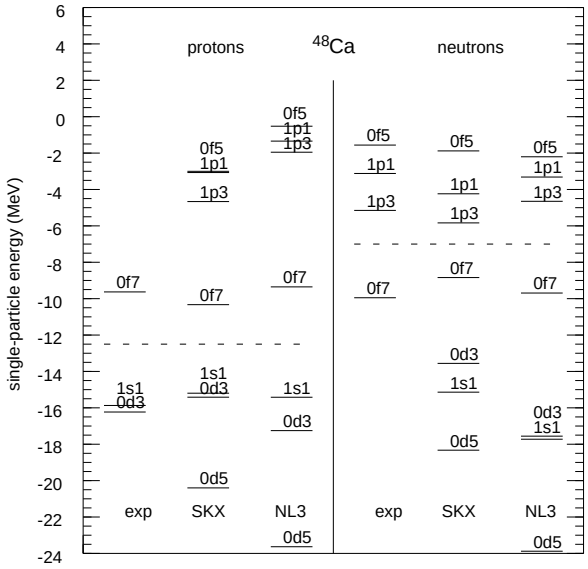

Figure 3: Experimental and theoretical proton and neutron single-particle energies for ^{48}Ca. The orbits are labeled by $(n, \ell, 2j)$, and the dashed line is the Fermi energy.

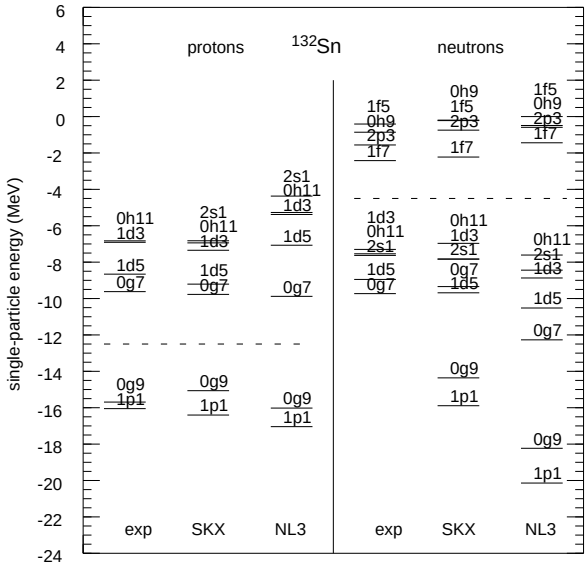

Figure 4: Experimental and theoretical proton and neutron single-particle energies for ^{132}Sn. The orbits are labeled by $(n, \ell, 2j)$, and the dashed line is the Fermi energy.

12.4.2 Single-particle energies

The experimental single-particle energies for ^{16}O, ^{40}Ca, ^{48}Ca, ^{132}Sn and ^{208}Pb are compared with the SKX Hartree-Fock and NL3 Dirac Hartree calculations in Figs. (12.2), (12.3), (12.4), and (12.5). Both mean-field calculations are in qualitative agreement with experiment. For light nuclei the NL3 results are in better, but for heavy nuclei the SKX results are better. The difference between SKX and NL3 is mainly related to the effective mass (m^*/m), which is about 1.0 for SKX and 0.6 for NL3. The effective mass for the Skyrme interaction can be tuned by the parameters [2] and those for SKX are determined primarily from the SPE of heavy nuclei where the spacing around the Fermi surface requires an effective mass of about 1.0 [14]. For NL3 on the other hand, an effective mass of about 0.6 is intrinsic to the model. An effective mass of 0.6 gives SPE in heavy nuclei which are spread out compared to experiment as shown by NL3 in Figs. (12.4) and (12.5). Typical Brueckner G matrix interactions also give an effective mass of about 0.6, and the reason for an empirical value of near unity in heavy nuclei is attributed to configuration mixing due to coupling of the single-particle states to surface vibrations [15], [16]. For a hamiltonian like SKX with an effective mass of unity, these surface vibrations effectively included in terms of a modified (renormalized) hamiltonian.

Experimental values of the SPE are usually used as input to shell-model calcula-

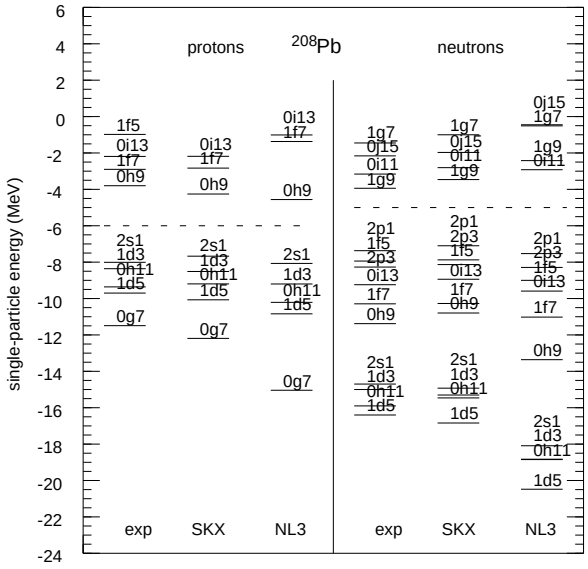

Figure 5: Experimental and theoretical proton and neutron single-particle energies for ^{132}Sn. The orbits are labeled by $(n, \ell, 2j)$, and the dashed line is the Fermi energy.

tions. For nuclei near the drip lines where the experimental SPE are not known, one needs a theoretical model for predicting or extrapolating the SPE. The HF parameter model such as SKX and NL3 provide perhaps the most reliable way to extrapolate the SPE from nuclei near stability to the most exotic nuclei near the drip lines. The predictions for the ^{60}Ca and ^{78}Ni SPE are given in Figs. (12.6) and (12.7), respectively. Other recent predictions for ^{60}Ca are given in [17]. It will remain for future experiments to test these extrapolations.

As a guide to the ordering of the single-particle states as a function of N and Z, I show in Fig. (12.8) the single-particle energies for nuclei with $N = Z$ obtained from with SKX . Fig. (12.9) shows the SKX single-particle energies for the calcium isotopes as a function of neutron number. Beyond ^{60}Ca one observes that the $0g_{9/2}$ orbital becomes bound, and thus ^{70}Ca will be bound with SKX . The even-even calcium nuclei between ^{60}Ca and ^{70}Ca will probably be bound due to pairing (which has been neglected in this particular SKX HF calculation).

12.4.3 Rms charge radii and charge densities

In this section I will discuss the results for rms charge and charge densities obtained with the Skyrme parameter sets SKX [14] and SKM* [18]

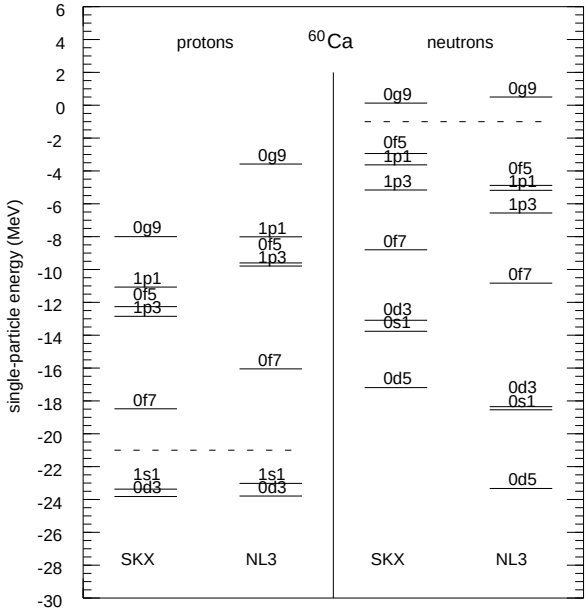

Figure 6: Theoretical proton and neutron single-particle energies for ^{60}Ca. The orbits are labeled by $(n, \ell, 2j)$, and the dashed line is the Fermi energy.

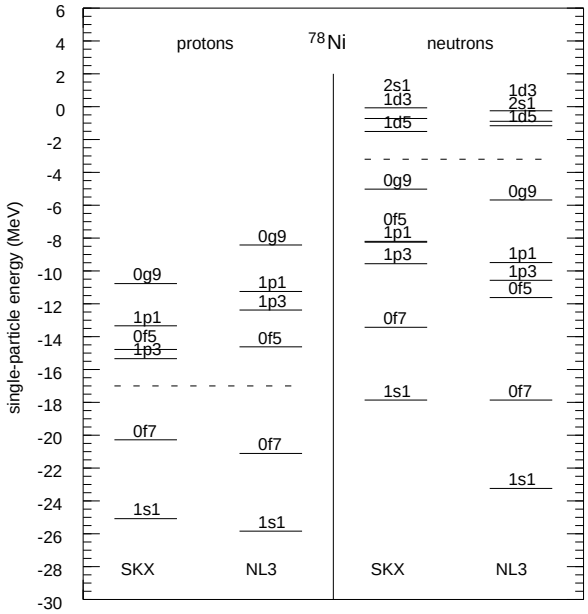

Figure 7: Theoretical proton and neutron single-particle energies for ^{78}Ni. The orbits are labeled by $(n, \ell, 2j)$, and the dashed line is the Fermi energy.

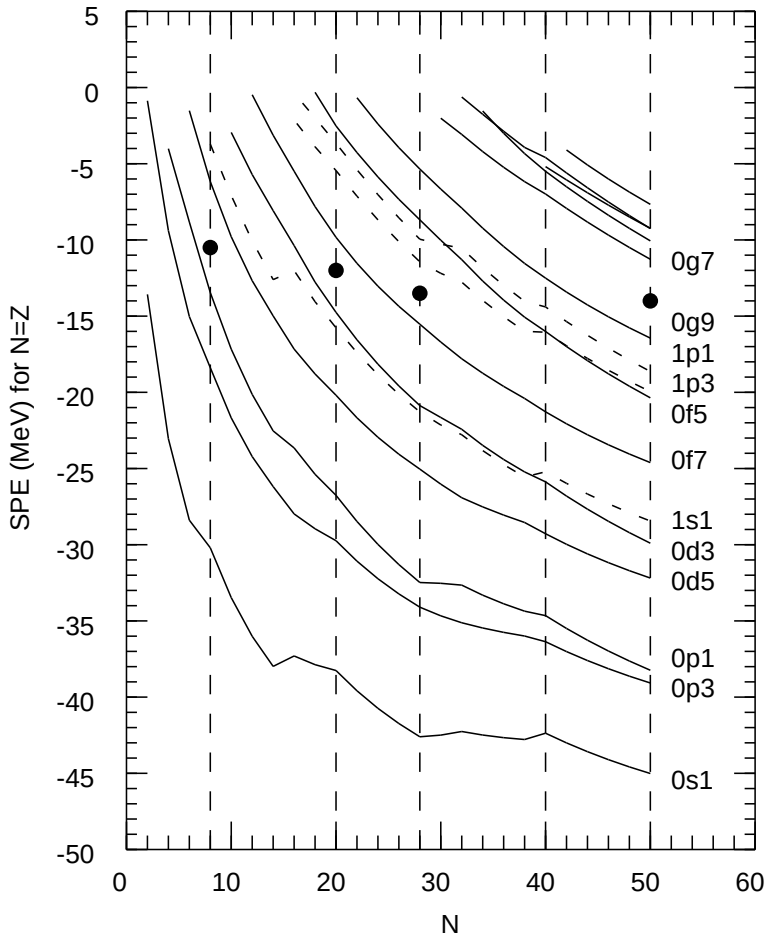

Figure 8: Neutron single-particle energies for nuclei with $N = Z$ as a function of neutron number obtained with the SKX spherical Hartree-Fock calculation. The vertical dashed lines show some of the magic number discussed in the text. The large circles show the approximate Fermi energies for ^{16}O, ^{40}Ca, ^{56}Ni and ^{100}Sn. The orbits are labeled by $(n, \ell, 2j)$.

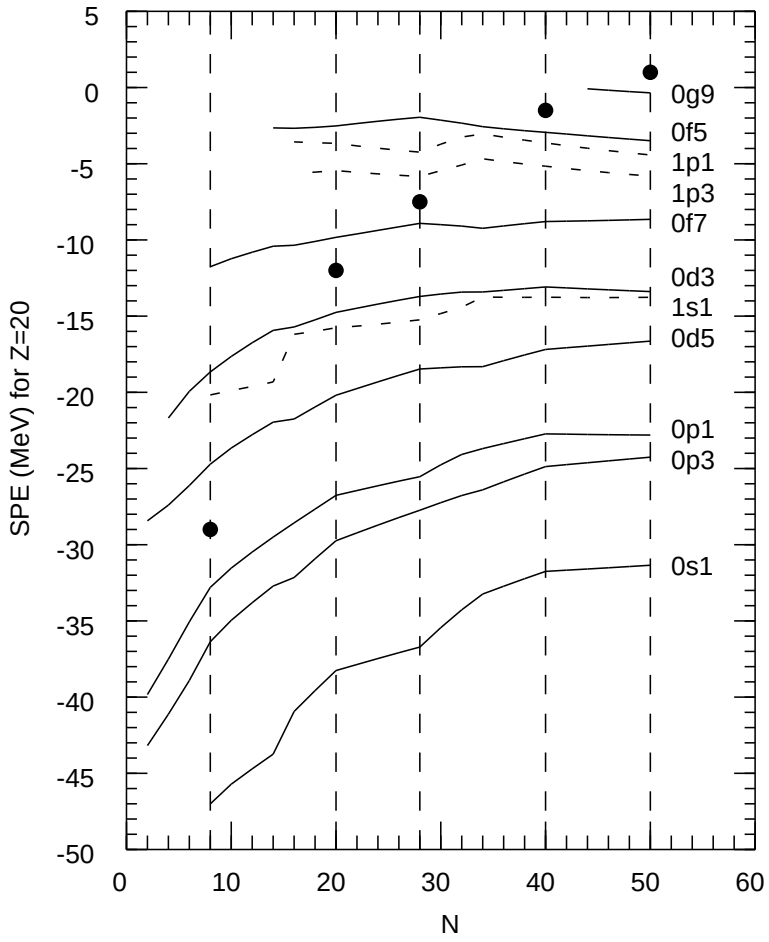

Figure 9: Neutron single-particle energies for the calcium isotopes obtained with the SKX spherical Hartree-Fock calculation. The vertical dashed lines show some of the magic number discussed in the text. The large circles show the approximate Fermi energies for ^{28}Ca, ^{40}Ca, ^{48}Ca, ^{60}Ca and ^{70}Ca. The orbits are labeled by $(n, \ell, 2j)$.

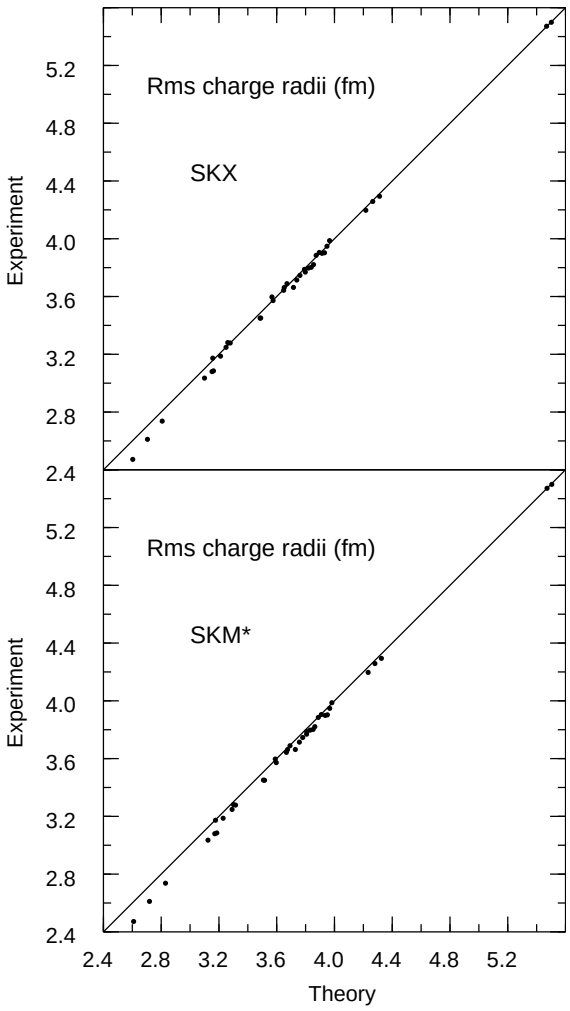

Figure 10: Comparison of experimental and theoretical rms charge radii for the Skyrme interactions SKX (top panel) and SKM* (bottom panel).

The experimental and theoretical rms charge radii are compared in Fig. (12.10). The experimental radii are from Refs. [19] and [20], with those with the smallest errors selected in the case of more than one data set. The error in the experimental data is typically smaller than the size of the data points. The Hartree-Fock results for the two interactions SKM* (bottom panel) and SKX (top panel) are obtained with the CM (fractional) occupations (those obtained with ESP occupations are essentially the same). The excellent overall agreement between experiment and theory is not surprising since these rms charge radii are used to constrain the values of the Skyrme parameters. The deviations increase for light nuclei going up to 5% for ^{12}C. In general one may expect the mean-field approximation to be less valid for light nuclei.

In order to illustrate how the features of the charge density are built out of the

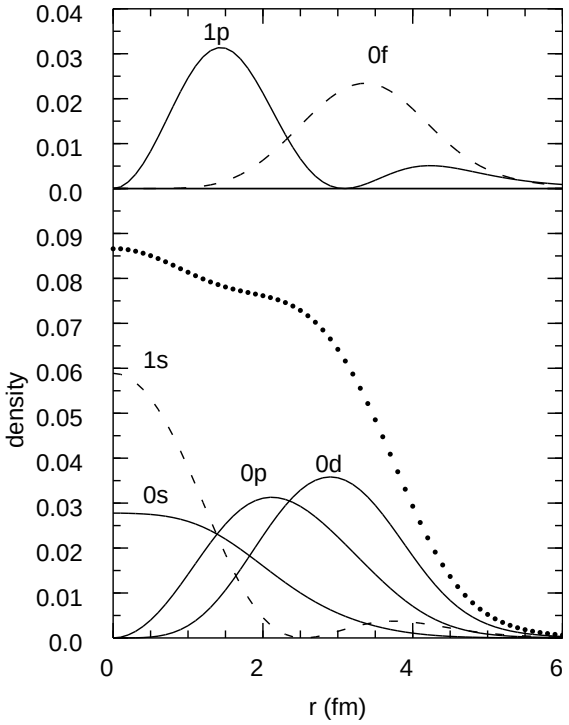

Figure 11: The point-proton density (points) of ^{40}Ca in the SKX model with a closed shell configuration. The total density is decomposed in terms of the contributions from the individual filled orbitals. In the upper panel the densities for protons in the orbitals just above the Fermi-surface of ^{40}Ca are shown, for eight protons in the $0f_{7/2}$ orbit and for four protons in the $1p_{3/2}$ orbit.

specific shell model orbitals which are filled, we show in Fig. (12.11) the point-proton density of ^{40}Ca (points) obtained with SKX with the assumption that the $0s, 0p, 1s$ and $0d$ orbits are filled. The individual contributions of the filled orbits to the proton density are shown. The $0s$ and $1s$ are the contributions from two protons in each of these orbits respectively. The $0p$ indicates the sum of the four protons in the $0p_{3/2}$ orbit and two protons in the $0p_{1/2}$ orbit. The $0d$ indicates the sum of the six protons in the $0d_{5/2}$ orbit and four protons in the $0d_{3/2}$ orbit. In the top panel the densities associated with the (unfilled) valence orbits above the Fermi-surface are shown; $0f$ for eight protons in the $0f_{7/2}$ orbit and $1p$ for four protons in the $1p_{3/2}$ orbit.

For comparison between experimental and theoretial charge densities I consider in Fig. (12.12) a set of data for nuclei that cover a wide mass range and which for which there is the good electron scattering data: ^{28}Si from Ref. [21], ^{32}S from Ref. [22] (circles) and Ref. [23] (squares), ^{40}Ca and ^{48}Ca from Ref. [24], ^{50}Ti and ^{52}Cr from Ref. [25], ^{54}Fe from Ref. [26], ^{58}Ni from Refs. [27] (circles) and [26] (squares),

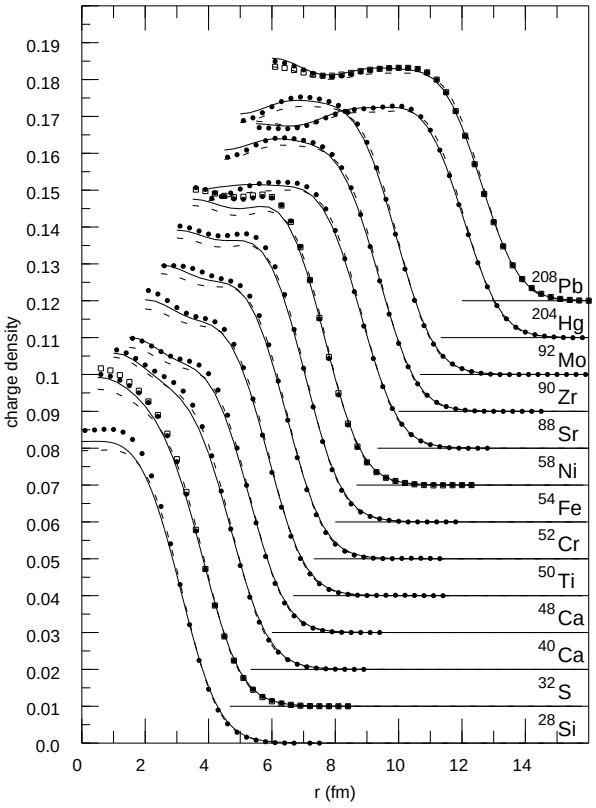

Figure 12: Experimental charge-density distributions (filled circles) compared with the SKX (dashed lines) and SKM* (solid lines) calculations. The charge density units are e fm^{-3}. Beyond ^{28}Si the curves and data have been progressively offset by 1 fm and 0.01 in the charge density. The data are discussed in the text.

^{88}Sr from Ref. [28], ^{90}Zr from Ref. [29], ^{92}Mo from Ref. [30], ^{204}Hg from Ref. [31], and ^{208}Pb from Refs. [32] (circles) and [33] (squares). The data are compared to the SKX (dashed lines) and SKM* (solid lines) are calculations. Both SKX and SKM* nicely reproduce the nucleus-dependent oscillations. The hamiltonian parameters are obtained from fits to the rms charge radii, binding energies and excited state energies of these nuclei. Thus the good agreement between experiment and theory for the nucleus-dependent oscillations observed in Fig. (12.12) are not a result of a "fit" to these data but arise naturally from the underlying shell structure.

The main difference between the SKX and SKM* results is that the interior density is about 5% higher with SKM* compared to SKX, with SKM* in best overall agreement with experiment. Close inspection of the curves in Fig. (12.12) in the region where the density falls off reveals a slightly larger surface diffuseness for SKM* com-

pared to SKX (the dashed line for SKX is slightly steeper than the line for SKM* in the surface). The correlation between the increased interior height with the increased diffuseness (when the rms radius is the same) is consistent with what is expected from the Fermi model shown in Fig. 3.2. The change between SKX and SKM* corresponds to a $\Delta a = 0.036$ fm for ^{208}Pb. The change in the diffuseness is connected to the difference in the density-dependent part of the hamiltonians, namely $[\rho(r)]^{1/2}$ for SKX and $[\rho(r)]^{1/6}$ for SKM*. There is agreement between experiment and theory to an accuracy of about 2% or better for $r > 1$ fm with SKM*. As discussed above, this is about the level of the accuracy with which these densities can be experimentally determined.

In the overview of Fig. (12.12) one can observe several interesting features associated with how the quantum waves change with shell structure and mass. Between ^{28}Si and ^{32}S in the sd shell there is a large increase in the interior density due to the filling of the $1s_{1/2}$ orbital (see also [23]). Likewise between ^{204}Hg and ^{208}Pb there is a large increase in the interior related to the filling of the $2s_{1/2}$ orbital. Between ^{40}Ca and ^{48}Ca one observes a redistribution of the charge (proton) density due to the interaction with the valence $0f_{7/2}$ neutrons. The theoretical density distributions for the sequence ^{48}Ca, ^{50}Ti, ^{52}Cr and ^{54}Fe show a smoothly varying trend due to dominance of the proton $0f_{7/2}$ subshell filling.

12.4.4 Displacement energies

The displacement energy is the binding energy difference between mirror nuclei (those with the same atomic number A but with the proton number Z and neutron number N interchanged). For a given mass A and isospin T the displacement energy is:

$$D(A,T) = BE(A,T_z^<) - BE(A,T_z^>), \tag{12.33}$$

where $T = \mid T_z^< \mid = \mid T_z^> \mid$, $BE(A,T_z^<)$ is the binding energy of the proton-rich nucleus and $BE(A,T_z^>)$ is the binding energy of the neutron-rich nucleus. If the nuclear force is charge symmetric, then this binding energy difference can be related to the well-understood Coulomb interaction between the protons. However, it was shown by Nolen and Schiffer [34] that there is a systematic increase in the experimental displacement energies compared to those calculated with a charge symmetric strong interaction (the Nolen-Schiffer anomaly). In the usual HF calculation one has both direct and exchange terms in the Coulomb-energy density functional. For the exchange one uses the Fermi-gas approximation which is a good approximation to the exact calculation [35]. The ground-state displacement energies obtained with the Coulomb plus Coulomb-exchange HF approach (from the SKXce interaction of [14]) are shown on the right-hand side of Fig. (12.13). One observes the systematic deviation between experiment and theory associated with the Nolen-Schiffer anomaly. For the heaviest

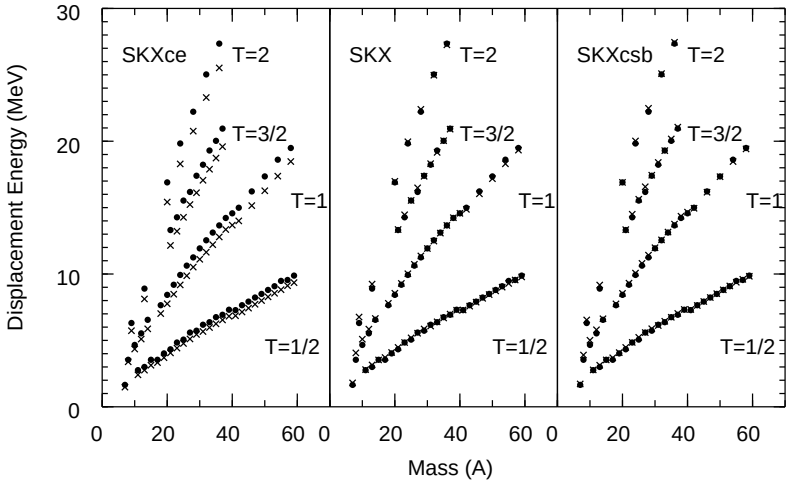

Figure 13: Ground-state displacement energies as a function of A for SKXce (with the normal Coulomb exchange term), SKX (without the exchange term) and SKXcsb (with the exchange term and with a CSB interaction). The experimental data are filled circles and the calculations are given as crosses.

nuclei the ratio shown in Fig. (12.14) goes to a constant value of about 1.06. It is well known [34] that the displacement energies are sensitive to the rms charge radii; the SKX interactions reproduce the experimental charge radii of ^{16}O, ^{40}Ca and ^{48}Ca to better than one percent (see Fig. 10 of [14]). The displacement energies are also sensitive to the rms radius of the valence orbits, and the SKX interactions give radii for the $d_{5/2}$ orbit in ^{17}O and the $0f_{7/2}$ orbit in ^{41}Ca which are within 2% of those deduced from the magnetic electron scattering form factors [36].

In the fit to closed-shell nuclei the displacement energy is represented by the pair of nuclei ^{48}Ni-^{48}Ca. The binding energy of ^{48}Ni is not measured but can be extrapolated to within an uncertainly of a few hundred keV from the $0f_{7/2}$ shell displacement energy systematics [37], [38], [39], [40], [41]. The recent discovery of ^{48}Ni [42] is consistent with the mass obtained from the $0f_{7/2}$ extrapolations.

In order to improve agreement with experiment it was found that the HF theory could be improved in two ways. One of them consists of leaving out the Coulomb exchange term, with the result shown in the middle panel of Figs. (12.13) and (12.14). This may be interpreted as a correction from nuclear correlation (configuration mixing) which happens to cancel the exchange term. This has been discussed in the general HF framework by Bulgac and Shaginyan [43], [44], [45] in terms of a surface-vibration contribution to the Coulomb correlation energy. I note that the relativistic approach leaves out the Coulomb exchange by default, and that most Woods-Saxon programs [46], [47] leave out the Coulomb exchange.

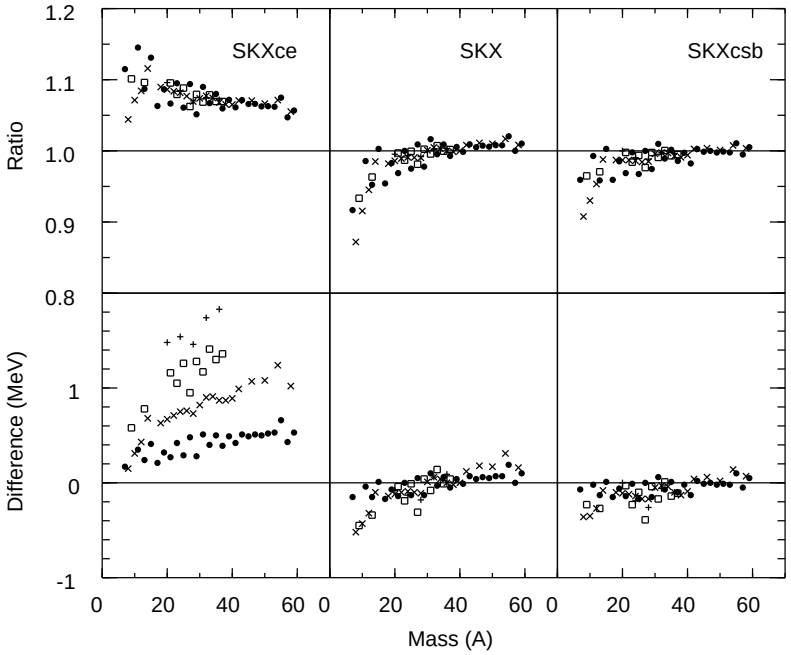

Figure 14: Top: the ratio experiment/theory for the data shown in Fig. (12.13); Bottom: the difference experiment–theory. The symbols are filled circles for $T = 1/2$, crosses for $T = 1$, squares for $T = 3/2$ and plus signs for $T = 2$.

Another way to improve agreement with experiment is to add a charge-symmetry breaking (CSB) term to the Skyrme interaction which can be expressed as a change to the proton-proton (pp) and neutron-neutron (nn) s-wave interactions:

$$V^{pp}_{\rm Skyrme} = t_0(1 - x_0)(1 + x_a)\delta$$

and

$$V^{nn}_{\rm Skyrme} = t_0(1 - x_0)(1 - x_a)\delta, \tag{12.34}$$

where x_a is a parameter to be determined.

The $A = 48$ closed shell nuclei require $x_a = -0.014 \pm 0.002$ for the interaction called SKXcsb The results for the all displacement energies are shown on the right-hand side of Figs. (12.13) and (12.14).

A correct description of the displacement energies within the mean field approximation is obviously important for understanding the position of the proton drip lines. $A = 99$ is the heaviest $T = 1/2$ isobaric doublet for which the proton-rich nucleus is expected to be bound. The calculated displacement energies for $A = 99$ are -13.54 MeV (SKXce), -14.03 MeV MeV (SKX) and -14.15 MeV (SKXcsb). The introduction of the extra terms in the Skyrme hamiltonian which are needed for the displacement energies, also has an influence on the neutron drip line; for example

the binding energy of ^{176}Sn is predicted to be -1158.0 MeV (SKXce), -1149.0 MeV (SKX) and -1148.4 MeV (SKXcsb).

The SKXcsb interaction should ultimately be related to the CSB nucleon-nucleon (NN) scattering data. Analysis of the NN scattering data together with a model for the NN interaction gives [48], [49] a value of $\Delta a_{CSB} = a_{pp} - a_{nn} = 1.5 \pm 0.5$ fm for the difference in the pp and nn scattering lengths. Modern NN potentials such as the AV18 [50] and CDbonn99 [51] are designed to reproduce this difference. It is not easy to interpret the CSB contribution to the displacement energies directly in terms of a NN potential due the short-range nuclear correlations and their dependence on the strong NN potential. Probably the most realistic way to do this is to consider the CSB contribution to the displacement energies obtained with the variational Monte Carlo approach for $A = 7$ [52] and the BHF approach for $A = 15$ and $A = 17$ [51]. For example, the CSB displacement energy for the $A = 17$, $d_{5/2}$ state is 92 keV with AV18 [51] to be compared with 355 keV with SKXcsb. From these comparisons one finds that the effect of the empirical CSB interaction obtained for SKXcsb is a factor of 3−4 larger than expected from AV18 or CDbonn99. Thus one concludes that either there is a significant NNN or many-body CSB contribution whose origin is unknown, or that a major part of the displacement energy anomaly is due to nuclear correlations. Possible many-body CSB effects at the quark level have recently been examined [53], [54].

The systematics associated with the Coulomb displacement energies can be used to obtain theoretical binding-energies of proton-rich nuclei from the experimental binding energies of neutron-rich nuclei. The displacement energies of Eq. (12.33) can be modeled on smooth systematics [38], [39], [55]; shell-model configuration mixing which contains the Coulomb and CSB interactions [37], [40], [41]; or on the mean-field models. One can combine the experimental binding energy for the neutron-rich nucleus $BE(A, T_z^>)_{exp}$ together with the calculated value for $D(A, T)$ to give an extrapolation for the proton-rich binding energy:

$$BE(A, T_z^<) = D(A, T)_{\text{theory}} + BE(A, T_z^>)_{exp}. \tag{12.35}$$

For most of the nuclei out to the proton drip line the binding energy $BE(A, T_z^>)_{exp}$ of the mirror neutron-rich nucleus is known to 100 keV or better. This method has been used to predict the binding energies and the drip line for $Z = 19 - 28$ [37], [41], [38] and $Z = 28 - 38$ [41], [56]. The latter calculations have been used [56] to study the rapid-proton (rp) capture path in the astrophysical explosive hydrogen burning process [57]. The rp-process in light nuclei depends upon theoretical calculations of the displacement energies of ground and excited states and upon the spectroscopic factors which enter into the (p,γ) reaction [58], [59].

References

[1] T. R. H. Skyrme. Philos. Mag. **1**, 1043 (1956); Nucl. Phys. **9**, 615 (1959); **9**, 635 (1959).

[2] D. Vautherin and D. M. Brink, Phys. Rev. C **5**, 626 (1972).

[3] C. B. Dover and N. Van Giai, Nucl. Phys. **A190**, 373 (1972).

[4] W. Kohn and L. J. Sham, Phys. Rev. **140** A1133 (1965).

[5] R. M. Dreizler and E. K. U. Gross, "Density Functional Theory: An Approach to the Quantum Many-Body Problem", (Springer, Berlin, 1990).

[6] M. M. Sharma, G. Lalazissis, J. Konig and P. Ring, Phys. Rev. Lett. **74**, 3744 (1995).

[7] B. Friedman and V. R. Pandharipande, Nucl. Phys. **A361**, 502 (1981).

[8] B. A. Brown, Phys. Rev. Lett. **85**, 5296 (2000).

[9] S. Typel and B. A. Brown, Phys. Rev. C **64**, 027302 (2001).

[10] B. A. Brown, W. A. Richter and R. Lindsay, Phys. Lett. B **483**, 49 (2000).

[11] S. Goriely, F. Tondeur and J. M. Pearson, At. Data Nucl. Data Sheets **77**, 311 (2001).

[12] J. D. Walecka, Ann. Phys. (N. Y.) **83**, 491 (1974).

[13] G. A. Lalazissis, J. König and P. Ring, Phys. Rev. C **55**, 540 (1997).

[14] B. A. Brown, Phys. Rev. C **58**, 220 (1998).

[15] S. O. Backman, G. E. Brown and J. A. Niskanen, Phys. Rep. **124**, 1 (1985).

[16] C. Mahaux, P. F. Bortignon, R. A. Broglia and C. G. Dasso, Phys. Rep. **120**, 1 (1985).

[17] I. Hamamoto, H. Sagawa and X . Z. Zhang, Phys. Rev. C **64**, 024313 (2001).

[18] J. Bartel, P. Quentin, M. Brack, C.Guet, and M. B. Hakansson, Nucl. Phys. **A386**, 79 (1982).

[19] H. de Vries, C. W. de Jager and C. de Vries, At. Data and Nucl. Data Tables **36**, 495 (1987).

[20] G. Fricke, C. Bernhardt, K. Heilig, L. A. Schaller, L. Shellenberg, E. B. Shera and C. W. de Jager, At. Data and Nucl. Data Sheets **60**, 177 (1995).

[21] H. Miessen, Ph.D. Thesis, University of Mainz, 1982 (unpublished).

[22] D. Rychel, Ph.D. Thesis, University of Mainz, 1983 (unpublished)

[23] J. Wesseling, C. W. de Jager, L. Lapikas, H. de Vries, L. W. Fagg, M. N. Harakeh, N. Kalantar-Nayestanaki, R. A. Lindgren, E. Moya De Guerra, and P. Sarriguren, Phys. Rev. **C55**, 2773 (1997)

[24] H. J. Emrich, Ph.D. Thesis, University of Mainz, 1983 (unpublished)

[25] J. W. Lightbody, Jr., J. B. Bellicard, J. M. Cavedon, B. Frois, D. Goutte, m. Huet, Ph. Leconte, A. Nakada, Phan Xuan Ho, S. K. Platchkov, S. Turck-Chieze, C. W. de Jager, J. J. Lapikas, and P. K. A. de Witt Huberts. Phys. Rev. **C27**, 113 (1983)

[26] H. D. Wohlfahrt, Habilitationsschrift, University of Mainz, 1976 (unpublished)

[27] G. Beuscher, Ph.D. Thesis, University of Mainz, 1983 (unpublished)

[28] G. Stephan, Ph.D. Thesis, University of Mainz, 1976 (unpublished)

[29] H. Rothhaas, Ph.D. Thesis, University of Mainz, 1976 (unpublished)

[30] B. Dreher, Phys. Rev. Lett **35**, 716 (1975)

[31] A. J. C. Burghardt, Ph.D. Thesis, University of Amsterdam, 1989 (unpublished)

[32] H. Euteneuer, J. Friedrich and N. Vögler, Nucl. Phys. **A298**, 452 (1978)

[33] J. L. Friar, J. Heisenberg and J. W. Negele, Proceedings of the June Workshop in Intermediate Energy Electromagnetic Interactions, edited by A. M. Bernstein, Massachusetts Institute of Technology (1977), p. 325

[34] J. A. Nolen and J.P. Schiffer, Ann. Rev. Nucl. Sci. **19**, 471 (1969).

[35] C. Titin-Schnaider and P. Quentin, Phys. Lett. **49B**, 397 (1974).

[36] T. Suzuki, H. Sagawa and A. Arima, Nucl. Phys. **A536**, 141 (1992)

[37] B. A. Brown, Phys. Rev. C **43**, R1513 (1991); C **44**, 924 (1991).

[38] B. J. Cole, Phys. Rev. C **54**, 1240 (1996).

[39] Phys. Rev. C **58**, 2831 (1998).

[40] W. E. Ormand, Phys. Rev. C **53**, 214 (1996); Phys. Rev. C **55**, 2407 (1997).

[41] W. E. Ormand, Phys. Rev. C **55**, 2407 (1997).

[42] B. Blank et al., Phys. Rev. Lett. **84**, 1116 (2000).

[43] A. Bulgac and V. R. Shaginyan, Nucl. Phys. **A601**, 103 (1996).

[44] A. Bulgac and V. R. Shaginyan, Phys. Lett. B **469**, 1 (1999).

[45] A. Bulgac and V. R. Shaginyan, Eur. Phys. J. A **5**, 247 (1999).

[46] R. Sherr and G. Bertsch, Phys. Rev. C **32**, 1809 (1985).

[47] B. A. Brown, A. Csoto and R. Sherr, Nucl. Phys. **A597**, 66 (1996).

[48] G. A. Miller, B. M. K. Nefkens and I. Slaus, Phys. Rep. **194**, 1 (1990).

[49] G. Q. Li and R. Machleidt, Phys. Rev. C **58**, 3153 (1998).

[50] R. B. Wiringa, V. G. J. Stoks and R. Schiavilla, Phys. Rev. C **49**, 2950 (1995).

[51] C. Harzer, H. Muther and R. Machleidt, Phys. Lett. B **459**, 1 (1999).

[52] B. S. Pudliner, V. R. Pandharipande, J. Carlson, S. C. Pieper, and R. B. Wiringa, Phys. Rev. C **56**, 1720 (1997).

[53] K. Tsushima, K. Saito and A. W. Thomas, Phys. Lett. B **465**, 36 (1999).

[54] C. J. Horowitz and J. Piekarewicz, Phys. Rev. C **63**, 01330(R), (2000).

[55] B. A. Brown and P. G. Hansen, Phys. Lett. B **391** (1996).

[56] B. A. Brown, R. Clement, H. Schatz, W. A. Richter, A. Volya and W. A. Richter, Phys. Rev. C65, 045802 (2002).

[57] H. Schatz et al., Phys. Rep. **294**, 167 (1998).

[58] H. T. Fortune, R. Sherr and B. A. Brown, Phys. Rev. C **61**, 057303 (2000).

[59] H. Herndl, J. Goerres, M. Wiescher, B. A. Brown and L. Van Wormer, Phys. Rev. C **52**, 1078 (1995).

13 Angular Momentum and Tensor Algebra

13.1 Angular momentum coupling

The total angular momentum of a system is conserved. The total angular momentum may be composed of the sum of orbital and intrinsic spins, or it may be composed of the sum of the angular momenta $\vec{j}$ for two or more nucleons. In this section $\vec{J}$ will denote a generalized angular momentum, it could be orbital, intrinsic-spin or some combinations of both. Results for the coupling of up to four angular momenta and the notation relating these to the $3j$, $6j$ and $9j$ coefficients will be summarized.

Explicit expressions for the $3j$, $6j$ and $9j$ coefficients are given in [1], [2] and [3]. Computer programs for these can be found in the books by Thompson [3] and [4] as well as in the OXBASH shell-model computer package [5]. The $3j$ and $6j$ coefficients are tabulated in many references for small values of angular momentum and in [6] for small and intermediate values of angular momentum. Some of the more useful special relations and values for these coefficients will be given below. Many others are available in the literature [1] [2] [3] [7] [8] [9] [10].

13.1.1 Coupling of Two Angular Momenta

The coupling of two angular momenta will be considered first. The total angular momentum, $\vec{J} = \vec{J_1} + \vec{J_2}$, is conserved, and the quantum numbers J associated with the vector $\vec{J}$ take on the integer values from $J_{min} = \mid J_1 - J_2 \mid$ to $J_{max} = J_1 + J_2$. This condition on the J values will be referred to as the triangle condition, $\Delta(J_1 J_2 J)$. The sum of the J values in the triangle condition, $J_t = J_1 + J_2 + J$ in this case, is always an integer, and the factor $(-1)^{2J_t} = 1$ can be multiplied in order to simplify a phase factor.

The wave functions associated with the states $\mid J_1 J_2 JM >$ are linear combinations of the states $\mid J_1 M_1 J_2 M_2 >$

$$\mid J_1 J_2 JM >= \sum_{M_1 M_2} \mid J_1 M_1 J_2 M_2 >< J_1 M_1 J_2 M_2 \mid J_1 J_2 JM >, \qquad (13.1)$$

where $M_1 + M_2 = M$. The Clebsch-Gordan coefficients [1] are a specific normalization and phase convention for the overlaps

$$< J_1 M_1 J_2 M_2 \mid JM > \equiv < J_1 M_1 J_2 M_2 \mid J_1 J_2 JM > .$$

In particular, they are all real and

$$< J_1 M_1 J_2 M_2 \mid J_{max}, M = J_{max} >= 1.$$

Since they are real,

$$< J_1M_1J_2M_2 \mid JM >=< JM \mid J_1M_1J_2M_2 > . \tag{13.2}$$

The Clebsch-Gordan coefficients can be used, for example, to couple the two wave functions $\Phi_a^{J_1}$ and $\Phi_b^{J_2}$ to the product wave function $\Phi_c(J_1,J_2)^J$

$$\Phi_c(J_1,J_2)^J_M = \sum_{M_1M_2} < J_1M_1J_2M_2 \mid J_1J_2JM > \Phi^{J_1}_{a,M_1}\Phi^{J_2}_{b,M_2} \equiv [\Phi_a^{J_1} \otimes \Phi_b^{J_2}]^J_M. \tag{13.3}$$

The Clebsch-Gordan coefficients obey the orthonormality conditions

$$\sum_{J,M} < J_1M_1J_2M_2 \mid JM >< J_1M_1'J_2M_2' \mid JM >= \delta_{M_1M_1'}\delta_{M_2M_2'}, \tag{13.4}$$

and

$$\sum_{M_1M_2} < J_1M_1J_2M_2 \mid JM >< J_1M_1J_2M_2 \mid J'M' >= \delta_{JJ'}\delta_{MM'}. \tag{13.5}$$

The symmetry properties of the Clebsch-Gordan coefficients are

$$< J_1M_1J_2M_2 \mid JM >= (-1)^{J_1+J_2-J} < J_2M_2J_1M_1 \mid JM >, \tag{13.6}$$

$$< J_1M_1J_2M_2 \mid JM >= (-1)^{J_1+J_2-J} < J_1,-M_1J_2,-M_2 \mid J,-M >, \tag{13.7}$$

and

$$< J_1M_1J_2M_2 \mid JM >= (-1)^{J_2+M_2}\sqrt{\frac{2J+1}{2J_1+1}} < J_2,-M_2JM \mid J_1M_1 > . \tag{13.8}$$

The $3j$ coefficient $\begin{pmatrix} J_1 & J_2 & J \\ M_1 & M_2 & M \end{pmatrix}$ is related to the Clebsch-Gordan coefficient by

$$< J_1M_1J_2M_2 \mid JM > \equiv (-1)^{J_1-J_2+M}\sqrt{2J+1}\begin{pmatrix} J_1 & J_2 & J \\ M_1 & M_2 & -M \end{pmatrix}, \tag{13.9}$$

where the sum of the M values in the bottom row must be zero: $M_1 + M_2 - M = 0$. The symmetry properties of the Clebsch-Gordan coefficients are given compactly in terms of those for the $3j$ coefficients and can be summarized by

$$\begin{pmatrix} J_1 & J_2 & J_3 \\ M_1 & M_2 & M_3 \end{pmatrix} = (-1)^p \begin{pmatrix} J_a & J_b & J_c \\ M_a & M_b & M_c \end{pmatrix}, \tag{13.10}$$

where $p = J_a + J_b + J_c$ when the $3j$ on the right is obtained by the interchange of any two neighboring columns (a permutation of the columns) of the $3j$ on the

left. Since p always an integer, two such interchanges gives $(-1)^{2p} = 1$. In addition, $p = J_a + J_b + J_c$ if the top row is unchanged but the bottom row is changed in sign. ($M_1 = -M_a$, $M_2 = -M_b$ and $M_3 = -M_c$). The orthogonality relations for the $3j$ coefficients which are equivalent to Eqs. (13.4) and (13.5) take the form

$$\sum_{J,M}(2J+1)\begin{pmatrix} J_1 & J_2 & J \\ M_1 & M_2 & M \end{pmatrix}\begin{pmatrix} J_1 & J_2 & J \\ M_1' & M_2' & M \end{pmatrix} = \delta_{M_1 M_1'}\delta_{M_2 M_2'}, \tag{13.11}$$

and

$$\sum_{M_1,M_2}(2J+1)\begin{pmatrix} J_1 & J_2 & J \\ M_1 & M_2 & M \end{pmatrix}\begin{pmatrix} J_1 & J_2 & J' \\ M_1 & M_2 & M' \end{pmatrix} = \delta_{JJ'}\delta_{MM'}. \tag{13.12}$$

Useful expressions for some special cases are

$$\begin{pmatrix} J & 0 & J \\ -M & 0 & M' \end{pmatrix} = \frac{(-1)^{J-M}\,\delta_{MM'}}{\sqrt{2J+1}}, \tag{13.13}$$

$$\begin{pmatrix} J & 1 & J \\ -M & 0 & M' \end{pmatrix} = \frac{(-1)^{J-M}\,M\,\delta_{MM'}}{\sqrt{J(2J+1)(J+1)}}, \tag{13.14}$$

and

$$\begin{pmatrix} J & 2 & J \\ -M & 0 & M' \end{pmatrix} = \frac{(-1)^{J-M}\,[3M^2 - J(J+1)]\,\delta_{MM'}}{\sqrt{(2J-1)J(2J+1)(J+1)(2J+3)}}. \tag{13.15}$$

13.1.2 Coupling of Three Angular Momenta

In this section we use the notation $\mid (J_1 J_2 J_{12}) J_3 J M >$ for the three particle wave functions formed from the Clebsch-Gordan coupling of J_1 and J_2 to make J_{12} and then the Clebsch-Gordan coupling of J_{12} to J_3 to make the total the total angular momutum J and projection M. The wave functions may require other quantum numbers for their complete specification, but only the explicit representation for J is required in this section. The three angular momenta can be coupled in various ways. For example,

$$\mid (J_1 J_2 J_{12}) J_3 J M >= \sum_{M_{12} M_3} < J_{12} M_{12} J_3 M_3 \mid J M > \mid (J_1 J_2 J_{12} M_{12}) J_3 M_3 >$$

$$= \sum_{M_1 M_2 M_3} < J_{12} M_{12} J_3 M_3 \mid J M >< J_1 M_1 J_2 M_2 \mid J_{12} M_{12} > \mid J_1 M_1 J_2 M_2 J_3 M_3 >, \tag{13.16}$$

and

$$\mid J_1(J_2J_3J_{23})J'M' >= \sum_{M_{23}M_1'} < J_1M_1'J_{23}M_{23} \mid J'M' >\mid J_1M_1'(J_2J_3J_{23}M_{23}) >$$

$$= \sum_{M_1'M_2'M_3'} < J_1M_1'J_{23}M_{23} \mid J'M' >< J_2M_2'J_3M_3' \mid J_{23}M_{23} >\mid J_1M_1'J_2M_2'J_3M_3' > . \tag{13.17}$$

The overlaps between these two ways of coupling are defined in terms of the $6j$ coefficients

$$< (J_1J_2J_{12})J_3JM \mid J_1(J_2J_3J_{23})J'M' >=$$

$$= \delta_{JJ'}\delta_{MM'} \sum_{M_1M_2M_3} < J_{12}M_{12}J_3M_3 \mid JM >< J_1M_1J_2M_2 \mid J_{12}M_{12} >$$

$$\times < J_1M_1J_{23}M_{23} \mid JM >< J_2M_2J_3M_3 \mid J_{23}M_{23} >$$

$$\equiv (-1)^{J_1+J_2+J_3+J}\sqrt{(2J_{12}+1)(2J_{23}+1)} \begin{Bmatrix} J_1 & J_2 & J_{12} \\ J_3 & J & J_{23} \end{Bmatrix}, \tag{13.18}$$

and thus

$$\mid J_1(J_2J_3J_{23})JM >= \sum_{J_{12}} (-1)^{J_1+J_2+J_3+J}\sqrt{(2J_{12}+1)(2J_{23}+1)}$$

$$\times \begin{Bmatrix} J_1 & J_2 & J_{12} \\ J_3 & J & J_{23} \end{Bmatrix} \mid (J_1J_2J_{12})J_3JM > . \tag{13.19}$$

The allowed values of J are restricted by the triangle conditions $\Delta(J_1J_2J_{12})$, $\Delta(J_3JJ_{12})$, $\Delta(J_3J_2J_{23})$ and $\Delta(J_1JJ_{23})$, as represented by the circles in

$$\begin{Bmatrix} o & o & o \\ & & \end{Bmatrix}, \begin{Bmatrix} & & o \\ o & o & \end{Bmatrix}, \begin{Bmatrix} & o & \\ o & & o \end{Bmatrix} \text{ and } \begin{Bmatrix} o & & \\ & o & o \end{Bmatrix}.$$

The symmetry properties of the $6j$ coefficient can be summarized by

$$\begin{Bmatrix} J_1 & J_2 & J_3 \\ J_1' & J_2' & J_3' \end{Bmatrix} = \begin{Bmatrix} J_a & J_b & J_c \\ J_a' & J_b' & J_c' \end{Bmatrix}, \tag{13.20}$$

when the columns (a, b, c) are any permutation of the columns $(1, 2, 3)$. In addition,

$$\begin{Bmatrix} J_1 & J_2 & J_3 \\ J_1' & J_2' & J_3' \end{Bmatrix} = \begin{Bmatrix} J_1' & J_2' & J_3 \\ J_1 & J_2 & J_3' \end{Bmatrix}. \tag{13.21}$$

An orthogonality condition for the $6j$ coefficients is

$$\sum_{J_3} (2J_3+1)(2J_6+1) \begin{Bmatrix} J_1 & J_2 & J_3 \\ J_4 & J_5 & J_6 \end{Bmatrix} \begin{Bmatrix} J_1 & J_2 & J_3 \\ J_4 & J_5 & J_6' \end{Bmatrix} = \delta_{J_6J_6'}. \tag{13.22}$$

Another useful relation for the $6j$ coefficients is

$$\sum_k (-1)^{k+k_1+k_2}(2k+1)\left\{\begin{array}{ccc} k_1 & J_1' & k \\ J_2' & J_2 & J \end{array}\right\}\left\{\begin{array}{ccc} k_1 & k_2 & k \\ J_1' & J_1 & J_2'' \end{array}\right\}\left\{\begin{array}{ccc} k_1 & k_2 & k \\ J_2' & J_2 & J_1'' \end{array}\right\}$$
$$= (-1)^{J_1+J_2+J_1'+J_2'+J_1''+J_2''+J}\left\{\begin{array}{ccc} J_1 & J_2 & J \\ J_1'' & J_2'' & k_1 \end{array}\right\}\left\{\begin{array}{ccc} J_1' & J_2' & J \\ J_1'' & J_2'' & k_2 \end{array}\right\}. \tag{13.23}$$

When one of the arguments is zero, the $6j$ coefficient reduces to

$$\left\{\begin{array}{ccc} J_1 & J_2 & J_3 \\ J_4 & J_5 & 0 \end{array}\right\} = \frac{(-1)^{J_1+J_2+J_3}\,\delta_{J_5J_1}\,\delta_{J_4J_2}}{\sqrt{(2J_1+1)(2J_2+1)}}. \tag{13.24}$$

13.1.3 Coupling of Four Angular Momenta

The $9j$ coefficient is defined by the overlap between two ways of coupling four angular momenta

$$< (J_1J_3J_{13})(J_2J_4J_{24})J \mid (J_1J_2J_{12})(J_3J_4J_{34})J >$$
$$\equiv \sqrt{(2J_{13}+1)(2J_{24}+1)(2J_{12}+1)(2J_{34}+1)}\left\{\begin{array}{ccc} J_1 & J_2 & J_{12} \\ J_3 & J_4 & J_{34} \\ J_{13} & J_{24} & J \end{array}\right\}$$
$$\equiv \left[\begin{array}{ccc} J_1 & J_2 & J_{12} \\ J_3 & J_4 & J_{34} \\ J_{13} & J_{24} & J \end{array}\right]. \tag{13.25}$$

The $\{\,\}$ symbol with nine arguments is the $9j$ coefficient, and the $[\,]$ symbol with nine arguments will be referred to as the normalized $9j$ coefficient. The allowed values of J are restricted by the triangle condition associated with any row or column. The value of the $9j$ coefficient is unchanged for any even permutation of the rows or columns and changes only by a phase factor $(-1)^{J_1+J_2+J_{12}+J_3+J_4+J_{34}+J_{13}+J_{24}+J}$ for any odd permutation of the rows or columns. An orthogonality condition for the normalized $9j$ coefficients is

$$\sum_{J_{13}J_{24}}\left[\begin{array}{ccc} J_1 & J_2 & J_{12} \\ J_3 & J_4 & J_{34} \\ J_{13} & J_{24} & J \end{array}\right]\left[\begin{array}{ccc} J_1 & J_2 & J_{12}' \\ J_3 & J_4 & J_{34}' \\ J_{13} & j_{24} & J \end{array}\right] = \delta_{J_{12}J_{12}'}\delta_{J_{34}J_{34}'}. \tag{13.26}$$

Another sum rule which will be used later is (see page 367 in Ref. [2])

$$\sum_J (2J+1)\left\{\begin{array}{ccc} J_1 & J_2 & J_{12} \\ J_3 & J_4 & J_{34} \\ J_{13} & J_{24} & J \end{array}\right\}\left\{\begin{array}{ccc} J_1' & J_2' & J_{12}' \\ J_3' & J_4' & J_{34}' \\ J_{13} & J_{24} & J \end{array}\right\}$$

$$= \sum_J (2J+1) \left\{ \begin{array}{ccc} J_1 & J_4 & J \\ J_{24} & J_{12} & J_2 \end{array} \right\} \left\{ \begin{array}{ccc} J_1 & J_4 & J \\ J_{34} & J_{13} & J_3 \end{array} \right\}$$

$$\times \left\{ \begin{array}{ccc} J_{24} & J_{12} & J \\ J'_1 & J'_4 & J'_2 \end{array} \right\} \left\{ \begin{array}{ccc} J_{34} & J_{13} & J \\ J'_1 & J'_4 & J'_3 \end{array} \right\}. \tag{13.27}$$

(This last sum rule is related to the $12j$ coefficient of the "Second Kind" [2]). When one of the arguments is zero, the $9j$ coefficient reduces to

$$\left\{ \begin{array}{ccc} J_1 & J_2 & J_{12} \\ J_3 & J_4 & J_{34} \\ J_{13} & J_{24} & 0 \end{array} \right\} = \frac{(-1)^{J_2+J_3+J_{12}+J_{13}} \delta_{J_{12}J_{34}} \delta_{J_{13}J_{24}}}{\sqrt{(2J_{12}+1)(2J_{13}+1)}} \left\{ \begin{array}{ccc} J_1 & J_3 & J_{13} \\ J_4 & J_2 & J_{12} \end{array} \right\}. \tag{13.28}$$

The $9j$ coefficient can be expressed as a sum over $6j$ coefficients

$$\sum_{J'} (-1)^{2J'} (2J'+1) \left\{ \begin{array}{ccc} J_1 & J_3 & J_{13} \\ J_{24} & J & J' \end{array} \right\} \left\{ \begin{array}{ccc} J_2 & J_4 & J_{24} \\ J_3 & J' & J_{34} \end{array} \right\} \left\{ \begin{array}{ccc} J_{12} & J_{34} & J \\ J' & J_1 & J_2 \end{array} \right\}$$

$$= \left\{ \begin{array}{ccc} J_1 & J_2 & J_{12} \\ J_3 & J_4 & J_{34} \\ J_{13} & J_{24} & J \end{array} \right\}. \tag{13.29}$$

13.2 Tensors and reduced matrix elements

A tensor T^λ_μ of rank λ is a set of $2\lambda+1$ operators, $\mu = -\lambda, -\lambda+1, \ldots, \lambda$, which obey the following commutation relations with the angular momentum operators $J_\pm$ and J_z

$$[J_\pm, T^\lambda_\mu] = [J_x \pm iJ_y, T^\lambda_\mu] = \sqrt{\lambda(\lambda+1) - \mu(\mu\pm 1)}\, T^\lambda_{\mu\pm 1}, \tag{13.30}$$

and

$$[J_z, T^\lambda_\mu] = \mu T^\lambda_\mu. \tag{13.31}$$

The spherical harmonics, Y^λ_μ, are the most obvious example of a tensor of rank λ. Based on the components of Y^1_μ in cartesian coordinates, the components of a vector $\vec{r}$ can be arranged into a tensor of rank $\lambda = 1$ as: $r^1_0 = z$, and $r^1_\pm = \mp(x \pm iy)/\sqrt{2}$. The use of tensor operators reduces the M-state dependence of matrix elements to a simple dependence on the Clebsch-Gordan or $3j$ coefficient via the Wigner-Eckhart theorem

$$\begin{aligned} < JM \mid T^\lambda_\mu \mid J'M' > &= (-1)^{J-M} \begin{pmatrix} J & \lambda & J' \\ -M & \mu & M' \end{pmatrix} < J||T^\lambda||J' > \\ &= (-1)^{2\lambda} < J'M'\lambda\mu \mid JM > \frac{< J||T^\lambda||J' >}{\sqrt{(2J+1)}}, \end{aligned} \tag{13.32}$$

where $< J||T^\lambda||J' >$ is referred to as the reduced matrix element. The reduced matrix element convention followed in this book is common [1] [11] [9] [7] [8] [12] [13] but not universal. By multiplying Eq. (13.32) on both sides by the $3j$ coefficient, summing over M, μ and M' and using the $3j$ sum rule of Eq. (13.12), one obtains the inverse relation

$$\begin{aligned} < J||T^\lambda||J' > &= (2\lambda+1) \sum_{MM'} (-1)^{J-M} \begin{pmatrix} J & \lambda & J' \\ -M & \mu & M' \end{pmatrix} < JM \mid T^\lambda_\mu \mid J'M' > \\ &= \sum_{M\mu M'} (-1)^{J-M} \begin{pmatrix} J & \lambda & J' \\ -M & \mu & M' \end{pmatrix} < JM \mid T^\lambda_\mu \mid J'M' > . \end{aligned} \tag{13.33}$$

If T^λ_μ is a tensor of rank λ, then its Hermitian conjugate, $(T^\lambda_\mu)^+$, is not a tensor of rank λ. However, the quantity

$$\tilde{T}^\lambda_\mu \equiv (-1)^{p+\mu} (T^\lambda_{-\mu})^+ \tag{13.34}$$

is a tensor of rank λ. This can be proven by taking the Hermitian conjugate of both sides of Eqs. (13.30) and (13.31) and then making the substitution

$$(T^\lambda_\mu)^+ = (-1)^{\mu-p} \tilde{T}^\lambda_{-\mu}.$$

The arbitrary phase factor p is chosen for convenience. In order to ensure that the phase factors are real, one can choose $p = 0$ for integer values of λ, and $p = \lambda$ for half-integer values of λ. When the phase factor is real, $(-1)^{\mu-p} = (-1)^{p-\mu}$.

The relationship between $< J||T^\lambda||J' >$ and $< J'||\tilde{T}^\lambda||J >$ can be obtained by considering

$$\begin{aligned} &< JM \mid T^\lambda_\mu \mid J'M' > = < J'M' \mid (T^\lambda_\mu)^+ \mid JM >^+ \\ &= < J'M' \mid (T^\lambda_\mu)^+ \mid JM >^* = (-1)^{p-\mu} < J'M' \mid \tilde{T}^\lambda_{-\mu} \mid JM >^* \\ &= (-1)^{p-\mu+J'-M'} \begin{pmatrix} J' & \lambda & J \\ -M' & -\mu & M \end{pmatrix} < J'||\tilde{T}^\lambda||J >^* \\ &= (-1)^{p+J'-M} \begin{pmatrix} J & \lambda & J' \\ -M & \mu & M' \end{pmatrix} < J'||\tilde{T}^\lambda||J >^*, \end{aligned}$$

where Eq. (13.10) has been used in the last line together with $M = M' + \mu$. Thus by comparison with Eq. (13.32)

$$< J||T^\lambda||J' > = (-1)^{p+J'-J} < J'||\tilde{T}^\lambda||J >^*, \tag{13.35}$$

and

$$< J||\tilde{T}^\lambda||J' > = (-1)^{J-J'+p} < J'||T^\lambda||J >^*, \tag{13.36}$$

where * indicates complex conjugation. The spherical harmonics have the property that $\tilde{Y}^\lambda_\mu = Y^\lambda_\mu$, and hence

$$< J||Y^\lambda||J' > = (-1)^{J-J'} < J'||Y^\lambda||J >^* . \tag{13.37}$$

If wave functions are chosen to be real (as will be the case in this book), this expression simplifies further to

$$< J||Y^\lambda||J' > = (-1)^{J-J'} < J'||Y^\lambda||J > . \tag{13.38}$$

13.2.1 Special reduced matrix elements

Reduced matrix element can be calculated from Eq. (13.33) or more simply by evaluating the left-hand side of Eq. (13.32) for a particular choice of M, μ and M' for which the $3j$ coefficient does not vanish. Reduced matrix elements for many types of operators can be found in the literature [7] [9] [1] [2]. Some commonly used reduced matrix elements are

$$< J||1||J' > = \delta_{JJ'}\sqrt{2J+1}\,, \tag{13.39}$$

$$< J||J^{\lambda=1}||J' >= \delta_{JJ'}\sqrt{J(J+1)(2J+1)}\,, \tag{13.40}$$

and

$$< \ell||Y^{\lambda}||\ell' >= (-1)^{\ell}\sqrt{\frac{(2\ell+1)(2\lambda+1)(2\ell'+1)}{4\pi}}\begin{pmatrix} \ell & \lambda & \ell' \\ 0 & 0 & 0 \end{pmatrix} \tag{13.41}$$

It is clear from Eqs. (13.13) and (13.32) (and from rotational invariance) that the matrix element of a scalar is independent of M and can be written as

$$< JM \mid T^{\lambda=0} \mid J'M' >= \delta_{JJ'}\delta_{MM'} < J \mid T^{\lambda=0} \mid J >= \delta_{JJ'}\delta_{MM'}\frac{< J||T^{\lambda=0}||J >}{\sqrt{2J+1}}. \tag{13.42}$$

13.2.2 Products of tensor operators

The components of two tensors T^{λ_1} and U^{λ_2} can be combined to form a third tensor S^{λ} by

$$S^{\lambda}_{\mu} = [T^{\lambda_1} \otimes U^{\lambda_2}]^{\lambda}_{\mu} = \sum_{\mu_1\mu_2} < \lambda_1\mu_1\lambda_2\mu_2 \mid \lambda\mu > T^{\lambda_1}_{\mu_1}U^{\lambda_2}_{\mu_2} \tag{13.43}$$

It is straightforward to show that the components of S^{λ} satisfy Eqs. (13.30) and (13.31). Useful results for the reduced matrix elements involving products of tensor operators will be discussed in this section. The dot product (e.g. $\vec{\ell}\cdot\vec{s}$) is related to this tensor cross product by

$$T^{\lambda_1}\cdot U^{\lambda_1} = (-1)^{\lambda_1}\sqrt{(2\lambda_1+1)}\,[T^{\lambda_1}\otimes U^{\lambda_1}]^0. \tag{13.44}$$

When T and U operate in the same space (e.g. $[Y^{\lambda_1}(\hat{r})\otimes Y^{\lambda_2}(\hat{r})]^{\lambda}$), the reduced matrix element can be evaluated by summing over a complete set of intermediate states J_c [9]

$$\begin{aligned} < J_a||[T^{\lambda_1}\otimes U^{\lambda_2}]^{\lambda}||J_b >= (-1)^{J_a+\lambda+J_b}\sqrt{(2\lambda+1)} \\ \times \sum_{J_c}\begin{Bmatrix} J_b & J_a & \lambda \\ \lambda_1 & \lambda_2 & J_c \end{Bmatrix} < J_a||T^{\lambda_1}||J_c >< J_c||U^{\lambda_2}||J_b > . \end{aligned} \tag{13.45}$$

When T and U operate in different spaces (e.g. $\vec{\ell}\cdot\vec{s}$), one obtains [9]

$$\begin{aligned} < J_aJ_bJ||[T^{\lambda_1}\otimes U^{\lambda_2}]^{\lambda}||J_cJ_dJ' >= \sqrt{(2J+1)(2\lambda+1)(2J'+1)} \\ \times \begin{Bmatrix} J_a & J_b & J \\ J_c & J_d & J' \\ \lambda_1 & \lambda_2 & \lambda \end{Bmatrix} < J_a||T^{\lambda_1}||J_c >< J_b||U^{\lambda_2}||J_d >, \end{aligned} \tag{13.46}$$

where T^{λ_1} operates in the space of $\mid J_a >$ and $\mid J_c >$, and U^{λ_2} operates in the space of $\mid J_b >$ and $\mid J_d >$.

Special cases of Eq. (13.46) can be obtained from the reduction of the $9j$ coefficient given in Eq. (13.28). For $\lambda = 0$ Eq. (13.46) reduces to

$$< J_a J_b J || [T^{\lambda_1} \otimes U^{\lambda_1}]^0 || J_c J_d J' >= \delta_{JJ'} (-1)^{J_b + J_c + J + \lambda_1} \sqrt{\frac{2J+1}{2\lambda_1 + 1}}$$

$$\times \left\{ \begin{array}{ccc} J_a & J_b & J \\ J_d & J_c & \lambda_1 \end{array} \right\} < J_a || T^{\lambda_1} || J_c >< J_b || U^{\lambda_1} || J_d > . \tag{13.47}$$

For $\lambda_1 = 0$ and $T^{\lambda_1} = 1$, Eq. (13.46) reduces to

$$< J_a J_b J || U^{\lambda_2} || J_c J_d J' >= (-1)^{J_c + J_d + J + \lambda_2} \sqrt{(2J+1)(2J'+1)}$$

$$\times \delta_{J_a J_c} \left\{ \begin{array}{ccc} J_b & J_d & \lambda_2 \\ J' & J & J_a \end{array} \right\} < J_b || U^{\lambda_2} || J_d >, \tag{13.48}$$

and for $\lambda_2 = 0$ and $U^{\lambda_2} = 1$, Eq. (13.46) reduces to

$$< J_a J_b J || T^{\lambda_1} || J_c J_d J' >= (-1)^{J_a + J_b + J' + \lambda_1} \sqrt{(2J+1)(2J'+1)}$$

$$\times \delta_{J_b J_d} \left\{ \begin{array}{ccc} J_a & J_c & \lambda_1 \\ J' & J & J_b \end{array} \right\} < J_a || T^{\lambda_1} || J_c > . \tag{13.49}$$

Eq. (13.49) can be used, for example, to obtain the single-particle j-coupled matrix element of Y^λ

$$< \ell s j || Y^\lambda || \ell' s j' >= (-1)^{\ell + 1/2 + j' + \lambda} \sqrt{(2j+1)(2j'+1)}$$

$$\times \left\{ \begin{array}{ccc} \ell & \ell' & \lambda \\ j' & j & 1/2 \end{array} \right\} < \ell || Y^\lambda || \ell' >, \tag{13.50}$$

which can be combined with Eq. (13.41) and simplified [1] to obtain

$$< \ell s j || Y^\lambda || \ell' s j' >= \frac{1}{2} [1 + (-1)^{\ell + \lambda + \ell'}] (-1)^{j + 1/2}$$

$$\times \sqrt{\frac{(2j+1)(2\lambda+1)(2j'+1)}{4\pi}} \left(\begin{array}{ccc} j & \lambda & j' \\ 1/2 & 0 & -1/2 \end{array} \right). \tag{13.51}$$

13.2.3 Other convensions for reduced matrix elements

Other conventions for reduced matrix elements analogous to Eq. (13.32) often used in the literature are that of Lawson [14]

$$< JM \mid T^{\lambda}_{\mu} \mid J'M' >=< J'M'\lambda\mu \mid JM >< J||T^{\lambda}||J' >_{L}, \tag{13.52}$$

and that of Brink and Satchler [10], Towner [15] and Thompson [3]

$$< JM \mid T^{\lambda}_{\mu} \mid J'M' >= (-1)^{2\lambda} < J'M'\lambda\mu \mid JM >< J||T^{\lambda}||J' >_{B} . \tag{13.53}$$

An advantage of using Eq. (13.32) instead of one of the above alternatives is that Eq. (13.38) only involves a phase factor, and a disadvantage is the extra $\sqrt{2J+1}$ factor which appears in Eqs. (13.39) and (13.42). When expressions involving reduced matrix elements are taken from the literature, it is obviously important to be consistent and to know which convention is being used.

References

[1] A. R. Edmonds, *Angular Momentum in Quantum Mechanics*, (Princeton University Press, 1957).

[2] D. A. Varshalovich, A. N. Moskalev and V. K. Khersonskii, *Quantum Theory of Angular Momentum*, (World Scientific, 1988).

[3] W. J. Thompson, *Angular Momentum*, (John Wiley and Sons, Inc., 1994)

[4] K. L. G. Heyde, *The Nuclear Shell Model*, (Springer-Verlag, 1994)

[5] B. A. Brown, et al., the computer code OXBASH.

[6] M. Rotenberg, R. Bivins, M. Metropolis and K. R. Wooten Jr., *The 3-j and 6-j Symbols*, (Technology Press MIT, Cambridge, 1959).

[7] A. de Shalit and I. Talmi, *Nuclear Shell Theory*, (Academic Press, 1963).

[8] I. Talmi, *Simple Models of Complex Nuclei*, (Harwood Academic Publishers, 1993).

[9] P. J. Brussaard and P. W. M. Glaudemans, *Shell Model Applications in Nuclear Spectroscopy*, (North Holland, 1977).

[10] D. M. Brink and G. R. Satchler, *Angular Momentum*, (Clarendon Press, Oxford, 1968).

[11] A. Messiah, *Quantum Mechanics*, Vol. 1, (North Holland, Amsterdam, 1975).

[12] A. Bohr and B. R. Mottelson, *Nuclear Structure*, Vol. I, (W. A. Benjamin, 1969), *Nuclear Structure* Vol. II, (W. A. Benjamin, 1975).

[13] A. de Shalit and H. Feshbach, *Theoretical Nuclear Physics Vol. I: Nuclear Structure*, (John Wiley and Sons, 1974).

[14] R. D. Lawson, *Theory of the Nuclear Shell Model*, (Clarendon Press, 1980).

[15] I. S. Towner, *A Shell Model Description of Light Nuclei*, (Clarendon Press, 1977).

14 Single-particle electromagnetic moments

14.1 General results and notation

Electromagnetic moments have the general form:

$$\mathcal{M}_{em} = < \Psi, J, M = J \mid \sum_k T^{\lambda}_{\mu=0}(k) \mid \Psi, J, M = J >, \tag{14.1}$$

where T^{λ}_{μ} is a one-body tensor operator of rank λ associated with the interaction of the nucleus with the multipole components of the electromagnetic field. This is a diagonal matrix element, and by definition we take M to have its maximum value $M = J$. The matrix elements with other M values are related to $\mathcal{M}_{em}$ by the Wigner-Eckart theorem:

$$< \Psi, J, M \mid \sum_k T^{\lambda}_{\mu=0}(k) \mid \Psi, J, M >= \frac{< J, M, \lambda, \mu = 0 \mid J, M >}{< J, J, \lambda, \mu = 0 \mid J, J >} \mathcal{M}_{em}. \tag{14.2}$$

For a given J value, the allowed values of the λ are determined by the triangle condition, $\Delta(J, \lambda, J)$. In particular, $\lambda_{max} = 2J$, and for $J = 0$ only $\lambda = 0$ is allowed.

There are two type of electromagnetic moments: the electric moments associated with the static distribution of charge and the magnetic moments associated with the magnetic currents. The parity conservation requires λ=even for the static moments and λ=odd for the magnetic moments. The names relate to the greek for the 2^{ℓ} poles. The lowest few are:

2^0 – monopole
2^1 – dipole
2^2 – quadrupole
2^3 – octupole
2^4 – hexadecapole
2^5 – triakontadupole

The electromagnetic moment for λ=0 is $\sum_k e_k$ which simply counts the number of particles with charge e_k. The operators for magnetic dipole (ℓ=1) and electric quadrupole (ℓ=2) moments will be discussed in the following subsections. A compilation of experimental magnetic and quadrupole moments is given on the web [1].

14.2 General results for closed-shell and single-particle configurations

We first consider the angular momenta allowed for these simple one-dimensional configurations, and then investigate the consequences for the electromagnetic moments. For the closed-shell configuration $\mid C >$ there are several (n_r, ℓ, j) orbits which are completely filled. For each of these orbits there is an m degeneracy of $(2j+1)$ states (for protons or neutrons) and the total M_j value is:

$$M_j = \sum_{\alpha} < j, m \mid \hat{j}_z \mid j, m > = \sum_{m=-j}^{m=j} < j, m \mid \hat{j}_z \mid j, m > = \sum_{m=-j}^{m=j} m = 0,$$

(The wavefunction $\mid j, m >$ also depends upon n_r and ℓ, but as in this example, sometimes they need not be written explicitly.) Thus each filled j orbit has $J = 0$. The sum over all M_j gives $M = 0$, and thus we have $J^\pi = 0^+$ for the closed shell. The parity is positive since the number of particles in each j orbit is even. Only the $\lambda = 0$ moment contributes for the closed shell.

For the single-particle configuration $\mid Ci >$, the extra nucleon will go into one of the empty states (n_r, ℓ, j, m) above the fermi surface. There are $(2j+1)$ allowed M values from $-j$ to j. Thus the total angular momentum is $J = j$, and the parity is $(-1)^\ell$. For the moments we need the $M-$state with $M = m = j$.

For the single-hole configuration, $\mid Ci^{-1} >$, the nucleon will be removed from one of the filled states (n_r, ℓ, j, m') below the fermi surface. The M value of the state is:

$$M = \sum_{m \neq m'} m = -m'.$$

There are $(2j+1)$ values for M from $-j$ to j. Thus the total angular momentum is $J = j$, and the parity parity is $(-1)^\ell$. If we want to have a many-body state with $M = J = j$, then the nucleon must be removed from the single-particle state with $m' = -j$.

Next we consider the moments for $\lambda > 0$. For one-particle outside of a closed-shell configuration, $\mid \Psi > = \mid Ci >$, the moment is:

$$\mathcal{M}(Ci)_{em} = \sum_{a} < \alpha \mid T^\lambda_{\mu=0} \mid \alpha > + < i \mid T^\lambda_{\mu=0} \mid i >, \tag{14.3}$$

where the sum over α runs over the states filled in the closed shell. Since the closed shell has $J^\pi = 0^+$ the first term in Eq. (14.3) is zero unless λ=0. For $\lambda > 0$ we have for the $\mid Ci >$ configuration:

$$\mathcal{M}(Ci)_{em} = < i \mid T^\lambda_{\mu=0} \mid i > = < j, m = j \mid T^\lambda_{\mu=0} \mid j, m = j > . \tag{14.4}$$

For the one-hole configuration:

$$\mathcal{M}(Ci^{-1})_{em} = \sum_a < \alpha \mid T^\lambda_{\mu=0} \mid \alpha > - < i \mid T^\lambda_{\mu=0} \mid i >, \tag{14.5}$$

and for $\lambda > 0$:

$$\mathcal{M}(Ci^{-1})_{em} = - < i \mid T^\lambda_{\mu=0} \mid i > = - < j, m = -j \mid T^\lambda_{\mu=0} \mid j, m = -j > . \tag{14.6}$$

Note that the particle is removed from the state $m = -j$ so that $M = J = j$. A special result of the Wigner-Eckart theorem of Eq. (14.2) is:

$$< j, m = -j \mid T^\lambda_{\mu=0} \mid j, m = -j > =$$

$$= \frac{< j, -j, \lambda, \mu = 0 \mid j, -j >}{< j, j, \lambda, \mu = 0 \mid j, j >} < j, m = j \mid T^\lambda_{\mu=0} \mid j, m = j >$$

$$= (-1)^\lambda < j, m = j \mid T^\lambda_{\mu=0} \mid j, m = j > . \tag{14.7}$$

Thus, for the hole states:

$$\mathcal{M}(Ci^{-1})_{em} = (-1)^{\lambda+1} < j, m = j \mid T^\lambda_{\mu=0} \mid j, m = j > . \tag{14.8}$$

The one-body operator T^λ will have terms which operate separately on the space and spin parts of the wave function. Thus, the general evaluation of the single-particle moments starts with the decomposition of the state j into its space and spin components:

$$\mid \ell, j, m > = \sum_{m_\ell, m_s} < \ell, m_\ell, s, m_s \mid j, m > \mid \ell, m_\ell, m_s \gg,$$

where the notation $\mid \gg$ will be used for the state where m_ℓ and m_s are good quantum numbers (n_r and s are implicit). The special cases we need for the moments are:

$$\mid \ell, j = \ell + \frac{1}{2}, m = j > = \mid \ell, \ell, \frac{1}{2} \gg, \tag{14.9}$$

and

$$\mid \ell, j = \ell - \frac{1}{2}, m = j > = \sqrt{\frac{1}{2\ell+1}} \mid \ell, \ell - 1, \frac{1}{2} \gg - \sqrt{\frac{2\ell}{2\ell+1}} \mid \ell, \ell, -\frac{1}{2} \gg . \tag{14.10}$$

The matrix elements of T^λ have the form:

$$< n_r, \ell, j = \ell + \frac{1}{2}, m = j \mid T^\lambda \mid n_r, \ell, j = \ell + \frac{1}{2}, m = j >$$

$$= \ll \ell, \ell, \frac{1}{2} \mid T^\lambda \mid \ell, \ell, \frac{1}{2} \gg, \tag{14.11}$$

and:

$$< n_r, \ell, j = \ell - \frac{1}{2}, m = j \mid T^\lambda \mid n_r, \ell, j = \ell - \frac{1}{2}, m = j >$$
$$= \left(\frac{1}{2\ell+1}\right) \ll \ell, \ell-1, \frac{1}{2} \mid T^\lambda \mid \ell, \ell-1, \frac{1}{2} \gg$$
$$+ \left(\frac{2\ell}{2\ell+1}\right) \ll \ell, \ell, -\frac{1}{2} \mid T^\lambda \mid \ell, \ell, -\frac{1}{2} \gg . \tag{14.12}$$

For these expressions I have used the fact that the electromagnetic operator T^λ is diagonal in m_s (it does not connect the states with $m_s = \frac{1}{2}$ and $m_s = -\frac{1}{2}$).

14.3 Magnetic moments

The magnetic moment operator is defined to be

$$T^{\lambda=1}_{\mu=0} = \hat{\mu}_z[\ell_z \; g^\ell_{t_z} + s_z \; g^s_{t_z}]\mu_N, \tag{14.13}$$

where $g^\ell_{t_z}$ and $g^s_{t_z}$ are the orbital and spin g-factors for the proton ($t_z = -\frac{1}{2}$) and neutron ($t_z = \frac{1}{2}$). The free-nucleon values for the g-factors are $g^\ell_p = 1$, $g^\ell_n = 0$, $g^s_p = 5.586$ and $g^s_n = -3.826$. The values of the magnetic moments are conventionally taken to be in units of the nuclear magneton,

$$\mu_N = \frac{e\hbar}{2m_p c} = 0.105 \; e\,\mathrm{fm} \tag{14.14}$$

where m_p is the mass of the proton.

From Eq. (14.8), the single-particle and single-hole magnetic moments are the same. From Eq. (14.11) for $m = j$ and $j = \ell + \frac{1}{2}$ we have

$$\frac{\mu(j = \ell + \frac{1}{2})}{\mu_N} = \ell \; g^\ell_{t_z} + \frac{1}{2} \; g^s_{t_z}, \tag{14.15}$$

and from Eq. (14.12) for $m = j$ and $j = \ell - \frac{1}{2}$ we have

$$\frac{\mu(j = \ell - \frac{1}{2})}{\mu_N} = \left[\frac{1}{(2\ell+1)}(\ell-1) + \frac{2\ell}{(2\ell+1)}\ell\right] g^\ell_{t_z} + \left[\frac{1}{2\ell+1}\left(\frac{1}{2}\right) + \frac{2\ell}{2\ell+1}\left(-\frac{1}{2}\right)\right] g^s_{t_z}$$
$$= \frac{(2\ell-1)(\ell+1)}{(2\ell+1)} g^\ell_{t_z} - \frac{(2\ell-1)}{(4\ell+2)} g^s_{t_z}. \tag{14.16}$$

The traditional and most compact way to write these expressions is:

$$\frac{\mu}{\mu_N} = j\left[g^\ell_{t_z} \pm \frac{g^s_{t_z} - g^\ell_{t_z}}{2\ell+1}\right], \tag{14.17}$$

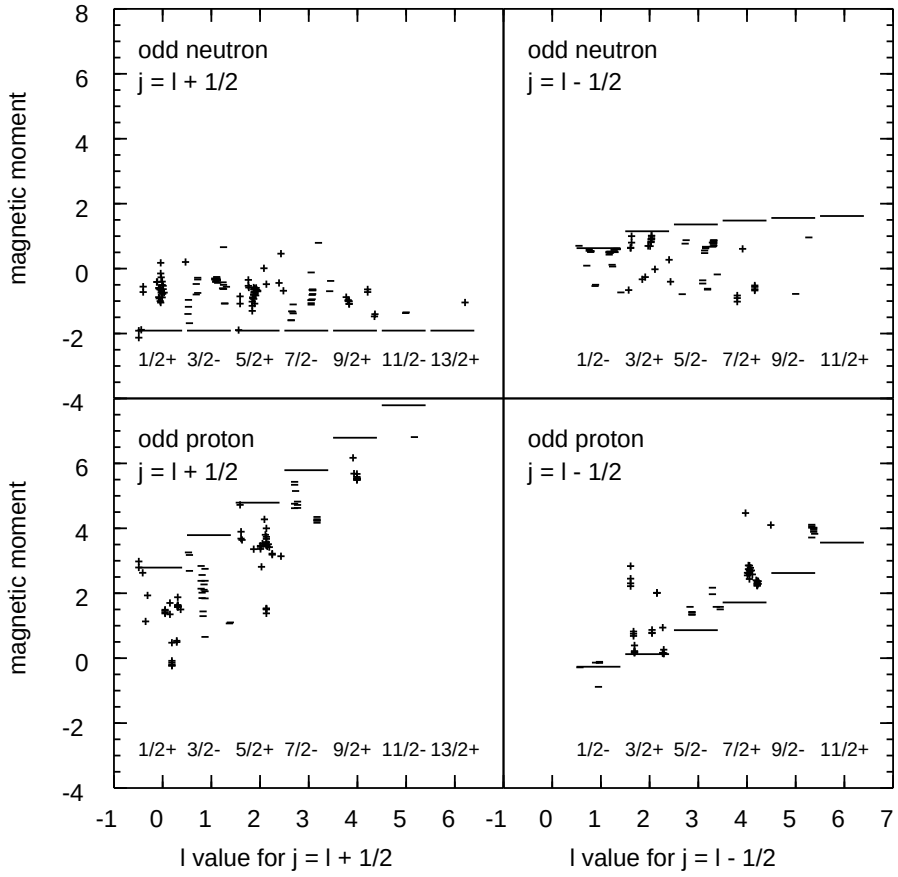

Figure 1: Experimental magnetic moments compared to the single-particle (Schmidt) values. For a given j^π value the data are plotted vs increasing neutron or proton number withplus signs for positive parity and minus signs for negative parity.

there the $\pm$ sign goes with $j \pm \frac{1}{2}$. The g-factor is defined as $\mu/(\mu_N J)$ which for the single-particle case gives:

$$g = \left[g^\ell_{t_z} \pm \frac{g^s_{t_z} - g^\ell_{t_z}}{2\ell + 1} \right]. \tag{14.18}$$

These single-particle magnetic moments are called the Schmidt values. The result for neutrons in the state $j = \ell + \frac{1}{2}$ with $g^\ell_n = 0$ reduces to

$$\mu(j = \ell + \frac{1}{2}\,, \text{neutron}) = \frac{g^s_n \mu_N}{2} = \mu_n = -1.913\,\mu_N$$

where μ_n is the magnetic moment of the neutron.

The magnetic moments data from the compilation of Stone [1] are shown in Fig.

(14.1) in comparison with the single-particle values. The data are shown for the odd-neutron and odd-proton nuclei. For a given j^π value one can associate the unique ℓ and the data can be divided into two groups with $j = \ell + 1/2$ and $j = \ell - 1/2$. There is a pronounced difference between the odd-neutron and odd-proton plots that is related to the influence of the orbital contribution for protons. With few exceptions all of the data for a given kind of nucleon lies in between the limits given by the $j = \ell \pm 1/2$ single-particle values. The reason for this can be understood as a result of configuration mixing byond the single-particle model.

There is a short-cut for deriving these results by using the projection theorem:

$$< j, m \mid v_z \mid j, m >= \frac{< j \mid (\vec{j} \cdot \vec{v}) \mid j >}{j(j+1)} < j, m \mid j_z \mid j, m >, \tag{14.19}$$

where v_z is any vector operating in the j-space, and the matrix element of $\vec{j} \cdot \vec{v}$ has been written without the m to indicate that the scalar matrix element does not depend upon m. This can be derived using the Wigner-Eckart theorem.

For the single-particle magnetic moment with $m = j$:

$$< j, m = j \mid \hat{\mu}_z \mid j, m = j >= \frac{< j \mid (\vec{j} \cdot \vec{\mu}) \mid j >}{(j+1)}. \tag{14.20}$$

We can save some algebra by writing:

$$\frac{\hat{\mu}_z}{\mu_N} = \ell_z \; g^\ell_{t_z} + s_z \; g^s_{t_z} = (\ell_z + s_z) \; g^\ell_{t_z} + s_z \; (g^s_{t_z} - g^\ell_{t_z}) = j_z \; g^\ell_{t_z} + s_z \; (g^s_{t_z} - g^\ell_{t_z})$$

The matrix elements for the magnetic moment is then:

$$\frac{< j, m = j \mid \hat{\mu}_z \mid j, m = j >}{\mu_N} = \frac{< j \mid j^2 g^\ell_{t_z} + (\vec{j} \cdot \vec{s})(g^s_{t_z} - g^\ell_{t_z}) \mid j >}{(j+1)}$$

$$= j g^\ell_{t_z} + \frac{< j \mid (\vec{j} \cdot \vec{s}) \mid j > (g^s_{t_z} - g^\ell_{t_z})}{(j+1)}$$

The scalar matrix element of $\vec{j} \cdot \vec{s}$ can be derived using the identity $\vec{j} - \vec{s} = \vec{\ell}$ to obtain

$$\vec{j} \cdot \vec{s} = \frac{j^2 + s^2 - \ell^2}{2}$$

whose expectation value is:

$$< j \mid \vec{j} \cdot \vec{s} \mid j >= \frac{j(j+1) + s(s+1) - \ell(\ell+1)}{2},$$

and after some simplification one obtains the same result as in Eq. (14.17).

14.4 Electric quadrupole moments

The electric quadrupole operator is defined to be

$$T^{\lambda=2}_{\mu=0} = \hat{Q} = (3z^2 - r^2)e_{t_z}e = \sqrt{\frac{16\pi}{5}}\ r^2\ Y^2_0(\hat{r})\ e_{t_z}e, \tag{14.21}$$

were Y^λ_μ are the spherical harmonics. The e_{t_z} are the charges for the proton and neutron in units of e. For the free-nucleon charge we would take $e_p = 1$ and $e_n = 0$, for the proton and neutron, respectively. Although the initial operator for quadrupole moments only acts upon the protons, we will keep the general expression in terms of e_{t_z} because later we will introduce "effective charges" for the proton and neutron. By convention the electric quadrupole moment is taken to be in units of e: Quadrupole moments are usually quoted in units of e fm^2 or eb where b is the "barn", $b = 100$ fm^2 (sometimes the e is implicit).

From Eq. (14.11) the single-particle quadrupole moment in the state $j = \ell + \frac{1}{2}$ is:

$$\frac{Q}{e} = \sqrt{\frac{16\pi}{5}} < Y^\ell_\ell \mid Y^2_0 \mid Y^\ell_\ell > < r^2 > e_{t_z}. \tag{14.22}$$

where

$$< r^2 > = \int f^2(r)\, r^4 dr = \int R^2_{n_r,\ell,j}\, r^2 dr.$$

The angular integral is given by Eqs. (13.32) and (13.41):

$$\begin{aligned} < Y^\ell_\ell \mid Y^2_0 \mid Y^\ell_\ell > &= (-1)^\ell \begin{pmatrix} \ell & 2 & \ell \\ -\ell & 0 & \ell \end{pmatrix} (2\ell+1)\sqrt{\frac{5}{4\pi}} \begin{pmatrix} \ell & 2 & \ell \\ 0 & 0 & 0 \end{pmatrix} \\ &= -\sqrt{\frac{5}{4\pi}} \left(\frac{\ell}{2\ell+3}\right). \end{aligned} \tag{14.23}$$

Thus, the single-particle quadrupole moment in the state $j = \ell + \frac{1}{2}$ simplifies to:

$$\frac{Q(i)}{e} = -\left(\frac{2\ell}{2\ell+3}\right) < r^2 > e_{t_z}. \tag{14.24}$$

From (14.8), the single-hole quadrupole moment in the state $j = \ell + \frac{1}{2}$ is:

$$\frac{Q(i^{-1})}{e} = \left(\frac{2\ell}{2\ell+3}\right) < r^2 > e_{t_z}. \tag{14.25}$$

The radial integrals can be evaluated with the chosen radial wavefunctions such as harmonic-oscillator or Woods-Saxon.

For the general case which includes both $j = \ell + \frac{1}{2}$ and $j = \ell - \frac{1}{2}$ one obtains for particle states:

$$\frac{Q(i)}{e} = -\left(\frac{2j-1}{2j+2}\right) < r^2 > e_{t_z}. \tag{14.26}$$

and for hole states:

$$\frac{Q(i^{-1})}{e} = \left(\frac{2j-1}{2j+2}\right) < r^2 > e_{t_z}. \tag{14.27}$$

A geometrical understanding of the sign of the quadrupole moment can be obtained from the form of the quadrupole operator in cartesian co-ordinates $(3z^2 - r^2) = (2z^2 - x^2 - y^2)$. Thus if the density is spherical $Q = 0$. If the density extends more along the z axis it has a prolate shape with $Q > 0$, and if the density is concentrated in the $x - y$ plan it has a oblate shape with $Q < 0$. The density distribution for the state $m_\ell = \ell$ is concentrated towards the $x - y$ plane and has $Q < 0$. For the single-hole state the density associated with this $m_\ell = -\ell$ state is missing and the remaining density has a prolate shape with $Q > 0$.

The experimental data for the quadrupole moments of the ground states of odd-even nuclei are shown in Fig. (14.2). In order to qualitatively divide out the mass dependence implied by the $< r^2 >$ matrix elements in Eqs. (14.26) and (14.27), the experimental moments can be divided by R^2 where $R = 1.2A^{1/3}$. These scaled quadrupole moments are shown in Fig. (14.3). The scaled data are shown for a region of the nuclear chart in Fig. (14.4).

There are several places where the sign change between particle (oblate) and hole (prolate) states can be observed, for example, for odd-protons in Fig. (14.5) just above and below $Z = 50$. But overall most nuclei have positive Q moments characteristic of a prolate shape.

In the single-particle model we would expect the Q moments for the neutrons to be zero or at least small compared to protons. But one observes that the Q moments for odd-proton and odd-nuetron nuclei are about the same. The single-particle values for the scaled Q moments are on the order of unity. In contrast the data for many regions of nuclei show Q which are up to an order of magnitude larger than this. Both of these deviations from the single-particle model are signatures of configuration mixing. Near the magic numbers this can be understood in terms of the interaction between the valence nucleon and the core nucleons producing a "core-polatization" that can be modeled in terms of an effective change for protons and neutrons. Away from the closed shell the interaction between valence nucleons results in a collective (coherent) motion between many nucleons that is qualitatively understood in the deformed model for nuclei.

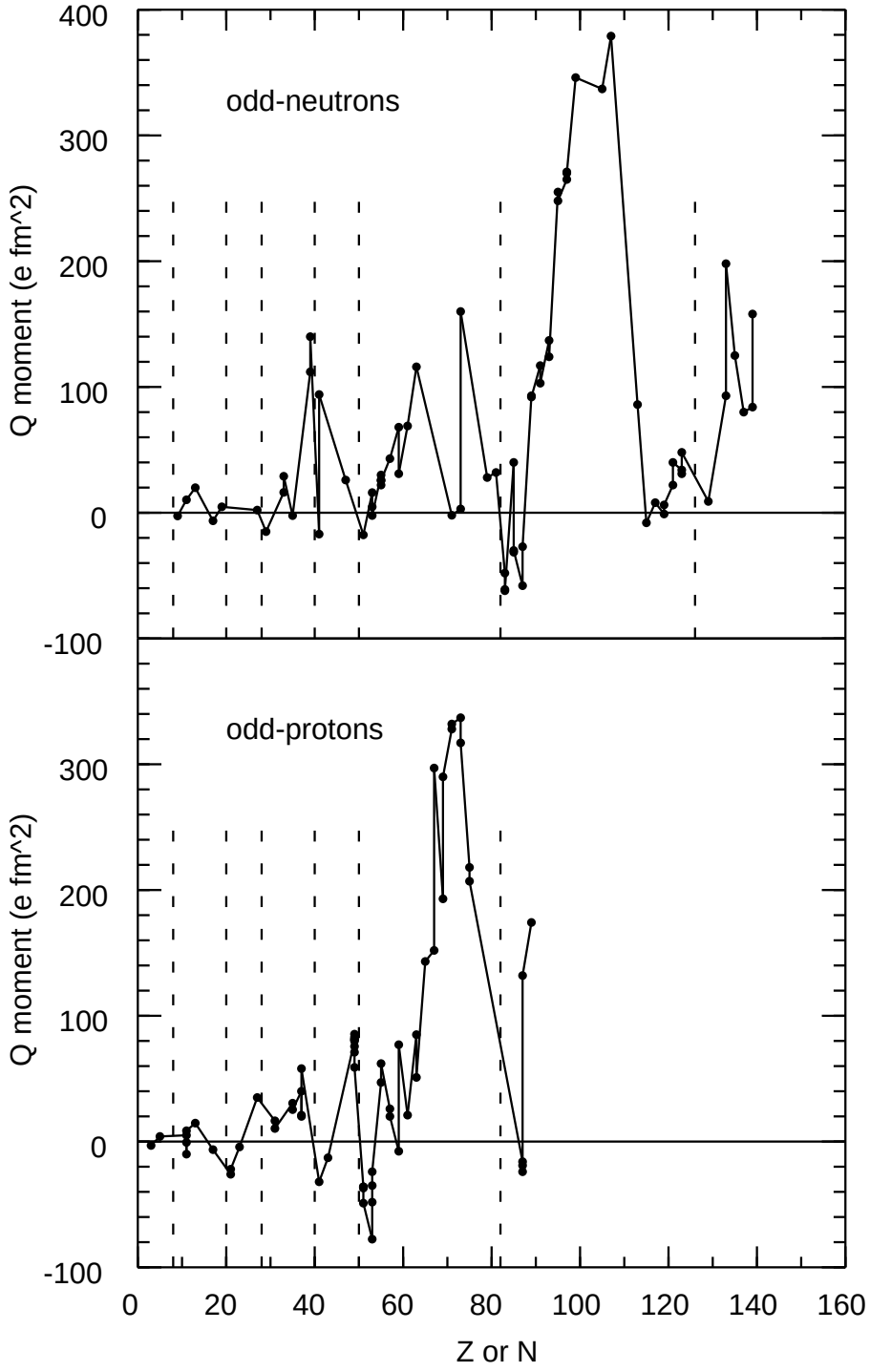

Figure 2: Experimental quadrupole moments for the ground states of odd-even nuclei. The dashed lines show the magic numbers 8, 20, 28, 40, 50, 82 and 126.

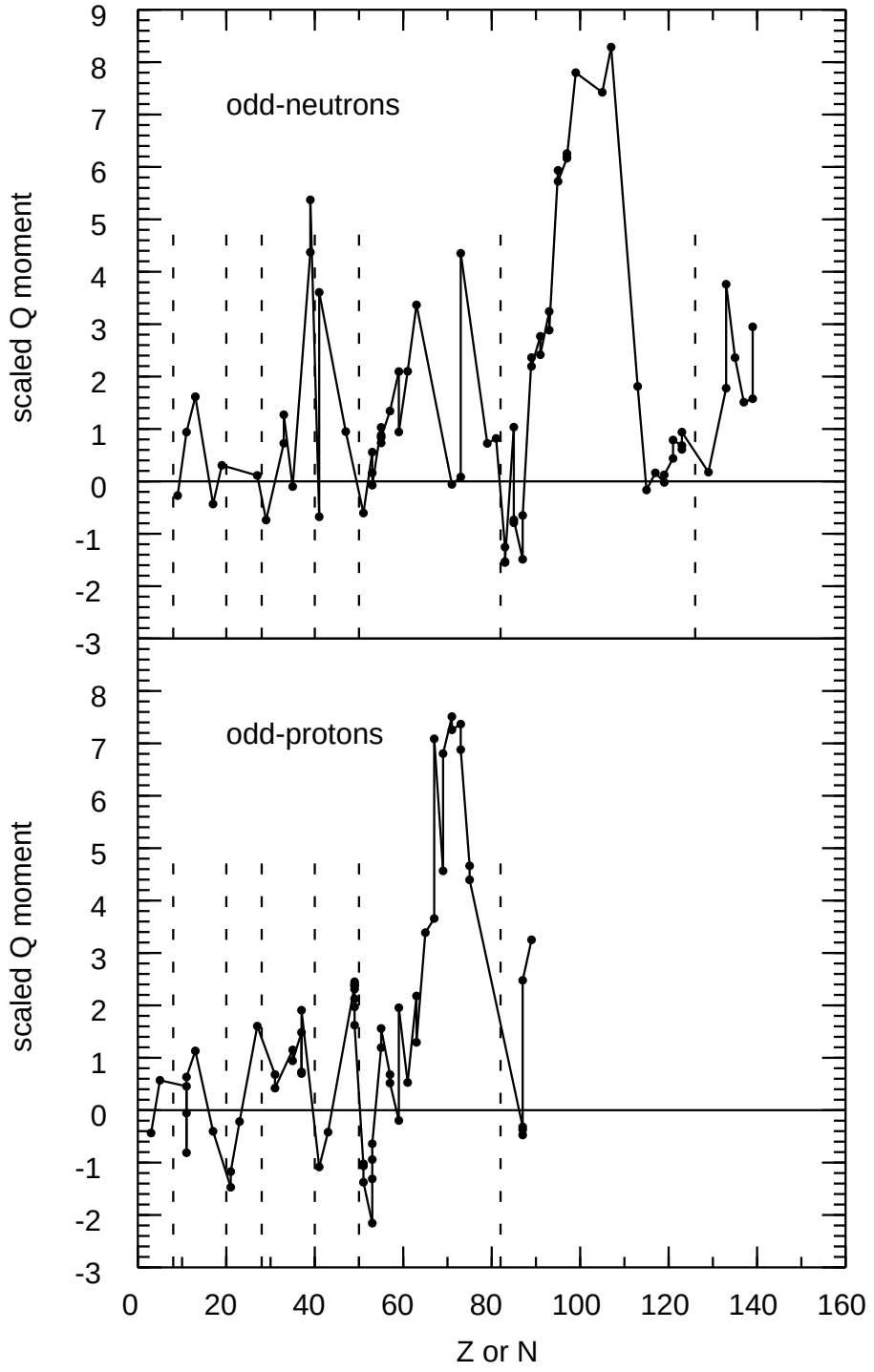

Figure 3: Scaled experimental quadrupole moments for the ground states of odd-even nuclei. The dashed lines show the magic numbers 8, 20, 28, 40, 50, 82 and 126.

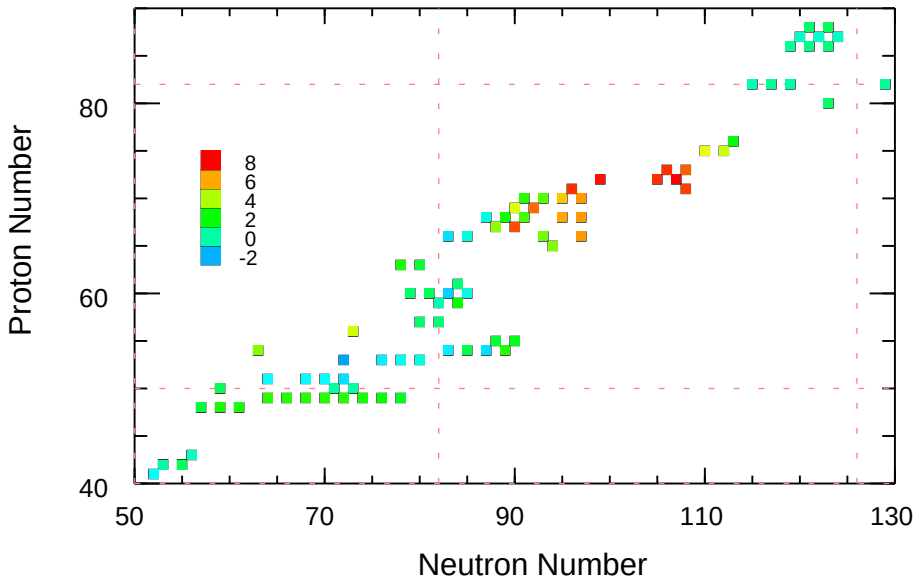

Figure 4: Scaled experimental quadrupole moments for the ground states of odd-even nuclei for a region of nuclei. The dashed lines show the magic numbers 50 and 82 for protons and 82 and 126 for neutrons.

References

[1] http://www.nndc.bnl.gov/publications/preprints/nuclear-moments.pdf

15 The Creation Operator Method

15.1 Introduction

A convenient method for taking into account the antisymmetry of the many-body wavefunctions is to express them in second-quantized form in terms of creation and destruction operators. The antisymmetry is enforced by the commutation relations of the operators. The next few sections summarize the properties of the creation operator and their use in constructing wavefunctions and operators. Some examples are given in the last section.

15.2 Creation Operators and Wavefunctions

The operator a_α^+ creates the one-particle state $\mid \alpha >$

$$a_\alpha^+ \mid > = \mid \alpha >, \tag{15.1}$$

where $\mid >$ represents the vacuum state. The label α represents, for example, the set of quantum numbers $(n_r \ell j m)$ used in the spherical shell-model basis. The n-particle state is formed from the product of these creation operators. For example, for $n = 3$

$$a_\lambda^+ a_\beta^+ a_\alpha^+ \mid > = \mid \alpha\beta\lambda > . \tag{15.2}$$

We use the convention that the order of the labels on the right-hand side is the inverse of that on the left hand side. The Hermitian conjugates of Eqs. (15.1) and (15.2) are

$$< \mid (a_\alpha^+)^+ = < \alpha \mid \equiv < \mid a_\alpha, \tag{15.3}$$

and

$$< \mid (a_\lambda^+ a_\beta^+ a_\alpha^+)^+ = < \mid a_\alpha a_\beta a_\lambda = < \alpha\beta\lambda \mid . \tag{15.4}$$

The a^+ and a operators obey the commutation relations

$$\{a_\lambda^+, a_\beta^+\} = a_\lambda^+ a_\beta^+ + a_\beta^+ a_\lambda^+ = 0, \tag{15.5}$$

$$\{a_\lambda, a_\beta\} = a_\lambda a_\beta + a_\beta a_\lambda = 0, \tag{15.6}$$

and

$$\{a_\lambda^+, a_\beta\} = a_\lambda^+ a_\beta + a_\beta a_\lambda^+ = \delta_{\lambda\beta}. \tag{15.7}$$

Use of the creation operators a^+ and annhilliation operators a together with their commutation relationships are completely equivalent to the results obtained from

Slater determinants, as will be shown in the next few paragraphs. In particular, we must show either that the commutation relations can be obtained directly from the structure of the antisymmetric wavefunctions, or that the commutation relations give the same result when applied to any wavefunction.

Antisymmetry of the Slater determinant means that

$$\mid \lambda\beta\alpha_1 \ldots \alpha_n >= - \mid \beta\lambda\alpha_1 \ldots \alpha_n >, \tag{15.8}$$

and

$$\mid \lambda\alpha_1 \ldots \alpha_n\beta >= (-1)^n \mid \lambda\beta\alpha_1 \ldots \alpha_n >, \tag{15.9}$$

Non-vanishing of the wavefunctions in Eqs. (15.8) and (15.9) implies that all of the labels are different. Eq. (15.8) implies that

$$a_\lambda^+ a_\beta^+ \mid \alpha_1 \ldots \alpha_n > \; + a_\beta^+ a_\lambda^+ \mid \alpha_1 \ldots \alpha_n > = 0. \tag{15.10}$$

Since the wavefunction itself is assumed not to vanish, one must have

$$a_\lambda^+ a_\beta^+ + a_\beta^+ a_\lambda^+ = 0, \tag{15.11}$$

which is the first the first commutation relation, Eq. (15.5). The Hermitian conjugate of this gives the second commutation relation, Eq. (15.6). The case when λ=β in Eqs. (15.5) and (15.6) implies in particular that

$$a_\lambda^+ a_\lambda^+ = a_\lambda a_\lambda = 0. \tag{15.12}$$

Before deriving Eq. (15.7), some intermediate results are useful, first:

$$a_\lambda^+ \mid \alpha_1 \ldots \alpha_n\lambda > = 0, \tag{15.13}$$

$$a_\lambda \mid \alpha_1 \ldots \alpha_n\lambda > = \mid \alpha_1 \ldots \alpha_n >, \tag{15.14}$$

$$a_\lambda^+ \mid \alpha_1 \ldots \alpha_n > = \mid \alpha_1 \ldots \alpha_n\lambda >, \tag{15.15}$$

and

$$a_\lambda \mid \alpha_1 \ldots \alpha_n > = 0, \tag{15.16}$$

Eq. (15.13) follows from Eq. (15.12), and Eq. (15.15) follows from the basic definition of Eq. (15.2). The results for operating with a to the right in Eqs. (15.14) and (15.16) can be inferred from the normalization condition

$$< \lambda \mid \beta > = <\mid a_\lambda \mid \beta > = \delta_{\lambda\beta}, \tag{15.17}$$

which can be satisfied by the two relations

$$a_\lambda \mid \beta > = 0 \quad \text{if} \quad \lambda \neq \beta \tag{15.18}$$

and

$$a_\lambda \mid \beta >= \mid > \quad \text{if} \quad \lambda = \beta. \tag{15.19}$$

In particular,

$$a_\lambda \mid > = 0, \tag{15.20}$$

and

$$a_\lambda \mid \lambda >= \mid > . \tag{15.21}$$

Next, from Eqs. (15.13)-(15.16) it is straightforward to show that

$$a_\lambda a_\lambda^+ \mid \alpha_1 \ldots \alpha_n \lambda >= 0, \tag{15.22}$$

$$a_\lambda^+ a_\lambda \mid \alpha_1 \ldots \alpha_n \lambda >= \mid \alpha_1 \ldots \alpha_n \lambda >, \tag{15.23}$$

$$a_\lambda a_\lambda^+ \mid \alpha_1 \ldots \alpha_n >= \mid \alpha_1 \ldots \alpha_n >, \tag{15.24}$$

and

$$a_\lambda^+ a_\lambda \mid \alpha_1 \ldots \alpha_n >= 0, \tag{15.25}$$

Note that $a_\lambda a_\lambda^+$ or $a_\lambda^+ a_\lambda$ cannot always be replaced by unity.

The commutation relation of Eq. (15.7) can now be proven by showing that it holds for its application on all possible wavefunctions. The results for the case $\lambda = \beta$:

$$(a_\lambda^+ a_\lambda + a_\lambda a_\lambda^+) \mid \alpha_1 \ldots \alpha_n \lambda >= \mid \alpha_1 \ldots \alpha_n \lambda >, \tag{15.26}$$

and

$$(a_\lambda^+ a_\lambda + a_\lambda a_\lambda^+) \mid \alpha_1 \ldots \alpha_n >= \mid \alpha_1 \ldots \alpha_n >, \tag{15.27}$$

are obtained immediately from Eqs. (15.22) $-$ (15.25). For $\lambda \neq \beta$ the results

$$(a_\lambda^+ a_\beta + a_\beta a_\lambda^+) \mid \alpha_1 \ldots \alpha_n \lambda >= 0, \tag{15.28}$$

and

$$(a_\lambda^+ a_\beta + a_\beta a_\lambda^+) \mid \alpha_1 \ldots \alpha_n >= 0, \tag{15.29}$$

follow immediately from Eqs. (15.13) and (15.16). The final case is

$$\begin{aligned}(a_\lambda^+ a_\beta + a_\beta a_\lambda^+) \mid \alpha_1 \ldots \alpha_n \beta >&= (a_\lambda^+ a_\beta a_\beta^+ - a_\beta a_\beta^+ a_\lambda^+) \mid \alpha_1 \ldots \alpha_n > \\ &= (a_\lambda^+ - a_\lambda^+) \mid \alpha_1 \ldots \alpha_n >= 0,\end{aligned} \tag{15.30}$$

where (15.24) has been used to replace the $a_\beta a_\beta^+$ by unity. Eqs. (15.26) $-$ (15.30) are equivalent to Eq. (15.7).

15.3 Operators

One- (O) and two-body (T) operators can be expressed in terms of these creation and destruction operators:

$$\hat{O} = \sum_{\alpha\beta} < \alpha \mid O \mid \beta > a_\alpha^+ a_\beta, \tag{15.31}$$

and

$$\hat{T} = \frac{1}{4} \sum_{\alpha\beta\gamma\delta} < \alpha\beta \mid T \mid \gamma\delta > a_\alpha^+ a_\beta^+ a_\delta a_\gamma. \tag{15.32}$$

Note the order of γ and δ at the end of this equation for T are different from their order in $\mid \gamma\delta >$. Angular momentum coupled versions of these operators will be given in a following chapter.

A basic one-body operators is the scalar number operator

$$N = \sum_{i=1}^{n} 1 = n,$$

which in second-quantized form becomes

$$\hat{N} = \sum_{\alpha\beta} < \alpha \mid 1 \mid \beta > a_\alpha^+ a_\beta = \sum_{\alpha} a_\alpha^+ a_\alpha. \tag{15.33}$$

When operating on a state to the right, $\hat{N}$ will give unity if the state α is occupied [Eq. (15.23)] and zero if it is unoccupied [Eq. (15.25)], and the sum will thus give the total number of particles, n.

The creation operator method is well suited for computer codes, since the basis states Φ can be represented by binary bit patterns, with (1) denoting an occupied state and (0) an unoccupied state. The operations amount to binary additions and keeping track of phase factors. Many computer codes have been developed which make use of these techniques. These computations are based on some finite set of single-particle quantum numbers $(\alpha_1, \ldots, \alpha_n)$. It is convenient to choose some arbitrary but fixed ordering for these. For example, if one considers only the state with $j = 3/2$, there are four m-states which could put in the order $(-3/2, -1/2, 1/2, 3/2)$. The complete set of many-body states for two particles in this basis is then, (0011), (0101), (1001), (0110), (1010) and (1100).

15.4 Examples of a^+ and a Matrix Elements

This section will provide a few explicit examples for evaluating matrix elements of operators in the a^+-a representation. The first examples are considered from the point of view of algebraically interchanging the a^+ and a operators until one has $a \mid > = 0$.

a) A normalization:

$$< i \mid k > = <\mid a_i a_k^+ \mid > = <\mid \delta_{ik} - a_k^+ a_i \mid > = \delta_{ik}. \tag{15.34}$$

b) The elementary one-body matrix element:

$$\begin{aligned}
< i \mid \hat{O} \mid k > &= \sum_{\alpha\beta} < \alpha \mid O \mid \beta >< i \mid a_\alpha^+ a_\beta \mid k > \\
&= \sum_{\alpha\beta} < \alpha \mid O \mid \beta ><\mid a_i a_\alpha^+ a_\beta a_k^+ \mid > \\
&= \sum_{\alpha\beta} < \alpha \mid O \mid \beta ><\mid a_i a_\alpha^+ [\delta_{\beta k} - a_k^+ a_\beta] \mid > \\
&= \sum_{\alpha\beta} < \alpha \mid O \mid \beta ><\mid a_i a_\alpha^+ \delta_{\beta k} \mid > \\
&= \sum_{\alpha\beta} < \alpha \mid O \mid \beta ><\mid \delta_{\alpha i} \delta_{\beta k} \mid > = < i \mid O \mid k > .
\end{aligned}$$

This is a tedious way to get an identity. However, the power of second quantization is apparent when the technique is applied to a more general case with help of a computer code. Next we consider some examples which are closer to how second quantization is used in computer programs.

c) The elementary one-body matrix element − a repeat of (b) above:

$$\begin{aligned}
< i \mid \hat{O} \mid k > &= \sum_{\alpha} < \alpha \mid O \mid k >< i \mid a_\alpha^+ a_k \mid k > \\
&= \sum_{\alpha} < \alpha \mid O \mid k >< i \mid a_\alpha^+ \mid \emptyset > = < i \mid O \mid k >< i \mid i > = < i \mid O \mid k > .
\end{aligned} \tag{15.35}$$

d) A more general diagonal one-body matrix element:

$$\begin{aligned}
< ikl|\hat{O} \mid ikl > &= \sum_{\alpha\beta} < \alpha \mid O \mid \beta >< ikl|a_\alpha^+ a_\beta \mid ikl > \\
&= \sum_{\alpha} \Big\{ < \alpha \mid O \mid i >< ikl|a_\alpha^+ \mid \emptyset kl > \\
&- < \alpha \mid O \mid k >< ikl|a_\alpha^+ \mid i\emptyset l > + < \alpha \mid O|l >< ikl|a_\alpha^+ \mid ik\emptyset > \Big\}
\end{aligned}$$

$$
\begin{aligned}
&= < i \mid O \mid i >< ikl|ikl > + < k \mid O \mid k >< ikl|ikl > \\
&\quad + < l \mid O \mid l >< ikl|ikl > \\
&= < i \mid O \mid i > + < k \mid O \mid k > + < l \mid O \mid l >, \qquad (15.36)
\end{aligned}
$$

which is result expected for a diagonal matrix element. The notation "$\emptyset$" in the above wavefunctions is to indicate that the single-particle state which normally would occupy this position is empty.

f) An off-diagonal one-body matrix element

$$
\begin{aligned}
< ikl|\hat{O} \mid ikm > &= \sum_{\alpha\beta} < \alpha \mid O \mid \beta >< ikl|a^+_\alpha a_\beta \mid ikm > \\
&= \sum_a \Big\{ < \alpha \mid O \mid i >< ikl|a^+_\alpha \mid \emptyset km > \\
&- < \alpha \mid O \mid k >< ikl|a^+_\alpha \mid i\emptyset m > + < \alpha \mid O \mid m >< ikl|a^+_\alpha \mid ik\emptyset > \Big\} \\
&= < i \mid O \mid i >< ikl|ikm > + < k \mid O \mid k >< ikl|ikm > \\
&\quad + < l|O \mid m >< ikl|ikl > = < l|O \mid m > . \qquad (15.37)
\end{aligned}
$$

16 Many-Body Wavefunctions

16.1 Wavefunctions in the m-scheme

For a spherical potential the single-particle wavefunctions are labeled by their radial, orbital angular momentum, and total angular momentum quantum numbers, n_r, ℓ and j, respectively. This set of quantum numbers will be denoted by $k \equiv (n_r, \ell, j)$. Each j value has $(2m+1)$ m-states, and the associated single-particle wavefunctions will be labeled by $\alpha \equiv (km)$. It is useful to think of k as unique numerical sequence of numbers associated with the complete set of single-particle states. A particular choice for this labeling which is often used [1] is $k = 1, 2, 3, 4, 5, 6, 7, 8, 9, 10, \ldots$, for the sequence $0s_{1/2}, 0p_{3/2}, 0p_{1/2}, 0d_{5/2}, 0d_{3/2}, 1s_{1/2}, 0f_{7/2}, 0f_{5/2}, 1p_{3/2}, 1p_{1/2}, \ldots$. The k value for a given $n\ell j$ can be computed from:

$$k = \frac{1}{2}[(2n+\ell)(2n+\ell+3) - 2j + 3]. \tag{16.1}$$

The formalism developed thus far is basically all that is needed for an M-scheme calculation [2]. In the M-scheme one starts with a set of basis states Φ for a given M value

$$M = \sum_\alpha m_\alpha, \tag{16.2}$$

where the sum is over the m values for the occupied states. In general there are an infinite number of basis states Φ, but a for a given situation one truncates the number of states based upon those that are lowest in unperturbed energy. Since the Hamiltonian is diagonal in M one need only consider the subset of basis states Φ with a single value of M in the construction of the many-particle wavefunctions Ψ. The many-body matrix elements of the relevant one- and two-body operators can then be calculated with the techniques of second quantization. Many computer codes have been written to do this.

A basis state with a given value of M does not in general have a definite (good) value of the total angular momentum J. However, since the Hamiltonian is spherically symmetric, the Hamiltonian is also diagonal in J. Thus, the eigenvalues of H, which are linear combinations of the Φ basis, will automatically have good a J value with $J \geq M$, as long as the basis contains the complete set of states that are connected by the $\hat{J}^2$ operator. The J value can be determined by calculating the expectation value $< \Psi \mid \hat{J}^2 \mid \Psi >$.

We can calculate the total number of states for a given J, the J-dimension $D(J)$, from the M-scheme dimensions $d(M)$. This is based upon the fact that for each J

Table 1: M values for the $[(j = 5/2)^2]$ configuration for identical nucleons. The x's under columns headed by $2m$ indicate that the state is occupied, and the total M value is given on the right-hand side.

$2m$	5	3	1	-1	-3	-5	
							M
	x	x					4
	x		x				3
	x			x			2
	x				x		1
	x					x	0
		x	x				2
		x		x			1
		x			x		0
		x				x	-1
			x	x			0
			x		x		-1
			x			x	-2
				x	x		-2
				x		x	-3
					x	x	-4

state there must be $(2J + 1)$ M-states. Thus we find:

$$D(J) = d(M = J) - d(M = J + 1). \tag{16.3}$$

The meaning of Eq. (16.3) is that the number of extra $M = J$ states compared to to the number of $M = J + 1$ states must be the number of states with angular momentum J. Since $d(-M) = d(M)$ one only has to consider $M \geq 0$. Eq. (16.3) will be illustrated with with some examples. The results for these examples only depend upon the (j, m) quantum numbers, and thus the (n_r, ℓ) values are not given explicitly.

Table (16.1) gives all possible M-states for the $[(j = 5/2)^2]$ configuration for identical nucleons. Due to the Pauli principle we cannot have $M = 5$, and thus $J = 5$ is not allowed. The M-scheme dimensions for this case are given in Table (16.2). From the number of states for each M, one can make up Table (16.2). $M_{max} = 4$ means that the highest J value is $J = 4$ and this will account for nine of the M states, M= 4, 3, 2, 1, 0, -1, -2, -3 and -4. $J = 3$ is not allowed since there is only one $M = 3$ state which must go with $J = 4$. The extra $M = 2$ state means that there is a state with $J = 2$ which accounts for five more M states M= 2, 1, 0, -1, and -2. $J = 1$ is not allowed since all of the $M = 1$ states are now used, and the extra $M = 0$ states means that there is one state with $J = 0$. Thus, the allowed J values are 0, 2 and 4.

A second example is given for the $[(j = 5/2)]^3$ configuration given in Table (16.3).

Table 2: Table of M-scheme dimensions for $[(j = 5/2)^2]$.

M	$d(M)$
4	1
3	1
2	2
1	2
0	3
-1	2
-2	2
-3	1
-4	1

Table 3: $M0$ values ($M \geq 0$) for the $[(j = 5/2)^3]$ configuration for identical nucleons. The x's under columns headed by $2m$ indicate that the state is occupied, and the total M value is given on the right-hand side.

$2m$	5	3	1	-1	-3	-5	
							$2M$
	x	x	x				9
	x	x		x			7
	x	x			x		5
	x	x				x	3
	x		x	x			5
	x		x		x		3
	x		x			x	1
	x			x	x		1
		x	x	x			3
		x	x		x		1

From the multiplicity of the M values one can deduce that only $J = 3/2, 5/2$ and $9/2$ are allowed.

In general, the maximum J-value allowed for a $[k^n]$ configuration is given by the sum of the n largest possible m values,

$$J_{max} = \sum_{i=1}^{n} m_i^{max}. \tag{16.4}$$

In the $[(j = 5/2)^3]$ example, $J_{max} = 5/2 + 3/2 + 1/2 = 9/2$. Lawson [3] discusses other rules which can be deduced from these counting procedures. In particular, the k^n state with $J = J_{max} - 1$ is not allowed by the Pauli principle.

A third example is given for the $[(j = 5/2)^2(j = 1/2)]$ configuration in Table

Table 4: M values ($M \geq 0$) for the $[(j = 5/2)^2(j = 1/2)^1]$ configuration for identical nucleons. The x's under columns headed by $2j$ and $2m$ indicate that the state is occupied, and the total M value is given on the right-hand side.

$2j$	5	5	5	5	5	5	1	1	
$2m$	5	3	1	-1	-3	-5	-1	1	
									$2M$
	x	x					x		9
	x	x						x	7
	x		x				x		7
	x		x					x	5
	x			x			x		5
	x			x				x	3
	x				x		x		3
	x				x			x	1
	x					x	x		1
		x	x				x		5
		x	x					x	3
		x		x			x		3
		x		x				x	1
		x			x		x		1
			x	x			x		1

(16.4). One finds that $J = 9/2$, $7/2$, $5/2$, $3/2$ and $1/2$ are allowed. The restrictions on the J values due to the Pauli principle are only related to those associated with putting several identical nucleons into one j-orbit. Thus these allowed J values can also be deduced by the all possible values allowed by the triangle condition of coupling $j = 1/2$ to the $J = 0$, 2 and 4 states allowed for two particles in the j =5/2 state.

A forth example is given for the $[(j = 5/2)^1(j = 1/2)^2]$ configuration in Table (16.5). One finds only $J = 5/2$, as expected from the coupling of $j = 5/2$ to the closed-shell $[(j = 1/2)^2]$ configuration.

If there is only one M value allowed, the wavefunctions of the J state is given by that of the single M state. If there is more that one M value allowed, then one must diagonalize the hamiltonian in a space which has the dimension $d(M)$. The states of good J will be linear combinations of the M states. For a given J value of interest, one usually chooses $M = J$, since the number of M states is minimized in this case. However, one could also choose any $M \leq \mid J \mid$ value.

Alternatively, the linear combination of M-states with good J can be calculated using angular-momentum projection methods. This is the method used by the code OXBASH to construct a matrix with dimension $D(J)$ corresponding to the states of

Table 5: M values ($M \geq 0$) for the $[(j = 5/2)^1(j = 1/2)^2]$ configuration for identical nucleons. The x's under columns headed by $2j$ and $2m$ indicate that the state is occupied, and the total M value is given on the right-hand side.

$2j$	5	5	5	5	5	5	1	1	
$2m$	5	3	1	-1	-3	-5	-1	1	
									$2M$
	x						x	x	5
		x					x	x	3
			x				x	x	1

good J in terms of the M-scheme basis.

A partition is defined as a specific distribution of the particles into the allowed (active) set of k states. The examples discussed above include the three partitions allowed for putting three particles into the $j = 5/2$ and $j = 1/2$ states, namely $[(j = 5/2)^3]$, $[(j = 5/2)^2(j = 1)]$ and $[(j = 5/2)(j = 1/2)^2]$. These are all of the partitions allowed for three particles in these two orbits. The first step in a shell model calculation is to specify the number of particles, the number of active orbits, and then to make a list of the complete set of partitions. Then for each partition we calculate $D_p(J)$ and the total J-dimension is obtained by summing D_p over all partitions. The calculation may proceed with the full set of partitions (a full-space calculation) or it may be restricted to some subset of the partitions (a truncated calculation).

Compilations of $D(J)$ for j^n configurations for some values of j are available in the literature [4], and computer codes are available for the general case [1], [5], [6].

16.2 Wavefunctions in the J-scheme

In order to reduce the size of the calculation it is useful to form a basis which has a definite J value. It is also useful to express the many-particle matrix elements in a way in which the trivial M-state dependence is taken into account. This section discusses the structure of the angular momentum-coupled wave functions. The structure of the operators and matrix elements, is considered in the next section.

The two-particle wavefunction in which particles in the states k_1 and k_2 with angular momentum $\vec{j}_1$ and $\vec{j}_2$, respectively, are coupled to a total angular momentum $\vec{J}$ is given in terms of the product wavefunctions by

$$\mid k_1 k_2 JM >_p = \sum_{m_1 m_2} < j_1 m_1 j_2 m_2 \mid JM > \mid k_1 m_1 \; k_2 m_2 >_p, \tag{16.5}$$

where $M = m_1 + m_2$, and the subscript p indicates the product wavefunctions. As usual, the allowed values of J are from $J_{min} = \mid j_1 - j_2 \mid$ to $J_{max} = j_1 + j_2$ in integer steps. The result for the Slater determinant is not as simple, but takes the form

$$\mid k_1 k_2 JM >= N_{12} \sum_{m_1 m_2} < j_1 m_1 j_2 m_2 \mid JM > \mid k_1 m_1 \; k_2 m_2 >, \tag{16.6}$$

where N_{12} can be evaluated by taking the norm of both sides

$$\begin{aligned}
&< k_1 k_2 JM \mid k_1 k_2 JM >= 1 \\
&= N_{12}^2 \sum_{m_1 m_2 m_3 m_4} < j_1 m_1 j_2 m_2 \mid JM >< j_1 m_3 j_2 m_4 \mid JM > \\
&\times \frac{1}{2}\Big\{ < k_1 m_1 \; k_2 m_2 \mid k_1 m_3 \; k_2 m_4 >_p - < k_1 m_1 \; k_2 m_2 \mid k_2 m_4 \; k_1 m_3 >_p \\
&- < k_2 m_2 \; k_1 m_1 \mid k_1 m_3 \; k_2 m_4 >_p + < k_2 m_2 \; k_1 m_1 \mid k_2 m_4 \; k_1 m_3 >_p \Big\} \\
&= N_{12}^2 \sum_{m_1 m_2 m_3 m_4} < j_1 m_1 j_2 m_2 \mid JM >< j_1 m_3 j_2 m_4 \mid JM > \\
&\times \{ \delta_{m_1 m_3} \delta_{m_2 m_4} - \delta_{m_1 m_4} \delta_{m_2 m_3} \delta_{k_1 k_2} \} \\
&= N_{12}^2 \Big\{ \sum_{m_1 m_2} | < j_1 m_1 j_2 m_2 \mid JM > |^2 - \delta_{k_1 k_2} \sum_{m_1 m_2} < j_1 m_1 j_1 m_2 \mid JM >< j_1 m_2 j_1 m_1 \mid JM > \Big\} \\
&= N_{12}^2 \{ 1 - \delta_{k_1 k_2} (-1)^{J - 2j_1} \} = N_{12}^2 \{ 1 + \delta_{k_1 k_2} (-1)^J \},
\end{aligned} \tag{16.7}$$

where the symmetry property of the Clebsch-Gordan coefficient has been used. Thus, $\mid k_1 k_2 JM >$ vanishes if J is odd and $k_1 = k_2$. When the two-particle wavefunction does not vanish

$$N_{12} = \frac{1}{\sqrt{(1 + \delta_{k_1 k_2})}}. \tag{16.8}$$

The inverse of Eq. (16.6) is

$$\mid k_1 m_1 k_2 m_2 >= \frac{1}{N_{12}} \sum_{JM} < JM \mid j_1 m_1 j_2 m_2 > \mid k_1 k_2 JM > . \tag{16.9}$$

Also note that

$$\mid k_2 k_1 JM >= (-1)^{j_1+j_2-J+1} \mid k_1 k_2 JM >, \tag{16.10}$$

where a phase factor of (-1) arises from the antisymmetry of the two-particle wavefunction.

In terms of the a^+ operators introduced in Sec. 16.7, the angular momentum coupled two-particle wavefunction is

$$\begin{aligned} \mid k_1 k_2 JM >= N_{12} \sum_{m_1 m_2} & < j_1 m_1 j_2 m_2 \mid JM > a^+_{k_2 m_2} a^+_{k_1 m_1} \mid > \\ = -N_{12} \sum_{m_1 m_2} & < j_1 m_1 j_2 m_2 \mid JM > a^+_{k_1 m_1} a^+_{k_2 m_2} \mid > \\ = -N_{12} & [a^+_{k_1} \otimes a^+_{k_2}]^J_M \mid > . \end{aligned} \tag{16.11}$$

In general, when more than two particles are coupled to good angular momentum, one finds that $N = 1$ as long as each particle is in a different k state. When more than two particles go into a single k state, the normalization factor becomes increasingly complicated. However, as discussed in the previous section, the number of allowed states for a given J value are easily deduced from the number of M values.

The wave functions associated with these allowed J values can be obtained with the projection operators discussed in Sec. 16.12. The n-particle wavefunction will be denoted by

$$\mid k^n \omega JM > \equiv \; Z^+(k^n \omega JM) \mid >, \tag{16.12}$$

where ω is the additional quantum number which must be introduced when there is more than one state for a given value of J, and where Z^+ are the linear combinations of a^+ operators which create the antisymmetric n-particle state. (In the literature, [7] one sometimes finds the notation Z in used place of Z^+.) In some cases ω may be a label associated with the seniority quantum number [8] or some group theoretical classification. It will be assumed that these states are constructed to be orthonormal. Computer programs are available for calculating the number of allowed J values in a k^n configuration. [9], [1]

When the n particles are distributed over two k-states, the wavefunctions take the form

$$\mid n\omega JM >= \mid (k_1^{n_1} \omega_1 J_1)(k_2^{n_2} \omega_2 J_2) JM >$$

$$= \sum_{M_1 M_2} < J_1 M_1 J_2 M_2 \mid JM > Z^+(k_2^{n_2}\omega_2 J_2 M_2) Z^+(k_1^{n_1}\omega_1 J_1 M_1) \mid >$$

$$= (-1)^{n_1 n_2} [Z^+(k_1^{n_1}\omega_1 J_1) \otimes Z^+(k_2^{n_2}\omega_2 J_2)]^J_M \mid >, \tag{16.13}$$

where $n = n_1 + n_2$, and where the operators Z^+ are defined in Eq. (16.12) above. The phase factor of $(-1)^{n_1 n_2}$ arises from commuting n_1 particles in state k_1 with n_2 particles in state k_2. Hermitian conjugation of this equation gives

$$< n\omega JM \mid = < (k_1^{n_1}\omega_1 J_1)(k_2^{n_2}\omega_2 J_2) JM \mid$$

$$= \sum_{M_1 M_2} < J_1 M_1 J_2 M_2 \mid JM > < \mid Z(k_1^{n_1}\omega_1 J_1 M_1) Z(k_2^{n_2}\omega_2 J_2 M_2)$$

$$= < \mid [Z(k_1^{n_1}\omega_1 J_1) \otimes Z(k_2^{n_2}\omega_2 J_2)]^J_M. \tag{16.14}$$

The values and multiplicities of J in Eq. (16.13) are those allowed by the vector coupling of all possible $\vec{J}_1$ and $\vec{J}_2$.

When the n particles are distributed over many k states, the wavefunctions take one of the possible forms allowed by the successive vector coupling of the angular momenta. As an example, for three states

$$\mid n\omega JM > = \mid [(k_1^{n_1}\omega_1 J_1)(k_2^{n_2}\omega_2 J_2) J_{12}][k_3^{n_3}\omega_3 J_3] JM >, \tag{16.15}$$

where $n = n_1 + n_2 + n_3$. For a given total number of particles n, the distribution $n_1, n_2 \ldots$ among the k states will be referred to as the partition.

16.3 Angular momentum projection

The angular-momentum projection operator can be used to construct explicit linear combinations of the M-scheme Slater determinants which have good total angular momentum. These linear combinations can thus be used to construct a Hamiltonian matrix which is block diagonal in J. Before discussing the angular-momentum projection operator, the results for the simpler types of angular-momentum operators will be reviewed.

The single-particle states $\mid k,m>$ are eigenfunctions of the j^2 and j_z operators

$$j^2 \mid km> = j(j+1) \mid km> \tag{16.16}$$

and

$$j_z \mid km> = m \mid km> . \tag{16.17}$$

The j^2 operator can be written in terms of the raising and lowering operators $j_\pm$

$$j^2 = j_- j_+ + j_z^2 + j_z = j^2 = j_+ j_- + j_z^2 - j_z, \tag{16.18}$$

where

$$j_\pm \mid km> = \sqrt{j(j+1) - m(m\pm 1)} \mid k, m\pm 1> . \tag{16.19}$$

The total angular momentum is a one-body operator given by a sum over the angular momenta of the particles

$$\vec{J} = \sum_{k=1}^{n} \vec{j}_k. \tag{16.20}$$

J^2 is a two-body operator given in terms of the vector components of Eq. (16.20) by

$$J^2 = J_- J_+ + J_z^2 + J_z. \tag{16.21}$$

The second-quantized form for the one-body vector operators are

$$\hat{J}_z = \sum_{\alpha\beta} <\alpha \mid J_z \mid \beta> a_\alpha^+ a_\beta = \sum_{\alpha\beta} m_\alpha \delta_{\alpha\beta} a_\alpha^+ a_\beta$$

$$= \sum_{km} m a_{km}^+ a_{km}, \tag{16.22}$$

and

$$\hat{J}_\pm = \sum_{km} \sqrt{j(j+1) - m(m\pm 1)}\, a_{k,m\pm 1}^+ a_{km}. \tag{16.23}$$

One can operate with $\hat{J}^2$ on any M-state Slater determinant to determine whether or not it has good angular momentum. For example, for the closed-shell configuration of a given single-particle state defined by

$$\mid C_k> = a_{kj}^+ a_{k,j-1}^+ \ldots a_{k,-j}^+ \mid> \tag{16.24}$$

one obtains

$$\hat{J}_z \mid C_k >= M \mid C_k >= \sum_{km} m \; a^+_{km} a_{km} \mid C_k >$$

$$= \sum_{m=-j}^{j} m \mid C_k >= 0 \mid C_k >, \tag{16.25}$$

and

$$\hat{J}_\pm \mid C_k >= \sum_{km} \sqrt{j(j+1) - m(m \pm 1)} \, a^+_{k,m\pm1} a_{km} \mid C_k >= 0, \tag{16.26}$$

since the state with quantum numbers $(k, m \pm 1)$ is already occupied in $|\mathrm{C}_k >$. Hence $M = 0$ and by Eq. (16.21) $J = 0$. That is, the closed-shell configuration is spherically symmetric. The general closed-shell configuration

$$\mid C >= \prod_a \mid C_{k_a} > \tag{16.27}$$

also has $J = M = 0$, and thus only partially filled shells contribute to non-zero angular momenta.

The closed-shell plus one-particle configuration (the single-particle configuration) can be represented by

$$\mid Ck_a > \equiv \; a^+_{k_a m_a} \mid C > . \tag{16.28}$$

This state is also an eigenstate of $\hat{J}^2$ and $\hat{J}_z$ with eigenvalues $j_a(j_a + 1)$ and m_a, respectively.

The closed-shell minus one-particle configuration (the single-hole configuration) with one particle absent in the state $(k_\alpha m_\alpha)$ is given by

$$\mid C(k_\alpha m_\alpha)^{-1} >= (-1)^{j_\alpha - m_\alpha} a_{k_\alpha m_\alpha} \mid C > \tag{16.29}$$

Operation of $\hat{J}_z$ and $\hat{J}^2$ on this state gives

$$\hat{J}_z \mid C(k_\alpha m_\alpha)^{-1} >= \sum_{m=-j, m\neq m_\alpha}^{m=j} m \mid C(k_\alpha, m_\alpha)^{-1} >$$

$$= -m_\alpha \mid C(k_\alpha, m_\alpha)^{-1} > . \tag{16.30}$$

and

$$\hat{J}^2 \mid C(k_\alpha, m_\alpha)^{-1} >= j_\alpha(j_\alpha + 1) \mid C(k_\alpha, m_\alpha)^{-1} > . \tag{16.31}$$

Hence, the single-hole configuration as defined by Eq. (16.29) has $J = j_\alpha$ and $M = -m_\alpha$. The single-hole configuration with $J = j_\alpha$ and $M = m_\alpha$ is given by the closed-shell configuration with one particle absent in the state $(k_\alpha, -m_\alpha)$

$$\mid Ck_\alpha^{-1} > \equiv \; (-1)^{j_\alpha + m_\alpha} a_{k_\alpha, -m_\alpha} \mid C > \equiv \; \tilde{a}_{k_\alpha m_\alpha} \mid C >, \tag{16.32}$$

where $\tilde{a}$ is the tensor operator of rank j_α.

In general, multi-particle M-states $\mid \Phi_\alpha(\mathrm{M})>$ are not eigenstates of $\hat{J}^2$ (they do not have a good J value). However, states with good J are linear combinations of the M-states:

$$\mid \Psi(\omega JM) >= \sum_{\alpha=1}^{d(M)} c_\alpha \mid \Phi_\alpha(M) > . \tag{16.33}$$

Conversely, the M-states are linear combinations of the J-states:

$$\mid \Phi_a(M) >= \sum_{J\geq M}^{J_{max}} \sum_{\omega=1}^{D(J)} d_{\omega J} \mid \Psi(\omega JM) > . \tag{16.34}$$

The $d(M)$ and $D(J)$ are the M-scheme and J-scheme dimensions, respectively. Any configuration which has $d(M) = 1$ must have good angular momentum $J = M_{max}$, since there is only one term in Eqs. (16.33). In particular, the state $\mid \Phi(\mathrm{M}_{max})>$ with $M = M_{max}$ has $J = M_{max}$. This can also be seen from the fact that

$$\hat{J}_+ \mid \Phi(M_{max}) >= 0, \tag{16.35}$$

and hence

$$\begin{aligned} \hat{J}^2 \mid \Phi(M_{max}) >&= (J_z^2 + J_z) \mid \Phi(M_{max}) > \\ &= (M_{max}+1)M_{max} \mid \Phi(M_{max}) > . \end{aligned} \tag{16.36}$$

An operator that projects out the component with $J = J_o$ leaving the component with $J = J_i$ unchanged is

$$\bar{P}_{J_iJ_o} \equiv \frac{\hat{J}^2 - J_o(J_o+1)}{J_i(J_i+1) - J_o(J_o+1)}. \tag{16.37}$$

This can be seen by operating with $\bar{P}$ on the wave function of Eq. (16.34)

$$\bar{P}_{J_iJ_o} \mid \Phi_a(M) >= \sum_{J\geq M, J\neq J_o}^{J_{max}} \sum_{\omega=1}^{D(J)} d'_{\omega J} \mid \Psi(\omega JM) >, \tag{16.38}$$

where

$$d'_{\omega J} = \frac{J(J+1) - J_o(J_o+1)}{J_i(J_i+1) - J_o(J_o+1)} d_{\omega J}. \tag{16.39}$$

That is, the component with $J = J_o$ is missing and the component with $J = J_i$ has $d' = d$.

The operator, which projects out all of the unwanted components with $J = J_o$ leaving only one component with $J = J_i$, is thus

$$P_{J_i} \equiv \prod_{J_o=M, J_o\neq J_i}^{J_{max}} \bar{P}_{J_iJ_o} = \prod_{J_o=M, J_o\neq J_i}^{J_{max}} \frac{\hat{J}^2 - J_o(J_o+1)}{J_i(J_i+1) - J_o(J_o+1)}. \tag{16.40}$$

P_{J_i} acting on the wave function of Eq. (16.34) gives

$$P_{J_i} \mid \Phi_a(M) >= \sum_{\omega=1}^{D(J)} d_{\omega J_i} \mid \Psi(\omega J_i M) > . \tag{16.41}$$

Since each of the states $\Psi(\omega JM)$ is a linear combination of M-states, the sum in the above equation is also be a linear combination of M-states

$$\sum_{\omega=1}^{D(J)} d_{\omega J_i} \mid \Psi(\omega J_i M) >= \sum_{b=1}^{d(M)} e_b \mid \Phi_b(M) > . \tag{16.42}$$

Evaluation of the real coefficients e_b will be illustrated below by some examples.

When $d(M) > D(J)$, the set of J-states obtained from operating P_{J_i} on all of the M-states is overcomplete. Also it may happen the projection from different M-states produces states which are not linearly independent (as in the above examples). Thus, one must carefully choose $D(J)$ out of the total set of $d(M)$ projected states which will form a complete basis. In addition, when $D(J) > 1$, the projected states will not necessarily be orthogonal, and they must be orthogonalized by the Gram-Schmidt orthogonalization procedure.

In general, the angular-momentum projection operator can be applied to configurations with particles distributed over several single-orbital states. The projection operator cannot change the partition (the number of particles in each single-orbital state). Thus the overlaps between the good J states in different partitions is automatically zero. Only one partition need be considered at a time for constructing the good J states.

The projection operator is unitary,

$$P_{J_i} P_{J_i} = P_{J_i}, \tag{16.43}$$

and it commutes with the spherically symmetric Hamiltonian operator,

$$[H, P_{J_i}] = 0. \tag{16.44}$$

Thus, matrix elements of the Hamiltonian operator with the states of good J can be obtained by projecting on only one side

$$< \Phi_a \mid P_{J_i} H P_{J_i} \mid \Phi_b >=< \Phi_a \mid H P_{J_i} P_{J_i} \mid \Phi_b >=< \Phi_a \mid H P_{J_i} \mid \Phi_b > . \tag{16.45}$$

16.3.1 Examples for $(j = 5/2)^n$ configurations

Example (i): For the $(j = 5/2)^2$ configuration there are two M-states with $M = 2$

$$\mid a >= a^+_{-1/2} a^+_{5/2} \mid > \tag{16.46}$$

and

$$\mid b >= a^+_{1/2}a^+_{3/2} \mid > . \tag{16.47}$$

($a^+_{-1/2} \equiv a^+_{j=5/2,m=-1/2}$, etc.) These must by associated with the J-states that have J =2 or 4. From Eq. (16.4), $J = 4$ is the maximum J-value allowed, and due to the Pauli principle [Eq. (16.7)] $J = 3$ is not allowed. Operation with $\hat{J}^2$ gives

$$\hat{J}^2 \mid a >= 15 \mid a > +\sqrt{45} \mid b > \tag{16.48}$$

and

$$\hat{J}^2 \mid b >= \sqrt{45} \mid a > +11 \mid b > . \tag{16.49}$$

The linear combination of $\mid a >$ and $\mid b >$ that has $J = 2$ can be obtained by projecting out the states with J_o =3 and 4 by operating on $\mid a >$ or $\mid b >$ with $P_{J=2}$ and projecting out the states with J_o =3 and 4; in particular $\mid a >$ gives

$$P_{J=2} \mid a >= \bar{P}_{J=2,J_o=3}\bar{P}_{J=2,J_o=4} \mid a >= \left\{\frac{\hat{J}^2-12}{6-12}\right\}\left\{\frac{\hat{J}^2-20}{6-20}\right\} \mid a >$$

$$= \left\{\frac{\hat{J}^2-12}{6-12}\right\}\sqrt{\frac{5}{14}}\left\{\sqrt{\frac{5}{14}} \mid a > -\sqrt{\frac{9}{14}} \mid b >\right\}$$

$$= \frac{5}{14} \mid a > -\frac{\sqrt{45}}{14} \mid b >= \sqrt{\frac{5}{14}}\left\{\sqrt{\frac{5}{14}} \mid a > -\sqrt{\frac{9}{14}} \mid b >\right\}. \tag{16.50}$$

(Note that the operation of projecting out $J_o = 3$ had no effect because $J_o = 3$ is forbidden by the Pauli principle.) The normalization factor taken out in front in the last line shows that the probability of finding the component $J = 2$ component in state $\mid a >$ is 5/14 (and thus the probability to find the $J = 4$ component must be 9/14). In this two-particle example the factors inside the {} brackets in the last line must be within a phase factor of the result obtained with Eq. (16.6) with $N_{12} = \frac{1}{\sqrt{2}}$

$$\frac{1}{\sqrt{2}}\,(2)\ < 5/2, -1/2, 5/2, 5/2 \mid 2, 2 >= -\sqrt{\frac{5}{14}} \tag{16.51}$$

and

$$\frac{1}{\sqrt{2}}\,(2)\ < 5/2, 1/2, 5/2, 3/2 \mid 2, 2 >= \sqrt{\frac{9}{14}}, \tag{16.52}$$

where the factor of (2) comes from the fact that there are two terms in Eq. (16.6) which contribute to a given antisymmetric M-scheme basis state. The normalized wave function is

$$\frac{P_{J=2} \mid a >}{N_a} = \sqrt{\frac{5}{14}} \mid a > -\sqrt{\frac{9}{14}} \mid b > \tag{16.53}$$

The same result (up to a phase factor) would be obtained from $P_{J=2}$ acting on the state $\mid b >$. In general the projection operator applied to any two-particle configuration gives results which are equivalent to those in Sec. 16.2. However, the projection operator can also be applied in the general case of the n-particle configuration to obtain wave functions with good J, as in the next example.

Example (ii): From Table 16.1 it is seen that there are two M-states for the $(j = 5/2)^3$ configuration with $M = 5/2$

$$|c> = a^+_{-3/2}a^+_{3/2}a^+_{5/2}\,|> \tag{16.54}$$

and

$$\mid d> = a^+_{-1/2}a^+_{1/2}a^+_{5/2}\,|> \tag{16.55}$$

The operation of $\hat{J}^2$ on these states gives

$$\hat{J}^2|c> = \frac{67}{4}|c> + \frac{32}{4}\mid d>$$

and

$$\hat{J}^2 \mid d> = \frac{67}{4}|c> + \frac{32}{4}\mid d> \tag{16.56}$$

Since there is no $J_o = 7/2$ component, the state with $J = 5/2$ can be obtained by projecting out the $J_o = 9/2$ component from state $|c>$

$$P_{J=5/2}|c> = \frac{(\hat{J}^2 - \frac{99}{4})}{(\frac{35}{4} - \frac{99}{4})}|c> = \frac{1}{\sqrt{2}}\left\{-\frac{1}{\sqrt{2}}\,|c> + \frac{1}{\sqrt{2}}\mid d>\right\}. \tag{16.57}$$

The normalized projected wave functions is given by

$$\frac{P_{J=5/2}|c>}{N_c} = \left\{-\frac{1}{\sqrt{2}}\,|c> + \frac{1}{\sqrt{2}}\mid d>\right\}. \tag{16.58}$$

16.4 General form for the matrix elements in the J scheme

In this section, a few general results for the matrix elements for creation operator in the J-scheme are given. These will be used in subsequent sections when the matrix elments of the J-coupled forms are derived.

In addition to the angular momentum recoupling, attention must be paid to the phase factors which occur due to the reordering of particles between groups. Examples of these phase factors for the wave functions themselves appear above in Eqs. (16.10) and (16.13). As an example for the particle-number-dependent phase factors in matrix elements of the creation and destruction operators, consider a matrix element involving the wave functions of Eqs. (16.13) and (16.14) with operators $O(k_i n_i'')$ which involve n_i'' creation and/or destruction operators for the state k_i

$$
\begin{aligned}
&< (k_1^{n_1}\omega_1 J_1)(k_2^{n_2}\omega_2 J_2) JM \mid O(k_1 n_1'')O(k_2 n_2'') \mid (k_1^{n_1'}\omega_1' J_1')(k_2^{n_2'}\omega_2' J_2') J'M' > \\
&\quad = \sum_{M_i M_i'} < J_1 M_1 J_2 M_2 \mid JM >< J_1' M_1' J_2' M_2' \mid J'M' > \\
&\quad \times <\mid Z(k_1^{n_1}\omega_1 J_1 M_1) Z(k_2^{n_2}\omega_2 J_2 M_2) O(k_1 n_1'') O(k_2 n_2'') \\
&\quad\quad \times Z^+(k_2^{n_2'}\omega_2' J_2' M_2') Z^+(k_1^{n_1'}\omega_1' J_1' M_1') \mid> \\
&= (-1)^{n_2 n_1'' + n_1'(n_2+n_2'+n_2'')} \sum_{M_i M_i'} < J_1 M_1 J_2 M_2 \mid JM >< J_1' M_1' J_2' M_2' \mid J'M' > \\
&\quad \times <\mid Z(k_1^{n_1}\omega_1 J_1 M_1) O(k_1 n_1'') Z^+(k_1^{n_1'}\omega_1' J_1' M_1') \\
&\quad \times Z(k_2^{n_2}\omega_2 J_2 M_2) O(k_2 n_2'') Z^+(k_2^{n_2'}\omega_2' J_2' M_2') \mid> .
\end{aligned}
\tag{16.59}
$$

The phase factor arises from first commuting the state operator Z for n_2 with the operator O for n_1'', and next commuting the state operator Z^+ for n_1' with the operators for n_2', n_2'' and n_2. The phase factor can be simplified by noting that $n_i + n_i' + n_i''$ is always even. This can be seen by considering n_i'' as a sum of the number of creation, c_i'', and destruction, d_i'', operators. It is clear that the total number of destruction operators, $n_i + d_i''$, must equal the total number of creation operators, $n_i' + c_i''$. Since $n_i + d_i'' = n_i' + c_i''$, and both are integers, the sum $n_i + d_i'' + n_i' + c_i'' = n_i + n_i' + n_i''$ must be even. This also means that $(-1)^{n_i''} = (-1)^{n_i + n_i'}$. Thus the phase factor becomes

$$
(-1)^{n_2 n_1'' + n_1'(n_2+n_2'+n_2'')} = (-1)^{n_2 n_1''} = (-1)^{n_2(n_1+n_1')}. \tag{16.60}
$$

A general angular momentum recoupling result that is often needed is the matrix element for an operator which acts only on particles in a set of active states $(n_a J_a)$ and not on those in a set of inactive states $(n_i J_i)$

$$
< (n_i\omega_i J_i)(n_a\omega_a J_a) J || O^\lambda(n_a'') || (n_i'\omega_i' J_i')(n_a'\omega_a' J_a') J' >
$$

$$= (-1)^{J'_i+J'_a+J+\lambda}\sqrt{(2J+1)(2J'+1)}\left\{\begin{array}{ccc} J_a & J'_a & \lambda \\ J' & J & J_i \end{array}\right\}$$
$$\times < n_a\omega_a J_a||O^\lambda(n''_a)||n'_a\omega'_a J'_a > \delta_{n_i n'_i}\delta_{J_i J'_i}\delta_{\omega_i\omega'_i}. \quad (16.61)$$

where Eq. 13.48 has been used and the number-dependent phase factor from Eq. (16.60) is $(-1)^{n_\alpha(2n_i)} = 1$. The matrix element with the active and inactive states interchanged is the same except for the phase factor; from Eq. 13.49

$$< (n_a\omega_a J_a)(n_i\omega_i J_i)J||O^\lambda(n''_a)||(n'_a\omega'_a J'_a)(n'_i\omega'_i J'_i)J' >$$
$$= (-1)^{J_a+J_i+J'+\lambda}\sqrt{(2J+1)(2J'+1)}\left\{\begin{array}{ccc} J_a & J'_a & \lambda \\ J' & J & J_i \end{array}\right\}$$
$$\times < n_a\omega_a J_a||O^\lambda(n''_a)||n'_a\omega'_a J'_a > \delta_{n_i n'_i}\delta_{J_i J'_i}\delta_{\omega_i\omega'_i}. \quad (16.62)$$

References

[1] W. D. M. Rae, A. Etchegoyen and B. A. Brown, *OXBASH, the Oxford-Buenos Aries-MSU Shell-Model Code*, Michigan State University Laboratory Report no. 524.

[2] R. R. Whitehead, A. Watt, B. J. Cole and I. Morrison, Advances in Nuclear Nuclear Physics **9**, 123, (1977); L. M. Mackenzie, A. M. Macleod, D. J. Berry and R. R. Whitehead, Comput. Phys. Comm. 48, 229 (1988).

[3] R. D. Lawson, *Theory of the Nuclear Shell Model*, (Clarendon Press, 1980).

[4] T. Sebe and M. Harvey, "Enumeration of Many-Body States of the Nuclear Shell Model with Definite Angular Momentum and Isobaric Spin with Mixed Single Particle Orbits", ARCL, Chalk River preprint 3007 (1968).

[5] D. K. Sunko, Phys. Rev. C33, 1811 (1986).

[6] J. P. Draayer and H. T. Valdes, Comput. Phys. Comm. 36, 313 (1985).

[7] P. J. Brussaard and P. W. M. Glaudemans, *Shell Model Applications in Nuclear Spectroscopy*, (North Holland, 1977).

[8] A. de Shalit and I. Talmi, *Nuclear Shell Theory*, (Academic Press, 1963).

[9] L. B. Hubbard, Comput. Phys. Commun. 1, 453 (1970).

17 The Two-Body Hamiltonian

17.1 Introduction

In this section we will discuss the methods used to calculate two-body hamiltonian matrix elements for use in microscopic nuclear structure studies. The starting point for the two-body interaction is the data on nucleon-nucleon (NN) scattering and its interpretation in terms of NN potentials. For very light nuclei $A \leq 8$ one can carry out calculations with Green's Function Monte-Carlo techniques in which the NN interaction is a direct input [1]. The result is that the theoretical binding energies are about 25% smaller than experiment. This corresponds to the interaction energy being about 5% to small (there is a large cancellation between kinetic and potential energy). To do better one has to introduce phenomenological three-body interactions for which direct experimental data does not exist.

Calculations for heavier nuclei are based upon a sub-space (a model space) within the shell-model basis. For these calculations the NN interaction must be renormalized to take into account the finite basis. This renormalization is usually divided into two steps. The first step uses Brueckner theory to deal with strongly repulsive short-range part of the interaction. This theory uses the NN interaction to obtain G matrix elements. The resulting G matrix elements can be expressed in terms of an effective one-boson exchange potential such as M3Y [2] or HKT [3]. Alternatively one may take only the low-momentum (low-k) part of the NN interaction to calculate the two-body matrix elements. In this section we will discuss methods used to calculate two-body interactions from effective potential models.

The second step is to renormalize the G matrix elements to take into account configurations which are omitted from the model space that are not included in the Brueckner G matrix. The are called "core-polarization" corrections and the two-body matrix elements are called G_{eff}. Calculations with G_{eff} are rather successful for the spectra of nuclei with a few valence nucleons removed from the closed shells [4], [5].

For systems with three or more valence nucleons, the agreement with experiment can be improved by using effective potentials or effective two-body matrix elements V_{eff} that are determined from the binding energy data. The differences between G_{eff} and V_{eff} are not well understood, but part of it may come from the omitted three-body interactions.

17.2 Form of the two-body matrix elements

Antisymmetric J-coupled two-body matrix elements are the primary ingredients for the setting up the Hamiltonian matrix. With the results of Sec. 16.2 they can be evaluated by expanding them into direct and exchange terms involving the product wavefunctions:

$$< k_1 k_2 J \mid V \mid k_3 k_4 J >$$

$$= N_{12} N_{34} \sum_{m_i} < j_1 m_1 j_2 m_2 \mid JM >< j_3 m_3 j_4 m_4 \mid JM >< k_1 m_1 k_2 m_2 \mid V \mid k_3 m_3 k_4 m_4 >$$

$$= N_{12} N_{34} \sum_{m_i} < j_1 m_1 j_2 m_2 \mid JM >< j_3 m_3 j_4 m_4 \mid JM >$$

$$\times \{< k_1 m_1 k_2 m_2 \mid V \mid k_3 m_3 k_4 m_4 >_p - < k_1 m_1 k_2 m_2 \mid V \mid k_4 m_4 k_3 m_3 >_p\}, \quad (17.1)$$

where the subscripte p indicates that this is the "product" wavefunction. With the symmetry properties of the Clebsch-Gordan coefficients the sums of m_i can be carried to obtain:

$$< k_1 k_2 J \mid V \mid k_3 k_4 J >= \frac{1}{\sqrt{[(1+\delta_{k_1 k_2})(1+\delta_{k_3 k_4})]}}$$

$$\times \Big\{< k_1 k_2 J \mid V \mid k_3 k_4 J >_p -(-1)^{j_3+j_4-J} < k_1 k_2 J \mid V \mid k_4 k_3 J >_p \Big\}. \quad (17.2)$$

Since the interaction V is Hermitian and the matrix elements are real, one has

$$< k_3 k_4 J \mid V \mid k_1 k_2 J >=< k_1 k_2 J \mid V \mid k_3 k_4 J > . \quad (17.3)$$

In addition, one has from the wavefunction symmetry:

$$< k_1 k_2 J \mid V \mid k_4 k_3 J >= -(-1)^{j_3+j_4-J} < k_1 k_2 J \mid V \mid k_3 k_4 J >, \quad (17.4)$$

and

$$< k_2 k_1 J \mid V \mid k_3 k_4 J >= -(-1)^{j_1+j_2-J} < k_1 k_2 J \mid V \mid k_3 k_4 J > . \quad (17.5)$$

Thus it is sufficient to calculate the two-body matrix element for only one-ordering of k_1, k_2, k_3 and k_4.

When isospin is introduced the factors associated with j and J are doubled with those involving $t = \frac{1}{2}$ and T and the last four equations become:

$$< k_1 k_2 JT \mid V \mid k_3 k_4 JT >= \frac{1}{\sqrt{[(1+\delta_{k_1 k_2})(1+\delta_{k_3 k_4})]}}$$

$$\times \Big\{< k_1 k_2 JT \mid V \mid k_3 k_4 JT >_p -(-1)^{j_3+j_4-J+1-T} < k_1 k_2 JT \mid V \mid k_4 k_3 JT >_p \Big\}, \quad (17.6)$$

$$< k_3k_4JT \mid V \mid k_1k_2JT >=< k_1k_2JT \mid V \mid k_3k_4JT >, \tag{17.7}$$

$$< k_1k_2JT \mid V \mid k_4k_3JT >= -(-1)^{j_3+j_4-J+1-T} < k_1k_2JT \mid V \mid k_3k_4JT >, \tag{17.8}$$

and

$$< k_2k_1JT \mid V \mid k_3k_4JT >= -(-1)^{j_1+j_2-J+1-T} < k_1k_2JT \mid V \mid k_3k_4JT > . \tag{17.9}$$

The M-scheme two-body matrix elements can be expressed in terms of these J-coupled two-body matrix elements

$$< k_1m_1k_2m_2 \mid V \mid k_3m_3k_4m_4 >= \sqrt{(1+\delta_{k_1\,k_2})(1+\delta_{k_3\,k_4})}$$

$$\times \sum_{JM} < JM \mid j_1m_1j_2m_2 >< JM \mid j_3m_3j_4m_4 >< k_1k_2J \mid V \mid k_3k_4J > . \tag{17.10}$$

When isospin is introduced this becomes

$$< (k_1m_1t_z)(k_2m_2t'_z) \mid V \mid (k_3m_3t_z)(k_4m_4t'_z) >= \sqrt{(1+\delta_{k_1\,k_2})(1+\delta_{k_3\,k_4})}$$

$$\times \sum_{JMTT_z} < JM \mid j_1m_1j_2m_2 >< JM \mid j_3m_3j_4m_4 >$$

$$\times < TT_z \mid \frac{1}{2}t_z\frac{1}{2}t'_z >< TT_z \mid \frac{1}{2}t_z\frac{1}{2}t'_z >< k_1k_2JT \mid V \mid k_3k_4JT > . \tag{17.11}$$

Conservation of charge means that there are two basic types of interactions. Those with $(t_z, t'_z) = (p, p)$ or $(t_z, t'_z) = (n, n)$ which must have $T = 1$, and those with $(t_z, t'_z) = (p, n)$ which are a linear combination of $T = 0$ and $T = 1$.

17.3 General types of interactions

The general form of the two-body potential consists of central (c), spin-orbit (s) and spin-tensor (t) components:

$$V_c = f_c(r), \tag{17.12}$$

$$V_s = f_s(r)\ \vec{L}\cdot\vec{S}, \tag{17.13}$$

and

$$V_t = f_t(r)\ S_{12}. \tag{17.14}$$

In these equations,

$$\vec{S} = (\vec{\sigma}_1 + \vec{\sigma}_2)/2, \tag{17.15}$$

$\vec{L}$ is relative angular momentum operator, and S_{12} is the spin-tensor operator

$$S_{12} = 3(\vec{\sigma}_1\cdot\hat{r})(\vec{\sigma}_2\cdot\hat{r}) - (\vec{\sigma}_1\cdot\vec{\sigma}_2), \tag{17.16}$$

where $\vec{r}$ is the relative coordinate

$$\vec{r} = \vec{r}_1 - \vec{r}_2,$$

with magnitude $r = \mid \vec{r} \mid$. (17.17)

In order to carry out the tensor algbra it is useful to rewite the potential in terms of tensor operators $U^{(q)}$ which act on the spacial coordinates and $X^{(q)}$ which act on the spin coordinates:

$$V = \sum_q V_q = \sum_q U^{(q)} \cdot X^{(q)}, \tag{17.18}$$

The interaction components are specified by $q = 0$ for central, $q = 1$ for spin-orbit and $q = 2$ for spin-tensor.

In order to carry out the tensor algebra one can rewrite the interaction of Eqs. (17.12)-(17.14) in the form of Eq. (17.18) with the spacial parts U given by:

$$U^{(0)}(\vec{r}) = f_c(r), \tag{17.19}$$

$$U^{(1)}(\vec{r}) = f_s(r)\ \vec{L}, \tag{17.20}$$

and

$$U^{(2)}(\vec{r}) = f_t(r)\ Y^{(2)}(\hat{r}), \tag{17.21}$$

and the spin parts X given by

$$X^{(0)} = 1, \tag{17.22}$$

$$X^{(1)} = \vec{S}, \tag{17.23}$$

and

$$X^{(2)} = \sqrt{\frac{24\pi}{5}}\,[\vec{\sigma}_1 \otimes \vec{\sigma}_2]^{(2)}. \tag{17.24}$$

To evaluate the space and spin components of the matrix elements of Eq. (17.18) we need to transform from jj to LS coupling:

$$< k_a k_b JT \mid V \mid k_c k_d JT >_p = \sum_{LSL'S'} \begin{bmatrix} \ell_a & 1/2 & j_a \\ \ell_b & 1/2 & j_b \\ L & S & J \end{bmatrix} \begin{bmatrix} \ell_c & 1/2 & j_c \\ \ell_d & 1/2 & j_d \\ L' & S' & J \end{bmatrix}$$

$$\times\ < k_A k_B LSJT \mid V \mid k_C k_D L'S'JT >_p\ . \tag{17.25}$$

k_A is shorthand for the set of quantum numbers $(n_a \ell_a)$ and k_a is shorthand for the set $(n_a \ell_a j_a)$, etc. The large square bracket is the LS to jj transformation coefficient given by Eq. 14.25. With Eq. (17.18), these LS coupled matrix elements are then expressed in terms of reduced matrix elements:

$$< k_A k_B LSJT \mid V \mid k_C k_D L'S'JT >_p$$

$$= \sum_q < k_A k_B LSJT \mid V_q \mid k_C k_D L'S'JT >_p = \sum_q (-1)^{S+L'+J} \left\{ \begin{array}{ccc} L & S & J \\ S' & L' & q \end{array} \right\}$$
$$\times < k_A k_B L||U^{(q)}||k_C k_D L' >< ST||X^{(q)}||S'T > . \quad (17.26)$$

17.4 Transformation from relative to center-of-mass coordinates

The shell-model wavefunctions are expressed in terms of the coordinates $\vec{r}_1$ and $\vec{r}_2$ with respect to a fixed center, but the NN interaction depends on the relative coordinate $\vec{r}$. The transformation between center-of-mass and relative coordinates can be carried out in an oscillator basis. The reason is that the oscillator hamiltonian is seperable in both coordinates:

$$H = \frac{p_1^2}{2m} + \frac{p_2^2}{2m} + \frac{1}{2}m\omega^2 r_1^2 + \frac{1}{2}m\omega^2 r_2^2$$
$$= \frac{Q^2}{2M} + \frac{1}{2}M\omega^2 R^2 + \frac{p^2}{2\mu} + \frac{1}{2}\mu\omega^2 r^2, \quad (17.27)$$

where $M = 2m$ and $\mu = m/2$ (m is the nucleon mass). The quantum numbers of the usual shell-model basis are:

$$\mid k_1 k_2 L > = \mid (n_1\ell_1)(n_2\ell_2)L >, \quad (17.28)$$

and the quantum numbers associated with the relative coordinates are:

$$\mid (n\lambda)(N\Lambda)L >, \quad (17.29)$$

where (n, λ) are the radial and angular-momentum quantum numbers associated with the relative coordinate $\vec{r}$, and (N, Λ) go with the center-of-mass coordinate $\vec{R}$. The transformation between these two sets of coordinates is given by:

$$\mid k_1 k_2 L > = \mid (n_1\ell_1)(n_2\ell_2)L > = \sum_{n\lambda N\Lambda} < n\lambda N\Lambda L \mid n_1\ell_1 n_2\ell_2 L > \mid (n\lambda)(N\Lambda)L > . \quad (17.30)$$

These transformation coefficients are called Moshinsky or Talmi-Moshinsky brackets after the authors who first calculated their properties. Note that changing the mass from m to $\mu = m/2$ for the relative motion means that the relative radial wavefunctions use an oscillator parameter which is effectively smaller than ω by a factor of two.

For the matrix element of Eq. (17.26) the spatial wavefunctions $\mid k_A k_B >$ and $\mid k_C k_D >$ are expressed in terms of the relative $(n\lambda)$ and center-of-mass $(N\Lambda)$ coordinates using the Talmi-Moshinsky transformation:

$$< k_A k_B L||U^{(q)}||k_C k_D L' > = \sum_{n\lambda n'\lambda' N\Lambda N'\Lambda'} < n\lambda N\Lambda \mid k_A k_B L >$$

$$\times \; < n'\lambda' N'\Lambda' \mid k_C k_D L' >< n\lambda N\Lambda L||U^{(q)}(\vec{r})||n'\lambda' N'\Lambda' L' > . \tag{17.31}$$

With Eq. 13.49 this last integral reduces to:

$$< n\lambda N\Lambda L||U^{(q)}(\vec{r})||n'\lambda' N'\Lambda' L' >= (-1)^{\lambda+\Lambda+L'+q}\sqrt{(2L+1)(2L'+1)}$$

$$\times \left\{ \begin{array}{ccc} \lambda & \lambda' & q \\ L' & L & \Lambda \end{array} \right\} < n\lambda||U^{(q)}(\vec{r})||n'\lambda' > \delta_{N\,N'}\delta_{\Lambda\,\Lambda'}. \tag{17.32}$$

With the $U(\vec{r})$ given by Eqs. (17.19)-(17.21) the relative integrals reduce to:

$$< n\lambda||U^{(0)}(\vec{r})||n'\lambda' >=< n\lambda \mid f_c(r) \mid n'\lambda' > \sqrt{2\lambda+1}\,\delta_{\lambda\,\lambda'}, \tag{17.33}$$

$$< n\lambda||U^{(1)}(\vec{r})||n'\lambda' >=< n\lambda \mid f_s(r) \mid n'\lambda' > \sqrt{\lambda(\lambda+1)(2\lambda+1)}\,\delta_{\lambda\,\lambda'}, \tag{17.34}$$

and

$$< n\lambda||U^{(2)}(\vec{r})||n'\lambda' >$$

$$= (-1)^{\lambda} < n\lambda \mid f_t(r) \mid n'\lambda' > \sqrt{(2\lambda+1)(2\lambda'+1)} \left\{ \begin{array}{ccc} \lambda & 2 & \lambda' \\ 0 & 0 & 0 \end{array} \right\}. \tag{17.35}$$

The central matrix element ($q = 0$) of Eq. (17.26) simplifies to

$$< k_A k_B LSJT \mid V_0 \mid k_C k_D L' S' JT >_p =$$

$$= \sum_{n\lambda n'\lambda' N\Lambda N'\Lambda'} < n\lambda N\Lambda \mid k_A k_B L >< n'\lambda' N'\Lambda' \mid k_C k_D L' >$$

$$\times \; < n\lambda \mid f_c(r) \mid n'\lambda' > \delta_{N\,N'}\delta_{\Lambda\,\Lambda'}\delta_{L\,L'}\delta_{S,S'}. \tag{17.36}$$

17.5 Simple potentials

The two-body Coulomb is given by the central interaction:

$$V_{coul} = e^2/r. \tag{17.37}$$

It is independent of spin and acts only between protons ($T = 1$).

The simplest short-ranged interaction might be approximated by a delta function:

$$V_{delta} = W\delta(r), \tag{17.38}$$

with a strength W which may depend upon the total spin S. Only λ=λ'=0 contributes to the integral. The spacial symmetry of two nucleons in an λ=0 state is symmetric, and thus $S + T$ must be odd to make the total two-nucleon wavefunction

antisymmetric. Thus the delta function only acts in the $(S,T) = (0,1)$ and $(1,0)$ states. The scalar operator for spin that selects out the S components is

$$(\vec{\sigma}_1 \cdot \vec{\sigma}_2) \mid S = 0 >= -3,$$

and

$$(\vec{\sigma}_1 \cdot \vec{\sigma}_2) \mid S = 1 >= 1. \tag{17.39}$$

Thus the most general delta-function interaction can be witten:

$$V_{delta} = W[1 + \alpha\ (\vec{\sigma}_1 \cdot \vec{\sigma}_2)]\delta(r), \tag{17.40}$$

with typical strength values of $W = -500$ MeV fm^3 and $\alpha = 0.12$. Thus for $(S,T) = (0,1)$ $W(1-3\alpha) = -180$ MeV fm^3, and for $(S,T) = (1,0)$ $W(1+\alpha) = -560$ MeV fm^3.

17.6 One boson exchange potentials

The one-pion exchange potential (OPEP) is the longest ranged part of the NN interaction due to the small mass of 140 MeV for the pion. The form of the OPEP interaction is:

$$V_{OPEP}(r) = g^2\ (\tau_1 \cdot \tau_2)\ [(\vec{\sigma}_1 \cdot \vec{\nabla})(\vec{\sigma}_2 \cdot \vec{\nabla})]f(r), \tag{17.41}$$

where g is the pion-nucleon coupling constant, and $f(r)$ is the Yukawa form:

$$f(r) = \frac{e^{-(r/\rho_\pi)}}{r/\rho_\pi}. \tag{17.42}$$

The range ρ_π is given by

$$\rho_\pi = \hbar/(m_\pi c) = 1.414 \text{ fm}. \tag{17.43}$$

Eq. (17.41) can be expanded and written in terms of the central and spin-tensor operators

$$V_{OPEP}(r) = \frac{g^2}{3}(\tau_1 \cdot \tau_2)\Big\{S_{12}\Big[\frac{3}{r^2} + \frac{3}{\rho_\pi r} + \frac{1}{\rho_\pi^2}\Big]f(r) + \frac{(\vec{\sigma}_1 \cdot \vec{\sigma}_2)}{\rho_\pi^2}f(r) - 4\pi(\vec{\sigma}_1 \cdot \vec{\sigma}_2)\delta(r)\Big\}. \tag{17.44}$$

In the G matrix one takes only the low-k components and the δ(r) term is dropped. The isospin operator is analogous to those for the spin in Eq. (17.39)

$$(\vec{\tau}_1 \cdot \vec{\tau}_2) \mid T = 0 >= -3,$$

and

$$(\vec{\tau}_1 \cdot \vec{\tau}_2) \mid T = 1 >= 1. \tag{17.45}$$

Thus, the central OPEP potential which contains the the term $(\tau_1 \cdot \tau_2)(\vec{\sigma}_1 \cdot \vec{\sigma}_2)$ gives a relative weighting of 9, -3, -3, and 1 to the (S,T) channels (0,0), (0,1), (1,0) and (1,1), respectively. The overall strength of the OPEP interaction as determined from pion-nucleon scattering data is $(g^2\rho_\pi^2) = 42$ MeV fm^3.

Another way to write the OPEP strength is in terms of the projection operators $P_{S,T} = P_S P_T$. These operators project out the part with specific S and T values. For the spin part:

$$P_{S=0} \mid S=0 >= 1, \quad P_{S=0} \mid S=1 >= 0,$$
$$P_{S=1} \mid S=0 >= 0, \quad P_{S=1} \mid S=1 >= 1, \tag{17.46}$$

or in terms of the spin operators:

$$P_{S=0} = \frac{1 - (\vec{\sigma}_1 \cdot \vec{\sigma}_2)}{4},$$
$$P_{S=1} = \frac{3 + (\vec{\sigma}_1 \cdot \vec{\sigma}_2)}{4}, \tag{17.47}$$

with a similar set of equations for the isospin projection. Thus we could write in terms of $P_{S,T}$:

$$(\tau_1 \cdot \tau_2)(\vec{\sigma}_1 \cdot \vec{\sigma}_2) = P_{11} - 3P_{01} - 3P_{10} + 9P_{00}.$$

Hosaka, Kubo and Toki (HKT) [3] parameterized their G-matrix in terms of one-boson-exchange potential (OBEP) forms [6]. In general the functions $f(r)$ can depend on the value of the total spin S and isospin T. Thus we introduce these two indicies as well strength parmeters W which depend on the channel; central (c), spin-orbit (s) or spin-tensor (t); the range index, i, and S and T:

$$f_{c,S,T}(r) = P_{S,T} \sum_i W_{c,i,S,T} \frac{e^{-x_i}}{x_i}, \tag{17.48}$$

$$f_{s,S,T}(r) = P_{S,T} \sum_i W_{s,i,S,T} \Big\{ 1 + \frac{1}{x_i} \Big\} \frac{e^{-x_i}}{x_i^2}, \tag{17.49}$$

and

$$f_{t,S,T}(r) = P_{S,T} \sum_i W_{t,i,S,T} \Big\{ 1 + \frac{3}{x_i} + \frac{3}{x_i^2} \Big\} \frac{e^{-x_i}}{x_i}. \tag{17.50}$$

The x_i is r divided by the range parameter ρ_i:

$$x_i = r/\rho_i. \tag{17.51}$$

The HKT parameterization requires four ranges for the central component: $\rho_i = 0.20$, 0.33, 0.50 and 1.414 fm; two ranges for the tensor component: $\rho_i = 0.25$ and 1.414 fm; and two ranges for the spin-orbit component: $\rho_i = 0.25$ and 0.40 fm. The range

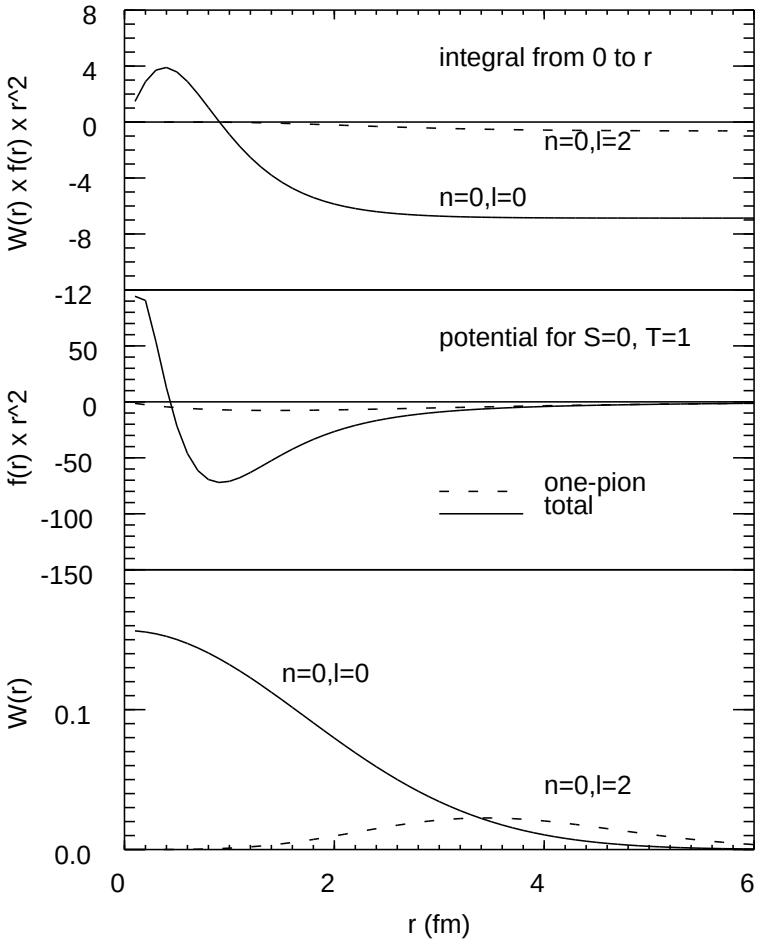

Figure 1: The central $S = 0$, $T = 1$ channel for the the HKT interaction.

1.414 fm is that for the one-pion exchange. The shorter ranges are associated with two-pion, rho and omega meson exchange. The strength parameters W were obtained from a fit to G-matrix elements calculated from the Paris N-N potential [7] and are given in Table 2 of [3].

Contributions to the integral

$$< n\lambda \mid f_c(r) \mid n\lambda > = \int \psi_{n,\lambda}(r) f_c(r) \psi_{n,\lambda} r^2 dr$$

for the central part of the HKT interaction are shown in Figs. (17.1) − (17.4). The bottom panels show the contribution $W = \psi^2_{n,\lambda}$ in the integrand from the relative radial wavefunctions y, the middle panels show the radial part of the potential multiplied by r^2 and the top panels show the integral evaluated out to radius r. Note that the orbital angular momentum of the relative wavefunction is restricted by the symmetry condition that $\ell + S + T$ is odd for a two-particle wavefunction. Thus, for

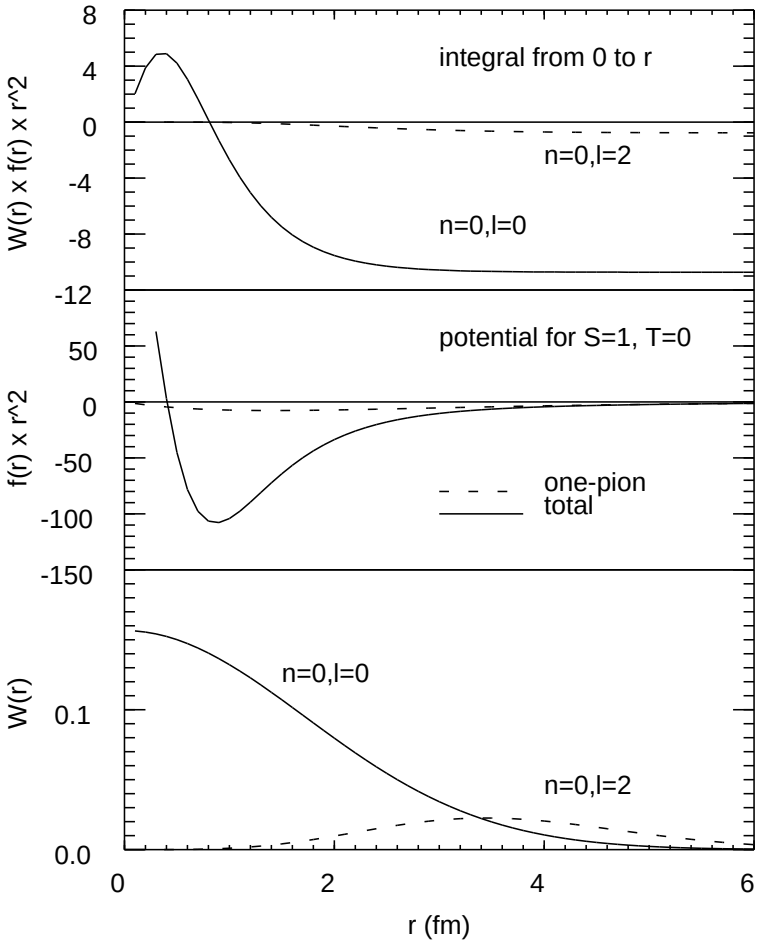

Figure 2: The central $S = 1$, $T = 0$ channel for the the HKT interaction.

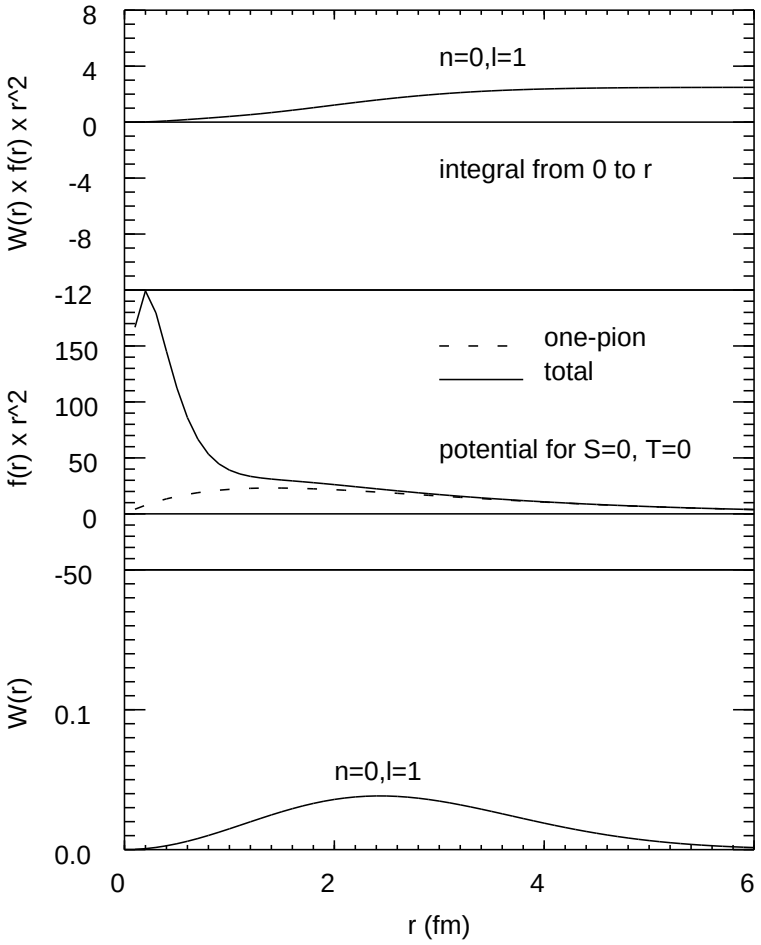

Figure 3: The central $S = 0$, $T = 0$ channel for the the HKT interaction.

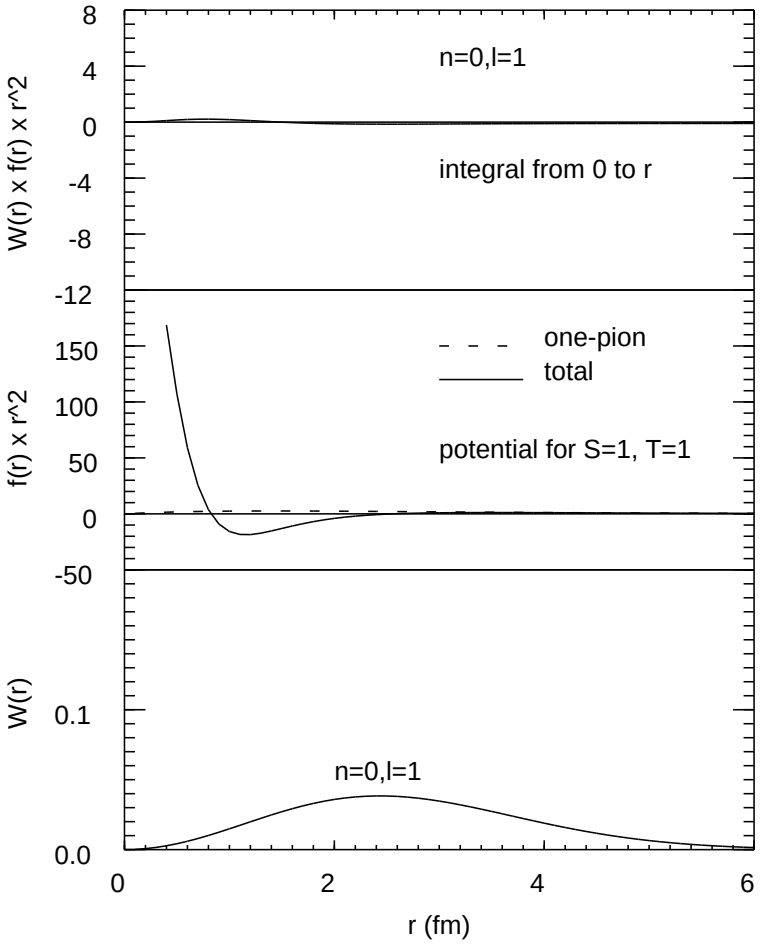

Figure 4: The central $S = 1$, $T = 1$ channel for the the HKT interaction.

a short range potential, the most important contributions are for ℓ=0 in the (S,T) = (0,1) and (1,0) channels.

The longest ranged part of the HKT interaction corresponds to the one-pion-exchange (OPEP) potential. The OPEP contribution to the bare G-matrix provides about 1/3 of the attractive interaction needed for the (S,T) = (0,1) and (1,0) channels of the central component. A common feature of this as well as other OBEP parameterizations is a strong attractive medium-range part which is partly cancelled out by a repulsive short-range part.

17.7 Numerical examples

In Table 1 and 2 I compared some typical values of the two-body matrix elements obtained with the potentials discussed in the proceeding section.

$V_{con} = 1$,

V_{coul} is the Coulomb potential of Eq. (17.37),

V_{del} is the delta-function potential of Eq. (17.40),

V_{OPEP} is the one-pion exchange from Eq. (17.44),

V_G is the HKT G-matrix potential from Eq. (17.48).

17.8 Density-dependent interactions

Phenomenological density-dependent interactions have long played an important role in Hartree-Fock calculations [8], [9], [10] as well as in shell-model calculations [11], [12], [13]. From a more fundamental point of view, density dependence enters into the calculations of the G-matrix in finite nuclei [14]. There also has been a renewed interest in density dependence because of recent developments with relativistic models [15]. For a density-dependent interaction there is an additional dependence on the center-of-mass coordinate:

$$\vec{R} = (\vec{r}_1 + \vec{r}_2)/2. \tag{17.52}$$

The spacial functions $U^{(q)}$ are extended to include a dependence on R:

$$\tilde{U}^{(q)}(R,\vec{r}) = U^{(q)}(\vec{r})\ F_q(R), \tag{17.53}$$

and Eq. (17.32) will become:

$$< n\lambda N\Lambda L||\tilde{U}^{(q)}||n'\lambda' N'\Lambda' L' >= (-1)^{\lambda+\Lambda+L+q}\sqrt{(2L+1)(2L'+1)}$$

Table 1: Values of some central potential matrix elements $< k_1k_2JT \mid V \mid k_3k_4JT >$ (in MeV) with $\hbar\omega$=13.9 MeV. They are labeled by $k = 4$ for $0d_{5/2}$ and $k = 6$ for $1s_{1/2}$.

k_1	k_2	k_3	k_4	J	T	V_{con}	V_{coul}	V_{del}	V_{OPEP}	V_G
4	4	4	4	0	1	1	0.493	−3.109	−0.873	−2.916
4	4	4	4	2	1	1	0.416	−0.711	−0.236	−1.052
4	4	4	4	4	1	1	0.387	−0.296	−0.063	−0.567
4	4	4	6	2	1	0	0.029	−0.496	−0.183	−0.687
4	4	6	6	0	1	0	0.046	−1.068	−0.291	−0.833
4	6	4	6	2	1	1	0.420	−0.740	−0.420	−1.523
4	6	4	6	3	1	1	0.388	0.000	0.156	−0.088
6	6	6	6	0	1	1	0.452	−2.529	−0.951	−2.514
4	4	4	4	1	0	1		−2.954	0.527	−1.027
4	4	4	4	3	0	1		−1.658	−0.038	−1.317
4	4	4	4	5	0	1		−2.591	−0.834	−3.740
4	4	4	6	3	0	0		−1.269	−0.268	−1.487
4	4	6	6	1	0	0		−1.277	−0.199	−0.916
4	6	4	6	2	0	1		−0.864	0.520	−0.239
4	6	4	6	3	0	1		−2.159	−0.804	−3.370
6	6	6	6	1	0	1		−4.426	−0.951	−3.784

Table 2: Values of some spin-orbit (s) and spin-tensor (t) potential matrix elements $< k_1k_2JT \mid V \mid k_3k_4JT >$ (in MeV) with $\hbar\omega$=13.9 MeV. They are labeled by $k = 4$ for $0d_{5/2}$ and $k = 6$ for $1s_{1/2}$.

k_1	k_2	k_3	k_4	J	T	$V_{OPEP}(t)$	$V_G(t)$	$V_G(s)$
4	4	4	4	0	1	1.078	0.732	0.343
4	4	4	4	2	1	0.089	0.043	−0.186
4	4	4	4	4	1	0.190	0.139	−0.049
4	4	4	6	2	1	0.052	0.071	−0.025
4	4	6	6	0	1	0.000	0.000	0.000
4	6	4	6	2	1	0.334	0.245	0.025
4	6	4	6	3	1	−0.239	−0.175	−0.124
6	6	6	6	0	1	0.000	0.000	0.000
4	4	4	4	1	0	0.977	0.450	0.011
4	4	4	4	3	0	0.657	0.414	−0.028
4	4	4	4	5	0	0.198	0.183	−0.034
4	4	4	6	3	0	0.076	0.094	−0.006
4	4	6	6	1	0	0.743	0.460	0.000
4	6	4	6	2	0	−0.124	−0.153	0.011
4	6	4	6	3	0	0.086	0.109	−0.057
6	6	6	6	1	0	0.000	0.000	0.000

$$\times \left\{ \begin{array}{ccc} \lambda & \lambda' & q \\ L' & L & \Lambda \end{array} \right\} < n\lambda||U^{(q)}(\vec{r})||n'\lambda' >< N\Lambda \mid F_q(R) \mid N'\Lambda' > \delta_{\Lambda\,\Lambda'}. \qquad (17.54)$$

A typical form for the density dependence is:

$$D(R) = 1 + A_d F(R)^{B_d}, \qquad (17.55)$$

where and

$$F(R) = 1 + \exp[(R - R_o)/a]^{-1}, \qquad (17.56)$$

where A_d and B_d are constants to be chosen. Initially we take $R_o = 1.1A^{1/3}$ fm (with A=16 for the sd shell) and $a = 0.6$ fm. In the original Skyrme Hartree-Fock calculations [16] and work by Migdal [13], linear density dependence ($B_d = 1$) was assumed. Note that $F(R)$ is the Fermi function which approaches unity as R goes to zero.

It is interesting to compare this density dependence with the commonly used surface-delta interaction (SDI) for the central component [11], [12]. For a zero-range interaction the radial dependence of the two-body matrix element reduces to the integral [11]

$$I = \int D(R)\psi_A(R)\psi_B(R)\psi_C(R)\psi_D(R)R^2 dR. \qquad (17.57)$$

For a surface-delta interaction, one could evaluate this integral with $D(R) = \delta(R - R_o)$ for some value of R_o near the surface. However, in practice one usually replaces the integral by unity times a phase factor which takes into account the fact that the radial wavefunctions ψ(R) conventionally are defined to be positive near the origin):

$$I = (-1)^{n_a+n_b+n_c+n_d}. \qquad (17.58)$$

A more realistic form of the density dependence is given by $D(R)$ in Eq. (17.55) with $A_d = -1$ (i.e., an interaction which goes smoothly to zero in the nuclear interior). In Table (17.1) the radial matrix elements for the sd shell calculated with a density-independent zero-range interaction and with various versions of the density-dependent, zero-range interactions are compared. Very large differences among the various models is noted. Also,it is noted that the linear density dependence gives results which are closest to the commonly used constant approximation of Eq. (17.58). Many of the successful phenomenological global interactions, such the D1 interaction of Decharge and Gogny [9], have a density-dependence which makes the interaction much smaller in the nuclear interior than on the surface.

References

[1] B. R. Wiringa, S. C. Pieper, J. Carlson and V. R. Pandharipande, Phys. Rev. C 62, 014001 (2000).

[2] N. Anantaraman, H. Toki, G. F. Bertsch, Nucl. Phys. A398, 269 (1983).

[3] A. Hosaka, K. I. Kubo, H. Toki, Nucl. Phys. A444, 76 (1985). Note the following corrections: in Eq. (2) the $\vec{\sigma}$ in Eq. (2) should be replaced by $\vec{s}$, in Eq. (3) the $Y_{LS}(x)$ term should have the factor e^{-x}/x^2 rather than e^{-x}/x, and in Table 3 the range should be 0.40 rather than 0.50.

[4] T. T. S. Kuo, Ann. Reviews of Nucl. Sc. 24, 101 (1974).

[5] J. Shurpin, T. T. S. Kuo and D. Strottman, Nucl. Phys. A408, 310 (1983).

[6] R. Bryan and B. L. Scott, Phys. Rev. C177, 1435 (1969).

[7] M. Lacombe, B. Loiseau, J. M. Richard, R. Vinh Mau, J. Cote, P. Pires and R. de Tourreil, Phys. Rev. C 21, 861 (1980).

[8] Nguyen van Giai and H. Sagawa, Phys. Lett. 106B, 379 (1981).

[9] J. Decharge and D. Gogny, Phys. Rev. C21, 1568 (1980).

[10] J. Friedrich and P. G. Reinhard, Phys. Rev. C33, 335 (1986).

[11] P. J. Brussaard and P. W. M. Glaudemans, *Shell Model Applications in Nuclear Spectroscopy* (North-Holland, 1977).

[12] P. W. M. Glaudemans, P. J. Brussaard and B. H. Wildenthal, Nucl. Phys. A102, 593 (1967).

[13] A. B. Migdal, *Nuclear Theory; The Quasiparticle Method* (Benjamin, New York, 1968); *Theory of Finite Fermi Systems and Applications to Atomic Nuclei* (Wiley, New York, 1967).

[14] J. W. Negele, Phys. Rev. C1, 1260 (1970).

[15] M. R. Anastasio, L. S. Celenza, W. S. Pong and C. M. Shakin, Physics Reports 100, 328 (1983); L. S. Celemza, W. S. Pong and C. M. Shakin, Phys. Rev. Lett. 47, 3 (1981).

[16] D. Vautherin and D. M. Brink, Phys. Rev. C5, 626 (1972).

18 Applications of the Two-Body Interactions

18.1 Interaction energies for closed shell, one-particle and one-hole configurations

The total energy for a diagonal configuration in the M-scheme is the sum of kinetic energy and interaction energy contributions.

$$E = E_K + E_I, \tag{18.1}$$

where the kinetic energy is

$$E_K = \sum_{\alpha} < \alpha \mid T \mid \alpha >, \tag{18.2}$$

and the interaction energy is

$$E_I = \frac{1}{2}\sum_{\alpha,\beta} < \alpha\beta \mid V \mid \alpha\beta > . \tag{18.3}$$

In this section we will derive the interaction energies for the closed-shell and closed-shell plus-or-minus one-particle configurations in terms of the J-coupled two-body matrix elements. For a closed shell the sum runs over all of the filled states labeled by (k, m), where k stands for (n_r, ℓ, j). In terms of explicit sums over the k orbits the kinetic energy is

$$E_K(C) = \sum_{k_a,m_a} < k_a m_a \mid T \mid k_a m_a >= \sum_{k_a} N_a < k_a \mid T \mid k_a >, \tag{18.4}$$

where the factor of

$$N_a = (2j_a + 1) \tag{18.5}$$

comes from number of degenerate m_a states which have the same kinetic energy. The interaction energy is

$$E_I(C) = \frac{1}{2}\sum_{k_a,k_b,m_a,m_b} < k_a m_a k_b m_b \mid V \mid k_a m_a k_b m_b > . \tag{18.6}$$

We can replace the M-scheme two-body matrix element with the J-scheme result given in Eq. 17.10:

$$E_I(C) = \frac{1}{2}\sum_{k_a,k_b,m_a,m_b} [1 + \delta_{k_a,k_b}] \sum_{JMJ'M'} < JM \mid j_a m_a j_b m_b > < J'M' \mid j_a m_a j_b m_b > \times < k_a k_b J \mid V \mid k_a k_b J > . \tag{18.7}$$

With $\sum_{m_a,m_b} < JM \mid j_a m_a j_b m_b > < J'M' \mid j_a m_a j_b m_b > = \delta_{J,J'}\delta_{M,M'}$ this becomes:

$$E_I(C) = \frac{1}{2}\sum_{k_a,k_b}[1+\delta_{k_a,k_b}]\sum_{JM} < k_a k_b J \mid V \mid k_a k_b J > . \tag{18.8}$$

Note that $\frac{1}{2}\Sigma_{k_a,k_b}[1+\delta_{k_a,k_b}]$ is equivalent to $\Sigma_{k_a \le k_b}$. Also $< V >$ does not depend on M and there are $(2J+1)$ values of M. Thus we have

$$E_I(C) = \sum_{k_a \le k_b}\sum_{J}(2J+1) < k_a k_b J \mid V \mid k_a k_b J > . \tag{18.9}$$

The average (monopole) interaction energy between two k orbits is defined as:

$$\bar{V}_{k_a k_b} = \frac{\sum_J (2J+1) < k_a k_b J \mid V \mid k_a k_b J >}{\sum_J (2J+1)}. \tag{18.10}$$

When $k_a \neq k_b$ we have $\Sigma_J(2J+1) = N_a N_b$, where $N = (2j+1)$ is the filled shell orbit occupancy. This represents the total number of two-body interactions when one particle is in orbit k_a and the other particle is in orbit k_b. When both particles are in the same orbit k_a, then $\Sigma_J(2J+1) = N_a(N_a-1)/2$, which represents the number of two-body interactions for the particles within orbit k_a. In terms of these average interactions the total closed-shell interaction energy is:

$$E_I(C) = \sum_{k_a}\frac{N_a(N_a-1)}{2}\bar{V}_{k_a k_a} + \sum_{k_a > k_b} N_a N_b \bar{V}_{k_a k_b}, \tag{18.11}$$

where $N = (2j+1)$.

We can use these average interactions to calculate the energy associated with one-hole and one-particle configurations. Thus for one-particle in orbit k_i outside the closed-shell we sum over the average interactions with the filled orbits k_a multiplied by the total number of particles $N_a = (2j_a+1)$ in that orbit:

$$\epsilon_{k_i} = E(C\ k_i) - E(C) = < k_i \mid T \mid k_i > + \sum_{k_a} N_a\ \bar{V}_{k_a,k_i}. \tag{18.12}$$

For one hole in orbit k_i the result is:

$$\epsilon_{k_i} = E(C) - E(C\ k_i^{-1}) = < k_i \mid T \mid k_i > + (N_i - 1)\ \bar{V}_{k_i,k_i} + \sum_{k_a \neq k_i} N_a \bar{V}_{k_a,k_i}, \tag{18.13}$$

where the factor in front of the $\bar{V}_{k_i,k_i}$ term is the difference between the total number of interactions for the filled shell, $N_a(N_a-1)/2$, and the total number of interactions for a filled shell minus one particle, $(N_a-1)(N_a-2)/2$.

When isospin is included the number of nucleons in the filled shell becomes:

$$N'_a = (2t+1)(2j_a+1) = 2(2j_a+1), \tag{18.14}$$

where $t = 1/2$. The closed-shell kinetic energy is:

$$E_K(C) = \sum_{k_a,m_a} < k_a m_a \mid T \mid k_a m_a >= \sum_{k_a} N'_a < k_a \mid T \mid k_a >, \tag{18.15}$$

the closed-shell interaction energy is:

$$E_I(C) = \sum_{k_a \le k_b} \sum_{J,T} (2T+1)(2J+1) < k_a k_b JT \mid V \mid k_a k_b JT >, \tag{18.16}$$

the average interaction is:

$$\bar{V}_{k_a k_b} = \frac{\sum_{JT}(2J+1)(2T+1) < k_a k_b JT \mid V \mid k_a k_b JT >}{\sum_{JT}(2J+1)(2T+1)}, \tag{18.17}$$

the single-particle energy is:

$$\epsilon_{k_i} = < k_i \mid T \mid k_i > + \sum_{k_a} N'_a \bar{V}_{k_a,k_i}, \tag{18.18}$$

and the single-hole energy is:

$$\epsilon_{k_i} = < k_i \mid T \mid k_i > + (N'_i - 1)\bar{V}_{k_i,k_i} + \sum_{k_a \ne k_i} N'_a \bar{V}_{k_a,k_i}. \tag{18.19}$$

As an example, we can calculate the interaction energy for ^{16}O with the matrix elements of the low-k NN interaction derived by Bogner et al. [1] (the sum of the central, spin-orbit and spin-tensor terms). We take oscillator potential with $\hbar\omega$=14 MeV provides an approximation to the Hartree-Fock potential. The required two-body matrix elements are given in Table 1. The total sum from Eq. (18.16) is E_I = −325.3 MeV. The total kinetic energy from Sec. 7.2 is $E_K = 18\hbar\omega = 252$ MeV. We should also subtract the center-of-mass kinetic energy $E_K(cm) = \frac{3}{4}\hbar\omega = 10.5$ MeV. Finally we can add the total Coulomb energy by using Eq. (18.9) to sum the proton-proton two-body matrix elements of the Coulomb interaction to get $E(coul)$ = 13.8 MeV. (The proton-proton matrix elements are given by the $T = 1$ Coulomb matrix elements in Table 1.) Thus the total energy is:

$$E = E_I + E_K - E_K(cm) + E(coul) =$$

$$= -325.3 + 252 - 10.5 + 13.8 \text{ MeV} = -70.0 \text{ MeV}. \tag{18.20}$$

Table 1: Values of the some $V(lowk)$ and Coulomb two-body matrix elements used in this section. The orbits are labeled by $k = 1$ for $0s_{1/2}$ $k = 2$ for $0p_{3/2}$, $k = 3$ for $0p_{1/2}$, and $k = 4$ for $0d_{5/2}$.

k_1	k_2	k_3	k_4	J T	V_{lowk}	V_{coul}
1	1	1	1	1 0	−7.86	
1	1	1	1	0 1	−6.72	0.67
				average	−7.29	0.67
1	2	1	2	1 0	−1.07	
1	2	1	2	2 0	−7.86	
1	2	1	2	1 1	−3.80	0.59
1	2	1	2	2 1	−1.00	0.44
				average	−2.87	0.50
1	3	1	3	0 0	−7.86	
1	3	1	3	1 0	−4.47	
1	3	1	3	0 1	−1.88	0.44
1	3	1	3	1 1	−0.88	0.52
				average	−2.18	0.50
2	2	2	2	1 0	−1.39	
2	2	2	2	3 0	−3.95	
2	2	2	2	0 1	−3.30	0.56
2	2	2	2	2 1	−1.37	0.47
				average	−2.22	0.48
2	3	2	3	1 0	−5.54	
2	3	2	3	2 0	−5.05	
2	3	2	3	1 1	−0.53	0.44
2	3	2	3	2 1	−2.50	0.49
				average	−2.63	0.47
3	3	3	3	1 0	−2.26	
3	3	3	3	0 1	−0.63	0.50
				average	−1.44	0.50
4	4	4	4	1 0	−0.28	
4	4	4	4	3 0	−0.72	
4	4	4	4	5 0	−2.94	
4	4	4	4	0 1	−1.79	
4	4	4	4	2 1	−1.15	
4	4	4	4	4 1	−0.51	

This should be compared with the experimental value of $E = -BE = -127.6$ MeV. That is, an difference of 58 MeV (corresponding to 18% in $E_I(lowk)$). To do better we need to include configurations beyond the closed-shell such as two-particle two-hole admixtures. Also perhaps three-body interactions must be added.

One can also use the two-body matrix elements from Table 1 to obtain the single-hole energies for $0s_{1/2}$, $0p_{3/2}$ and $0p_{1/2}$. For example, for the $0p_{1/2}$ we would use Eq. (18.19) with $\bar{V}_{33} = -1.44$ MeV, $\bar{V}_{23} = -2.63$ MeV, and $\bar{V}_{13} = -2.18$ MeV to get $3\bar{V}_{33} + 8\bar{V}_{23} + 4\bar{V}_{13} = -34.1$ MeV for the interaction energy. The kinetic energy is $\frac{5}{4}\hbar\omega = 17.5$ MeV and the single-hole energy from the sum is -16.58 MeV. This is not too far from the experimental value of $\epsilon_n = -[BE(^{16}O) - BE(^{15}O)] = -15.66$ MeV for the neutron.

To get the $0p_{1/2}$ proton single-hole energy we would also include the contribution from the Coulomb interaction between protons. From Eq. (18.13) and Table 1 this is $(0.50) + 4(0.47) + 2(0.50) = 3.38$ MeV (for the sum over $0p_{1/2}$, $0p_{3/2}$ and $0s_{1/2}$, respectively). The proton $0p_{1/2}$ hole energy is thus $-16.58 - 3.38 = -13.20$ MeV compared to the experimental value of $\epsilon_p = -[BE(^{16}O) - BE(^{15}N)] = -12.13$ MeV. Finally we could also compare the calculated value for $\epsilon_p - \epsilon_n = 3.38$ MeV (just the Coulomb energy term) with the experimental value of 3.54 MeV.

18.2 Interaction energies for diagonal two-particle configurations

The diagonal matrix element of the hamiltonian for two-particles outside of a closed shell as given by Eq. 12.4 is:

$$E(C+2) = < C\alpha\beta \mid H \mid C\alpha\beta >= E(C) + \epsilon_\alpha + \epsilon_\beta + < \alpha\beta \mid V \mid \alpha\beta >, \qquad (18.21)$$

where C represents all of the orbitals in the closed shell, and where ϵ are interpreted in Hartree-Fock theory as the single-particle energies for a single-particle outside the closed shell. In the M-scheme the α and β could be in two different m values in the same $k = (n_r, \ell, j)$ orbital or in two different orbitals k_a and k_b. It is useful to define an energy relative to that of the closed shell:

$$\Delta E = E(C+2) - E(C) = \epsilon_\alpha + \epsilon_\beta + < \alpha\beta \mid V \mid \alpha\beta >, \qquad (18.22)$$

These energy differences provide a different kind of test for the shell-model methods.

In the J-scheme with both particles in the same k orbit we would have:

$$\Delta E = E(C+2) - E(C) = 2\epsilon_k + < k^2 J \mid V \mid k^2 J > . \qquad (18.23)$$

For example, as a model for ^{18}O we could use Eq. (18.23) with the observed single-particle energy of the lowest $5/2^+$ state in ^{17}O.

$$\epsilon_{0d_{5/2}} = -[BE(^{17}O) - BE(^{16}O)] = -4.14 \text{ MeV} \tag{18.24}$$

For two neutrons in $j = 5/2$ we can have $J = 0$, 2 and 4. If we take the lowest states with these spins in ^{18}O (the 2^+ and 1.98 MeV and the 4^+ at 3.55 MeV) has having these configurations we have from the experimental binding energies:

$$\Delta E_{exp}(0^+) = -[BE(^{18}O), 0^+) - BE(^{16}O)] = -12.19 \text{ MeV},$$

$$\Delta E_{exp}(2^+) = -[BE(^{18}O), 2^+) - BE(^{16}O)] = -10.21 \text{ MeV},$$

and

$$\Delta E_{exp}(4^+) = -[BE(^{18}O), 4^+) - BE(^{16}O)] = -8.64 \text{ MeV}. \tag{18.25}$$

These can be compared to those calculated with the experimental single-particle energy of -4.14 MeV and the theoretical two-body matrix elements from Table 1:

$$\Delta E_{th}(0^+) = 2(-4.14) - 1.79 = -10.07 \text{ MeV},$$

$$\Delta E_{th}(2^+) = 2(-4.14) - 1.15 = -9.43 \text{ MeV},$$

and

$$\Delta E_{th}(4^+) = 2(-4.14) - 0.51 = -8.79 \text{ MeV}. \tag{18.26}$$

The deviation between experiment and theory is largest for $J = 0$. This difference is mainly due to mixing with other configurations as will be discussed in the next section.

This simple model for two-particles in one orbit outside of a closed shell works best when that one orbit is isolated in energy from the others. The best examples of these $T = 1$ two-particle spectra are found in ^{50}Ti for two $0f_{7/2}$ protons outside of ^{48}Ca, ^{92}Mo for two $0g_{9/2}$ protons outside of ^{90}Zr and ^{210}Po for two $0h_{9/2}$ protons outside of ^{208}Pb.

In this one-orbit approximation, we can use the equations to deduce "experimental" values for the $(T = 1)$ two-body matrix elements:

$$\begin{aligned} < k^2 J \mid V \mid k^2 J >_{exp} &= [E(C+2) - E(C)] - 2\epsilon \\ &= [E(C+2) - E(C)] - 2[E(C+1) - E(C)] \\ &= -[BE(C+2) - BE(C)] + 2[BE(C+1) - BE(C)]. \end{aligned} \tag{18.27}$$

In the example for ^{18}O

$$< (0d_{5/2})^2 J = 0 \mid V \mid (0d_{5/2})^2 J = 0 >_{exp} = -3.91 \text{ MeV},$$

$$< (0d_{5/2})^2 J = 0 \mid V \mid (0d_{5/2})^2 J = 0 >_{exp} = -1.93 \text{ MeV},$$

and

$$< (0d_{5/2})^2 J = 0 \mid V \mid (0d_{5/2})^2 J = 0 >_{exp} = -0.36 \text{ MeV}. \tag{18.28}$$

These can be compared to the theoretical values of -1.79, -1.15 and -0.51 MeV, respectively.

18.3 Interaction energies for diagonal two-hole configurations

The diagonal matrix element of the hamiltonian for two-particles outside of a closed shell as given by Eq. 12.7 is:

$$E(C-2) = < C\alpha^{-1}\beta^{-1} \mid H \mid C\alpha^{-1}\beta^{-1} > = E(C) - \epsilon_\alpha - \epsilon_\beta + < \alpha\beta \mid V \mid \alpha\beta >, \tag{18.29}$$

where C represents all of the orbitals in the closed shell, and where ϵ are interpreted in Hartree-Fock theory as the single-particle energies for the one-hole configuration. The energy relative to that of the closed shell is:

$$\Delta E = E(C-2) - E(C) = -\epsilon_\alpha - \epsilon_\beta + < \alpha\beta \mid V \mid \alpha\beta >, \tag{18.30}$$

The formalism for two-holes is identical to that of two-particles except for the sign in front of ϵ. This result can be generalized to many holes; the formalism for n holes is the same as that for n particles except for the sign in front of ϵ.

In the J-scheme for two holes in the same orbit:

$$\Delta E = E(C-2) - E(C) = -2\epsilon_k + < k^2 J \mid V \mid k^2 J > . \tag{18.31}$$

A comparison of Eqs. (18.23) and (18.31) shows that the energy spectra for the hole configuration is the same as that of the particle configuration, as long as the two-body matrix elements are the same. Experimental values for the two-body matrix elements can be derived for the properties of the hole nuclei by:

$$\begin{aligned} < k^2 J \mid V \mid k^2 J >_{exp} &= [E(C-2) - E(C)] + 2\epsilon \\ &= [E(C-2) - E(C)] + 2[E(C) - E(C-1)] \\ &= [BE(C) - BE(C-2)] - 2[BE(C) - BE(C-1)]. \end{aligned} \tag{18.32}$$

One of best examples can be found in the nucleus ^{54}Fe with two holes in the $0f_{7/2}$ orbit relative to a closed shell for ^{56}Ni.

18.4 Interaction energies for particle-hole configurations

The diagonal matrix element of the hamiltonian for a particle-hole state is:

$$E(ph) = < C\alpha\beta^{-1} \mid H \mid C\alpha\beta^{-1} >= E(C) + \epsilon_\alpha - \epsilon_\beta - < \alpha\tilde{\beta} \mid V \mid \alpha\tilde{\beta} >, \quad (18.33)$$

where C represents all of the orbitals in the closed shell, and where ϵ are interpreted in Hartree-Fock theory as the single-particle energies. $\tilde{b}$ is the m-scheme wavefunction for the state

$$\mid \tilde{\beta} >= (-1)^{j_\beta + m_\beta} \mid k_\beta, -m_\beta > . \quad (18.34)$$

The energy of the particle-hole state coupled to total angular momentum J relative to that of the closed shell is:

$$\Delta E(ph, J) = E(ph) - E(C) = \epsilon_\alpha - \epsilon_\beta + V(ph, J), \quad (18.35)$$

where $V(ph, J)$ is as linear combinations of two-body matrix elements known as the Pandya transformation [2]

$$V(ph, J) = -\sum_{J'}(2J'+1) \left\{ \begin{array}{ccc} j_\alpha & j_\beta & J \\ j_\alpha & j_\beta & J' \end{array} \right\} < k_\alpha k_\beta J' \mid V \mid k_\alpha k_\beta J' > . \quad (18.36)$$

Extension to isospin formalism gives:

$$\Delta E(ph, JT) = E(ph) - E(C) = \epsilon_\alpha - \epsilon_\beta + V(ph, JT), \quad (18.37)$$

where

$$V(ph, JT) = -\sum_{J'T'}(2J'+1)(2T'+1) \left\{ \begin{array}{ccc} j_\alpha & j_\beta & J \\ j_\alpha & j_\beta & J' \end{array} \right\} \left\{ \begin{array}{ccc} 1/2 & 1/2 & T \\ 1/2 & 1/2 & T' \end{array} \right\}$$
$$\times < k_\alpha k_\beta J'T' \mid V \mid k_\alpha k_\beta J'T' > . \quad (18.38)$$

Puttng in the values of the isospin factors one has:

$$V(ph, JT = 0) = -\sum_{J'}(2J'+1) \left\{ \begin{array}{ccc} j_\alpha & j_\beta & J \\ j_\alpha & j_\beta & J' \end{array} \right\}$$

$$\times [\frac{3}{2} < k_\alpha k_\beta J'T' = 1 \mid V \mid k_\alpha k_\beta J'T' = 1 > -\frac{1}{2} < k_\alpha k_\beta J'T' = 0 \mid V \mid k_\alpha k_\beta J'T' = 0 >], \quad (18.39)$$

and

$$V(ph, JT = 1) = -\sum_{J'}(2J'+1) \left\{ \begin{array}{ccc} j_\alpha & j_\beta & J \\ j_\alpha & j_\beta & J' \end{array} \right\}$$

$$\times [\frac{1}{2} < k_\alpha k_\beta J'T' = 1 \mid V \mid k_\alpha k_\beta J'T' = 1 > +\frac{1}{2} < k_\alpha k_\beta J'T' = 0 \mid V \mid k_\alpha k_\beta J'T' = 0 >]. \quad (18.40)$$

References

[1] S. Bogner, T. T. S. Kuo, L. Coraggio, A. Covello and N. Itaco, Phys. Rev. C 65, 051130(R) (2002).

[2] S. P. Pandya, Phys. Rev. **103**, 956 (1956).

19 Configuration mixing

19.1 Two-particle configurations

In ^{17}O one observes that the $1s_{1/2}$ orbit lies only 0.87 MeV above the $0d_{5/2}$ ground states. Thus both of these orbits should be considered for the two-particle configuration in ^{18}O. For $J^\pi = 0^+$ we take the two J-coupled basis states:

$$\mid \Phi_1 >= \mid C, aa\ J >= \mid C, (0d_{5/2})^2 J >,$$

and

$$\mid \Phi_2 >= \mid C, bb\ J >= \mid C, (1s_{1/2})^2 J >, \tag{19.1}$$

where C indicates all orbits in the ^{16}O closed shell. The ground state will be a linear combination of these two basis states which are determined by diagonalizing the hamiltonian matrix:

$$\begin{bmatrix} \tilde{H}_{11} & \tilde{H}_{12} \\ \tilde{H}_{21} & \tilde{H}_{22} \end{bmatrix}, \tag{19.2}$$

where

$$\tilde{H}_{11} = < C, aa\ J \mid H \mid C, aa\ J >= E(C) + 2\epsilon_a + < aa\ J \mid V \mid aa\ J >,$$

$$\tilde{H}_{22} = < C, bb\ J \mid H \mid C, bb\ J >= E(C) + 2\epsilon_b + < bb\ J \mid V \mid bb\ J >,$$

and

$$\tilde{H}_{12} = \tilde{H}_{21} = < C, aa\ J \mid H \mid C, bb\ J >= < aa\ J \mid V \mid bb\ J > . \tag{19.3}$$

For the off-diagonal matrix element, $\tilde{H}_{21} = \tilde{H}_{12}$, since the matrix is real and hermitian. Since the two basis states differ by the change of two particles between orbits a and b, the only contribution to H_{12} comes from the operator $\Sigma_{\alpha\beta\gamma\delta} a^+_\alpha a^+_\beta a_\gamma a_\delta$ acting to move the two particles between orbits a and b (if H operates on a state other than those in a and b the remaining overlaps of the form $< a \mid b >$ will give zero).

The core energy $E(C)$ appears as a constant in the diagonal of the matrix. Thus we can consider the energies E relative to the closed-shell energy given by the eigenvalues of

$$H = \tilde{H} - E(C)$$

as given by the matrix

$$\begin{bmatrix} H_{11} & H_{12} \\ H_{21} & H_{22} \end{bmatrix}, \tag{19.4}$$

$$H_{11} = 2\epsilon_a + < aa\ J \mid V \mid aa\ J >,$$

$$H_{22} = 2\epsilon_b + < bb\ J \mid V \mid bb\ J >,$$

and

$$H_{12} = < aa\ J \mid V \mid bb\ J > . \tag{19.5}$$

We will assume that the matrix is arranged such that:

$$H_{11} < H_{22} \ldots ,$$

e.g. H_{11} is the lowest diagonal energy. The eigenvalues E for this two-by-two matrix are given by the two solutions of the quadratic equation obtained from determinant $\mid H - E \mid$:

$$E_{1/2} = \frac{1}{2}\left[H_{22} + H_{11} \pm \sqrt{(H_{22} - H_{11})^2 + 4H_{12}^2}\right]. \tag{19.6}$$

The subscripts 1(2) indicate the eigenstates which are associated with $\Phi_{1(2)}$ when $H_{12} = 0$. We can write the energies as:

$$E_1 = H_{11} - \delta,$$

and

$$E_2 = H_{22} + \delta, \tag{19.7}$$

where

$$\delta = \frac{1}{2}\left[\sqrt{(H_{22} - H_{11})^2 + 4H_{12}^2} - (H_{22} - H_{11})\right], \tag{19.8}$$

where $\delta > 0$. In terms of δ the eigenfunctions are given by:

$$\mid \Psi_1 > = \frac{1}{N}\left[\mid \Phi_1 > -(\delta/H_{12}) \mid \Phi_2 >\right],$$

and

$$\mid \Psi_2 > = \frac{1}{N}\left[\mid \Phi_2 > +(\delta/H_{12}) \mid \Phi_1 >\right], \tag{19.9}$$

with normalization:

$$N^2 = 1 + (\delta/H_{12})^2$$

Note that $- \mid \Psi_i >$ are also eigenstates. Thus there are "random" phase factors in the wave functions which must be kept consistent throughout the calculations of physical observables (which always involve a given wavefunction twice).

It is useful to look at various limits of these results. When the states start out degenerate $H_{11} = H_{22}$, then $\delta = H_{12}$, and the states are repelled to have a total separation energy of $E_2 - E_1 = 2\delta$, and the eigenstates are equal mixtures of the basis states $\mid \Phi_1 >$ and $\mid \Phi_2 >$.

When the diagonal separation energy is large compared to off-diagonal matrix element; $H_{22} - H_{11} \gg \mid H_{12} \mid$, then

$$E_1 = H_{11} - \delta \approx H_{11} - \frac{H_{12}^2}{H_{22} - H_{11}},$$

Table 1: Values of the some $V(lowk)$ two-body matrix elements used in this section. The orbits are labeled $j = 5$ for $0d_{5/2}$, $j = 3$ for $0d_{3/2}$ and $j = 1$ for $1s_{1/2}$.

j_1	j_2	j_3	j_4	J T	V_{lowk}
5	5	5	5	0 1	−1.79
5	5	3	3	0 1	−3.47
5	5	1	1	0 1	−0.83
3	3	3	3	0 1	−0.37
3	3	1	1	0 1	−0.68
1	1	1	1	0 1	−2.53
5	5	5	5	2 1	−1.15
5	5	5	3	2 1	−0.44
5	5	5	1	2 1	−0.63
5	5	3	3	2 1	−0.69
5	5	3	1	2 1	−0.60
5	3	5	3	2 1	−0.42
5	3	5	1	2 1	−0.23
5	3	3	3	2 1	−0.87
5	3	3	1	2 1	0.69
5	1	5	1	2 1	−1.27
5	1	3	3	2 1	−0.80
5	1	3	1	2 1	1.51
3	3	3	3	2 1	−0.28
3	3	3	1	2 1	0.07
3	1	3	1	2 1	−0.66
5	5	5	5	4 1	−0.51
5	5	5	3	4 1	−1.09
5	3	5	3	4 1	−2.15

$$E_2 = H_{22} + \delta \approx H_{22} + \frac{H_{12}^2}{H_{22} - H_{11}}, \tag{19.10}$$

$$| \Psi_1 > \approx | \Phi_1 > - \frac{H_{12}}{H_{22} - H_{11}} | \Phi_2 >,$$

$$| \Psi_2 > \approx | \Phi_2 > + \frac{H_{12}}{H_{22} - H_{11}} | \Phi_1 >, \tag{19.11}$$

where the normalization in the wavefunction is ignored since the last term is small. These are equivalent to the perturbation theory results given in Eq. 9.13 and 9.15, respectively. When $H_{12} = 0$ the eigenstates start out at energies of H_{11} and H_{22} and as H_{12} is turned on the states repel each other by an additional amount 2δ.

19.2 Application to ^{18}O

We can apply these results to the ^{18}O $J^\pi = 0^+$ state by using the experimental single-particle energies:

$$\epsilon_5 = \epsilon_{0d_{5/2}} = -[BE(^{17}O, 5/2^+,\ gs) - BE(^{16}O] = -4.14 \text{ MeV},$$

and

$$\epsilon_1 = \epsilon_{1s_{1/2}} = -[BE(^{17}O, 1/2^+,\ 0.87 \text{ MeV}) - BE(^{16}O] = -3.27 \text{ MeV},$$

where we have introduced a short-hand notation $(2j+1)$. The basis states for $J = 0$ are:

$$\mid \Phi_1 > = \mid 55J > = \mid (0d_{5/2})^2 J = 0 >,$$

and

$$\mid \Phi_2 > = \mid 11J > = \mid (1s_{1/2})^2 J = 0 >, \tag{19.1}$$

The single-particle energies together with the low-k two-body matrix elements from Table 1 give the hamiltonian matrix elements:

$$H_{11} = 2\epsilon_5 + < 55J \mid V \mid 55J > = 2(-4.14) - 1.79 = -10.07 \text{ MeV}$$

$$H_{22} = 2\epsilon_1 + < 11J \mid V \mid 11J > = 2(-3.27) - 2.53 = -9.07 \text{ MeV}$$

and

$$H_{12} = < 55J \mid V \mid 11J > = -0.83 \text{ MeV}, \tag{19.12}$$

The lowest eigenenergy is -10.54 MeV which is an improvement over the single-orbit $(0d_{5/2})$ result of -10.07 MeV, but still not as low as the experimental value of -12.19 MeV.

For the 0^+ state the next configuration to consider would be

$$\mid \Phi_3 > = \mid 33J > . \tag{19.13}$$

for the $0d_{3/2}$ orbit. If we take the $3/2^+$ state at 5.08 MeV as the single-particle state in ^{17}O, its single-particle energy is:

$$\epsilon_3 = \epsilon_{0d_{3/2}} = -[BE(^{17}O, 3/2^+,\ 5.08 \text{ MeV}) - BE(^{16}O] = 0.94 \text{ MeV},$$

The hamiltonian matrix is then a 3x3 matrix of the form:

$$\begin{bmatrix} H_{11} & H_{12} & H_{13} \\ H_{21} & H_{22} & H_{23} \\ H_{31} & H_{32} & H_{33} \end{bmatrix}, \tag{19.14}$$

where in addition to the terms given in Eq. (19.12) we need:

$$H_{33} = 2\epsilon_3 + < 33J \mid V \mid 33J > = 2(0.94) - 0.37 = 1.51 \text{ MeV},$$

$$H_{13} = < 55J \mid V \mid 33J > = -3.47 \text{ MeV},$$

and

$$H_{23} = < 11J \mid V \mid 33J > = -0.68 \text{ MeV}. \tag{19.15}$$

The lowest eigenvalue of the 3x3 matrix is -11.44 MeV which is getting close to the experimental value of -12.19 MeV. To get better results we will need to include configurations which will break the closed shell of ^{16}O.

From the matrix elements given in Table 1 we can also consider configuration mixing for $J = 2$. There are five ways to make $J = 2$:

$$\mid \Phi_1 > = \mid 55J >,$$

$$\mid \Phi_2 > = \mid 53J >,$$

$$\mid \Phi_3 > = \mid 51J >,$$

$$\mid \Phi_4 > = \mid 33J >,$$

and

$$\mid \Phi_5 > = \mid 31J > . \tag{19.16}$$

There will be off-diagonal matrix elements in which one-particle in moved from one orbit to another. For example:

$$H_{12} = < 55J \mid V \mid 53J > . \tag{19.17}$$

Single-particle matrix elements of the kinetic energy (or the Hartree-Fock potential U_{HF}) are non-zero only for the diagonal M-scheme matrix elements of the type $< \alpha \mid T \mid \alpha >$, and thus can only enter into the diagonal part of the hamiltonian matrix. Matrix elements of the type, $< \alpha \mid T \mid \beta >$ with $\alpha \neq \beta$ are zero since the one-body scalar operators cannot change m or j.

19.3 Many-particle configurations

The basic ideas explored in the previous section for the configuration mixing of two particles can be extended to many-particle systems. We start with a J-coupled basis of the form:

$$\begin{aligned} \mid n\omega J > &= \mid [(k_1^{n_1}\omega_1 J_1)(k_2^{n_2}\omega_2 J_2)J_{12}][k_3^{n_3}\omega_3 J_3]J >, \\ \mid n\omega' J > &= \mid [(k_1^{n'_1}\omega'_1 J'_1)(k_2^{n'_2}\omega'_2 J'_2)J'_{12}][k_3^{n'_3}\omega'_3 J'_3]J >, \end{aligned} \tag{19.18}$$

where $n = n_1 + n_2 + n_3 = n'_1 + n'_2 + n'_3$. For a given total number of particles n, the distribution $n_1, n_2 \ldots$ among the k states is called the partition. The maximum number of particles in one orbit is $n = (2j+1)$. The ω indices distinguish the various basis states with the same J value.

The diagonal hamiltonian matrix elements have the form:

$$< n\omega J \mid H \mid n\omega J > = n_1\epsilon_{k_1} + n_2\epsilon_{k_2} + n_3\epsilon_{k_3} + \sum_i D_i(\omega, \omega, J) \ < V >_i, \qquad (19.19)$$

and the off-diagonal matrix elements have the form:

$$< n\omega J \mid H \mid n\omega' J > = \sum_i D_i(\omega, \omega', J) \ < V >_i \ . \qquad (19.20)$$

The $< V >_i$ represent the list of possible two-body matrix elements in the model space, and the D_i are numerical coefficients obtained from the matrix elements of $\Sigma_{\alpha\beta\gamma\delta} a^+_\alpha a^+_\beta a_\gamma a_\delta$. For example if we take the closed-shell configuration:

$$\mid n\omega J > = \mid [k_1^{2j_1+1} J = 0 >,$$

then $D_i = (2J'+1)$ and $V_i = < k_1^2 J' \mid V \mid k_1^2 J' >$ for the allowed J' values. If we take the two-particle configuration:

$$\mid n\omega J > = \mid [k_1^2 J >,$$

then there is only one non-zero value of D with $D_i = 1$ for $V_1 = < k_1^2 J \mid V \mid k_1^2 J >$. In general one must write an $M-$scheme or a $J-$scheme shell-model computer code to calculate D_i. If isospin is introduced, then all of the J in the equations are replaced by (J, T) and the maximum number of particles in one orbit is $n = 2(2j+1)$.

Note that the off-diagonal matrix element does not contain the single-particle energies for the same reasons as discussed in the two-particle example. The off-diagonal matrix element if zero if the set of numbers (n_1, n_2, n_3) differs from (n'_1, n'_2, n'_3) by the change of more than two particles. Thus if the basis states are ordered by their diagonal energy, the matrix will be "banded" with regions off-diagonal regions in which are zero. An example of this banded matrix is shown in Fig. 1 for the 0^+, T=0 levels for 12 particles in the sd-shell ($0d_{5/2}$,$0d_{3/2}$,$1s_{1/2}$) model space for the nuclus ^{28}Si [1]. The J, T matrix dimension is 839.

For the energy level spectrum I will use the example of the 0^+, $T = 0$ states obtained for the nucleus ^{24}Mg with 8 nucleons in the ($0d_{5/2}$,$0d_{3/2}$,$1s_{1/2}$) model space. For this calculation there are 35 partitions and $\omega_{max} = 325$ basis states. In the sd-shell there are 63 independent (J, T) two-body matrix elements, so the sums over i in Eqs. (19.19) and (19.20) is over 63 terms. The hamiltonian matrix is shown in Fig. 1 where

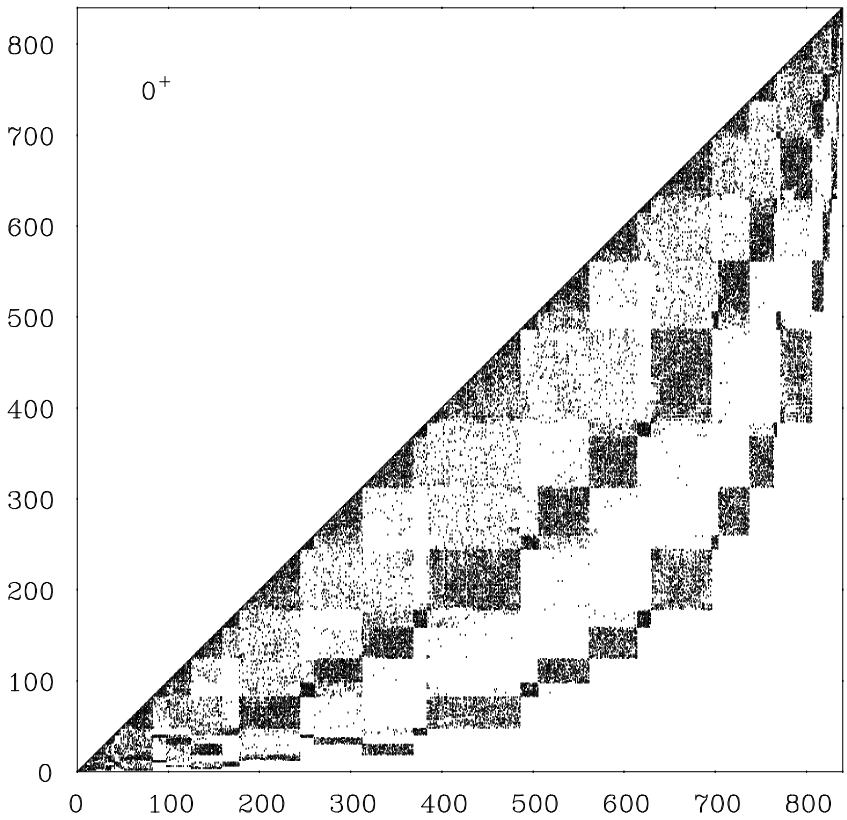

Figure 1: The hamiltonian matrix for the 0^+, $T = 0$ sd-shell basis in ^{28}Si. The points represent the non-zero matrix elements. The matrix is symmetric and only the bottom half is shown.

one observes the bands of zeros corresponding to the regions where the partitions differ by the change of more than two particles. Fig. 2 shows the eigenvalues has a function of the strength of the off-diagonal part of the matrix. 100 percent corresponds to the standard strength. Fig. 2 shows an expanded region of the results in Fig. 2. One observes an overall level repulsion with the lowest state decreasing monotonically in energy. The levels never cross but always show a repulsion typical of the two-level mixing model.

References

[1] V. Zelevinsky, B. A. Brown and M. Horoi, Phys. Rep. **276**, 85 (1996).

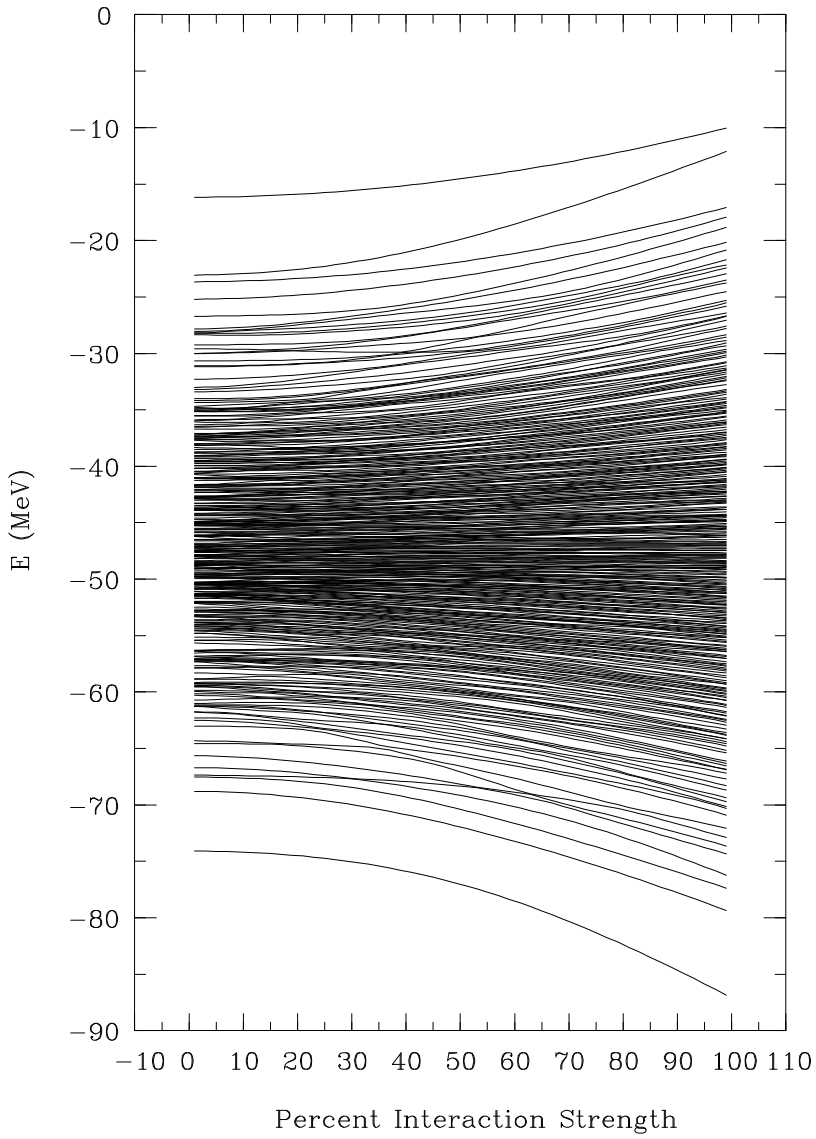

Figure 2: The spectrum of 0^+ states in ^{24}Mg as a function of the strength (in percent) of the off-diagonal part of the hamiltonian matrix.

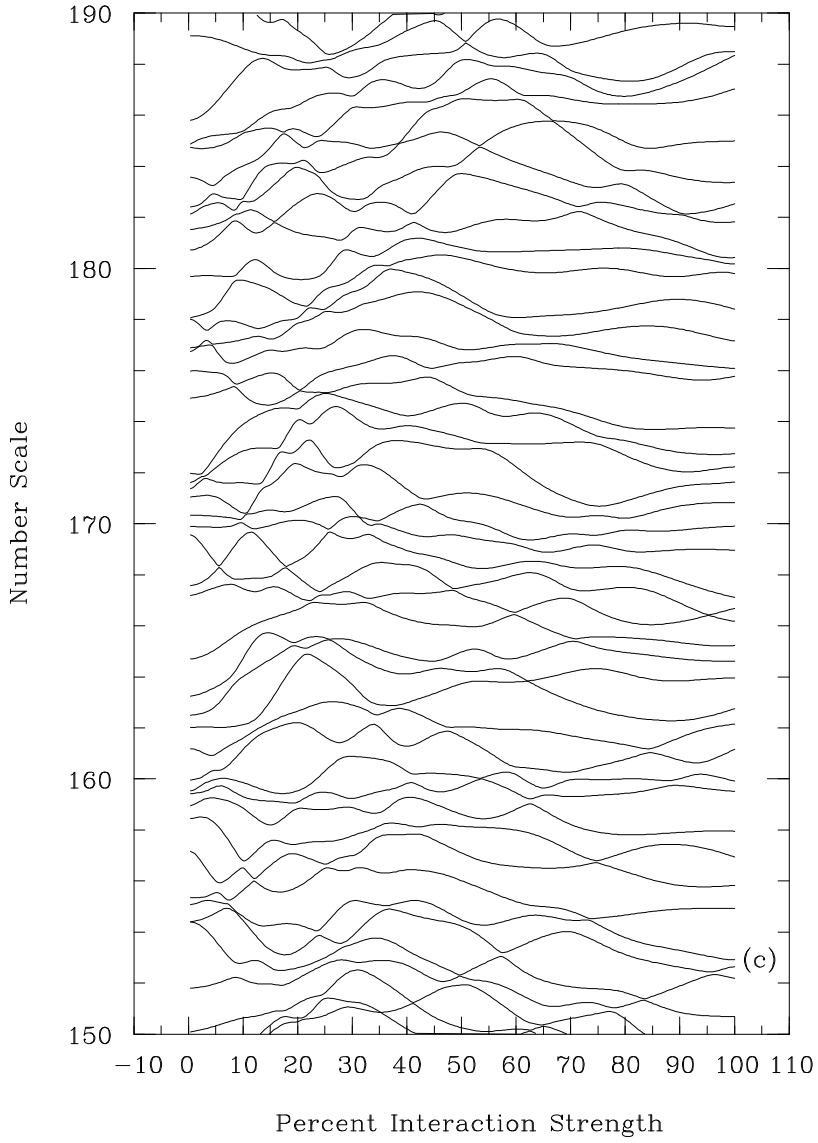

Figure 3: An expanded part of the previous figure.

20 One-particle transfer

20.1 Fractional parentage coefficients

20.1.1 One orbit

Observables for the removal or addition of a nucleon from a specific initial state to a specific final state are related to the matrix elements of the creation and destruction operators. In this section we will study the basic properties of these matrix elements and their sum-rules. The reduced matrix elements of the creation and destruction operators are used to define the spectroscopic factors associated with nuclear reactions. They are also the building blocks for the more complicated operators associated with one-body (such as electromagnetic and beta decay) and two-body transition amplitudes.

The creation operator a^+_{km} is a tensor of rank j since it creates the single-particle state $\mid km >$ (k stands for the set of single-particle quantum numbers $n\ell j$). The destruction operator a_{km} is not a tensor of rank j, however, by Eq. [13.34],

$$\tilde{a}_{km} \equiv (-1)^{j+m}[a^+_{k,-m}]^+ = (-1)^{j+m}a_{k,-m} \tag{20.1}$$

is a tensor of rank j. The inverse of Eq. (20.1) is

$$a_{km} = (-1)^{j-m}\tilde{a}_{k,-m}. \tag{20.2}$$

Eq. [13.35] (with the matrix elements being real and $p = j$) can be used to relate the reduced matrix elements involving $\tilde{a}$ to those involving a^+

$$< k^{n-1}\omega' J'||\tilde{a}_k||k^n\omega J >= (-1)^{j+J'-J} < k^n\omega J||a^+_k||k^{n-1}\omega' J' >, \tag{20.3}$$

All many-body matrix elements of a^+ can be reduced to these involving a single k-state.

Wave-function expansion relations and sum-rules for the states in the $n-1$ particle system can be obtained by operating with the number operator

$$\hat{N}_k = \sum_m a^+_{km}a_{km} \tag{20.4}$$

on the k^n configuration and then inserting a complete set of states with $n-1$ particles

$$\hat{N}_k \mid k^n\omega JM >= \sum_m a^+_{km}a_{km} \mid k^n\omega JM >= n \mid k^n\omega JM >$$

$$= \sum_{m\omega' J'M'} a^+_{km} \mid k^{n-1}\omega' J'M' >< k^{n-1}\omega' J'M' \mid a_{km} \mid k^n\omega JM > .$$

The matrix element of $a_{k,m}$ can be reduced with the Wigner-Eckhart theorem

$$< k^{n-1}\omega' J' M' \mid a_{km} \mid k^n \omega J M >= (-1)^{j-m} < k^{n-1}\omega' J' M' \mid \tilde{a}_{k,-m} \mid k^n \omega J M >$$

$$= (-1)^{j-m+J'-M'} \begin{pmatrix} J' & j & J \\ -M' & -m & M \end{pmatrix} < k^{n-1}\omega' J' || \tilde{a}_k || k^n \omega J >,$$

and by Eq. (20.3) the reduced matrix element of $\tilde{a}$ can be converted in a reduced matrix element of a^+ to obtain the final result:

$$\hat{N}_k \mid k^n \omega J M >= n \mid k^n \omega J M >= \sum_{m\omega' J' M'} (-1)^{-m-M'+J} \begin{pmatrix} J' & j & J \\ -M' & -m & M \end{pmatrix}$$

$$\times a^+_{km} \mid k^{n-1}\omega' J' M' >< k^n \omega J || a^+_k || k^{n-1}\omega' J' > . \qquad (20.5)$$

We can thus expand the k^n wavefunction in terms of those in the k^{n-1} basis:

$$\mid k^n \omega J M >= (-1)^n \sum_{\omega' J'} \frac{< k^n \omega J || a^+_k || k^{n-1}\omega' J' >}{n\sqrt{(2J+1)}} [Z^+(k^{n-1}\omega' J') \otimes a^+_k]^J_M \mid> . \quad (20.6)$$

A phase factor of $(-1)^{n-1}$ arises from commuting a^+ with the $n-1$ particles in the state k^{n-1}.

A sum-rule for the matrix elements of a^+ can be obtained by multiplying both sides of Eq. (20.5) by $< k^n \omega'' J'' M'' \mid$ to obtain

$$n\delta_{JJ''}\delta_{MM''}\delta_{\omega\omega''} = \sum_{m\omega' J' M'} (-1)^{-m-M'+J} \begin{pmatrix} J' & j & J \\ -M' & -m & M \end{pmatrix}$$

$$\times < k^n \omega'' J'' M'' \mid a^+_{km} \mid k^{n-1}\omega' J' M' >< k^n \omega J || a^+_k || k^{n-1}\omega' J' >$$

$$= \sum_{m\omega' J' M'} \begin{pmatrix} J' & j & J \\ -M' & -m & M \end{pmatrix} \begin{pmatrix} J'' & j & J' \\ -M'' & m & M' \end{pmatrix}$$

$$\times < k^n \omega'' J'' || a^+_k || k^{n-1}\omega' J' >< k^n \omega J || a^+_k || k^{n-1}\omega' J' >$$

$$= \frac{\delta_{JJ''}\delta_{MM''}}{(2J+1)} \sum_{\omega' J'} < k^n \omega'' J'' || a^+_k || k^{n-1}\omega' J' >< k^n \omega J || a^+_k || k^{n-1}\omega' J' >, \qquad (20.7)$$

where Eq. [13.12] has been used for the summation over $3j$ coefficients. Thus one finds the sum-rule:

$$\sum_{\omega' J'} < k^n \omega'' J'' || a^+_k || k^{n-1}\omega' J' >< k^n \omega J || a^+_k || k^{n-1}\omega' J' >= n(2J+1)\delta_{\omega\omega''}\delta_{JJ''}. \quad (20.8)$$

Thus:

$$\sum_{\omega' J'} |< k^n \omega J || a^+_k || k^{n-1}\omega' J' >|^2 = \sum_{\omega' J'} |< k^{n-1}\omega' J' || \tilde{a}_k || k^n \omega J >|^2 = n(2J+1). \quad (20.9)$$

The matrix elements in which the sum over final states is normalized to unity are historically called coefficients of fractional parentage [1] (CFP) defined by:

$$< j^n \omega J \,|\} j^{n-1} \omega' J' > \equiv \frac{< k^n \omega J || a_k^+ || k^{n-1} \omega' J' >}{\sqrt{n(2J+1)}}. \tag{20.10}$$

The j is used in the CFP rather than k, in order to emphasize the fact that these coefficients depend only on j and not on n and ℓ. In terms of CFP the sum-rule of Eq. (20.9) becomes:

$$\sum_{\omega' J'} |< j^n \omega J \,|\} j^{n-1} \omega' J' >|^2 = 1. \tag{20.11}$$

Thus, the square of the one-particle CFP is the probability of taking one particle in the state k from the configuration $\mid k^n \omega J >$ leaving and leaving it in the configuration $\mid k^{n-1} \omega' J' >$.

A sum-rule related to the connection between states in the n and $n+1$ particle systems can be obtained with the number operator written in the form:

$$\hat{N}_j = \sum_m (1 - a_{jm} a_{jm}^+). \tag{20.12}$$

Multiplying this on the state k^n and inserting a complete set of states of k^{n+1} gives:

$$\sum_{\omega' J'} |< k^{n+1} \omega' J' || a_k^+ || k^n \omega J >|^2 = (2J+1)(2j+1-n). \tag{20.13}$$

Combining Eqs. (20.9) and (20.13) we obtain a sum-rule for the sum over all states in both k^{n-1} and k^{n+1}:

$$\sum_{\omega' J'} |< k^{n-1} \omega' J' || \tilde{a}_k || k^n \omega J >|^2 + \sum_{\omega' J'} |< k^{n+1} \omega' J' || a_k^+ || k^n \omega J >|^2$$
$$= (2J+1)(2j+1). \tag{20.14}$$

When there is only one initial and final state, the CFP are unity. The basic examples are:

$$|< j^1, J = j \,|\} j^0, J' = 0 >| = 1, \tag{20.15}$$
$$|< j^2 J \,|\} j^1, J' = j >| = 1, \tag{20.16}$$

where J is even, and

$$|< j^{2j+1}, J = 0 \,|\} j^{2j}, J' = j >| = 1. \tag{20.17}$$

The wavefunctions for a closed-shell minus n particles can be expressed in terms of those for holes:

$$\mid k^{-n} \omega J > \equiv \mid k^{2j+1-n} \omega J > . \tag{20.18}$$

The matrix elements of $\tilde{a}$ for the hole-configurations are algebraically the same as the matrix elements of a^+ for particle configurations:

$$< k^{-n}\omega' J'||\tilde{a}_k||k^{-(n-1)}\omega J >=< k^n\omega' J'||a_k^+||k^{n-1}\omega J > . \tag{20.19}$$

Thus from Eq. (20.3) we can relate the matrix elements of a^+ for hole states to those for particle states:

$$\begin{aligned} < k^{-(n-1)}\omega J||a_k^+||k^{-n}\omega' J' >&= (-1)^{j+J'-J} < k^{-n}\omega' J'||\tilde{a}_k||k^{-(n-1)}\omega J > \\ &= (-1)^{j+J'-J} < k^n\omega' J'||a_k^+||k^{n-1}\omega J >, \end{aligned} \tag{20.20}$$

or

$$< k^{2j+1-(n-1)}\omega J||a_k^+||k^{2j+1-n}\omega' J' >= (-1)^{j+J'-J} < k^n\omega' J'||a_k^+||k^{n-1}\omega J > . \tag{20.21}$$

In terms of the one-particle CFP this becomes

$$\begin{aligned} < j^{-(n-1)}\omega J \,|\}j^{-n}\omega' J' > &\equiv < j^{2j+1-(n-1)}\omega J \,|\}j^{2j+1-n}\omega' J' > \\ = (-1)^{j+J'-J}&\sqrt{\frac{n(2J'+1)}{(2j+2-n)(2J+1)}} \; < j^n\omega' J' \,|\}j^{n-1}\omega J > . \end{aligned} \tag{20.22}$$

We can convert the special results of Eqs. (20.15) and (20.16) for particles to those for holes. When $n = 1$, $J' = j$, and $J = 0$ one obtain the same result as in Eq. (20.17). For the case when $n = 2$ and $J = j$ one obtains

$$|< j^{2j}, J = j \,|\}j^{2j-1}J' >|= \sqrt{\frac{(2J'+1)}{j(2j+1)}} \;\; |< j^2 J' \,|\}j^1, J = j >|= \sqrt{\frac{(2J'+1)}{j(2j+1)}}, \tag{20.23}$$

where J' is even. For example when we take one particle from the $[(j = 5/2)^5, J = 5/2]$ configuration the probability to leave the system in the states $[(j = 5/2)^4, J']$ is $\frac{2}{30}$ $\frac{10}{30}$ and $\frac{18}{30}$, for $J' = 0$, 2 and 4, respectively.

There are a variety of methods and computer programs for calculating the one-particle CFP [2], [3], [4], and they are tabulated in the literature [1], [5], [6] for small values of n and j. Also the projection operator method discussed in the next section can be used to calculate these CFP. All matrix elements in the J-scheme can be reduced to equations involving these one-particle CFP, and thus they are a primary input to any calculation or computer code that utilizes a J-coupled basis. As an example, the one-particle CFP for the $(j = 5/2)^3$ and $(j = 7/2)^3$ configuration [1] are given in Tables (20.1) and (20.2).

The results for specific CFP given in the text and tables implicitly have associated a choice for the phase factors of the initial and final wavefunctions. It is important to keep these phase factors consistent throughout the intermediate stages of a calculation, especially when the CFP are combined with the outputs of other programs.

Table (20.1). One-particle CFP for the $(j = 5/2)^3$ configuration.

$J \backslash J'$	0	2	4
3/2	0	$-\sqrt{\frac{5}{7}}$	$\sqrt{\frac{2}{7}}$
5/2	$-\sqrt{\frac{2}{9}}$	$\sqrt{\frac{5}{18}}$	$\sqrt{\frac{1}{2}}$
9/2	0	$\sqrt{\frac{3}{14}}$	$-\sqrt{\frac{11}{14}}$

Table (20.2). One-particle CFP for the $(j = 7/2)^3$ configuration.

$J \backslash J'$	0	2	4	6
3/2	0	$\sqrt{\frac{3}{14}}$	$-\sqrt{\frac{11}{14}}$	0
5/2	0	$\sqrt{\frac{11}{18}}$	$\sqrt{\frac{2}{33}}$	$-\sqrt{\frac{65}{198}}$
7/2	$-\sqrt{\frac{1}{4}}$	$\sqrt{\frac{5}{36}}$	$\sqrt{\frac{1}{4}}$	$\sqrt{\frac{13}{36}}$
9/2	0	$\sqrt{\frac{13}{126}}$	$-\sqrt{\frac{50}{77}}$	$\sqrt{\frac{49}{198}}$
11/2	0	$-\sqrt{\frac{5}{18}}$	$\sqrt{\frac{13}{66}}$	$-\sqrt{\frac{52}{99}}$
15/2	0	0	$\sqrt{\frac{5}{22}}$	$-\sqrt{\frac{17}{22}}$

20.2 Many orbits

The reduced matrix elements of the creation and destruction operators for the full many-body wave functions have the form:

$$< \Psi_f^{A-1}\omega_f J_f||\tilde{a}_k||\Psi_i^A\omega_i J_i >= (-1)^{j+J_f-J_i} < \Psi_i^A\omega_i J_i||a_k^+||\Psi_f^{A-1}\omega_f J_f > . \quad (20.24)$$

One can use the number operator to derive the sum-rules:

$$\sum_{\omega_f J_f} |< \Psi_f^{A-1}\omega_f J_f||\tilde{a}_k||\Psi_i^A\omega_i J_i >|^2= (2J_i+1) < n_k >_i, \quad (20.25)$$

and

$$\sum_{\omega_f J_f} |< \Psi_f^{A+1}\omega_f J_f||a_k^+||\Psi_i^A\omega_i J_i >|^2= (2J_i+1)[(2j+1)- < n_k >_i]. \quad (20.26)$$

In these expressions $< n_k >_i$ is the number of particle in orbit k in state Ψ_i. If one has a pure configuration this number is an integer, but for a mixed configuration this is the average number of particles in orbit k. For example, if one has a basis states from a single partition, e.g.

$$\mid n\omega J >_i= \mid [(k_1^{n_1}\omega_1 J_1)(k_2^{n_2}\omega_2 J_2)J_{12}][k_3^{n_3}\omega_3 J_3]J >_i,$$

then

$$< n_{k_a} >_i= n_a,$$

for $a = 1, 2$ and 3. If one has a wavefunction that contains two or more different partitions, e.g.

$$\mid \Psi >_i= c \mid \Phi >_i +c' \mid \Phi' >_i,$$

where

$$\mid \Phi >_i= \mid [(k_1^{n_1}\omega_1 J_1)(k_2^{n_2}\omega_2 J_2)J_{12}][k_3^{n_3}\omega_3 J_3]J >,$$

and

$$\mid \Phi' >_i= \mid [(k_1^{n'_1}\omega'_1 J'_1)(k_2^{n'_2}\omega'_2 J'_2)J'_{12}][k_3^{n'_3}\omega'_3 J'_3]J >, \quad (20.27)$$

then

$$< n_{k_a} >_i= c^2 n_a + c'^2 n'_a,$$

for $a = 1, 2$ and 3.

20.3 Spectroscopic factors

20.3.1 Basic definitions and sum-rules

The spectroscopic is defined in terms for the reduced matrix elements of a^+ by:

$$S = \frac{|< \Psi^A \omega J||a_k^+||\Psi^{A-1}\omega' J' >|^2}{(2J+1)} = \frac{|< \Psi^{A-1}\omega' J'||\tilde{a}_k||\Psi^A \omega J >|^2}{(2J+1)}, \tag{20.28}$$

where the $(2J+1)$ factor is by convention associated with the heavier mass A. S implicitly depends upon all quantities in the expressions (explicit labels are added when they are needed).

When the wavefunction is restricted to one orbital k with angular momentum j the spectroscopic factor is related to the coefficient of fractional parentage given in Eq. [20.10] by:

$$S = n \; |< j^n \omega J \; |\} j^{n-1} \omega' J' >|^2 \; . \tag{20.29}$$

The cross section for reactions involving the removal of a particle (proton or neutron) from nucleus A is proportional to the full matrix element of $\tilde{a}$ summed over m and the final M-states M_f, and averaged over the initial M-states M_i:

$$\sigma^- \sim \frac{1}{2J_i+1} \sum_{M_i,M_f,m} |< \Psi_f^{A-1} \omega_f J_f M_f \mid \tilde{a}_{k,m} \mid \Psi_i^A \omega_i J_i M_i >|^2$$

$$= \sum_{M_i,M_f,m} \begin{pmatrix} J_f & j & J_i \\ -M_f & m & M_i \end{pmatrix} \begin{pmatrix} J_f & j & J_i \\ -M_f & m & M_i \end{pmatrix} \frac{|< \Psi_f^{A-1} \omega_f J_f||\tilde{a}_k||\Psi_i^A \omega_i J_i >|^2}{(2J_i+1)}$$

$$= \frac{|< \Psi_f^{A-1} \omega_f J_f||\tilde{a}_k||\Psi_i^A \omega_i J_i >|^2}{(2J_i+1)} = S. \tag{20.30}$$

From the reaction theory one usually calculates a "single-particle" cross section σ_{sp} (i.e. assuming that $S = 1$) for the removal of one particle (proton or neutron) in orbit k and thus:

$$\sigma^- = S \; \sigma_{sp}. \tag{20.31}$$

Similarly the cross section for the addition of a particle to nucleus A is obtained from the full matrix element of a^+ summed over m and M_f and averaged over M_i:

$$\sigma^+ \sim \frac{1}{2J_i+1} \sum_{M_i,M_f,m} |< \Psi_f^{A+1} \omega_f J_f M_f \mid a_{k,m}^+ \mid \Psi_i^A \omega_i J_i M_i >|^2$$

$$= \sum_{M_i,M_f,m} \begin{pmatrix} J_f & j & J_i \\ -M_f & m & M_i \end{pmatrix} \begin{pmatrix} J_f & j & J_i \\ -M_f & m & M_i \end{pmatrix} \frac{|< \Psi_f^{A+1} \omega_f J_f||a_k^+ \mid \Psi_i^A \omega_i J_i >|^2}{(2J_i+1)}$$

$$= \frac{|< \Psi_f^{A+1}\omega_f J_f||a_k^+||\Psi_i^A\omega_i J_i >|^2}{(2J_i+1)} = \frac{(2J_f+1)}{(2J_i+1)}S, \tag{20.32}$$

where S is the spectroscopic factor associated with the removal of a particle from $A+1$ to A. Thus the cross section for the addition of a particle is given by:

$$\sigma^+ = \frac{(2J_f+1)}{(2J_i+1)}\ S\ \sigma_{sp}, \tag{20.33}$$

where the spectroscopic factor S is for the removal of a nucleon from $(A+1)$ to A, and the extra J factors take into account the different M state averaging for the two type of reactions.

The particle removal sum-rule for spectroscopic factors is obtained from Eq. [20.26] by summing over all states in the $(A-1)$ nucleus (denoted by $f-$):

$$\sum_{f-} S_{i,f,k} = < n_k >_i \quad [A \rightarrow (A-1)], \tag{20.34}$$

and the particle addition sum-rule for spectroscopic factors is obtained from Eq. [20.27] by summing over all states in the $(A+1)$ nucleus (denoted by $f+$):

$$\sum_{f+} \frac{(2J_f+1)}{(2J_i+1)}S_{i,f,k} = (2j+1) - < n_k >_i \quad [A \rightarrow (A+1)], \tag{20.35}$$

where $< n_k >_i$ is the average occupation of protons or neutrons in orbit k in the initial state i [with a maximum possible value of $(2j+1)$]. The total sum-rule is:

$$\sum_{f-} S_{i,f,k} + \sum_{f+} \frac{(2J_f+1)}{(2J_i+1)}S_{i,f,k} = (2j+1). \tag{20.36}$$

If we also sum Eq. (20.34) over all orbits we have a sum-rule for the total number of particles (protons or neutrons) in the nucleus:

$$\sum_{f-,k} S_{i,f,k} = Z \text{ or } N \quad [A \rightarrow (A-1)]. \tag{20.37}$$

20.3.2 Isospin dependence

The spectroscopic factors S as defined in Sec. 21.1 apply to protons or neutrons without regard to isospin. One can generalize the results to nucleons in the state (J,T) by adding the isospin labels. Eq. (20.28) becomes:

$$S(T) = \frac{|< \Psi^A\omega JT|||a_k^+|||\Psi^{A-1}\omega' J'T' >|^2}{(2J+1)(2T+1)} = \frac{|< \Psi^{A-1}\omega' J'T'|||\tilde{a}_k|||\Psi^A\omega J >|^2}{(2J+1)(2T+1)}, \tag{20.38}$$

where the triple bar matrix element indicates that it is reduced in both space and isospin. The sum-rules can be applied to the nucleon occupancies, e.g.

$$\sum_{f-} S_{i,f,k}(T) = < n_k >_i \quad [A \rightarrow (A-1)], \tag{20.39}$$

where $< n_k >_i$ is the average occupation of nucleons in orbit k in the initial state i (with a maximum possible value of $2(2j+1)$), and

$$\sum_{f-,k} S_{i,f,k}(T) = A \quad [A \rightarrow (A-1)], \tag{20.40}$$

When isospin is introduced we can also make explicit relationships between proton and neutron spectroscopic factors and nucleon spectroscopic factors. Starting with Eq. (20.28) but adding the explicit T_z dependence:

$$S(t_z) = \frac{|< \Psi^A \omega J T T_z || a^+_{k,t_z} || \Psi^{A-1} \omega' J' T' T'_z >|^2}{(2J+1)}, \tag{20.41}$$

where our convention is $(t, t_z) = (\frac{1}{2}, \frac{1}{2})$ for a neutron and $(t, t_z) = (\frac{1}{2}, -\frac{1}{2})$ for a proton, we use the Wigner-Eckhart theorem in isospin space to obtain:

$$S(t_z) = \begin{pmatrix} T & \frac{1}{2} & T' \\ -T_z & t_z & T'_z \end{pmatrix}^2 \frac{|< \Psi^A \omega J T ||| a^+_k ||| \Psi^{A-1} \omega' J' T' >|^2}{(2J+1)}$$

$$= |< T T_z \mid T' T'_z t t_z >|^2 \, \frac{|< \Psi^A \omega J T ||| a^+_k ||| \Psi^{A-1} \omega' J' T' >|^2}{(2J+1)(2T+1)}, \tag{20.42}$$

for the removal of a nucleon and:

$$S(t_z) = |< T T_z \mid T' T'_z t t_z >|^2 \, \frac{|< \Psi^{A+1} \omega J T ||| a^+_k ||| \Psi^A \omega' J' T' >|^2}{(2J+1)(2T+1)}, \tag{20.43}$$

for the addition of a nucleon. Thus in shorthand notation:

$$S(t_z) \equiv C^2 \, S(T), \tag{20.44}$$

where C^2 is the square the isospin Clebsch and $S(T)$ is the nucleon spectroscopic factor given by Eq. (20.38). In these expressions (T, T_z) are always associated with the heavier nucleus.

Although $S(t_z)$ are always the basic quantities measured, for nuclei not too far from $N = Z$ it is often convenient to calculate $S(T)$ in isospin formalism and then use Eq. (20.44) to convert to $S(t_z)$. In addition, some tables of experimental values and compilations [7] are given in terms of $S(T)$ by dividing the experimental $S(t_z)$

value by C^2. With good isospin there is an isospin selection rule given by the triangle condition $\Delta(T_f, \frac{1}{2}, T_i)$.

For an initial nucleus with $N = Z$, $S(t_z) = S(-t_z)$ by mirror symmetry. If we add a nucleon to $(T = 0, T_z = 0)$ then we must go to $T_f = 1/2$ with $C^2 = 1$. If we remove a nucleon from $(T = 0, T_z = 0)$ then we go to $T_f = 1/2$ with $C^2 = \frac{1}{2}$. In a neutron-rich nucleus, proton removal involves only one isospin value in the final state:

$$(T, T_z) \rightarrow \text{ proton } \rightarrow (T + \frac{1}{2}, T_z + \frac{1}{2}) = (T_>, T_z + \frac{1}{2}), \tag{20.45}$$

(transitions to the final state with higher isospin are forbidden by the triangle condition). Neutron removal can go to two isospin values:

$$(T, T_z) \rightarrow \text{ neutron } \rightarrow (T + \frac{1}{2}, T_z - \frac{1}{2}) = (T_>, T_z - \frac{1}{2}), \tag{20.46}$$

that are the isobaric analogues of the $(T + \frac{1}{2}, T_z + \frac{1}{2})$ states, and

$$(T, T_z) \rightarrow \text{ neutron } \rightarrow (T - \frac{1}{2}, T_z - \frac{1}{2}) = (T_<, T_z - \frac{1}{2}). \tag{20.47}$$

The $T_>$ and $T_<$ are referred to as the "T-upper" and "T-lower" states, respectively. The C^2 values for these three types of transitions are:

$$|< T, T_z \mid T + \frac{1}{2}, T_z + \frac{1}{2}, t, -\frac{1}{2} >|^2 = \left(\frac{2T+1}{2T+2}\right), \tag{20.48}$$

$$|< T, T_z \mid T + \frac{1}{2}, T_z - \frac{1}{2}, t, +\frac{1}{2} >|^2 = \left(\frac{1}{2T+2}\right), \tag{20.49}$$

and

$$|< T, T_z \mid T - \frac{1}{2}, T_z - \frac{1}{2}, t, +\frac{1}{2} >|^2 = 1. \tag{20.50}$$

The explicit relations between $S(t_z)$ and $S(T)$ are:

$$S(\text{proton}) = \left(\frac{2T+1}{2T+2}\right) S(T_>), \tag{20.51}$$

$$S(>, \text{neutron}) = \left(\frac{1}{2T+2}\right) S(T_>) = \left(\frac{1}{2T+1}\right) S(\text{proton}), \tag{20.52}$$

and

$$S(<, \text{neutron}) = S(T_<). \tag{20.53}$$

Thus, in neutron-rich nucleus one can measure "proton" spectroscopic factors, by neutron removal to the $T_>$ states. Although these $T_>$ states lie at a high excitation energy and are a often unbound to proton decay, their widths are small because

their nucleonic decay is isospin forbidden. These type of transitions have only been observed in nuclei not too far from $N = Z$ since where the $(2T + 1)$ factor is not too large.

French-Macfarlane sum-rules [8] are obtained from these results. For proton removal to $T_> = T_i + \frac{1}{2}$ ($T_z = T_i + \frac{1}{2}$) states:

$$\sum_f S(\text{proton}) = < n_{k,\text{proton}} >_i, \tag{20.54}$$

for neutron removal to the isobaric analogues of $T_>$ ($T_z = T_i - \frac{1}{2}$) states:

$$\sum_f S(>, \text{neutron}) = \frac{< n_{k,\text{proton}} >_i}{2T + 1}. \tag{20.55}$$

For the total neutron removal:

$$\sum_f S(\text{neutron}) = S(<, \text{neutron}) + S(>, \text{neutron}) = < n_{k,\text{neutron}} >_i, \tag{20.56}$$

and thus for neutron removal to the $T_<$ ($T_z = T_i - \frac{1}{2}$) states:

$$\sum_f S(<, \text{neutron}) = < n_{k,\text{neutron}} >_i \; - \frac{< n_{k,\text{proton}} >_i}{2T + 1}. \tag{20.57}$$

20.3.3 Simple situations

If we make a simple model for the initial and final states the values for the spectroscopic factors are sometimes easy to calculate. The results given in Sec. 20 for the special values of CFP in simple situations can be used to obtain the spectroscopic factors for the corresponding cases.

For example, ^{16}O might be assumed to be the closed-shell configuration $(0s_{1/2})^4$ $(0p_{3/2})^8$ $(0p_{1/2})^4$. One nucleon removal to $A = 15$ would then go to only three states each of which has a definite sum: $1/2^-$ with $S(0p_{1/2}) = 4$, $3/2^-$ with $S(0p_{3/2}) = 8$ and $1/2^+$ with $S(0s_{1/2}) = 4$. One proton or neutron removal for $T_i = 0$ going to $T_f = 1/2$ has $C^2 = 1/2$ and the sum rules are 2, 4 and 2, respectively, the same result one would obtain from the proton and neutron occupancies. (Center-of-mass corrections for these quantities will be discussed below.)

The spectroscopic factor for adding a $0\text{d}_{5/2}$ neutron to the closed-shell configuration for ^{16}O to make ^{17}O is $S_{0d_{5/2}} = 1$ and the stripping sum rule of Eq. (20.35) ($J_f = 5/2$ and $J_i = 0$) gives 6 which is the number of $0\text{d}_{5/2}$ neutron holes outside of ^{16}O.

20.3.4 Center-of-mass corrections

The center-of-mass (CM) correction to spectroscopic factors is closely associated with the problem of spurious states. Lets consider again the ^{16}O to $A = 15$ transition with a closed-shell configuration $(0s_{1/2})^4(0p_{3/2})^8(0p_{1/2})^4$ for ^{16}O. We take a single-particle basis that corresponds to the motion of the nucleons around a fixed center. In actuality, we should take them with respect to the CM of of the $A - 1$ nucleons. However, with harmonic-oscillator wave functions, the CM of the nucleus is in a 0s state as long as the nucleons fill the lowest possible oscillator states. There are effects due to CM motion, but they are the simple ones associated with the CM being on its 0s state. We will refer to these as "non-spurious" states. All oscillator states of the form $(0s_{1/2})^4(0p_{3/2})^n(0p_{1/2})^m$ are non-spurious and in particular the $A = 15$ the $1/2^-$ and $3/2^-$ states formed in this way are non-spurious.

Starting from a non-spurious state we can make $1\hbar\omega$ excited states either by an intrinsic $1\hbar\omega$ excitation leaving the CM in the 0s state, or by the $1\hbar\omega$ excitation of the CM state from 0s to 1p. These latter are spurious states in the nuclear shell model. A method for generating spurious states it to construct a two-body hamiltonian corresponding to the oscillator CM motion and then diagonalize this in the shell-model basis. If the coefficient in front of the CM hamiltonian is large enough, the spurious states will be pushed to a high excitation energy and are prevented from mixing into the low-lying (non-spurious) states.

The lowest $1\hbar\omega$ excitation for $A = 15$, $1/2^+$ corresponds to a mixture of $(0s)^3(0p)^8$ and $(0s)^4(0p)^7(1s0d)^1$ configurations (e.g. the notation 0p stands for all possible arrangements involving the $0p_{1/2}$ and $0p_{3/2}$). There are a total of 18 basis states and diagonalization of the CM hamiltonian results in two spurious states that are linear combinations of these basis states.

We can calculate the summed spectroscopic strength from the closed-shell configuration of ^{16}O to the non-spurious $A = 15$ states. The result is $S = 12$ for the 0p shell and $S = 3.2$ for the 0s shell - the remaining $S = 0.8$ for the 0s shell is in the two spurious states. However, the sum rule of $S = 16$ still applies to the wave-functions the intrinsic frame, and in order to recover this result we must make the following correction to the $0p$ spectroscopic factors [9]:

$$S_{0p} \rightarrow \frac{A}{(A-1)} S_{0p}. \tag{20.58}$$

where $A = 16$ in this example. This correction is the largest at the lower end of the 0p shell, e.g. (7/6) for the 0p-shell A=7 to A=6 spectroscopic factors. The general

derivation and result is given in [9]:

$$S_k \rightarrow \left[\frac{A}{(A-1)}\right]^{2n_r+\ell} S_k. \tag{20.59}$$

For example, for the removal of the $0d_{5/2}$ in ^{17}O to ^{16}O, the CM correction factor is $(17/16)^2 = 1.129$, and for the removal of the $0f_{7/2}$ in ^{48}Ca to ^{47}Ca the CM correction factor is $(48/47)^3 = 1.065$. [The first Variational Monte Carlo (VMC) calculations [10] for the ^{16}O(e,e′p) reaction indicated that the CM correction had the effect of reducing the 0p spectroscopic factor by about 12 percent, however subsequently an error was found [11] and the new VMC result is consistent with the 7 percent enhancement expected from from the CM correction.]

20.3.5 Computation of shell-model spectroscopic factors

In simple situations, the spectroscopic factors can be obtained from the sum rules. In particular, pickup from a closed shell configuration has a value of $2(2j+1)$ for nucleons or $(2j+1)$ for protons or neutrons. Pickup from a state which is represented by single-particle outside of a closed shell is unity. Often the j^n configuration allows only a single state with a given J value and the spectroscopic factor in this situation can be calculated with the use of tabulated coefficients of fractional parentage. For complicated situation one must use a shell-model computer code. For example, in Oxbash [12] one first calculates the wave functions and then takes the one-particle overlaps. The outputs are in files labeled *.LSA for the spectroscopic amplitudes and *.LSF for the spectroscopic factors.

20.4 Overlap functions

20.4.1 Definition and properties

Spectroscopic factors are related to the expansion of the wave function for a specific state Ψ_i^A in the initial nucleus with A nucleons in terms of a summation over the complete set of states Ψ_f^{A-1} in the final nucleus with $A-1$ nucleons:

$$\Psi_i^A = \sum_{f,\ell,j} \theta_{i,f,\ell,j}(\vec{r}\,)\ \Psi_f^{A-1}, \tag{20.60}$$

In the reaction for the removal of particles from state Ψ_i to a specific state Ψ_f one requires the overlap function θ:

$$< \Psi_f^{A-1} \mid \Psi_i^A > = \sum_{\ell,j} \theta_{i,f,\ell,j}(\vec{r}\,), \tag{20.61}$$

where an explicit summation over all possible ℓ and j values of the single-particle overlap function θ is made. The spectroscopic amplitude A is defined by the normalization of the overlap function:

$$A_{i,f,\ell,j} = \int \theta_{i,f,\ell,j}(\vec{r}\,)\ d\tau, \tag{20.62}$$

and the related spectroscopic factor is:

$$S_{i,f,\ell,j} = \mid A_{i,f,\ell,j} \mid^2 . \tag{20.63}$$

The explicit dependence on ℓ and j is kept because the angular distributions in a particular reaction depend upon ℓ and j, and thus is it possible to separate each of these components in a given transition. Often the dependence on j is small in which case one measures the sum over the two possible j values for a given ℓ:

$$S_{i,f,\ell} = \sum_j S_{i,f,\ell,j}. \tag{20.64}$$

For example, for a $J_i \rightarrow J_f = \frac{3}{2}^+ \rightarrow 2^+$ transition both $0d_{5/2}$ and $0d_{3/2}$ could contribute and one will measure:

$$S_{\ell=2} = S_{0d_{5/2}} + S_{0d_{3/2}}$$

The radial size of the spectroscopic amplitude can be characterized in terms of its mean-square radius:

$$< r^2 >_A = \frac{\int \theta(\vec{r}\,)\ r^2\ d\tau}{\int \theta(\vec{r}\,)\ d\tau}. \tag{20.65}$$

One can expand the overlap function in terms of a complete set of single-particle wave functions:

$$\theta_{i,f,\ell,j}(\vec{r}\,) = \sum_{n_r} B_{i,f,k}\ \phi_k(\vec{r}\,) \tag{20.66}$$

where the ϕ are normalized to unity and k stands for (n_r, ℓ, j). The single-particle states are given by:

$$\phi_k(\vec{r}\,) = \frac{R_k(r)}{r}[Y^{(\ell)}(\hat{r}) \otimes \chi^s]^j, \tag{20.67}$$

where χ^s is the intrinsic-spin wave function. For the single-particle states ϕ_k, one could take a basis of states generated from a mean-field potential. In practical terms one often approximates the mean-field with harmonic-oscillator or Woods-Saxon potentials. With the general expansion:

$$S_{i,f,l,j} = \sum_{n_r} \mid B_{i,f,k} \mid^2 . \tag{20.68}$$

One often assumes that sum in Eq. (20.66) is restricted to only one radial quantum number n_r, in which case $B = A$, and $S = \mid A \mid^2 = \mid B \mid^2$.

The possible ℓ and j values are restricted by the total angular momenta J and parities of the initial and final states. In general one must use a complete set of single-particle states in the overlap function. But the quantum numbers associated with j are restricted by the spin and parities of the initial and final states. In particular parity is conserved, and if $J_i^\pi = 0^+$ then $j = J_f$ and $\pi_f = (-1)^\ell$.

The overlap function is exact to the extent that the many-body calculation is exact and the sum in Eq. (20.66) extends over all (n_r) values. However, simplified nuclear models usually lead to the use of only a few (n_r) values related to orbits near the fermi surface. For example, a Hartree-Fock calculation for ^{17}O may be based upon a closed-shell configuration for ^{16}O plus a neutron in the $0d_{5/2}$ orbital. Then the overlap function for the ^{17}O to ^{16}O reaction has $A_{0d_{5/2}} = 1$ and is given by $\theta(\vec{r}\,) = \phi_{0d_{5/2}}(\vec{r}\,)$ (the Hartree-Fock single-particle wave function).

In order to meaningfully use spectroscopic factors we require that the reaction theory reproduce the observed dependence on projectile, energy and angle. The spectroscopic factor is a single number whose value should not depend on the reaction. When this is not the case, the reaction model or the model assumed for the overlap function must be questioned. A theoretical review is given by Bang et al. [13].

20.4.2 Asymptotic properties

We can consider the overlap in Eq. (20.62) as a function of r. At large r where the nuclear interactions are negligible this overlap must be governed by the kinematical

asymptotics appropriate for the energy difference $\Delta E = E_f - E_i$ ($E = -$BE where BE is the binding energy). For example for ^{17}O($5/2^+$) to ^{16}O(0^+), $\Delta E = -4.14$ MeV and there is an exponential decay appropriate for a d wave bound by 4.14 MeV.

In some reactions such as (^{3}He,d) and (d,^{3}He), the optical potentials are such that only the part of the overlap function near the nuclear surface is important. In the extreme case (e.g. at incident energies far below the Coulomb barrier) it is only the asymptotic part of the overlap function which is important. The assumptions about the potential only influence the overall normalization, $N_{\ell,j}$, of the asymptotic wave function:

$$\theta_{i,f,\ell,j}(\vec{r}\,) \rightarrow N_{\ell,j}\ f_\ell(r), \tag{20.69}$$

where $f_l(r)$ is an asymptotic form independent of the strong potential that depends upon ℓ due to the the centrifugal barrier. It is usually taken as the Whittaker function [14]. In the single-particle model the aymptotic behaviour is that of the single-particle radial wavefunction

$$\frac{R_k(r)}{r} \rightarrow N_k\ f_\ell(r), \tag{20.70}$$

The radial part of the overlap integral for large r is:

$$< \Psi_f^{A-1} \mid \Psi_i^A > \rightarrow \sum_{\ell,j} A_{i,f,\ell,j}\ N_{\ell,j}\ f_\ell(r). \tag{20.71}$$

In this case the nuclear structure part of the reaction cross section for a given (ℓ, j) depends only on the square of the asymptotic normalization $A_{i,f,\ell,j}N_{\ell,j}$.

20.4.3 The well-depth prescription

In some cases the nuclear model may explicitly contain the correct asymptotic behavior, such as a Hartree-Fock model for ^{17}O in which the last neutron is bound by 4.14 MeV. But usually many-body nuclear models are developed which do not explicitly contain the correct asymptotic form. For example, a typical shell-model calculation for ^{18}O consists of calculating the sd-shell configuration mixing and total energy by evaluating the G matrix elements of a two-body residual interaction in an harmonic-oscillator basis. The implicit radial wave functions used are the same for both ^{17}O and ^{18}O and have the incorrect (oscillator) asymptotics for both the ^{17}O to ^{16}O and the ^{18}O to ^{17}O overlaps.

The general method for generating an overlap function with the correct asymptotic form is to start with a realistic mean-field potential for the single-particle wave functions and then to modify this potential such that the single-particle (ϵ) energy is equal to the actual energy difference (ΔE). One way to do this is to multiply the mean-field potential by a constant such that the $\epsilon = \Delta E$. This is the "well-depth"

prescription. Historically, the well-depth prescription was easy to apply numerically and has become the default method in many codes and analyses. For example, for the ^{18}O(gs) to ^{17}O($5/2^+$ gs) reaction one would increase the potential depth in order to bind the $0d_{5/2}$ orbital by the experimental energy difference $\Delta E = -12.19$ MeV. Likewise for the ^{18}O(gs) to ^{17}O($1/2^+$ 0.87 MeV excited state) reaction one would increase the potential for the $1s_{1/2}$ orbital in order to give the experimental energy difference of $\Delta E = -13.06$ MeV.

In cases where the single-particle wave function generated by the well-depth prescription is close to that of a realistic mean-field (e.g. the multiplying factor is not too difference from unity) this method is a reasonable procedure. This usually applies to cases where the spectroscopic factor is near the sum-rule limit. But when the spectroscopic factor is small, this prescription may be questioned. For example, in the $(0\mathrm{d}_{5/2})^3$ configuration there are states with J =3/2, 5/2 and 9/2. The overlap function between $(0\mathrm{d}_{5/2})^2$, $J = 0$ and $(0\mathrm{d}_{5/2})^3$, $J = 3/2$ must vanish ($S = 0$) since the $J = 3/2$ does not match the $j = 5/2$ of the transferred particle. A nonvanishing spectroscopic factor would result from a small $(0\mathrm{d}_{5/2})^2(0\mathrm{d}_{3/2})$ admixture into the $(0\mathrm{d}_{5/2})^3$ wave functions. The single-particle potential needed to give the correct asymptotics for this small component is quite different from the mean-field potential. Thus rather than multiply the mean-field potential it may be more appropriate to add a surface peaked term to the mean-field potential as discussed in the next section.

A common way to implement the well-depth prescription is to generate an overlap function from the single-particle wave functions obtained from a Woods-Saxon potential. For the well-depth prescription, one would adjust the strength of the central potential to obtain a single-particle wave function ϕ_j which has a single-particle energy equal to the energy difference between the initial and final states under consideration. This wave function goes into the reaction theory to calculate a cross section, and then from comparison to experiment one deduces the spectroscopic factor S. However, one should keep in mind that the value for S depends upon the assumptions made about the reaction models and about the overlap function.

20.4.4 Beyond the well-depth prescription

One would like to carry out an experiment which is sensitive to the shape as well as the magnitude of the overlap function. But the nuclear reactions are generally only sensitive to the surface or asymptotic part, and thus the assumption about the fixed Woods-Saxon shape cannot be easily tested. As mentioned above the prescription based on the adjustment of the depth of a central potential is appropriate only when the transition under consideration is actually close to single-particle in nature. When the single-particle strength is fragmented due to residual interactions (beyond the

mean-field) one should consider additions to the central potential which are related to the residual interaction.

Pinkston and Satchler [15] discussed the situation for the (p,d) reactions in the $0f_{7/2}$ shell region, for example ^{48}Ti(p,d) leading to the lowest $T_< = 3/2$ and $T_> = 5/2$ states in ^{47}Ti which differ in separation energy by 7.3 MeV. This isospin splitting of the $0f_{7/2}$ orbit can be related to an isovector residual interaction which peaks near the nuclear surface and might be modeled on the derivative of the central Woods-Saxon potential. Thus the shape as well as the strength of the central potential must be considered. In terms of the original Woods-Saxon shape, the surface potential has the effect of effectively increasing the radius r_o for the $T_>$ state (in contrast to the well-depth prescription where the well-depth V_o is increased). This results in a relatively larger radius for the overlap function, a larger DWBA cross section, and hence a smaller spectroscopic factor. Similar considerations regarding the shape of the potential are related to the collective model. [15] More detailed models of these residual-interaction effects have discussed some of which involve solving a set of coupled equations for the bound state [16], [17], [18], [19], [20].

The examples above apply to removal from a partially filled orbit. In this situation the energy difference ΔE for the transition in question is usually larger than the single-particle energy. The well-depth prescription thus gives an rms radius for the overlap function which is smaller than the rms radius of the single-particle state. The surface effect of the residual interaction correction leads to an overlap function which has a relatively larger rms radius (back in the direction the single-particle rms radius). In the $0f_{7/2}$ shell it was found that a practical prescription is to fix the Woods-Saxon well depth and radius to give the correct energy difference and a *state-independent* rms radius for the overlap function [21]. The spectroscopic factors obtained with the residual interaction corrections are typically up to a factor of two smaller than than those obtained with the well-depth prescription.

The other extreme is stripping to a nearly filled orbit. For example ^{40}Ca(d,p)^{41}Ca leading to the $3/2^+$ state (at 2.04 MeV). The spectroscopic factor would be zero in the limit where the $0d_{3/2}$ orbit is filled in ^{40}Ca. The energy difference is $\Delta E = -10.4$ MeV as compared to the single-particle energy of about $\epsilon = -15.6$ MeV (e.g. the ^{40}Ca - ^{39}Ca binding energy difference). The well-depth prescription thus leads to an rms radius for the overlap function ($\Delta E = -10.4$ MeV) which is larger than that of the single-particle state ($\Delta E = -15.6$ MeV). The surface property of the residual interaction leads to an overlap function which has a relatively smaller rms radius [22] (again back in the direction of the single-particle rms radius).

References

[1] A. de Shalit and I. Talmi, *Nuclear Shell Theory*, (Academic Press, 1963).

[2] L. B. Hubbard, Comput. Phys. Commun. 1, 225 (1970); D. Zwart, Comput. Phys. Commun. **38**, 656 (1985); L. D. Skouras and S. Kossionides, Comput. Phys. Commun. **39**, 197 (1986).

[3] A. Novoselsky, J. Katriel and R. Gilmore, Jour. Math. Phys. **29**, 1368 (1988).

[4] X. Ji and M. Vallieres, Phys. Rev. C **35**, 1583 (1987).

[5] R. D. Lawson, *Theory of the Nuclear Shell Model*, (Clarendon Press, 1980).

[6] B. F. Bayman and A. Lande, Nucl. Phys. **77**, 1 (1966); I. S. Towner and J. C. Hardy, Nucl. Data Tables A6, 153 (1969); L. B. Hubbard, Nucl. Data Tables A9, 85 (1971); S. Shlomo, Nucl. Phys. **A184**, 545 (1972).

[7] "Spectroscopic Factors for Single Nucleon Transfer for A = 21-44", P. M. Endt, Atomic and Nuclear Data Tables **19**, 23 (1977).

[8] J. B. French and M. H. Macfarlane, Nucl. Phys. **26**, 168 (1961).

[9] A. E. L. Dieperink and T. de Forest, Phys. Rev. C **10**, 543 (1974); M. Ichimura, A. Arima, E. C. Halbert and T. Terasawa, Nucl. Phys. **A204**, 225 (1973).

[10] M. Radici, S. Boffi, S. C. Pieper and V. R. Pandharipande, Phys. Rev. C **50**, 3010 (1994).

[11] D. Van Neck, M. Waroquier, A. E. L. Dieperink, S. C. Pieper and V. R. Pandharipande, Phys. Rev. C **57**, 2308 (1998).

[12] W. D. M. Rae, A. Etchegoyen and B. A. Brown, *OXBASH, the Oxford-Buenos Aries-MSU Shell-Model Code*, Michigan State University Laboratory Report no. 524.

[13] J. M. Bang, F. G. Gareev, W. T. Pinkston and J. S. Vaagen, Phys. Rep. **125**, 253 (1985).

[14] P. G. Hansen and J. A. Tostevin, Ann. Rev. Nucl. Part. Sci. **53**, 219 (2003).

[15] W. T. Pinkston and G. R. Satchler, Nucl. Phys. **72**, 641 (1965).

[16] E. Rost, Phys. Rev. **154**, 994 (1967).

[17] T. Tamura, Phys. Rev. Lett. **19**, 321 (1967); Phys. Rev. **165**, 1123 (1968).

[18] A. Prakash, Phys. Rev. Lett. **20**, 864 (1968); A. Prakash and N. Austern, Ann. of Phys. **51**, 418 (1969).

[19] J. L. Hutton, Nucl. Phys. **A210**, 567 (1968).

[20] R. J. Philpott, W. T. Pinkston and G. R. Satchler, Nucl. Phys. **A119**, 241 (1968).

[21] A. Moalem, J. F. A. van Heinen and E. Kashy, Nucl. Phys. **A307**, 277 (1978).

[22] W. T. Pinkston, R. I. Philpott and G. R. Satchler, Nucl. Phys. **A125**, 176 (1969).

21 Experiments related to spectroscopic factors

21.1 Experimental results for specific nuclei

There have been many experimental papers related to the extraction of spectroscopic factors. The details obtained have been and continue to be tremendously important in guiding the our understanding of nuclear structure. In this section we will give a few examples of the wide range of data available.

We will mainly look at examples where nucleons are removed from the nucleus. Reactions such as (d,^{3}He) or (p,d) are called "pickup" reactions since a nucleon is picked up by the light projectile and removed from the target nucleus. Reactions such as (e,e′p) are called "knockout" reactions since the electron hits the proton and knocks it out of the nucleus. The collision of radioactive beams with light and heavy targets can also knockout protons or neutrons from the radioactive beam. In addition, the spontaneous decay of a proton or neutron from an unbound state removes a nucleon from the nucleus.

We will also look at examples for spectroscopic factors when nucleons are added to the nucleus. Reactions such as (^{3}He,d) or (d,p) are often called "stripping" reactions since since a nucleon is stripped from the light projectile and added to the target nucleus. Sometimes the spectroscopic factors for the a given pair of states can be studied in both stripping and pickup reactions. For consistency the same spectroscopic factor should be obtained from both reactions.

21.1.1 ^{51}V → ^{50}Ti

One of the best examples for proton removal spectroscopic factors in a one-orbit model is given by the reaction ^{51}V → ^{50}Ti. In this mass region the $0f_{7/2}$ orbit is rather well isolated. In this model the structure of ^{51}V is a closed shell, $(0f_{7/2})^8$, for neutrons and $(0f_{7/2})^3$ for protons. For this configuration there is only one $J = 7/2$ state, and the spectroscopic factors can be obtained immediately from the Table of CFP together with the relationship:

$$S = n \mid< j^n \omega_i J_i \mid\} j^{n-1} \omega_f J_f >|^2 . \tag{21.1}$$

This gives the values in the first column of Table [22.1] whose sum is three - the total number of protons in the $0f_{7/2}$. This particular structure leads to nontrivial values for the spectroscopic factors which are in excellent agreement with the original ^{51}V(d,^{3}He) (52 MeV) experiment (Table 22.1.a) [1]. An analysis of ^{51}V(d,^{3}He) data at several energies [2] shows that absolute spectroscopic factors are sensitive to the

Table 1: Proton spectroscopic factors for $^{51}V \rightarrow {}^{50}Ti$

J_f	$(f_{7/2})^3$ model	(d,^{3}He) (a)	(d,^{3}He) (b)	(e,e′p) (c)	(d,^{3}He) (c)
0	0.75	0.73	0.40(1)	0.37(3)	0.30
2	0.42	0.39	0.21(1)	0.16(2)	0.15
4	0.75	0.64	0.42(1)	0.33(3)	0.26
6	1.08	1.05	0.66(1)	0.49(4)	0.39
sum	3.00	2.81	1.69	1.35(7)	1.10

a) 1967 analysis of Hinterberger et al. [1] for 52 MeV data.
b) 1976 analysis of Craig et al. [2] for 80 MeV data.
c) 2001 analysis of Kramer et al. [3].

reaction model, but the relative spectroscopic factors for the various J_f values are rather insensitive. A more recent finite-range DWBA analysis of 80 MeV data results in spectroscopic factors which are about 0.6 of those expected from the $0f_{7/2}$ shell model (Table 22.1.b). This reduction from unity is consistent with the more recent (e,e′p) results (Table 22.1c) which will be discussed in more detail below.

21.1.2 (^{3}He,d) in the sd shell

The sd-shell provides one of the best examples of how shell-model configuration mixing can be applied consistently over a wide mass range. One can find an effective two-body interaction [4] which is able to reproduce the energies of about 1000 levels for nuclei over the mass range A=17-39 to within an rms deviation of a few hundred keV [5]. The electromagnetic and beta decay properties of these levels are also rather well understood in this sd-shell model [6].

Endt has made a compilation of spectroscopic factors for the sd-shell [7]. Vernotte et al. [8] has made an analysis of spectroscopic factors in the sd-shell with a unified analysis of (^{3}He,d) (nucleon removal) data obtained with a ^{3}He energy of 25 MeV. The data themselves are rather precise and the statistical error is relatively small. Most of the uncertainty associated with the extracted spectroscopic factors is related to the reaction-model interpretation. The data provides information for 39 transitions between specific initial and final states over the mass region A=17-40. The analysis depends upon a zero-range DWBA analysis for which one must provide optical potentials for the ^{3}He and d. The overlap function is based upon the well-depth method.

The initial analysis was carried out with Woods-Saxon shape parameters r_o =

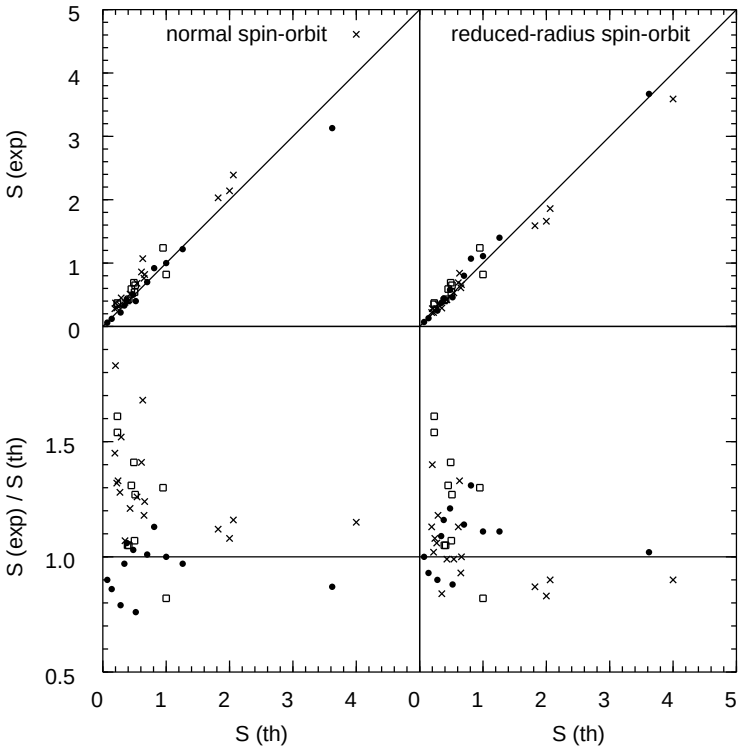

Figure 1: Theoretical vs experimental spectroscopic factors for 39 transitions in the sd shell. The parameters of the Woods-Saxon potential are $r_o = 1.25$ fm and $a = 0.65$ fm. The results on the left-hand side were obtained with the normal spin-orbit potential $r_{so} = r_o$ and $a_{so} = a_o$. The results on the right-hand side were obtained with the reduced-radius spin-orbit potential $r_{so} = 1.00$ fm and $a_{so} = 0.52$ fm. The points are for $0d_{5/2}$ (filled circles), $0d_{3/2}$ (crosses) and $1s_{1/2}$ (squares).

1.25 fm and $a = 0.65$ fm. Initially the same shape parameters were used for the spin-orbit potential. The experimental and theoretical spectroscopic factors are shown on the left-hand side of Fig. (21.1) (In [8] the results for the nucleonic spectroscopic factors are given, but here I have converted these to proton spectroscopic factors by dividing by the C^2 factor.) In the top one observes good agreement in terms of the variation from large to small values. The largest value for $0d_{5/2}$ (filled circle) corresponds to the ^{27}Al ($5/2^+$ gs) to ^{28}Si(0^+ gs) transition. In the simplest $(0d_{5/2})^n$ model the theoretical value would be six, but this gets reduced to 3.61 due to configuration mixing in the full sd shell. The largest value for $0d_{3/2}$ (cross) is for the ^{39}K($3/2^+$) $\rightarrow$ ^{40}Ca(0^+) transition. In the simple $(0d_{3/2})^n$ model as well as in the full sd-shell model it has a theoretical value of four.

In the bottom of Fig. (21.1) the ratios are plotted vs the theoretical value. The ratios for $0d_{3/2}$ (crosses) are systematically higher than those for $0d_{5/2}$ (filled circles). A way to correct this problem was noted by Vernotte et al., and I will discuss this in some detail to illustrate the problems which can arise in the model dependence

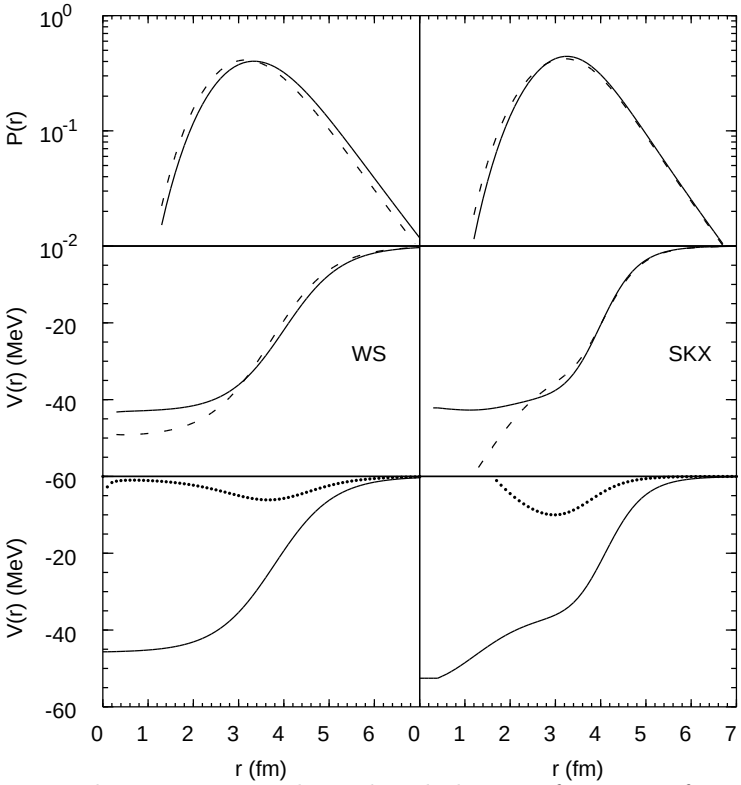

Figure 2: Bound state potentials and radial wave functions for the Woods-Saxon (left-hand side) and SKX Skyrme Hartree Fock (right-hand side). The bottom panel shows the cental (line) and spin-orbit (dots) potentials for $A = 28$. The middle panel shows the effective total potentials for $0d_{5/2}$ (line) and $0d_{3/2}$ (dashes) required to bind the orbitals by 3 MeV. The top panel shows the radial density probability for $0d_{5/2}$ (line) and $0d_{3/2}$ (dashes) resulting from the effective potentials.

in the analysis. Namely, the ratios can be improved if the value of r_{so} used in the Woods-Saxon potential is reduced from 1.25 to 1.00 fm. To better understand how this works, the central and spin-orbit Woods-Saxon potentials are plotted on the bottom left-hand of Fig. (21.2). The central potential is the one required to bind a 0d orbit by 3 MeV (no spin-orbit). The spin-orbit potential plotted represents the total change in potential between the $0d_{5/2}$ and $0d_{3/2}$ orbits which is required to reproduce the spin-orbit energy difference of about 6 MeV. The well-depth prescription is now used to generate a wave function for the $0d_{5/2}$ and $0d_{3/2}$ orbits with a fixed binding energy of 3 MeV (an arbitrary but typical value) by adjusting the strength V_o of the central potential. The "effective" total potential (the sum of the adjusted central and spin-orbit terms and excluding Coulomb) for the $0d_{5/2}$ and $0d_{3/2}$ are shown in the middle part of Fig. (21.2). The square of the radial wave functions are shown at the top. The effective potential for $0d_{5/2}$ has an effectively larger radius than that for $0d_{3/2}$ and the resulting $0d_{5/2}$ radial density is larger than that $0d_{3/2}$.

The (^{3}He,d) cross section is mainly sensitive to the overlap function near the surface, and essentially only the asymptotic normalization is important. On the left-hand side of Fig. (21.2) this asymptotic normalization is 25% larger for $0d_{5/2}$ compared to $0d_{3/2}$ which arises from the spin-orbit potential. Thus for a given separation energy, the spin-orbit potential causes the extracted spectroscopic factor for $0d_{5/2}$ to be 25% less than that for $0d_{3/2}$ (in the direction of the deviation noted in Fig. (21.1)).

Vernotte et al. were able to improve this situation by reducing the range of the spin-orbit potential to from 1.25 fm to 1.00 fm (the ratio of the diffuseness to the range of the spin-orbit potential was fixed at 0.52). This results in effective potentials for $0d_{5/2}$ and $0d_{3/2}$ that are nearly the same at the nuclear surface. The resulting spectroscopic factors shown in Fig. (21.1) have a more consistent average ratio for $0d_{5/2}$ and $0d_{3/2}$.

This analysis brings into focus the model dependence of extracting spectroscopic factors. One could use other models for the bound states. I show, as an example, the potentials which one obtains from the SKX Skyrme Hartree-Fock model [9] at the bottom of Fig. (21.2), together with the effective potentials obtained by adjusting the central part of the HF potential to obtain binding energies of 3 MeV for $0d_{5/2}$ and $0d_{3/2}$. It turns out that the spin-orbit potential from the Skyrme interaction is peaked at a smaller radius compared to the conventional Woods-Saxon model and that this leads to very similar effective potentials near the surface. In this sense the Skyrme HF justifies the empirical result obtained by Vernotte et al. The reason why the Skyrme spin-orbit potential peaks at a smaller radius is that it is obtained from the derivative of the matter density which has a smaller effective radius than the potential.

At small radii there are also large differences between the Woods-Saxon and Skyrme potentials, (21.2), but this does not have much influence on the analysis of spectroscopic factors. This small radius behavior has an influence on the interior density which can be determined from the charge density measured in elastic electron scattering. Some charge densities extracted from experiments are compared with Hartree-Fock calculations [11] based upon the SKX [9] and SKM* [10] Skyrme interactions are shown in Fig. [12.12]. For the sd-shell the occupancies from the sd-shell model calculations were used. The good agreement between experiment and theory together with the relatively strong nucleus to nucleus variation tends to confirm the Skyrme HF approach.

The possible uncertainty in the spin-orbit potential is part of a larger question as to how accurately the central potential and the resulting asymptotic normalizations can be calculated. In terms of the (^{3}He,d) reaction Vernotte et al. pointed out the strong dependence of the extracted spectroscopic factors on the range of the central potential. They noted that an increase of 0.01 fm in r_o decreased the extracted

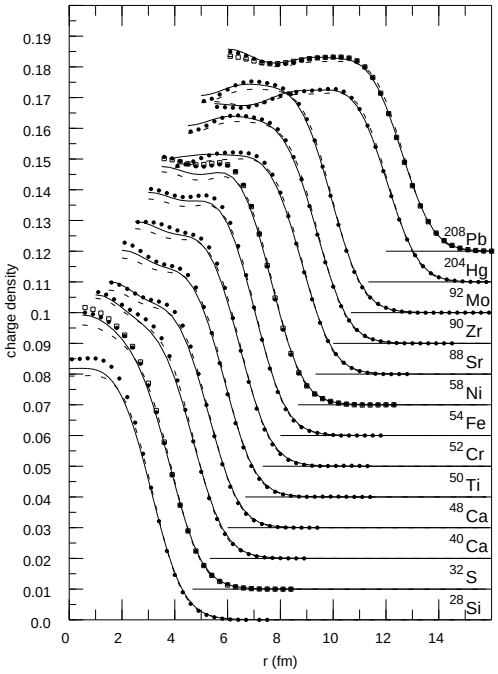

Figure 3: Charge densities for a range of nuclei. The filled circles are the experimental densities obtained from a Fourier-Bessel analysis of the electron scattering form factor data. The Hartree-Fock results are shown for the SKX [9] and SKM* [10] Skyrme interactions.

spectroscopic factors by 3-4% (see Fig. 8 in [8]). Since the reaction takes place at the nuclear surface and depends mainly on the asymptotic normalization, there is very little dependence of the shape of the angular distributions on r_o.

There are also issues related to the reaction model. Vernotte et al. used the convenient zero-range form of DWBA, but they noted that non-locality corrections and finite-range correction would decrease the overall spectroscopic factors by about 25%. Thus to attempt to summarize the sd-shell data in terms of absolute spectroscopic factors I show in Fig. (21.4) the values obtained with the new reduced-radius spin-orbit interaction and multiplied by 0.75 are plotted as the ratio of experiment over theory vs the mass value.

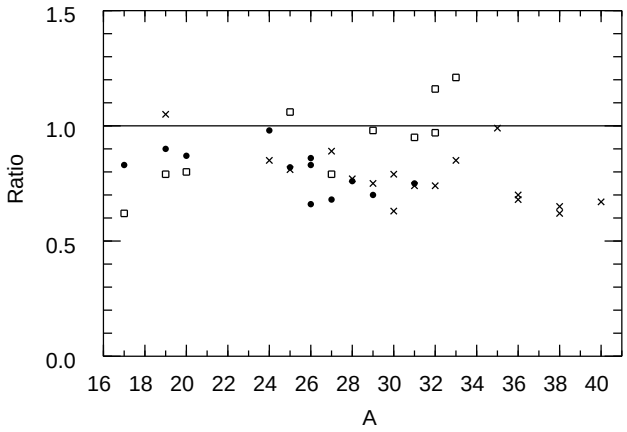

Figure 4: Ratio of the experimental to theoretical spectroscopic factors for $(A-1)(^3\mathrm{He,d})A$ in the sd shell. The experimental values obtained from the reduced-radius spin-orbit potential model are multiplied by 0.75. (Center-of-mass corrections are not included in the theory.) Filled circles are for $0\mathrm{d}_{5/2}$ crosses are for $0\mathrm{d}_{3/2}$ and squares are for $1\mathrm{s}_{1/2}$.

21.1.3 (e,e′p)

The (e,e′p) reaction is perhaps the most direct way to measure the proton spectroscopic factor. It is largely determined by the well understood electromagnetic interaction and the only hadronic reaction theory involved is for the final-state interactions of the protons as they leave the nucleus. [12], [3] Unlike the reactions such as the (^{3}He,d) and (d,^{3}He) discussed above which depend mainly on the surface part of the overlap function, the (e,e′p) reaction is sensitive to the overlap function at all radii. The shape of the momentum proton distributions is sensitive to the radial shape of the overlap function. Thus, one can adjust the well depth and the radius of the potential to give the separation energy and the shape of the momentum distribution. The analysis of many data have recently been carried out Kramer et al. [3] and I give the some of the resulting proton spectroscopic factors in Table [22.2].

Table [22.2] also gives the spectroscopic factors obtained from the conventional analysis of (d,^{3}He) data based upon zero-range DWBA and a Woods-Saxon potential with a radius of $r_o = 1.25$ fm. The spectroscopic factors deduced from (e,e′p) are systematically smaller than those from the old (d,^{3}He) analysis by a factor of 0.6-0.7. They are also about this much smaller than that expected from a shell-model or sum-rule estimate. An explanation of this is that the old (d,^{3}He) analysis is based upon a simple (zero-range) reaction theory and a shape for the form factor which are rather arbitrarily chosen to give the expected (sum-rule) result. Kramer et al., also carry out a new analysis of the (d,^{3}He) data based on a finite-range DWBA and with Woods-Saxon wave functions for the overlap function with r_o adjusted to give the correct shape of the (e,e′p) momentum distributions. A non-locality correction [3] was also

Table 2: Proton spectroscopic factors for a range of nuclei.

Nuclei	E_x (MeV)	J_f	(e,e′p)(a) NR(b)	(e,e′p) R(c)	(d,^{3}He)(a) (old)	(d,^{3}He)(a) (new)
$^{12}C \rightarrow {}^{11}B$	0.00	$3/2^-$	1.72(11)		2.98	1.72
	2.12	$1/2^-$	0.26(2)		0.69	0.27
	5.02	$3/2^-$	0.20(2)		0.31	0.11
$^{16}O \rightarrow {}^{15}N$	0.00	$1/2^-$	1.27(13)	1.46(e)	2.30	1.02
	6.32	$3/2^-$	2.25(22)	2.8(e)	3.64	1.94
	9.93	$3/2^-$	0.133(15)(d)			
	10.70	$3/2^-$	0.222(4)(d)			
$^{30}Si \rightarrow {}^{29}Al$	0.00	$5/2^+$	2.21(20)(g)		3.96(g)	
$^{31}P \rightarrow {}^{30}Si$	0.00	0^+	0.40(3)		0.62	0.36
$^{40}Ca \rightarrow {}^{39}K$	0.00	$3/2^+$	2.58(19)	3.32(f)	3.70	2.30
	2.52	$1/2^+$	1.03(7)		1.65	1.03
$^{48}Ca \rightarrow {}^{47}K$	0.00	$1/2^+$	1.07(7)		1.55	0.96
	0.36	$3/2^+$	2.26(16)		4.16	2.39
$^{51}V \rightarrow {}^{50}Ti$	0.00	$(0,2,4,6)^+$	1.35(7)		2.81	1.10
$^{208}Pb \rightarrow {}^{207}Tl$	0.00	$1/2^+$	0.98(9)	1.40(8)(h)	1.8	1.5
	0.35	$3/2^+$	2.31(22)	2.92(16)(h)	3.8	2.2
	1.35	$11/2^-$	6.85(68)		7.7	5.4
	1.67	$5/2^+$	2.93(28)		3.5	3.1
	3.47	$7/2^+$	2.06(20)		3.5	2.9

a) From Kramer et al. [3] except where noted.
b) Nonrelativistic analysis from Kramer et al. [3] except where noted.
c) Relativistic analyses.
d) From Leuschner et al. [13].
e) From Gao et al. [14].
d) From Wessling et al. [15].
g) From Jin et al. [16].
h) From Udias et al. [17].

applied to the Woods-Saxon wave functions. This adjustment of bound state wave functions has the effect of increasing the rms radius of the orbitals, increasing the asymptotic normalization, and hence reducing the spectroscopic factors. The total effect of changing the reaction model and overlap function is to bring the spectroscopic factors deduced from the new (d,^{3}He) analysis into much better agreement with those from (e,e′p) (see Table [22.2]).

The values of r_o which are needed to fit the (e,e′p) momentum distributions [3] are typically in the range 1.20 to 1.30 fm - close to the average accepted value of 1.25 fm. But there are exceptional cases, such as the value of $r_o = 1.65$ required for the relatively weak ^{12}C to ^{11}B($1/2^-$, 2.1 MeV) transition.

For consistency we can compare the spectroscopic factors obtained from the nucleon removal reactions in Table [22.2] to those from the (^{3}He,d) nucleon addition reaction of Vernotte [8]. The results based on the discussion in the previous section with the reduced-radius spin-orbit potential and then multiplied by 0.75 are $C^2S = 0.49$ for $^{30}\mathrm{Si} \rightarrow {}^{31}\mathrm{P}$ and $C^2S = 2.69$ for $^{39}\mathrm{K} \rightarrow {}^{40}\mathrm{Ca}$. These are close to those obtained in (e,e′p) but somewhat larger than those from the new (d,^{3}He) analysis given in Table 3.

Most of the (e,e′p) data in Table [22.2] is for the pickup of states below the fermi surface. One of the few (e,e′p) data available for states above the fermi surface is from the ^{209}Bi data of Branford et al. [18]. The data for ^{209}Bi(e,e′p)^{208}Pb(gs) are not very good, but from the most accurate data points in Fig. 2 of [18] one would interpret this experiment as giving $C^2S = 1$ for $0\mathrm{h}_{11/2}$ knockout. as expected in the extreme single-particle shell model. Branford et al. also study the excited states in ^{208}Pb corresponding to knocking out the hole states given in Table [22.2] and leaving ^{208}Pb in multiplet of states corresponding to the one-particle one-hole configurations. From a comparison to the ^{208}Pb(e,e′p)^{207}Tl data, they conclude that the model of ^{209}Bi based on a $0\mathrm{h}_{9/2}$ proton coupled to an inert ^{208}Pb core has a high degree of validity.

It is important that the spectroscopic factor extracted from the (e,e′p) data does not depend on the electron energy and/or the reaction model which is used to understand the data. For the (e,e′p) data typical of those for Table [22.2], the electron energy is about 500 MeV and the outgoing proton kinetic energy is about 100 MeV. The relevant variable is the four-momentum squared, Q^2, transferred by the virtual photon to the knocked-out nucleon which is about 0.2 (GeV/c)^2 in this case. For these low Q^2 a proton optical potential was used for the final-state interactions. The ^{12}C(e,e′p) data has been taken and analyzed over a wide range of Q^2. At high Q^2 values (0.8 and higher) one usually uses a Glauber model for the final-state interactions of the protons. At an intermediate Q^2 of about 0.6 both the optical model and the Glauber model can be used. Lapikas et al. [19] found that the two methods of

analysis gave different spectroscopic factors. For sum of the three 0p shell states in Table [22.2], the proton spectroscopic factors deduced from the optical-model analysis is about 2.2 (consistent with Table [22.2]) but the Glauber model analysis gave 3.56 (much closer to the simple shell model result of 4). However, more recently Radici et al. [20] have analyzed a similarly wide range of data for ^{16}O(e,e′p) and find a consistently small spectroscopic factor over the whole range of Q^2 values.

Data for ^{40}Ca(e,e′p) with 460 MeV electrons have been analyzed in the DWIA (distorted-wave impulse approximation) bound state (overlap functions) from the relativistic potential and also a relativistic model for the scattering state and the current operators [16]. The spectroscopic factor of 3.32 obtained for the $3/2^+$ state is 25% larger than the nonrelativistic results of Lapikas given in Table [22.2]. A relativistic DWIA analysis has also been carried out for ^{16}O(e,e′p) with 2.4 GeV electrons [14]. The proton spectroscopic factors obtained are $S(1/2^-, gs) = 1.46$ and $S(3/2^-, 6.32MeV) = 2.8$. These are about 20% larger than those of Table [22.2]. There is also a relativistic DWIA analysis of the ^{208}Pb(e,e′p) data [17] which gives a proton spectroscopic factors of 1.40(8) and 2.92(16) for the $1/2^+$ and $3/2^+$ states, respectively, again considerably larger than the nonrelativistic-analysis of 0.98(9) and 2.31(22), respectively. In [17] the difference between the nonrelativistic and relativistic results in mainly attributed to the proton optical potential which produces relatively more absorption in the relativistic model and hence gives rise to larger spectroscopic factors.

21.1.4 Proton decay

The widths for proton or neutron decay are related the spectroscopic factors. The usual method for calculating these decay widths is to multiply the single-particle width for the decay of a nucleon in orbital j with the spectroscopic factor:

$$\Gamma = (C^2S)\,\Gamma_{sp} \tag{21.2}$$

where Γ_{sp} is the single-particle width calculated from the scattering of a nucleon from a central potential. Usually a Woods-Saxon potential is used and the well depth V_o is adjusted to reproduce the experimental centroid of the state.

Millener [21] has analyzed the proton decay widths for several cases in the mass region $A = 11 - 16$ and his results are summarized in Table [22.3]. He used a Woods-Saxon potential with $r_o = 1.25$ fm and $a_o = 0.60$ fm. The calculated widths are based upon spectroscopic factors obtained with the Millener-Kurath interaction [22] (which are similar to those obtained with WBP [23]). There is good overall agreement between experiment and theory.

Table 3: Observed and calculated [21] proton decay widths for $1\hbar\omega$ states which have dominantly $1s_{1/2}$ or $0d_{5/2}$ character. (Center-of-mass corrections are not included in the theory.)

Nucleus	J^π	Γ^{th}	Γ^{exp}	Dominant Component
^{11}N	$\frac{1}{2}^+$	1467	1440	81% $s_{1/2}$(gs)
^{12}N	2^-	87	118(14)	70% $s_{1/2}$(gs)
	1^-	894	750(250)	76% $s_{1/2}(gs)$
	1^-	311	260(30)	77% $s_{1/2}$ $(\frac{1}{2}^-)$
^{13}N	$\frac{1}{2}^+$	32	31.7(8)	89% $s_{1/2}(gs)$
	$\frac{3}{2}^+$	84	115(5)	87% $s_{1/2}(2^+)$
	$\frac{5}{2}^+$	7	11	74% $s_{1/2}(2^+)$
^{14}O	1^-	28.8	30(1)	76% $s_{1/2}$(gs)
^{15}F	$\frac{1}{2}^+$	934	1000(200)	98% $s_{1/2}$(gs)
^{16}F	0^-	21	40(20)	100% $s_{1/2}$(gs)
	1^-	78	< 40	97% $s_{1/2}$(gs)
^{11}N	$\frac{5}{2}^+$	535	600(50)	67% $d_{5/2}$(gs)
^{12}N	3^-	220	220(25)	88% $d_{5/2}$(gs)
	4^-	610	744(25)	82% $d_{5/2}$(gs)
	3^-	280	180(23)	70% $d_{5/2}(\frac{1}{2}^-)$
^{13}N	$\frac{9}{2}^+$	258	280(30)	91% $d_{5/2}(2^+)$
	$\frac{7}{2}^+$	3	9.0(5)	92% $d_{5/2}(2^+)$
	$\frac{5}{2}^+$	45	47(7)	80% $d_{5/2}$(gs)
^{14}O	3^-	13.4	16(2)	84% $d_{5/2}$(gs)
	2^-	38.2	41(2)	66% $d_{5/2}$(gs)
^{15}F	$\frac{5}{2}^+$	222	240(30)	93% $d_{5/2}$(gs)
^{16}N	2^-	3.5	40(30)	96% $d_{5/2}$(gs)
	3^-	12	< 15	96% $d_{5/2}$(gs)

An increase of 0.01 fm in r_o increases the calculated single-particle with by about 1%, and an increase of 0.01 fm in a_o increases the calculated single-particle with by about 2% [21]. Thus for example a change of a_o from 0.60 to 0.65 would increase the calculated width by about 10%.

21.1.5 Radioactive beams

It has recently become possible to carry out one-nucleon transfer reactions with radioactive beams. One way is to do the traditional reactions such as (p,d) in inverse kinematics. A new way which has been developed is to knockout a loosely bound nucleon in a reaction on a light target such as ^{9}Be. The spectroscopic factor for a specific final state is obtained by analyzing the momentum distribution of the $(A-1)$ fragment in coincidence with gamma rays. A summary [24] of the spectroscopic factors obtained from the analysis of several experiments at the NSCL is shown in Fig. (21.5). The spectroscopic factors are obtained with an overlap function calculated with the traditional Woods-Saxon well-depth method.

21.2 Structure models for specific nuclei

The mean-field model for nuclear structure corresponds to the extreme single-particle value for the spectroscopic factor. The residual interaction results in correlations in the nuclear wave function beyond the mean field which will change the spectroscopic factors. We can attempt to distinguish between long- and short-range correlation. By long range correlation I mean the mixing of the configurations near the fermi surface. This results in a spread of the orbital occupations and fractionation of the spectroscopic strength into many states up to about 10 MeV in the spectrum. Short-range interactions can scattering the nucleons into very high single-particle states and spread the spectroscopic strength up to as high as 100 MeV in excitation. In this section I will discuss the results in terms of these long- and short-range correlations.

Shell-model configuration mixing takes into account the residual interaction for single-particle states near the fermi surface (the valence states). This type of configuration mixing is mainly related to the long-range correlations. The short-range correlation enters implicitly in terms of a renormalization of the two-body interaction (the G matrix). I will first concentrate on the spectroscopic factors obtained from shell-model calculations. The ratio of the experimental spectroscopic factors to the extreme single-particle model will be denoted by R and the ratio to the configuration mixed shell-model spectroscopic factors will be denoted by R_s. The subscript s means that its deviation from unity will be attributed to the effect of short-range

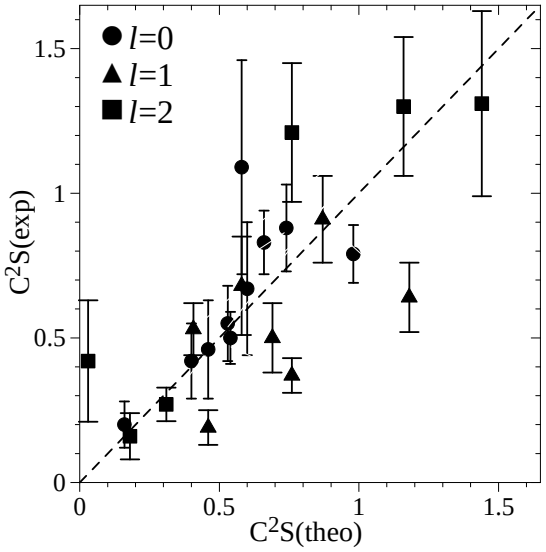

Figure 5: Comparison of experimental and calculated spectroscopic factors for reactions at approximately 60 MeV/nucleon leading to specific final levels in the nuclei ^{25,26,27}Si [25]. ^{10}Be [26], ^{11}Be [27], ^{13}B [28] and ^{14,15,16,18}C [29]. Circles, triangles and squares correspond to ℓ=0,1,2, respectively. The dashed line corresponds to $R = 1$.

correlations. There is actually no clear boundary between what we can attribute to long and short range correlations, but this will serve as a working definition. Also as we will discuss, there may be other types of effects such as clustering left out of the shell-model calculations which may contribute to R_s. The notation R'_s will be used when using (e,e′p) experimental data interpreted with a relativistic model the reaction. A summary of R values from the results discussed below is given in Table [22.4].

21.2.1 ^{7}Li

The ^{7}Li(e,e′p) reaction has recently been studied by Lapikas et al. [30] The spectroscopic factors for nonrelativistic analysis of the ^{7}Li(e,e′p) data summed over the 0^+ and 2^+ states in ^{6}He is 0.58(5). The 0p sum-rule value is 1.00 and typical 0p shell configuration mixing leads to about 0.95 in these lowest two states. Thus we would

Table 4: Ratio between experimental and shell-model spectroscopic factors

Nucleus	J_f	R(a)	R_s(b)	R'_s(c)
^{7}Li	$3/2^-$	0.52	0.52	
^{12}C	$1/2^-$,$3/2^-$	0.50	0.51	0.84
^{16}O	$1/2^-$,$3/2^-$	0.60	0.66	0.81
^{30}Si	$5/2^+$	0.37	0.58	
^{40}Ca	$3/2^+$	0.64	0.70	0.90
^{48}Ca	$3/2^+$	0.56	0.75	
^{51}V	$(0,2,4,6)^+$	0.45	0.50	
^{208}Pb	$3/2^+$	0.58	0.65	0.82

a) Non-relativistic analysis of Kramer et al. [3] compared to the extreme single-particle model.
b) Non-relativistic analysis of Kramer et al. [3] compared to valence shell-model calculations.
c) Relativistic or Glauber model analyses compared to valence shell-model calculations.

infer $R_s = (6/7) \times (0.58)/(0.95) = 0.52$, where (6/7) is the center-of-mass correction.

21.2.2 ^{12}C

^{12}C can easily be treated in the full 0p-shell. The WBP interaction [23] gives a ground state wave function with 48% $(0p_{3/2})^8$, 41% $(0p_{3/2})^6$-$(0p_{1/2})^4$, 4.7% $(0p_{3/2})^5$-$(0p_{1/2})^3$ and 5.5% $(0p_{3/2})^4$-$(0p_{1/2})^4$. The proton occupancies are 3.41 for $0p_{3/2}$ and 0.59 for $0p_{1/2}$. The spectroscopic strength gets split into $C^2S = 3.16$ to the $3/2^-$ ^{11}B ground state, 0.58 to a $1/2^-$ state at 1.85 MeV and 0.19 to a $3/2^-$ state at 4.31 MeV. The small remainder of 0.07 is fragmented over many states above 10 MeV in excitation. A common feature of all calculations within the 0p shell with a variety of effective interactions is that most (3.9 out of 4.0) of the p-shell sum-rule strength is contained in the lowest three states in ^{11}B. The sum of the spectroscopic strength obtained from the nonrelativistic analysis of the ^{12}C(e,e′p) data for the lowest three states in ^{13}B is 2.18 (Table [22.2]) giving $R_s = (11/12) \times (2.18)/(3.9) = 0.51$. The Glauber model analysis gives $R'_s = (11/12) \times (3.56)/(3.9) = 0.84$.

21.2.3 ^{16}O

For ^{16}O it is possible to go up to $4\hbar\omega$ beyond the closed-shell configuration explicit configuration mixing [31]. Configuration mixing for ^{16}O with the WBP interaction

[23] gives a ground state wave function with 49% closed-shell configuration and 39% $2\hbar\omega$ (mainly 2p-2h) and 12% $4\hbar\omega$ (mainly 4p-4h). The proton occupation numbers are 2.00 ($0s_{1/2}$), 3.70 ($0p_{3/2}$), 1.68 ($0p_{1/2}$), 0.36 ($0d_{5/2}$), 0.17 ($0d_{3/2}$) and 0.07 ($1s_{1/2}$) (with about 0.01 in the 1p0f shell). For the $^{16}O \rightarrow {}^{15}N$ transition, the transition to the $1/2^-$ ground state has C^2S=1.65 (most of the $0p_{1/2}$ strength) and the transition to the lowest $3/2^-$ state has C^2S=3.29 (89% of the $0p_{3/2}$ strength. The ratio of the spectroscopic factors obtained from the nonrelativistic analysis of the (e,e′p) data (Table [22.2]) to these calculated values is $R_s(1/2^-, gs) = (15/16) \times (1.27)/(1.65) = 0.72$ and $R_s(3/2^-, 6.32MeV) = (15/16) \times (2.25)/(3.29) = 0.64$, or $R_s = 0.66$ for the sum. The relativistic analysis gives a higher value of $R'_s = 0.81$.

21.2.4 The sd-shell

One of the most complete models available is for configuration mixing in the sd shell. In Fig. (21.6) I show the proton occupation numbers which result from the wave functions obtained with the USD interaction in the full sd-shell basis. They are compared to the extreme single-particle (ESP) model. For ^{28}Si in the middle of the sd-shell the ESP model corresponds to a closed-shell $(0d_{5/2})^{12}$ configuration with a proton occupation of number of 6 and a proton spectroscopic model of 6. In the full sd-shell model with 839 basis states, the ground-state wave function has only 22% of the $(0d_{5/2})^{12}$ state. However, the other basis states contain some nucleons in the $0d_{5/2}$ orbital and the proton occupancy is 4.62. Thus the sum-rule strength for $0d_{5/2}$ pickup in the full sd-shell model is 4.62. The transition to the ^{27}Al ground state gets 3.61 of this sum and the rest gets fragmented over several excited states in ^{27}Al. The spectroscopic factor from the (^{3}He,d) of Vernotte et al. (with the 0.75 DWBA reduction) of 2.75 is 25% smaller that the sd-shell value.

The ^{28}Si(e,e′p) reaction was studied at low resolution in one of the first experiments of this type [32], and an unexpectedly large spectroscopic factor of 5.5 for protons in 0d orbit inferred (it would be nice to have a new experiment on ^{28}Si). In place of ^{28}Si, we can consider the ^{30}Si(e,e′p)^{29}Al result from [15] which gives an experimental spectroscopic factor of 2.21(20) for the transition to the ground state which when compared to the sd-shell calculation of 3.79 gives $R_s = 0.58(6)$.

The ratio of experiment to theory for 39 transitions in the sd-shell is plotted vs mass in Fig. (21.4). For the 0d states one observes a mass-dependent ratio from about $R_s = 0.9$ at the lower end to $R_s = 0.6$ at the upper end. An interpretation of this will be discussed below.

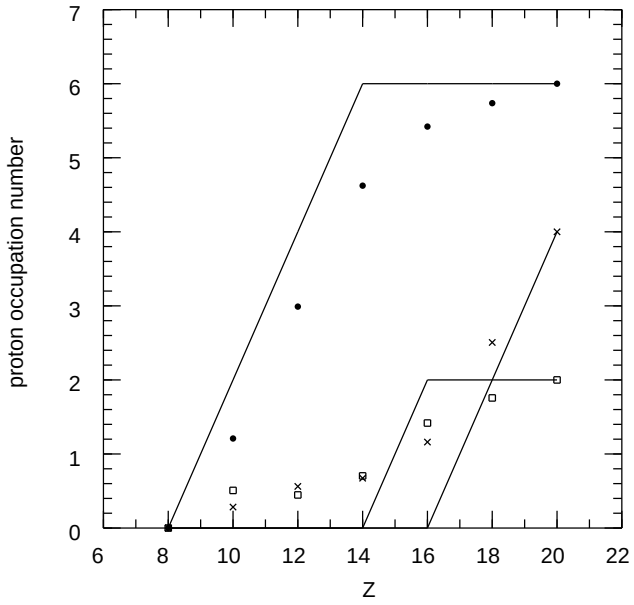

Figure 6: Proton occupation numbers for the even-even $N = Z$ sd shell nuclei as a function of mass. The lines are those expected in the extreme single-particle shell model and the symbols are those from the USD interaction: $0d_{5/2}$ (filled circles), $0d_{3/2}$ (crosses) and $1s_{1/2}$ (squares).

21.2.5 ^{40}Ca and ^{48}Ca

One can treat configuration mixing in ^{40}Ca in terms of $(0d_{3/2},0f_{7/2})^n$ configuration outside of an assumed closed shell for ^{32}S. The ground state obtained with the HJMW interaction [33] has 76% $(0d_{3/2})^8$, 21% $(0d_{3/2})^6$-$(0f_{7/2})^2$, 2.4% $(0d_{3/2})^4$-$(0f_{7/2})^4$, and 0.13% $(0d_{3/2})^2$-$(0f_{7/2})^6$. The $0d_{3/2}$ proton occupancy is 3.73 and and most of this (3.70) goes to the spectroscopic factor for the ^{39}K $3/2^+$ ground state. Taking the (e,e′p) experimental value from Table [22.2] gives $R_s = 0.70$ for the nonrelativistic model and $R'_s = 0.90$ for the relativistic model. The $0f_{7/2}$ occupancy is 0.27 and 0.18 of this goes to the lowest ^{39}K $7/2^-$ state at 2.34 MeV.

For ^{48}Ca the HJMW ground state has has 92% $(0d_{3/2})^8$-$(0f_{7/2})^8$, 7% $(0d_{3/2})^6$-$(0f_{7/2})^{10}$ and 0.17% $(0d_{3/2})^4$-$(0f_{7/2})^{12}$. The $0d_{3/2}$ proton occupancy is 3.85 and and 3.00 of this goes to the spectroscopic factor of the ^{47}K $3/2^+$ state. Taking the (e,e′p) experimental value of 2.26 from Table [22.2] gives $R_s = 0.75$.

21.2.6 ^{51}V

Calculations can be carried out in the full pf shell [34]. The dimension for the ^{51}V ground state is large, 938,626 J=7/2, T=t5/2 states, but the wave function is still

dominated by the $0f_{7/2}$ configurations and the average occupation proton number obtained with the FPD6 interaction [35] is about 2.68. Most of this into the spectroscopic factors in the lowest states of ^{50}Ti given in Table [22.2]. The ratio of experiment (Table [22.2]) to the full pf shell value is $R_s = 0.50$.

21.2.7 ^{208}Pb

It has recently become possible to consider the nucleus ^{208}Pb in a 24 orbit model space with 2p-2h mixtures into the closed-shell ground state [36]. The resulting wave function is 32% closed shell plus 68% 2p-2h. The resulting proton occupation numbers for the orbits observed in Table [22.2] are 7.91 ($0g_{7/2}$), 5.88 ($1d_{5/2}$), 11.83 ($0h_{11/2}$), 3.85 ($0d_{3/2}$) and 1.91 ($2s_{1/2}$). Although the ground state is only 32% closed shell the occupations are close to the $(2j+1)$ ESP limit. Of this total occupation about 90% (with the exception of $0g_{7/2}$) goes into the lowest state of each spin. About 60% of the $0g_{7/2}$ strength goes into the lowest state with the rest fragmented over more highly excited states. The average ratio of experiment to theory is to shell-model theory is about $R_s = 0.65$ for the nonrelativistic analysis and $R'_s = 0.82$ for the relativistic analysis.

21.3 Short-range correlations

Summarizing the results from previous sections, we find that there usually a reduction in the spectroscopic strength compared to valence shell-model calculations. The reduction appears to be largest for cases in which a nucleon is picked up from a closed-shell configuration leading to a single-particle state which is below the fermi surface. The size of the reduction has some reaction model-dependence ranging from an average value of $R_s = 0.65$ for the nonrelativistic analysis of (e,e′p) data to $R'_s = 0.85$ for a relativistic analysis of the same data. I will express this result in terms of a correction factor δ_s defined by:

$$R_s = (1 - \delta_s) \tag{21.3}$$

There is a trend for the 0d orbit within the sd-shell, Fig. (21.6) for a smaller correction factor ($\delta_s \approx 0.1$) at the beginning of the shell (A=17) where the single-particle state is above the fermi surface to a larger correction factor ($\delta_s \approx 0.4$) at the upper end of the shell (A=39) where the state is below the fermi surface. [However, the mass dependence observed in Fig. (21.4) may also be related to the incorrect use of a constant value of $r_o = 1.25$ fm for all sd-shell nuclei.] Other examples for spectroscopic factors of states above the fermi surface where the correction factor is

small are those obtained from the radioactive beam studies [24] and those obtained from the proton decay of unbound states discussed above.

One might expect that the correction factor due to short-range correlations to depend on the radial size of the overlap function relative to the size of the core density. When the overlap function is composed of orbitals below the fermi surface, the nucleon being removed will be spatially close to the core nucleons and the interaction may result in a relatively large short-range correlation. On the other hand if the nucleon being removed is above the fermi surface, there is a smaller spacial overlap with the core and the short-range correlation will be smaller. A semi-quantitative model for a hard-core potential of radius a_h has been derived by Birse and Clement [37]. (Birse and Clement [37] also discuss the effect of short-range correlations on the spin-dependent sum rules [38].) The correction is given in terms of an integral containing the valence density, $\rho_v(r)$, and the total matter density, $\rho_m(r) = \rho_p(r) + \rho_n(r)$:

$$\delta_s = \frac{4}{3}\pi a_h^3 \int \rho_v(r)\rho_m(r)r^2 dr \tag{21.4}$$

(The Pauli principle leads to a dependence on the core density that is proportional to [37] $\frac{1}{2}\rho_{t_z}(r) + \rho_{-t_z}(r)$ where t_z is the isospin of the transferred nucleon and $\rho_{t-z}(r)$ are the densities of the core protons/neutrons. In Eq. (21.4) I ignore the factor of $\frac{1}{2}$.) In Fig. (21.7) I plot the components of this integral for a selection of neutron valance orbits in the closed-shell configurations of ^{16}O and ^{40}Ca obtained from SKX Skyrme Hartree-Fock calculations [9]. For ^{16}O the valence states below the fermi surface are $0s_{1/2}$ bound by -30 MeV and $0p_{3/2}$ bound by -18 MeV. For ^{16}O the valence states above the fermi surface are $0d_{5/2}$ bound by 5 MeV (a typical value at the beginning of the shell) and $1s_{1/2}$ bound by 0.5 MeV (the value of its separation energy in ^{11}Be). For ^{40}Ca the valence state below the fermi surface is the $0d_{3/2}$ bound by 14.8 MeV. The relative value of the integrals are are 0.200, 0.144, 0.097, 0.048 and 0.160 for $0s_{1/2}$, $0p_{3/2}$, $0d_{5/2}$, $1s_{1/2}$ and $0d_{3/2}$, respectively. Thus we find that a significant binding energy dependence for the short-range corrections with the most loosely bound states having the smallest values.

Variational Monte-Carlo (VMC) calculations should contain both long and short ranged correlations. VMC calculations for the ^{7}Li(e,e′p) reaction give good agreement with the data. The small R_s value in this case may be influenced by the difference in structure between ^{7}Li and ^{6}He caused by the small binding (and large neutron radius) of ^{6}He. The alpha-triton clustering aspects of ^{7}Li may also enter. Both of these are relatively long-range effects which are special to light nuclei and which should be taken into account within the VMC. Thus the relative importance of short-range correlations in the VMC calculations for ^{7}Li is not clear.

The VMC calculation [39], [40] for ^{16}O(e,e′p) gives $R^{th} = 0.90$ for the ratio to the extreme single-particle model (without center-of-mass corrections) for the $0p_{3/2}$

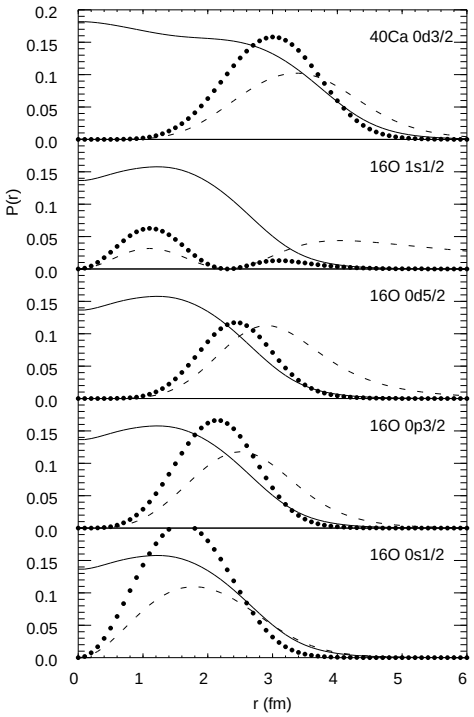

Figure 7: Components of the overlap function of Eq. (21.4). The solid line is the matter density, ρ_m(r), (normalized by $4\pi \int \rho_m(\mathrm{r})\ \mathrm{r}^2\mathrm{dr} = \mathrm{A}$). The dashed line is $r^2\rho_v(r)$ (in arbitrary units) and the dotted line is $r^2\rho_m(r)\rho_v(r)$ (in arbitrary units).

orbit. The role of the various types of short-range correlations has been studied in the correlated-basis-function theory [41] where it was found that tensor correlations are most important. Since the VMC calculations do not include the effect of fragmentation of the hole strength, but should contain the long-range correlations, we should compare this to the ratio obtained from the sum of the $3/2^-$ states in Table [22.2], e.g. $R = (15/16) \times (2.60)/(4.0) = 0.61$. Use of the relativistic (e,e′p) reaction model [14] would bring this up to about $R' = 0.76$. If we assume that the VMC calculation does not include the long-range correlation included in the shell-model calculation then we should compare $R^{th} = 0.90$ to the value of $R'_s = 0.81$ found in the previous section.

21.4 Conclusions

It appears possible to quantitatively understand spectroscopic factors in terms of a sum of short and long-long-range correlations for the overlap function and with the relativistic analysis of the (e,e′p) data. When the spectroscopic factors obtained

from the relativistic reaction theory are compared to valence shell-model calculations (which account for the long-range correlations) one obtains an average value of about $R'_s = 0.85$ for states below the fermi surface. This 15% reduction could be attributed to short-range correlations. Calculations based upon the NN interaction [39], [40] can account for most of this, $R_s^{th} = 0.90$.

The long-range correlations have the effect of fragmenting the spectroscopic strength over many states in the $A+1$ and $A-1$ nuclei, and are strongly dependent on the spacing and occupancy of the single-particle states around the fermi surface. Configuration mixing with empirical two-body matrix elements or renormalized G matrix interaction can account for the observed fragmentation, but the details are sensitive to the use of the correct single-particle energies. The details of the fragmentation and comparison to experiment is one of the most direct ways of testing nuclear structure models.

References

[1] F. Hinterberger et al., Z. Phys. **202**, 236 (1967).

[2] J. N. Craig, N. S. Wall and R. H. Bassel, Phys. Rev. Lett. **36**, 656 (1976).

[3] G. J. Kramer, H. P. Blok and L. Lapikas, Nucl. Phys. **A679**, 267 (2001).

[4] B. H. Wildenthal, Prog. in Part. and Nucl. Physcis **11**, 5 (1984).

[5] http://www.nscl.edu/~brown/sde.htm

[6] B. A. Brown and B. H. Wildenthal, Ann. Rev. Nucl. Part. Sci. **38**, 29 (1988).

[7] "Spectroscopic Factors for Single Nucleon Transfer for A = 21-44", P. M. Endt, Atomic and Nuclear Data Tables **19**, 23 (1977).

[8] J. Vernotte et al., Nucl. Phys. **A571**, 1 (1994).

[9] B. A. Brown, Phys. Rev. C **58**, 220 (1998).

[10] J. Bartel, P. Quentin, M. Brack, C. Guet and M. B. Hakansson, Nucl. Phys. **A386**, 79 (1982).

[11] W. A. Richter and B. A. Brown, submitted for publication.

[12] J. W. A. den Herder et al., Phys. Rev. Lett. **57**, 1843 (1986).

[13] M. Leuschner et al., Phys. Rev. C **49**, 955 (1994).

[14] J. Gao et al., Phys. Rev. Lett. **84**, 3265 (2000).

[15] J. Wesseling et al., Nucl. Phys. **A547**, 519 (1992).

[16] Y. Jin, J. K. Zhang, D. S. Onley and L. E. Wright, Phys. Rev. C **47**, 2024 (1993).

[17] J. M. Udias, P. Sarriguren, E. Moya de Guerra, E. Garrido and J. A. Caballero, Phys. Rev. C **48**, 2731 (1993).

[18] D. Branford et al., Phys. Rev. C **63**, 014310 (2000).

[19] L. Lapikas, G. van der Steenhoven, L. Frankfurt, M. Strikman and M. Zhalov, Phys. Rev. C **61**, 064325 (2000); L. Frankfurt, M. Strikman and M. Zhalov, Phys. Lett. B **503**, 73 (2001).

[20] M. Radici, W. H. Dickhoff and E. Roth Stoddard, Phys. Rev. C **66**, 014613 (2002).

[21] D. J. Millener, to by published.

[22] D. J. Millener and D. Kurath, Nucl. Phys. **A255**, 315 (1975).

[23] W. K. Warburton and B. A. Brown, Phys. Rev. C **46**, 923 (1992).

[24] P. G. Hansen and B. M. Sherrill, "Reactions and Single-Particle Structure of Nuclei Near the Drip Lines", Nucl. Phys. A (to be published).

[25] A. Navin et al., Phys. Rev. Lett. **81**, 5089 (1998).

[26] T. Aumann, et al., Phys. Rev. Lett. **84**, 35 (2000).

[27] A. Navin et al., Phys. Rev. Lett. **85**, 266 (2000).

[28] V. Guimaraes et al., Phys. Rev. C **61**, 06409 (2000).

[29] V. Maddalena et al., Phys. Rev. C **63**, 024613 (2001).

[30] L. Lapikas, J. Wesseling and R. B. Wiringa, Phys. Rev. Lett. **82**, 4404 (1999).

[31] E. K. Warburton, B. A. Brown and D. J. Millener, Phys. Lett. **B293**, 7 (1992).

[32] J. Mougy et al., Nucl. Phys. **A262**, 461 (1976).

[33] S. T. Hsieh, X. Ji, R. Mooy and B. H. Wildenthal, AIP Conference Proceedings **142**, 357 (1986).

[34] M. Honma, private communication.

[35] W. A. Richter, M. G. van der Merwe, R. E. Julies and B. A. Brown, Nucl. Phys. **A523**, 325 (1991).

[36] B. A. Brown, Phys. Rev. Lett. **85**, 5300 (2000).

[37] M. C. Birse and C. F. Clement, Nucl. Phys. **A351**, 112 (1981).

[38] C. F. Clement, Nucl. Phys. **A213**, 469 (1973); C. F. Clement, Nucl. Phys. **A213**, 493 (1973); C. F. Clement and S. M. Perez, Phys. Lett. **81B**, 269 (1979); C. F. Clement and S. M. Perez, Nucl. Phys. **A362**, 86 (1981).

[39] M. Radici, S. Boffi, S. C. Pieper and V. R. Pandharipande, Phys. Rev. C **50**, 3010 (1994).

[40] D. Van Neck, M. Waroquier, A. E. L. Dieperink, S. C. Pieper and V. R. Pandharipande, Phys. Rev. C **57**, 2308 (1998).

[41] D. Van Neck, L. Van Daele, Y. Dewulf and M. Waroquier, Phys. Rev. C **56**, 1398 (1997).

22 One-body transition operators and the OBTD

The M-scheme one-body transition operator is:

$$\hat{O}^{\lambda}_{\mu} = \sum_{\alpha\beta} < \alpha \mid O^{\lambda}_{\mu} \mid \beta > a^{+}_{\alpha} a_{\beta}$$

The tensor coupled form for this operator is:

$$\hat{O}^{\lambda}_{\mu} = \sum_{k_\alpha k_\beta} < k_\alpha || O^{\lambda} || k_\beta > \sum_{m_\alpha m_\beta} (-1)^{j_\alpha - m_\alpha} \begin{pmatrix} j_\alpha & \lambda & j_\beta \\ -m_\alpha & \mu & m_\beta \end{pmatrix} a^{+}_{\alpha} a_{\beta}$$

$$= \sum_{k_\alpha k_\beta} < k_\alpha || O^{\lambda} || k_\beta > \frac{[a^{+}_{k_\alpha} \otimes \tilde{a}_{k_\beta}]^{\lambda}_{\mu}}{\sqrt{(2\lambda+1)}}. \tag{22.1}$$

Where α stands for $(n_\alpha \ell_\alpha j_\alpha m_\alpha)$, and k_α stands for $(n_\alpha \ell_\alpha j_\alpha)$. It is convenient to express the reduced matrix element for the n-particle wave function in the form of a product over one-body transition densities (OBTD) times reduced single-particle matrix elements

$$< f || \hat{O}^{\lambda} || i > = < n\omega J || \hat{O}^{\lambda} || n\omega' J' > = \sum_{k_\alpha k_\beta} \mathrm{OBTD}(f i k_\alpha k_\beta \lambda) < k_\alpha || O^{\lambda} || k_\beta >, \tag{22.2}$$

where the OBTD is given by

$$\mathrm{OBTD}(f i k_\alpha k_\beta \lambda) = \frac{< n\omega J || [a^{+}_{k_\alpha} \otimes \tilde{a}_{k_\beta}]^{\lambda} || n\omega' J' >}{\sqrt{(2\lambda+1)}}. \tag{22.3}$$

The labels i and f are a short-hand notation for the initial and final state quantum numbers $(n\omega' J')$ and $(n\omega J)$, respectively. The OBTD represents in a compact form, the most general information needed to calculate the matrix elements of one-body operators between a given initial and final state. The OBTD can be calculated in an M-scheme basis by dividing a nonvanishing expectation value of the M-scheme matrix element by the $3j$ factor from the Wigner-Eckhart theorem

$$< J || [a^{+}_{k_\alpha} \otimes \tilde{a}_{k_\beta}]^{\lambda} || J' > = \frac{< JM \mid [a^{+}_{k_\alpha} \otimes \tilde{a}_{k_\beta}]^{\lambda}_{\mu} \mid J'M' >}{(-1)^{J-M} \begin{pmatrix} J & \lambda & J' \\ M & \mu & M' \end{pmatrix}} \tag{22.4}$$

The OBTD can be evaluated in a J-coupled basis by inserting a complete set of states with $(n-1)$ particles between the a^{+} and $\tilde{a}$ operators in Eq. (22.3) with Eq. [13.45] to obtain:

$$\mathrm{OBTD}(f i k_\alpha k_\beta \lambda) = (-1)^{J+\lambda+J'} \sum_{\omega'' J''} \begin{Bmatrix} J' & J & \lambda \\ j_\alpha & j_\beta & J'' \end{Bmatrix}$$

$$\times \; < n\omega J||a^+_{k_\alpha}||(n-1)\omega'' J'' >< (n-1)\omega'' J''||\tilde{a}_{k_\beta}||n\omega' J' >$$
$$= \sum_{\omega'' J''} (-1)^{J+\lambda+J''+j_\beta} \left\{ \begin{array}{ccc} J' & J & \lambda \\ j_\alpha & j_\beta & J'' \end{array} \right\}$$
$$\times \; < n\omega J||a^+_{k_\alpha}||(n-1)\omega'' J'' >< n\omega' J'||a^+_{k_\beta}||(n-1)\omega'' J'' > . \qquad (22.5)$$

These last two matrix elements can also be expressed as one-particle CFP. The explicit forms of the OBTD for the cases of a single-k configuration and for a two-orbital configuration are derived in the next two sections.

22.1 Isospin and proton-neutron formalism

The formulae in the previous section are immediately applicable to the proton-neutron formalism. In this case the labels for the orbits k implicitly include the proton or neutron label for the orbital. For example for β^- decay or (p,n) reactions we would destroy a neutron ($q = 1/2$) and create a proton ($q' = -1/2$):

$$\mathrm{OBTD}(fik_{\alpha,q'}k_{\beta,q}\lambda) = \frac{< n\omega J||[a^+_{k_\alpha,q'} \otimes \tilde{a}_{k_\beta,q}]^\lambda||n\omega' J' >}{\sqrt{(2\lambda+1)}}. \qquad (22.6)$$

To obtain the equivalent expression in terms of a reduced matrix element in isospin formalism we would label the wavefunctions explicitly with their (T, T_z) values and the operator in terms of the isospin rank $(\Delta T, \Delta T_Z)$ and then use the Wigner-Eckhart theorm in isospin space to obatin:

$$\mathrm{OBTD}(fik_{\alpha,q'}k_{\beta,q}\lambda) = \frac{< n\omega JTT_z||[a^+_{k_\alpha,q'} \otimes \tilde{a}_{k_\beta,q}]^{\lambda,\Delta T,\Delta T_z}||n\omega' J'T'T'_z >}{\sqrt{(2\lambda+1)}}$$
$$= (-1)^{T-T_z} \left(\begin{array}{ccc} T & \Delta T & T' \\ -T_z & \Delta T_z & T'_z \end{array} \right) \frac{< n\omega JT||[a^+_{k_\alpha,q'} \otimes \tilde{a}_{k_\beta,q}]^{\lambda,\Delta T}||n\omega' J'T' >}{\sqrt{(2\lambda+1)}}$$
$$=< T'T'_z\Delta T\Delta T_z \mid TT_z > \sqrt{\frac{(2\Delta T+1)}{(2T+1)}} \frac{< n\omega JT||[a^+_{k_\alpha,q'} \otimes \tilde{a}_{k_\beta,q}]^{\lambda,\Delta T}||n\omega' J'T' >}{\sqrt{(2\lambda+1)(2\Delta T+1)}}$$
$$=< T'T'_z\Delta T\Delta T_z \mid TT_z > \sqrt{\frac{(2\Delta T+1)}{(2T+1)}}\, \mathrm{OBTD}(fik_\alpha k_\beta \lambda \Delta T) \qquad (22.7)$$

where the last line contains the one-body transition density in isospin formalism:

$$\mathrm{OBTD}(fik_\alpha k_\beta \lambda \Delta T) = \frac{< n\omega JT||[a^+_{k_\alpha} \otimes \tilde{a}_{k_\beta}]^{\lambda,\Delta T}||n\omega' J'T' >}{\sqrt{(2\lambda+1)(2\Delta T+1)}}. \qquad (22.8)$$

22.2 OBTD for a single-orbital configuration

The OBTD for a single-orbital configuration is given by

$$\mathrm{OBTD}(f,i) = \sum_{\omega'' J''} (-1)^{J+\lambda+J''+j_\beta} \left\{ \begin{array}{ccc} J' & J & \lambda \\ j_\alpha & j_\beta & J'' \end{array} \right\}$$

$$\times < k^n \omega J || a^+_{k_\alpha} || k^{n-1} \omega'' J'' >< k^n \omega' J' || a^+_{k_\beta} || k^{n-1} \omega'' J'' > \qquad (22.9).$$

The only possibility for the set $(k_\alpha k_\beta)$ in the summation in Eq. (22.5) is (k,k) and one has in terms of the one-particle CFP:

$$\mathrm{OBTD}(fi) = n\delta_{k_\alpha k}\delta_{k_\beta k}\sqrt{(2J+1)(2J'+1)} \sum_{\omega'' J''} (-1)^{J+\lambda+J''+j}$$

$$\times \left\{ \begin{array}{ccc} J' & J & \lambda \\ j & j & J'' \end{array} \right\} < j^n \omega J \,|\} j^{n-1} \omega'' J'' >< j^n \omega' J' \,|\} j^{n-1} \omega'' J'' > . \qquad (22.10)$$

22.3 OBTD for a two-orbital configuration

First, the two-orbital configuration in which the initial and final states have the same partition is considered

$$< i \,| \equiv < n\omega' J' \,| = < (k_1^{n_1} \omega'_1 J'_1)(k_2^{n_2} \omega'_2 J'_2) J' \,| \qquad (22.11),$$

and

$$< f \,| \equiv < n\omega J \,| = < (k_1^{n_1} \omega_1 J_1)(k_2^{n_2} \omega_2 J_2) J \,| \qquad (22.12).$$

Consideration of Eq. (22.5) shows that there are two possible intermediate states

$$| \, a > \equiv | \, (n-1)\omega'' J''(a) > = | \, (k_1^{n_1-1} \omega''_1 J''_1)(k_2^{n_2} \omega''_2 J''_2) J'' >, \qquad (22.13)$$

and

$$| \, b > \equiv | \, (n-1)\omega'' J''(b) > = | \, (k_1^{n_1} \omega''_1 J''_1)(k_2^{n_2-1} \omega''_2 J''_2) J'' > . \qquad (22.14)$$

The OBTD will be a sum of the two terms

$$\mathrm{OBTD}(fi) = \mathrm{OBTD}^a(fi) + \mathrm{OBTD}^b(fi). \qquad (22.15)$$

For state (a)

$$\mathrm{OBTD}^a(fi) = \sum_{\omega''_1 J''_1 \omega''_2 J''_2 J''} (-1)^{J+\lambda+J''+j_\beta} \left\{ \begin{array}{ccc} J' & J & \lambda \\ j_1 & j_1 & J'' \end{array} \right\}$$

$$\times < (k_1^{n_1} J_1)(k_2^{n_2} J_2) J || a^+_{k_\alpha} || (k_1^{n_1-1} J''_1)(k_2^{n_2} J''_2) J'' >$$

$$\times \; < (k_1^{n_1} J_1')(k_2^{n_2} J_2') J' || a_{k_\beta}^+ || (k_1^{n_1-1} J_1'')(k_2^{n_2} J_2'') J'' > \tag{22.16}$$

(the ω labels are implicit in the wave functions) and the set $(\alpha\beta)$ must be $(1,1)$. Application of Eq. [13.49] together with the sum-rule of Eq. [13.23] for the $6j$ coefficients gives

$$\begin{aligned}
\mathrm{OBTD}^a(fi) = \delta_{(\alpha\beta)(1,1)} & \sum_{\omega_1'' J_1'' \omega_2'' J_2'' J''} (-1)^{J+\lambda+J''+j_1+J_1+J_2-J_1'-J_2'} \\
& \times (2J''+1)\sqrt{(2J+1)(2J'+1)}\,\delta_{\omega_2\omega_2''}\delta_{J_2 J_2''}\delta_{\omega_2'\omega_2''}\delta_{J_2' J_2''} \\
& \times \left\{ \begin{array}{ccc} J' & J & \lambda \\ j_\alpha & j_\beta & J'' \end{array} \right\} \left\{ \begin{array}{ccc} J_1 & J_1'' & j_1 \\ J'' & J & J_2 \end{array} \right\} \left\{ \begin{array}{ccc} J_1' & J_1'' & j_1 \\ J'' & J' & J_2' \end{array} \right\} \\
\times \; < k_1^{n_1} \omega_1 J_1 || a_{k_1}^+ || k_1^{n_1-1} \omega_1'' J_1'' > & < k_1^{n_1} \omega_1' J_1' || a_{k_1}^+ || k_1^{n_1-1} \omega_1'' J_1'' > \qquad (22.17) \\
= n_1 \delta_{(\alpha\beta)(1,1)} & \delta_{\omega_2\omega_2'}\delta_{J_2 J_2'} \sqrt{(2J+1)(2J'+1)(2J_1+1)(2J_1'+1)} \\
& \times \left\{ \begin{array}{ccc} J' & J & \lambda \\ J_1 & J_1' & J_2 \end{array} \right\} \sum_{\omega_1'' J_1''} (-1)^{J'-j_1+J_2'-J_1''} \left\{ \begin{array}{ccc} J_1 & J_1' & \lambda \\ j_1 & j_1 & J_1'' \end{array} \right\} \\
& \times \; < j_1^{n_1} \omega_1 J_1 \; | \} j_1^{n_1-1} \omega_1'' J_1'' > < j_1^{n_1} \omega_1' J_1' \; | \} j_1^{n_1-1} \omega_1'' J_1'' > . \qquad (22.18)
\end{aligned}$$

The contribution from intermediate state $\mid b >$ is related to this result by interchanging the subscripts 1 and 2, and multiplying by the phase factor $(-1)^{J_1+J_2-J+J_1'+J_2'-J'}$ to obtain

$$\begin{aligned}
\mathrm{OBTD}^b(fi) = n_2 \delta_{(\alpha\beta)(2,2)} & \delta_{\omega_1\omega_1'}\delta_{J_1 J_1'} \sqrt{(2J+1)(2J'+1)(2J_2+1)(2J_2'+1)} \\
& \times \left\{ \begin{array}{ccc} J' & J & \lambda \\ J_2 & J_2' & J_1 \end{array} \right\} \sum_{\omega_2'' J_2''} (-1)^{j_2+J_1+J_2''-J_2+J-J_2'} \left\{ \begin{array}{ccc} J_2 & J_2' & \lambda \\ j_2 & j_2 & J'' \end{array} \right\} \\
& \times \; < j_2^{n_2} \omega_2 J_2 \; | \} j_2^{n_2-1} \omega_2'' J_2'' > < j_2^{n_2} \omega_2' J_2' \; | \} j_2^{n_2-1} \omega_2'' J_2'' > . \qquad (22.19)
\end{aligned}$$

For the two-orbit case, there is also a OBTD connecting an initial state and with a final state which differs by a change of one particle from one orbit to another

$$< i \mid \equiv < n\omega J \mid = < (k_1^{n_1} \omega_1 J_1)(k_2^{n_2} \omega_2 J_2) J \mid \tag{22.20},$$

and

$$< f' \mid \equiv < n\omega' J' \mid = < (k_1^{n_1-1} \omega_1' J_1')(k_2^{n_2+1} \omega_2' J_2') J' \mid \tag{22.21}.$$

Consideration of Eq. (22.5) shows that there is only one possible type of intermediate state

$$\mid a > \equiv \mid (n-1)\omega'' J'' > = \mid (k_1^{n_1-1} \omega_1'' J_1'')(k_2^{n_2} \omega_2'' J_2'') J'' > . \tag{22.22}$$

The OBTD is obtained by application of Eqs. [13.48] and [13.49] together with the sum rule of Eq. [13.29]

$$\mathrm{OBTD}(f'i) = \delta_{(\alpha\beta)(1,2)} (-1)^{j_2+J_2-J_2'} \sqrt{n_1(n_2+1)}$$

$$\times \sqrt{(2J+1)(2J'+1)(2J_1+1)(2J_2'+1)} \left\{ \begin{array}{ccc} J_2' & J_1' & J' \\ J_2 & J_1 & J \\ j_2 & j_1 & \lambda \end{array} \right\}$$

$$\times \; < j_1^{n_1}\omega_1 J_1 \; |\} j_1^{n_1-1}\omega_1' J_1' >< j_2^{n_2+1}\omega_2' J_2' \; |\} j_2^{n_2}\omega_2 J_2 > . \qquad (22.23)$$

The matrix elements for the other possible cases where the final-state partition differs from the initial-state partition by the moving of one particle can be derived in an analogous manner and will have a form similar to Eq. (22.23). The OBTD for the case when two or more particles are moved between partitions vanishes.

22.4 Scalar one-body matrix elements

For the Hamiltonian one is interested in matrix elements of scalar operators. For the special case of a scalar (λ=0) one-body operator the results simplify and it is useful to define a new quantity OBTDS related to the unreduced matrix elements by

$$< n\omega J \mid \hat{O}^{\lambda=0} \mid n\omega' J' >= \sum_{k_\alpha k_\beta} \mathrm{OBTDS}(fik_\alpha k_\beta) < k_\alpha \mid O^{\lambda=0} \mid k_\beta >, \qquad (22.24)$$

where OBTDS is given by

$$\mathrm{OBTDS}(fik_\alpha k_\beta) = \delta_{j_\alpha j_\beta}\delta_{JJ'}\sqrt{\frac{(2j_\alpha+1)}{(2J+1)}}\,\mathrm{OBTD}(fik_\alpha k_\beta \lambda = 0)$$

$$= \sqrt{\frac{(2j_\alpha+1)}{(2J+1)}} < n\omega J||[a_{k_\alpha}^+ \otimes \tilde{a}_{k_\beta}]^{\lambda=0}||n\omega' J' >= \sqrt{2j_\alpha+1} \; < n\omega J \mid [a_{k_\alpha}^+ \otimes \tilde{a}_{k_\beta}]^{\lambda=0} \mid n\omega' J' >$$

$$= \frac{1}{(2J+1)}\delta_{j_\alpha j_\beta}\delta_{JJ'} \sum_{\omega'' J''} < n\omega J||a_{k_\alpha}^+||(n-1)\omega'' J'' >< n\omega' J'||a_{k_\beta}^+||(n-1)\omega'' J'' > . \qquad (22.25)$$

For a single-orbital configuration considered in Eq. (22.10), OBTDS reduces to

$$\mathrm{OBTDS}(fi) = n\delta_{k_\alpha k}\delta_{k_\beta k}\delta_{JJ'} \sum_{\omega'' J''} < j^n \omega J \; |\} j^{n-1}\omega'' J'' >$$

$$\times \; < j^n \omega' J' \; |\} j^{n-1}\omega'' J'' >= n\delta_{\omega\omega'}\delta_{JJ'}. \qquad (22.26)$$

where the last line follows from the sum rule of Eq. [20.8]. Similarly for a two-orbital configuration one obtains

$$\mathrm{OBTDS}^a(fi) = n_1\delta_{(\alpha\beta)(1,1)}\delta_{J_1 J_1'}\delta_{\omega_1\omega_1'}\delta_{\omega_2\omega_2'}\delta_{J_2 J_2'}, \qquad (22.27)$$

$$\mathrm{OBTDS}^b(fi) = n_2\delta_{(\alpha\beta)(2,2)}\delta_{\omega_1\omega_1'}\delta_{J_1 J_1'}\delta_{\omega_2\omega_2'}\delta_{J_2 J_2'}, \qquad (22.28)$$

and

$$\mathrm{OBTDS}(f'i) = \delta_{(\alpha\beta)(1,2)}\delta_{j_1 j_2}\delta_{JJ'}(-1)^{J+J'_1+J'_2}\sqrt{n_1(n_2+1)}$$
$$\times (2J_1+1)(2J'_2+1)\left\{ \begin{array}{ccc} J'_2 & J_2 & j_1 \\ J_1 & J'_1 & J \end{array} \right\}$$
$$\times < j_1^{n_1}\omega_1 J_1 \,|\}\, j_1^{n_1-1}\omega'_1 J'_1 >< j_2^{n_2+1}\omega'_2 J'_2 \,|\}\, j_2^{n_2}\omega_2 J_2 > . \qquad (22.29)$$

A special case of Eq. (22.25) is obtained for $k_\alpha = k_\beta = k_o$

$$\mathrm{OBTDS}(fi, k_\alpha = k_\beta = k_o) \equiv \sqrt{2j_o+1} < n\omega J \mid [a^+_{k_o} \otimes \tilde{a}_{k_o}]^{\lambda=0} \mid n\omega' J >$$
$$= \sqrt{2j_o+1}\sum_m < j_o m j_o, -m \mid 0,0 >< n\omega J \mid a^+_{k_o m}\tilde{a}_{k_o,-m} \mid n\omega' J >$$
$$= \sum_m < n\omega J \mid a^+_{k_o m}a_{k_o m} \mid n\omega' J >=< n\omega J \mid \hat{N}_{k_o} \mid n\omega' J >, \qquad (22.30)$$

where in the last line the single-state number operator

$$\hat{N}_{k_o} = \sum_m a^+_{k_o m}a_{k_o m}. \qquad (22.31)$$

has been introduced. In general $\mid n\omega J >$ are not eigenstates of $\hat{N}_{k_o}$. However, they can be expanded in terms of basis state Φ_a each of which has a fixed partition (an integer number of particles $n_o(a)$ in state k_o) and hence are eigenstates of $\hat{N}_{k_o}$;

$$\mid n\omega J >= \sum_a c_a \mid \Phi_a >, \qquad (22.32)$$

and

$$\hat{N}_{k_o} \mid \Phi_a >= n_o(a) \mid \Phi_a > . \qquad (22.33)$$

Thus one obtains

$$\mathrm{OBTDS}(fi, k_\alpha = k_\beta = k_o) =< n\omega J \mid \hat{N}_{k_o} \mid n\omega' J >$$
$$= \sum_{ab}(c_b)^* c'_a < \Phi_b \mid \hat{N}_{k_o} \mid \Phi_a >= \sum_a (c_a)^* c'_a n_o(a). \qquad (22.34)$$

In particular, for the diagonal matrix element, $f = i$ ($\omega' = \omega$ and $c'_a = c_a$),

$$\mathrm{OBTDS}(f = i, k_\alpha = k_\beta = k_o) =< n\omega J \mid \hat{N}_{k_o} \mid n\omega J >$$
$$= \sum_a |c_a|^2 \, n_o(a) \equiv < p_o >_{n\omega J} . \qquad (22.35)$$

where $< p_o >_{n\omega J}$ is the average number of k_o particles in the state $\mid n\omega J >$.

Eqs. (22.999), (22.999), and (22.999) are consistent with the general result of Eqs. (22.35). One should not confuse the condition $k_\alpha = k_\beta$ with the condition $j_\alpha = j_\beta$. For

example, the pair of states $k = 3$ $[(n\ell j) = (0, 1, 1/2)]$ and $k = 6$ $[(n\ell j) = (1, 0, 1/2)]$ obviously fulfills the latter condition but not the former condition, and thus one must use Eq. (22.25) to evaluate OBTDS. However, often the calculation is restricted to a set of active orbits for which $j_\alpha = j_\beta$ also implies that $k_\alpha = k_\beta$, and hence one can use the simpler results of Eqs. (22.34) and (22.35) for all scalar matrix elements in the model space. This is the case, for example, when the model space is restricted to a single major harmonic oscillator shell.

A useful sum rule for the one-particle transfer matrix elements can be obtained from a comparison of Eqs. (22.25) and (22.35)

$$\sum_{\omega'' J''} |< n\omega J||a^+_{k_o}||(n-1)\omega'' J'' >|^2 = (2J+1) < p_o >_{n\omega J} . \tag{22.36}$$

A related sum rule can be obtained by rewriting the number operator as

$$\hat{N}_{k_o} = \sum_m (1 - a_{k_o m} a^+_{k_o m}). \tag{22.37}$$

By methods similar to the above derivation one obtains

$$\sum_{\omega'' J''} |< (n+1)\omega'' J''||a^+_{k_o}||n\omega J >|^2$$

$$= (2J+1)\{(2j_o+1) - < p_o >_{n\omega J}\} \equiv (2J+1) < h_o >_{n\omega J} . \tag{22.38}$$

where $< h_o >_{n\omega J}$ is the average number of k_o holes in the state $\mid n\omega J >$.

23 Two-particle transfer operators

The operator that creates an antisymmetric state of two particles coupled to angular momentum J is defined by

$$A^+(k_\alpha k_\beta J_o M_o)\ |> = \mid k_\alpha k_\beta J_o M_o >, \tag{23.1}$$

and hence from Sec. 16.2:

$$A^+(k_\alpha k_\beta J_o M_o) = N_{12} \sum_{m_\alpha m_\beta} < j_\alpha m_\alpha j_\beta m_\beta \mid J_o M_o > a^+_{k_\beta m_\beta} a^+_{k_\alpha m_\alpha}$$

$$= -N_{12} \sum_{m_\alpha m_\beta} < j_\alpha m_\alpha j_\beta m_\beta \mid J_o M_o > a^+_{k_\alpha m_\alpha} a^+_{k_\beta m_\beta} = -N_{12}[a^+_{k_\alpha} \otimes a^+_{k_\beta}]^{J_o}_{M_o}, \tag{23.2}$$

where $N_{12} = \frac{1}{\sqrt{(1+\delta_{k_\alpha k_\beta})}}$. The two-particle destruction operator is

$$A(k_\alpha k_\beta J_o M_o) = \{A^+(k_\alpha k_\beta J_o M_o)\}^+ =$$

$$= N_{12} \sum_{m_\alpha m_\beta} < j_\alpha m_\alpha j_\beta m_\beta \mid J_o M_o > a_{k_\alpha m_\alpha} a_{k_\beta m_\beta}. \tag{23.3}$$

The tensor form of the two-particle destruction operator is

$$\tilde{A}(k_\alpha k_\beta J_o M_o) = (-1)^{J_o - M_o} \{A^+(k_\alpha k_\beta J_o, -M_o)\}^+$$

$$= N_{12}(-1)^{J_o - M_o} \sum_{m_\alpha m_\beta} < j_\alpha m_\alpha j_\beta m_\beta \mid J_o, -M_o > a_{k_\alpha m_\alpha} a_{k_\beta m_\beta} = N_{12}[\tilde{a}_{k_\alpha} \otimes \tilde{a}_{k_\beta}]^{J_o}_{M_o}. \tag{23.4}$$

Matrix elements involving $\tilde{A}$ can be converted into those involving A^+:

$$< (n-2)\omega J || \tilde{A}(k_\alpha k_\beta J_o) || n\omega' J' >$$

$$= (-1)^{J_o + J - J'} < n\omega' J' || A^+(k_\alpha k_\beta J_o) || (n-2)\omega J > . \tag{23.5}$$

All matrix elements of A^+ can be reduced to two types of matrix elements involving active states. The first type with $\alpha = \beta$ involves a matrix element related to the two-particle CFP, denoted by $< j^n \omega J \ |\} j^2(J_o); j^{n-2}\omega' J' >$ and defined by:

$$< j^n \omega J || A^+(k k J_o) || j^{n-2} \omega' J' >$$

$$\equiv \sqrt{\frac{n(n-1)(2J+1)}{2}}\ < j^n \omega J \ |\} j^2(J_o); j^{n-2}\omega' J' > . \tag{23.6}$$

There are a variety of notations in the literature for the two-particle CFP and the particular choice made in Eq. (23.6) is made to reflect the structure of the A^+ matrix element. Note that j is used in the two-particle CFP rather than k in order to

emphasize the fact that it does not depend on the $(n\ell)$ quantum number. Wave function expansion relations and sum rules for the two-particle CFP can be derived by applying the two-particle number operator

$$\sum_{J_oM_o} A^+(kkJ_oM_o)A(kkJ_oM_o)$$

$$= \frac{1}{2}\sum_{J_oM_om_i} < jm_1jm_2 \mid J_oM_o >< jm_3jm_4 \mid J_oM_o > a^+_{km_2}a^+_{km_1}a_{km_3}a_{km_4}$$

$$= \frac{1}{2}\sum_{m_1m_2} a^+_{km_2}a^+_{km_1}a_{km_1}a_{km_2} = \frac{1}{2}(\hat{N}_k^2 - \hat{N}_k) \tag{23.7}$$

to the k^n configuration and inserting a complete set of states with $(n-2)$ particles to obtain

$$\frac{1}{2}(\hat{N}_k^2 - \hat{N}_k) \mid k^n\omega JM >= \frac{1}{2}n(n-1) \mid k^n\omega JM >$$

$$= \sum_{\omega''J''J_o} \frac{< k^n\omega J||A^+(kkJ_o)||k^{n-2}\omega''J'' >}{\sqrt{(2J+1)}}[Z^+(k^{n-2}\omega''J'') \otimes A(kkJ_o)]^J_M \mid >, \tag{23.8}$$

and

$$\sum_{\omega''J''J_o} < j^n\omega'J' \mid\}j^2(J_o); j^{n-2}\omega''J'' >< j^n\omega J \mid\}j^2(J_0); j^{n-2}\omega''J'' >= \delta_{\omega\omega'}\delta_{JJ'}. \tag{23.9}$$

The square of the two-particle CFP is the probability that the removal of two particles in state k coupled to angular momentum J_o from the state $\mid k^n(\omega J) >$ will leave the system in the state $\mid k^{n-2}(\omega''J'') >$. Since the CFP are normalized to unity, the square of the CFP for a given initial state leading only one possible final state is unity, and thus

$$|< j^2J \mid\}j^2(J_o); j^0, J' = 0 >|= \delta_{JJ_o}. \tag{23.10}$$

One finds for the two-particle CFP

$$< j^{-(n-2)}\omega J \mid\}j^2(J_o); j^{-n}\omega'J' > \equiv < j^{2j+1-(n-2)}\omega J \mid\}j^2(J_o); j^{2j+1-n}\omega'J' >$$

$$= (-1)^{J_o+J'-J}\sqrt{\frac{n(n-1)(2J'+1)}{[(2j+3-n)(2j+2-n)(2J+1)]}} < j^n\omega'J' \mid\}j^2(J_o); j^{n-2}\omega J > . \tag{23.11}$$

The case when $n = 2$ and $J = 0$ gives

$$|< j^{-0}, J = 0 \mid\}j^2(J_o); j^{-2}J' >|$$

$$= \sqrt{\frac{2J'+1}{j(2j+1)}} \; |< j^2J' \mid\}j^2(J_o); j^0, J = 0 >|= \sqrt{\frac{2J'+1}{j(2j+1)}}\,\delta_{J'J_o}. \tag{23.12}$$

For the k^3 configuration the matrix element of A^+ can be related to the matrix element of a^+:

$$< k^3 J||a_k^+||k^2 J' >= (-1)^{J+J'+j} < k^3 J||A^+(kkJ')||kj >, \tag{23.13}$$

which in terms of CFP is

$$< j^3 J\ |\}j^2 J' >= (-1)^{J+J'+j} < j^3 J\ |\}j^2(J'); j^1 j > . \tag{23.14}$$

The two-particle CFP can also be reduced to a sum over one-particle CFP by inserting a complete set of intermediate states with $(n-1)$ particles between the a^+ of Eq. (23.2) (with $\delta_{jj} = 1$):

$$\begin{aligned} &< k^n \omega J||A^+(kkJ_o)||k^{n-2}\omega' J' > \\ &= -\frac{1}{\sqrt{2}}(-1)^{J+J_o+J'}\sqrt{2J_o+1}\sum_{\omega'' J''}\left\{\begin{array}{ccc} J' & J & J_o \\ j & j & J'' \end{array}\right\} \\ &\times < k^n \omega J||a_k^+||k^{n-1}\omega'' J'' >< k^{n-1}\omega'' J''||a_k^+||k^{n-2}\omega' J' > \\ &= \frac{1}{\sqrt{2}}(-1)^{J+J_o+J'+1}\sqrt{(2J_o+1)(2J+1)n(n-1)} \\ &\times \sum_{\omega'' J''}\sqrt{2J''+1}\left\{\begin{array}{ccc} J' & J & J_o \\ j & j & J'' \end{array}\right\} < j^n \omega J\ |\}j^{n-1}\omega'' J'' >< j^{n-1}\omega'' J''\ |\}j^{n-2}\omega' J' > . \end{aligned} \tag{23.15}$$

In terms of CFP this becomes

$$\begin{aligned} &< j^n \omega J\ |\}j^2(J_o); j^{n-2}\omega' J' >= (-1)^{J+J_o+J'+1}\sqrt{2J_o+1} \\ &\times \sum_{\omega'' J''}\sqrt{2J''+1}\left\{\begin{array}{ccc} J' & J & J_o \\ j & j & J'' \end{array}\right\} < j^n \omega J\ |\}j^{n-1}\omega'' J'' >< j^{n-1}\omega'' J''\ |\}j^{n-2}\omega' J' > . \end{aligned} \tag{23.16}$$

In the second type of matrix element for A^+, two different k-states are active and Eqs. (23.2) (with $\delta_{k_\alpha k_\beta} = 0$) can be used to express the matrix element in terms of one-particle CFP

$$\begin{aligned} &< (k_\alpha^{n_\alpha}\omega_\alpha J_\alpha)(k_\beta^{n_\beta}\omega_\beta J_\beta)J_{\alpha\beta}||A^+(k_\alpha k_\beta J_o)||(k_\alpha^{n_\alpha-1}\omega'_\alpha J'_\alpha)(k_\beta^{n_\beta-1}\omega'_\beta J'_\beta)J'_{\alpha\beta} > \\ &= (-1)^{n_\beta+1}\sqrt{(2J_{\alpha\beta}+1)(2J_o+1)(2J'_{\alpha\beta}+1)} \\ &\times \left\{\begin{array}{ccc} J_\alpha & J_\beta & J_{\alpha\beta} \\ J'_\alpha & J'_\beta & J'_{\alpha\beta} \\ j_\alpha & j_\beta & J_o \end{array}\right\} < k_\alpha^{n_\alpha}\omega_\alpha J_\alpha||a_{k_\alpha}^+||k_\alpha^{n_\alpha-1}\omega'_\alpha J'_\alpha >< k_\beta^{n_\beta}\omega_\beta J_\beta||a_{k_\beta}^+||k_\beta^{n_\beta-1}\omega'_\beta J'_\beta > \\ &= (-1)^{n_\beta+1}\sqrt{n_\alpha n_\beta(2J_{\alpha\beta}+1)(2J_o+1)(2J'_{\alpha\beta}+1)(2J_\alpha+1)(2J_\beta+1)} \end{aligned} \tag{23.17}$$

$$\times \left\{ \begin{array}{ccc} J_\alpha & J_\beta & J_{\alpha\beta} \\ J'_\alpha & J'_\beta & J'_{\alpha\beta} \\ j_\alpha & j_\beta & J_o \end{array} \right\} < j_\alpha^{n_\alpha} J_\alpha \,|\} j_\alpha^{n_\alpha - 1} J'_\alpha >< j_\beta^{n_\beta} J_\beta \,|\} j_\beta^{n_\beta - 1} J'_\beta > . \tag{23.18}$$

The phase factor arises from the $(-1)^{n_\beta}$ factor of Eq. [16.60] times the (-1) from Eq. (23.2).

24 Two-body transition operators and the TBTD

The M-scheme form for the two-body transition operator is:

$$\hat{T}^{\lambda}_{\mu} = \frac{1}{4}\sum_{\alpha\beta\gamma\delta} < \alpha\beta \mid T^{\lambda}_{\mu} \mid \gamma\delta > a^{+}_{\alpha}a^{+}_{\beta}a_{\delta}a_{\gamma} \tag{24.1}$$

The tensor coupled form for this two-body operator is:

$$\hat{T}^{\lambda}_{\mu} = \frac{1}{4}\sum_{\substack{k_\alpha k_\beta k_\gamma k_\delta \\ m_\alpha m_\beta m_\gamma m_\delta}} < k_\alpha m_\alpha k_\beta m_\beta \mid T^{\lambda}_{\mu} \mid k_\gamma m_\gamma k_\delta m_\delta > a^{+}_{k_\alpha m_\alpha}a^{+}_{k_\beta m_\beta}a_{k_\delta m_\delta}a_{k_\gamma m_\gamma} \tag{24.2}$$

$$= \frac{1}{4}\sum_{\substack{k_\alpha k_\beta k_\gamma k_\delta \\ J_o M_o J'_o M'_o}} \sqrt{(1+\delta_{k_\alpha k_\beta})}\sqrt{(1+\delta_{k_\gamma k_\delta})} < k_\alpha k_\beta J_o M_o \mid T^{\lambda}_{\mu} \mid k_\gamma k_\delta J'_o M'_o >$$

$$\times \sum_{\substack{m_\alpha m_\beta \\ m_\gamma m_\delta}} < J_o M_o \mid j_\alpha m_\alpha j_\beta m_\beta >< J'_o M'_o \mid j_\gamma m_\gamma j_\delta m_\delta > a^{+}_{k_\alpha m_\alpha}a^{+}_{k_\beta m_\beta}a_{k_\delta m_\delta}a_{k_\gamma m_\gamma} \tag{24.3}$$

$$= \frac{1}{4}\sum_{\substack{k_\alpha k_\beta k_\gamma k_\delta \\ J_o M_o J'_o M'_o}} < k_\alpha k_\beta J_o M_o \mid T^{\lambda}_{\mu} \mid k_\gamma k_\delta J'_o M'_o >$$

$$\times (1+\delta_{k_\alpha k_\beta})(1+\delta_{k_\gamma k_\delta}) A^{+}(k_\alpha k_\beta J_o M_o) A(k_\gamma k_\delta J'_o M'_o) \tag{24.4}$$

$$= \frac{1}{4}\sum_{\substack{k_\alpha k_\beta k_\gamma k_\delta \\ J_o J'_o}} < k_\alpha k_\beta J_o || T^{\lambda} || k_\gamma k_\delta J'_o >$$

$$\times (1+\delta_{k_\alpha k_\beta})(1+\delta_{k_\gamma k_\delta}) \frac{[A^{+}(k_\alpha k_\beta J_o) \otimes \tilde{A}(k_\gamma k_\delta J'_o)]^{\lambda}_{\mu}}{\sqrt{2\lambda+1}} \tag{24.5}$$

$$= \sum_{\substack{k_\alpha \le k_\beta k_\gamma \le k_\delta \\ J_o J'_o}} < k_\alpha k_\beta J_o || T^{\lambda} || k_\gamma k_\delta J'_o > \frac{[A^{+}(k_\alpha k_\beta J_o) \otimes \tilde{A}(k_\gamma k_\delta J'_o)]^{\lambda}_{\mu}}{\sqrt{2\lambda+1}}. \tag{24.6}$$

Eq. (24.3) is obtained by the M-scheme expansion of the J-coupled two-body matrix elements, Eq. [16.9], Eq. (24.4) comes from the definition of the two-particle operators in Eqs. [23.2] and [23.3], and Eq. (24.5) comes from the tensor coupling of the A^{+} and A opertors. Also note in Eq. (24.5) that the (-1) obtained from commuting $a_{k_\delta m_\delta}$ with $a_{k_\gamma m_\gamma}$ is cancelled by the (-1) from Eq. [23.2]. It is convenient to express the reduced matrix element for the n-particle wave function in the form of a product over two-body transition densities (TBTD) times reduced two-particle matrix elements

$$< n\omega J || \hat{T}^{\lambda} || n\omega' J' >= \sum_{\substack{k_\alpha \le k_\beta, k_\gamma \le k_\delta \\ J_o J'_o}} \mathrm{TBTD}(fikJ_oJ'_o\lambda) < k_\alpha k_\beta J_o || T^{\lambda} || k_\gamma k_\delta J'_o >, \tag{24.7}$$

where the TBTD is given by

$$\mathrm{TBTD}(fikJ_oJ'_o\lambda) = \frac{< n\omega J||[A^+(k_\alpha k_\beta J_o)\otimes \tilde{A}(k_\gamma k_\delta J'_o)]^\lambda||n\omega' J' >}{\sqrt{2\lambda+1}}\,. \tag{24.8}$$

We can evaluate these in terms of matrix elements of the two-particle transfer operators by interting a complete set of states for the $(n-2)$ particle system

$$\mathrm{TBTD}(fikJ_oJ'_o\lambda) = (-1)^{J+\lambda+J'}\sum_{\omega'' J''}\left\{\begin{array}{ccc} J' & J & \lambda \\ J_o & J'_o & J'' \end{array}\right\}$$

$$\times\ < n\omega J||A^+(k_\alpha k_\beta J_o)||(n-2)\omega'' J'' >< (n-2)\omega'' J''||\tilde{A}(k_\gamma k_\delta J'_o)||n\omega_\prime J' >$$

$$= \sum_{\omega'' J''}(-1)^{J+\lambda+J''+J'_o}\left\{\begin{array}{ccc} J' & J & \lambda \\ J_o & J'_o & J'' \end{array}\right\}$$

$$\times\ < n\omega J||A^+(k_\alpha k_\beta J_o)||(n-2)\omega'' J'' >< n\omega' J'||A^+(k_\gamma k_\delta J'_o)||(n-2)\omega'' J'' > . \tag{24.9}$$

The dependence of the TBTD on $k_\alpha, k_\beta, k_\gamma$ and k_δ is abreviated by k, and the dependence of the TBTD on the initial and final states is abreviated by i and f, respectively. The TBTD represents in a compact form, the most general information needed to calculate the matrix elements of two-body operators between a given initial and final state. The results given in Sec. 23 can be used to reduce the matrix elements of A^+ to one-particle and two-particle CFP. The TBTD can be evaluated for specific configurations following the procedures given in Sec. 22 for the OBTD. The analogous results for a scalar two-body operator will be given in the next section.

24.1 Scalar two-body operators

For the special case of a scalar (λ=0) two-body operator, it is useful to define a new quantity TBTDS related to the unreduced matrix elements by

$$< n\omega J \mid \hat{T}^{\lambda=0} \mid n\omega' J' >$$

$$= \sum_{\substack{k_\alpha \le k_\beta \\ k_\gamma \le k_\delta J_o}} \mathrm{TBTDS}(fikJ_o) < k_\alpha k_\beta J_o \mid T^{\lambda=0} \mid k_\gamma k_\delta J_o >, \tag{24.10}$$

where TBTDS is given by

$$\mathrm{TBTDS}(fikJ_o) = \delta_{J_oJ'_o}\delta_{JJ'}\sqrt{\frac{(2J_o+1)}{(2J+1)}}\,\mathrm{TBTD}(fikJ_oJ_o\lambda=0)$$

$$= (2J+1)^{-1}\sum_{\omega'' J''} < n\omega J||A^+(k_\alpha k_\beta J_o)||(n-2)\omega'' J'' >$$

$$\times \; < n\omega' J||A^+(k_\gamma k_\delta J_o)||(n-2)\omega'' J'' > . \qquad (24.11)$$

This result is most often used with respect to the scalar two-body interaction V

$$< n\omega J \mid V \mid n\omega' J >= \sum_{\substack{k_\alpha \le k_\beta \\ k_\gamma \le k_\delta, J_o}} \mathrm{TBTDS}(fikJ_o) < k_\alpha k_\beta J_o \mid V \mid k_\gamma k_\delta J_o >, \qquad (24.12)$$

In the next few subsections, the TBTDS for some simple configurations will be evaluated.

24.2 Scalar TBTD for a single-orbital configuration

First consider the evaluation of the TBTDS for a single-orbital configuration

$$\mathrm{TBTDS}(fikJ_o) = (2J+1)^{-1} \sum_{\omega'', J''} < k^n \omega J||A^+(k_\alpha k_\beta J_o)||k^{n-2}\omega'' J'' >$$

$$\times \; < k^n \omega' J||A^+(k_\gamma k_\delta J_o)||k^{n-2}\omega'' J'' > . \qquad (24.13)$$

The only possibility for the set $(k_\alpha k_\beta k_\gamma k_\delta)$ in the summation in Eq. (24.12) is $(kkkk)$ and, in terms of the two-particle CFP:

$$\mathrm{TBTDS}(fikJ_o) = \delta_{(k_\alpha k_\beta k_\gamma k_\delta),(kkkk)} \frac{n(n-1)}{2}$$

$$\times \sum_{\omega'' J''} < j^n \omega J \; |\}j^2(J_o); j^{n-2}\omega'' J'' >< j^n \omega' J \; |\}j^2(J_o); j^{n-2}\omega'' J'' > . \qquad (24.14)$$

24.3 Scalar TBTD for a two-orbital configuration

For the second example, consider the interaction energy coefficient for the two-orbital configuration in which the initial and final states have the form

$$< i \mid \equiv < n\omega' J \mid = < (k_1^{n_1} J_1')(k_2^{n_2} J_2') J \mid,$$

and

$$< f \mid \equiv < n\omega J \mid = < (k_1^{n_1} J_1)(k_2^{n_2} J_2) J \mid .$$

Consideration of Eq. (24.11) shows that there are three possible intermediate states

$$\mid a > \equiv \mid (n-2)\omega'' J'' > = \mid (k_1^{n_1-2} J_1'')(k_2^{n_2} J_2'') J'' >,$$

$$\mid b > \equiv \mid (n-2)\omega'' J'' > = \mid (k_1^{n_1-1} J_1'')(k_2^{n_2-1} J_2'') J'' >,$$

and

$$|c> \equiv |\ (n-2)\omega'' J'' > = |\ (k_1^{n_1} J_1'')(k_2^{n_2-2} J_2'') J'' > .$$

The TBTDS is given by Eq. (24.12) with a sum of three terms corresponding to these three types intermediate states

$$\text{TBTDS} = \text{TBTDS}^a + \text{TBTDS}^b + \text{TBTDS}^c.$$

In case (a), the set $(\alpha\beta\gamma\delta)$ must be $(1,1,1,1)$, in case (b), the set $(\alpha\beta\gamma\delta)$ must be $(1,2,1,2)$, and in case (c), the set $(\alpha\beta\gamma\delta)$ must be $(2,2,2,2)$. For case (a), the TBTDS can be obtained after application of Eq. [13.49] and the sum rule of Eq. [13.27] for the $6j$ coefficients

$$\begin{aligned}
\text{TBTDS}^a &= \delta_{(\alpha\beta\gamma\delta),(1,1,1,1)} (2J+1)^{-1} \\
&\times \sum_{\omega_1'' J_1'' \omega_2'' J_2'' J''} (-1)^{2J_2''+J_1'+J_1+2J+2J_o} \delta_{\omega_2,\omega_2''} \delta_{J_2 J_2''} \delta_{\omega_2' \omega_2''} \delta_{J_2' J_2''} \\
&\times < k_1^{n_1} J_1 || A^+(k_1 k_1 J_o) || k_1^{n_1-2} J_1'' >< k_1^{n_1} J_1' || A^+(k_1 k_1 J_o) || k_1^{n_1-2} J_1'' > \\
&\times (2J+1)(2J''+1) \left\{ \begin{array}{ccc} J_1 & J_1'' & J_o \\ J'' & J & J_2 \end{array} \right\} \left\{ \begin{array}{ccc} J_1' & J_1'' & J_o \\ J'' & J & J_2 \end{array} \right\} \\
&= \delta_{(\alpha\beta\gamma\delta),(1,1,1,1)} \frac{n_1(n_1-1)}{2} \delta_{\omega_2 \omega_2'} \delta_{J_2 J_2'} \delta_{J_1 J_1'} \\
&\times \sum_{\omega_1'' J_1''} < j_1^{n_1} \omega_1 J_1 \ |\} j_1^2(J_o); j_1^{n_1-2} \omega_1'' J_1'' >< j_1^{n_1} \omega_1' J_1 \ |\} j_1^2(J_o); j_1^{n_1-2} \omega_1'' J_1'' > . \qquad (24.15)
\end{aligned}$$

Similarly the contribution from intermediate state (c) is

$$\begin{aligned}
\text{TBTDS}^c &= \delta_{(\alpha\beta\gamma\delta),(2,2,2,2)} \frac{n_2(n_2-1)}{2} \delta_{\omega_1 \omega_1'} \delta_{J_1 J_1'} \delta_{J_2 J_2'} \\
&\times \sum_{\omega_2'' J_2''} < j_2^{n_2} \omega_2 J_2 \ |\} j_2^2(J_o); j_2^{n_2-2} \omega_2'' J_2'' >< j_2^{n_2} \omega_2' J_2 \ |\} j_2^2(J_o); j_2^{n_2-2} \omega_2'' J_2'' > . \qquad (24.16)
\end{aligned}$$

The contribution from the intermediate state $|\ b>$ is obtained by application of Eq. [13.46]

$$\begin{aligned}
\text{TBTDS}^b &= \delta_{(\alpha\beta\gamma\delta),(1,2,1,2)} (2J_o+1) n_1 n_2 \sqrt{(2J_1+1)(2J_2+1)(2J_1'+1)(2J_2'+1)} \\
&\times \sum_{\omega_1'' J_1'' \omega_2'' J_2''} < j_1^{n_1} \omega_1 J_1 \ |\} j_1^{n_1-1} \omega_1'' J_1'' >< j_2^{n_2} \omega_2 J_2 \ |\} j_2^{n_2-1} \omega_2'' J_2'' > \\
&\times < j_1^{n_1} \omega_1' J_1' \ |\} j_1^{n_1-1} \omega_1'' J_1'' >< j_2^{n_2} \omega_2' J_2' \ |\} j_2^{n_2-1} \omega_2'' J_2'' > \\
&\times \sum_{J''} (2J''+1) \left\{ \begin{array}{ccc} J_1 & J_2 & J \\ J_1'' & J_2'' & J'' \\ j_1 & j_2 & J_o \end{array} \right\} \left\{ \begin{array}{ccc} J_1' & J_2' & J \\ J_1'' & J_2'' & J'' \\ j_1 & j_2 & J_o \end{array} \right\} . \qquad (24.17)
\end{aligned}$$

There are two types of off-diagonal two-orbital terms. One in which the final states have partitions which differ from the initial state by the change of one particle

$$< f' |= < (k_1^{n_1-1}\omega_1 J_1)(k_2^{n_2+1}\omega_2 J_2)J |,$$

and another in which the final states have partitions which differ from the initial state by the change of two particles

$$< f'' |= < (k_1^{n_1-2}\omega_1 J_1)(k_2^{n_2+2}\omega_2 J_2)J | .$$

In analogy with the derivation given above for the diagonal case, explicit formulaes for the TBTDS can be derived. The result for the case $| f'' >$ is given in [1]. Although the general analytical results for the many-orbital case become quite complicated, [2], [3] they are easily obtained numerically by using an M-scheme shell-model code or a J-projection shell-model code such as OXBASH [4].

24.4 Sample calculations for interaction energies

As a sample application, the interaction energy for the $(j = 5/2)^3$ configuration will be calculated. This is obtained from Eqs. (24.12) and (24.14) by making use of the relationship between one- and two-particle CFP as given by Eq. [23.14] together with the one-particle CFP in Table [20.1]. For $J = 9/2$ one obtains

$$\text{TBTDS}(J = 9/2, J_o = 2) = \frac{9}{14},$$

and

$$\text{TBTDS}(J = 9/2, J_o = 4) = \frac{33}{14},$$

and thus

$$< j^3, J = 9/2 \mid V \mid j^3, J = 9/2 >= \frac{9}{14} < j^2, J_o = 2 \mid V \mid j^2, J_o = 2 >$$

$$+\frac{33}{14} < j^2, J_o = 4 \mid V \mid j^2, J_o = 4 > .$$

As a check, note that for a constant two-body interaction, $V = C$

$$< j^2, J_o = 2 \mid C \mid j^2, J_o = 2 >=< j^2, J_o = 4 \mid C \mid j^4, J_o = 4 >= C,$$

giving

$$< j^3, J = 9/2 \mid C \mid j^3, J = 9/2 >= 3C = \frac{n(n-1)C}{2},$$

where $n = 3$.

As an example of the application for the two-orbital configuration, the interaction energy for the configuration

$$| [(5/2)^2, J_1 = 4], [(1/2)^1, j_2 = 1/2], J = 9/2 >$$

is obtained with $\mathrm{TBTDS}^a = 1$ ($J_1'' = 0$), $\mathrm{TBTDS}^c = 0$, and

$$\mathrm{TBTDS}^{\mathrm{b}} = 18(2J_o + 1) \left\{ \begin{array}{ccc} 5/2 & 4 & 5/2 \\ 1/2 & J_o & 9/2 \end{array} \right\},$$

giving

$$\begin{aligned} < J = 9/2 \mid V \mid J = 9/2 > = & < (5/2)^2, 4 \mid V \mid (5/2)^2, 4 > \\ & +0.17\times \ < 5/2, 1/2, 2 \mid V \mid 5/2, 1/2, 2 > \\ & +1.83\times \ < 5/2, 1/2, 3 \mid V \mid 5/2, 1/2, 3 > . \end{aligned}$$

References

[1] I. Talmi, *Simple Models of Complex Nuclei*, (Harwood Academic Publishers, 1993).

[2] J. B. French, E. C. Halbert, J. B. McGrory and S. S. M. Wong, Advances in Nuclear Physics **3**, 193 (1969).

[3] J. Q. Chen, A. Novoselsky, M. Valliers and R. Gilmore, Phys. Rev. C **39**, 1088 (1989).

[4] B. A. Brown, et al., the computer code OXBASH.

25 Electromagnetic transitions

25.1 Operators and transition rates

The interaction of the electromagnetic field with the nucleons can be expressed in terms of a sum of electic and magnetic multipole operators with tensor rank λ

$$\mathcal{O} = \sum_{\lambda,\mu} [\mathcal{O}(E\lambda)_\mu + \mathcal{O}(M\lambda)_\mu]. \tag{25.1}$$

The total rate for a specific set of states and a given operator is given by:

$$T_{i,f,\lambda} = \left(\frac{8\pi(\lambda+1)}{\lambda[(2\lambda+1)!!]^2} \right) \left(\frac{k^{2\lambda+1}}{\hbar} \right) B(i \to f), \tag{25.2}$$

where k is the wave-number for the electromagnetic transition of energy E_γ given by:

$$k = \frac{E_\gamma}{\hbar c} = \frac{E_\gamma}{197 \text{ MeV fm}}. \tag{25.3}$$

The last factor in Eq. (25.2) is referred to as a "reduced transition probability" B defined by:

$$B(i \to f) = \frac{|< J_f||\mathcal{O}(\lambda)||J_i >|^2}{(2J_i+1)}. \tag{25.4}$$

With our definition of the reduced matrix element,

$$|< J_f||\mathcal{O}(\lambda)||J_i >|^2 = |< J_i||\mathcal{O}(\lambda)||J_f >|^2 \ . \tag{25.5}$$

B depends upon the direction of the transition by the factor of $(2J_i + 1)$. For electromagnetic transitions J_i is that for the higher-energy initial state. But in Coulomb excitation the initial usually taken as the ground state, and one can use the notation $B(\uparrow)$ for this situation.

The electric transition operator given by:

$$O(E\lambda) = r^\lambda \ Y^\lambda_\mu(\hat{r}) \ e_{t_z} e, \tag{25.6}$$

were Y^λ_μ are the spherical harmonics. Gamma transitions with λ=0 are forbidden because the photon must carry off at least one unit of angular momentum. The e_{t_z} are the electric charges for the proton and neutron in units of e. For the free-nucleon charge we would take $e_p = 1$ and $e_n = 0$, for the proton and neutron, respectively. Although the bare operator acts upon the protons, we will keep the general expression in terms of e_{t_z} in order to incorporate the "effective charges" for the proton and

neutron, which represent the center-of-mass corrections and the average effects of the renormalization from wavefunction admixtures outside the model space.

The magnetic transition operator is given by:

$$O(M\lambda) = \left[\vec{\ell}\,\frac{2g^{\ell}_{t_z}}{(\lambda+1)} + \vec{s}\,g^{s}_{t_z}\right]\,\vec{\nabla}[r^{\lambda}Y^{\lambda}_{\mu}(\hat{r})]\,\mu_N$$

$$= \sqrt{\lambda(2\lambda+1)}\,\left[[Y^{\lambda-1}\otimes\vec{\ell}]^{\lambda}_{\mu}\,\frac{2g^{\ell}_{t_z}}{(\lambda+1)} + [Y^{\lambda-1}\otimes\vec{s}]^{\lambda}_{\mu}\,g^{s}_{t_z}\right] r^{\lambda-1}\,\mu_N, \tag{25.7}$$

where μ_N is the nuclear magneton,

$$\mu_N = \frac{e\hbar}{2m_pc} = 0.105\ e\text{fm}, \tag{25.8}$$

and where m_p is the mass of the proton. The g-factors $g^{\ell}_{t_z}$ and $g^{s}_{t_z}$ are the orbital and spin g-factors for the proton and neutron, respectively. The free-nucleon values for the g-factors are $g^{\ell}_{p}=1$, $g^{\ell}_{n}=0$, $g^{s}_{p}=5.586$ and $g^{s}_{n}=-3.826$. We may use effective values for these g-factors to take into account the truncation of the model space.

The most probable types of transitions are $E1$, $E2$ and $M1$. The $E1$ transition operator is given by Eq. (25.6) with λ=1:

$$O(E1) = r\,Y^{(1)}_{\mu}(\hat{r})\,e_{t_z}e = \sqrt{\frac{3}{4\pi}}\,\vec{r}\,e_{t_z}e, \tag{25.9}$$

The $E2$ transition operator is given by Eq. (25.6) with λ=2:

$$O(E2) = r^2\,Y^{(2)}_{\mu}(\hat{r})\,e_{t_z}e, \tag{25.10}$$

The $M1$ transition operator is given by Eq. (25.7) with λ=1 and $Y^0 = 1/\sqrt{4\pi}$:

$$O(M1) = \sqrt{\frac{3}{4\pi}}\,[\vec{\ell}\,g^{\ell}_{t_z} + \vec{s}\,g^{s}_{t_z}]\,\mu_N. \tag{25.11}$$

The selection rules are given by the triangle condition for the angular momenta in Eq. (25.5), $\Delta(J_i, J_f, \lambda)$. The electromagnetic interaction conserves parity, and the elements of the operators for $E\lambda$ and $M\lambda$ can be classified according to their transformation under parity change:

$$POP^{-1} = \pi_O O. \tag{25.12}$$

$\pi_O = (-1)^{\lambda}$ for Y^{λ}, $\pi_O = -1$ for the vectors $\vec{r}$, $\vec{\nabla}$ and $\vec{p}$, and $\pi_O = +1$ for pseudo vectors $\vec{l} = \vec{r}\times\vec{p}$ and $\vec{\sigma}$. For a given matrix element we have:

$$<\Psi_f\mid\mathcal{O}\mid\Psi_i> = <\Psi_f\mid P^{-1}P\mathcal{O}P^{-1}P\mid\Psi_i> = \pi_i\pi_f\pi_O<\Psi_f\mid\mathcal{O}\mid\Psi_i>. \tag{25.13}$$

The matrix element will vanish unless $\pi_i\pi_f\pi_O = +1$. Thus the transitions are divided into two classes, the ones which do not change parity change $\pi_i\pi_f = +1$ which go by the operators with $\pi_O = +1$:

$$\pi_i\pi_f = +1 \text{ for } M1, E2, M3, E4\ldots, \tag{25.14}$$

and the ones which do change parity change $\pi_i\pi_f = -1$ which go by the operators with $\pi_O = -1$:

$$\pi_i\pi_f = -1 \text{ for } E1, M2, E3, M4\ldots. \tag{25.15}$$

25.2 Moments in terms of electromagnetic operators

The operator for electromagnetic moment can be expressed in terms of the electromagnetic transition operators. By the parity selection rule of Eq. (25.14), the moments are nonzero only for $M1$, $E2$, $M3.$, $E4$, ... The most common are:

$$\begin{aligned}\mu &= \sqrt{\frac{4\pi}{3}} < J, M = J \mid \mathcal{O}(M1) \mid J, M = J > \\ &= \sqrt{\frac{4\pi}{3}} \begin{pmatrix} J & 1 & J \\ -J & 0 & J \end{pmatrix} < J||\mathcal{O}(M1)||J >,\end{aligned} \tag{25.16}$$

and

$$\begin{aligned}Q &= \sqrt{\frac{16\pi}{5}} < J, M = J \mid \mathcal{O}(E2) \mid J, M = J > \\ &= \sqrt{\frac{16\pi}{5}} \begin{pmatrix} J & 2 & J \\ -J & 0 & J \end{pmatrix} < J||\mathcal{O}(E2)||J > .\end{aligned} \tag{25.17}$$

25.3 Nuclear matrix elements

Electromagnetic transitions and moments depend upon the reduced nuclear matrix elements $< f||\mathcal{O}(\lambda)||i >$. With the formalism of Sec. 23, these can be expressed as a sum over one-body transition densities times single-particle matrix elements:

$$< f||\mathcal{O}(\lambda)||i >= \sum_{k_\alpha k_\beta} \text{OBTD}(fik_\alpha k_\beta\lambda) < k_\alpha||O(\lambda)||k_\beta >, \tag{25.18}$$

where the OBTD is given by

$$\text{OBTD}(fik_\alpha k_\beta\lambda) = \frac{< f||[a^+_{k_\alpha} \otimes \tilde{a}_{k_\beta}]^\lambda||i >}{\sqrt{(2\lambda+1)}}. \tag{25.19}$$

The labels i and f are a short-hand notation for the initial and final state quantum numbers $(n\omega_i J_i)$ and $(n\omega_f J_f)$, respectively. Thus the problem is divided into two parts, one involving the nuclear structure dependent one-body transition densities OBTD, and the other involving the reduced single-particle matrix elements (SPME).

The SPME for $E\lambda$ operator of (25.6) is given by:

$$< k_a||O(E\lambda)||k_b >= (-1)^{j_a+1/2}\frac{[1+(-1)^{\ell_a+\lambda+\ell_b}]}{2}$$

$$\times\sqrt{\frac{(2j_a+1)(2\lambda+1)(2j_b+1)}{4\pi}}\begin{pmatrix} j_a & \lambda & j_b \\ 1/2 & 0 & -1/2\end{pmatrix} < k_a|r^\lambda \mid k_b > e_{t_z}e. \qquad (25.20)$$

The SPME for the spin part of the magnetic operator of Eq. (25.7) is:

$$< k_a||O(M\lambda,s)||k_b >=$$

$$=\sqrt{\lambda(2\lambda+1)}\ < j_a||[Y^{\lambda-1}\otimes\vec{s}]^\lambda||j_b >< k_a|r^{\lambda-1}\mid k_b >\ g^s_{t_z}\ \mu_N$$

$$=\sqrt{\lambda(2\lambda+1)}\sqrt{(2j_a+1)(2j_b+1)(2\lambda+1)}\begin{Bmatrix} \ell_a & 1/2 & j_a \\ \ell_b & 1/2 & j_b \\ \lambda-1 & 1 & \lambda\end{Bmatrix}$$

$$\times\ < \ell_a||Y^{\lambda-1}||\ell_b >< s||\vec{s}||s >< k_a|r^{\lambda-1}\mid k_b >\ g^s_{t_z}\ \mu_N, \qquad (25.21)$$

where

$$< s||\vec{s}||s >= \sqrt{3/2}\,. \qquad (25.22)$$

The SPME for the orbital part of the magnetic operator of (25.7) is:

$$< k_a||O(M\lambda,\ell)||k_b >=$$

$$=\frac{\sqrt{\lambda(2\lambda+1)}}{\lambda+1}< j_a||[Y^{\lambda-1}\otimes\vec{\ell}]^\lambda||j_b >< k_a|r^{\lambda-1}\mid k_b >\ g^\ell_{t_z}\ \mu_N$$

$$=\frac{\sqrt{\lambda(2\lambda+1)}}{\lambda+1}(-1)^{\ell_a+1/2+j_b+\lambda}\sqrt{(2j_a+1)(2j_b+1)}$$

$$\times\begin{Bmatrix} \ell_a & \ell_b & \lambda \\ j_b & j_a & 1/2\end{Bmatrix} < \ell_a||[Y^{\lambda-1}\otimes\vec{\ell}]^\lambda||\ell_b >< k_a|r^{\lambda-1}\mid k_b >\ g^\ell_{t_z}\ \mu_N, \qquad (25.23)$$

where

$$< \ell_a||[Y^{\lambda-1}\otimes\vec{\ell}]^\lambda||\ell_b >= (-1)^{\lambda+\ell_a+\ell_b}\sqrt{(2\lambda+1)\ell_b(\ell_b+1)(2\ell_b+1)}$$

$$\times\begin{Bmatrix} \lambda-1 & 1 & \lambda \\ \ell_b & \ell_a & \ell_b\end{Bmatrix} < \ell_a||Y^{\lambda-1}||\ell_b >, \qquad (25.24)$$

with

$$< \ell_a||Y^{\lambda-1}||\ell_b >= (-1)^{\ell_a}\sqrt{\frac{(2\ell_a+1)(2\ell_b+1)(2\lambda-1)}{4\pi}}\begin{pmatrix} \ell_a & \lambda-1 & \ell_b \\ 0 & 0 & 0 \end{pmatrix}. \quad (25.25)$$

For the $M1$ operator of (25.11) the radial matrix element is:

$$< k_a|r^0 \mid k_b >= \delta_{n_a,n_b}, \quad (25.26)$$

and the SPME simplify to:

$$< k_a||O(M1,s)||k_b >= \sqrt{\frac{3}{4\pi}} < j_a||\vec{s}||j_b > \delta_{n_a,n_b}\, g^s_{t_z}\, \mu_N$$

$$= \sqrt{\frac{3}{4\pi}}(-1)^{\ell_a+j_a+3/2}\sqrt{(2j_a+1)(2j_b+1)}\begin{Bmatrix} 1/2 & 1/2 & 1 \\ j_b & j_a & \ell_a \end{Bmatrix}$$
$$\times < s||\vec{s}||s > \delta_{\ell_a,\ell_b}\delta_{n_a,n_b}\, g^s_{t_z}\, \mu_N, \quad (25.27)$$

where

$$< s||\vec{s}||s >= \sqrt{3/2}\,,$$

and

$$< k_a||O(M1,\ell)||k_b >= \sqrt{\frac{3}{4\pi}} < j_a||\vec{\ell}||j_b > \delta_{n_a,n_b}\, g^\ell_{t_z}\, \mu_N$$

$$= \sqrt{\frac{3}{4\pi}}(-1)^{\ell_a+j_b+3/2}\sqrt{(2j_a+1)(2j_b+1)}\begin{Bmatrix} \ell_a & \ell_b & 1 \\ j_b & j_a & 1/2 \end{Bmatrix}$$
$$\times < \ell_a||\vec{\ell}||\ell_b > \delta_{n_a,n_b}\, g^\ell_{t_z}\, \mu_N, \quad (25.28)$$

where

$$< \ell_a||\vec{\ell}||\ell_b >= \delta_{\ell_a,\ell_b}\sqrt{\ell_a(\ell_a+1)(2\ell_a+1)}\,.$$

Thus the $M1$ operator can connect only a very limited set of orbits, namely those which have the same n and ℓ values.

25.4 Applications to simple situations

25.4.1 Closed shell plus one particle

For a closed shell plus one particle one finds that OBTD=1 and the only term contributing to the sum (for $\lambda > 0$) comes from the transition between two specific particle states with $J = j$ (since $J_c = 0$)

$$< J_f = j_f||\mathcal{O}(\lambda)||J_i = j_i >=< k_f||O(\lambda)||k_i >, \quad (25.29)$$

Table (25.1). Coefficients C for k^2 E2 transitions.

transition	$(3/2)^2$	$(5/2)^2$	$(7/2)^2$	$(9/2)^2$	$(11/2)^2$	$(13/2)^2$
$2 \rightarrow 0$	0.800	0.914	0.952	0.970	0.979	0.985
$4 \rightarrow 2$		0.630	0.950	1.114	1.207	1.265
$6 \rightarrow 4$			0.433	0.771	0.990	1.132
$8 \rightarrow 6$				0.308	0.612	0.841
$10 \rightarrow 8$					0.229	0.491
$12 \rightarrow 10$						0.177

and the reduced transition probability for this cases is:

$$B(\lambda) = \frac{|< k_f||O(\lambda)||k_i >|^2}{(2j_i+1)}. \tag{25.30}$$

25.4.2 Single-orbit configurations

For a closed shell plus n particles in a single state k these expressions (for $\lambda >0$) reduce to:

$$< k^n, \omega_f, J_f||\mathcal{O}(\lambda)||k^n, \omega_i, J_i >= \mathrm{OBTD}(fik\lambda) < k||O(\lambda)||k >, \tag{25.31}$$

$$\mathrm{OBTD}(fik\lambda) = n\sqrt{(2J_f+1)(2J_i+1)} \sum_{\omega J} (-1)^{J_f+\lambda+J+j}$$

$$\times \left\{ \begin{array}{ccc} J_i & f & \lambda \\ j & j & J \end{array} \right\} < j^n \omega_f J_f \,|\}j^{n-1}\omega J >< j^n \omega_i J_i \,|\}j^{n-1}\omega J > . \tag{25.32}$$

For $n = 1$ this simplifies to the equivalent to Eq. (25.29)

$$< J_f = j||\mathcal{O}(\lambda)||J_i = j >=< k||O(\lambda)||k >, \tag{25.33}$$

which is the reduced matrix element which can be used in Eqs. (25.16) and (25.17) for the single-particle moments of the state k.

For $n = 2$, the CFP are unity and the sum only contains $J = j$ in which case Eq. (25.32) simplifies to

$$\mathrm{OBTD}(fik\lambda) = (-1)^{J_f+\lambda+1} n\sqrt{(2J_f+1)(2J_i+1)} \left\{ \begin{array}{ccc} J_i & J_f & \lambda \\ j & j & j \end{array} \right\}. \tag{25.34}$$

The reduced transition rate becomes:

$$B(\lambda) = n^2(2J_f+1)\left\{ \begin{array}{ccc} J_i & J_f & \lambda \\ j & j & j \end{array} \right\}^2 |< k||O(\lambda)||k >|^2 \, . \tag{25.35}$$

$$= n^2(2J_f+1)(2j+1)\left\{ \begin{array}{ccc} J_i & J_f & \lambda \\ j & j & j \end{array} \right\}^2 \frac{|< k||O(\lambda)||k >|^2}{(2j+1)}$$

$$= C(J_i, J_f, j)\frac{|< k||O(\lambda)||k >|^2}{(2j+1)}, \tag{25.36}$$

where the last line is written in terms of a coefficient which depends upon J_i and J_f times a reduced "single-particle" transition rate. These coefficients for some j value are given in Table 1.

26 Allowed beta decay

The study of nuclear beta decay provides information both about the nature of the weak interaction and about the structure of nuclear wave functions. The types of beta decay can be classified by the angular momenta carried away by the electron and neutrino. The most important are those for $\Delta\ell$=0 which are referred to as "allowed" beta decay. There are two type of allowed beta decay − Fermi (F) and Gamow-Teller (GT). The operator associated with Fermi decay is proportional to the isospin raising and lowering operator. As such it can only connect isobaric analogue states and it provides an exacting test of isospin conservation in the nucleus. The operator associated with Gamow-Teller decay also contains the nucleon spin operator. Since the total spin S is not a good quantum number, Gamow-Teller beta decay goes in general to many final states and provides a sensitive test of shell-model configuration mixing in the nucleus.

26.1 Formulation of allowed beta decay

The allowed beta decay rate T between a specific set of initial and final states is given by

$$T_{i,f} = (f/K_o)\left[g_V^2\ B_{i,f}(F_\pm) + g_A^2\ B_{i,f}(GT_\pm)\right], \tag{26.1}$$

where f is dimensionless three-body phase-space factor which depends upon the beta-decay Q value, and K_o is a specific combination of fundamental constants

$$K_o = \frac{2\pi^3\hbar^7}{m_e^5c^4} = 1.8844 \times\ 10^{-94}\ \mathrm{erg}^2\ \mathrm{cm}^6\ \mathrm{s}. \tag{26.2}$$

The $\pm$ refer to $\beta_\pm$ decay of nucleus (A_i, Z_i) into nucleus $(A_i, Z_i \mp 1)$. The weak-interaction vector (V) and axial-vector (A) coupling constants for the decay of neutron into a proton are denoted by g_V and g_A, respectively.

The total decay rate for a given initial state is obtained by summing the partial rates over all final states

$$T = \sum_f T_{if}, \tag{26.3}$$

with the branching fraction to a specific final state

$$b_{if} = \frac{T_{if}}{T}. \tag{26.4}$$

Beta decay lifetime are usually given in terms of the half-life with a total half-life of

$$T_{1/2} = \ln(2)\tau = \frac{\ln(2)}{T}. \tag{26.5}$$

The partial half-life for a particular final state will be denoted by $t_{1/2}$

$$t_{1/2} = \frac{T_{1/2}}{b_{if}}. \tag{26.6}$$

Historically one combines the partial half-life for a particular decay with the calculated phase-space factor f to obtain from Eq. (26.1) an "ft" value given by

$$ft_{1/2} = \frac{C}{[B(F_\pm) + (g_A/g_V)^2 B(GT_\pm)]} \tag{26.7}$$

where

$$C = \frac{\ln(2)\, K_o}{(g_V)^2} \tag{26.8}$$

One often compiles the allowed beta decay rates in terms of a "logft" which stands for $\log_{10}$ of the $ft_{1/2}$ value.

The values of the coupling constants for Fermi decay, g_V, and Gamow-Teller decay, g_A, in the combinations in which they appear in Eq. (26.7) are obtained as follows. For a $0^+ \to 0^+$ nuclear transition $B(GT) = 0$, and for a transition between $T = 1$ analogue states with $B(F) = 2$ Eq. (26.7) reduces to

$$C = 2t_{1/2} f. \tag{26.9}$$

The partial half-lives and Q values for several $0^+ \to 0^+$ analogue transitions have been measured to an accuracy of about one part in 10000. With the phase space factors discussed in Sec. 4.3.3 (including the correction δ_V), one obtains [1]

$$C = 6170(4) \tag{26.10}$$

This result, which together with the value of K_o in Eq. (26.2), can be used with Eq. (26.8) to obtain g_V.

At the quark level $g_V = -g_A$. But for nuclear structure we use the value obtained from the neutron to proton beta decay [2]

$$\mid g_A/g_V \mid = 1.261(8). \tag{26.11}$$

26.2 Operators for allowed beta decay

26.2.1 Fermi decay

The operator for Fermi beta decay in terms of sums over the nucleons is

$$\mathcal{O}(F_\pm) = \sum_k t_{k\pm}. \tag{26.12}$$

The matrix element is

$$B(F) = |< f \mid T_\pm \mid i >|^2, \tag{26.13}$$

where

$$T_\pm = \sum_k t_\pm \tag{26.14}$$

is the total isospin raising and lowering operator for total isospin constructed out of the basic nucleon isospin raising and lowering operators

$$t_- \mid n >= \mid p >, \;\; t_- \mid p >= 0,$$

and

$$t_+ \mid p >= \mid n >, \;\; t_+ \mid n >= 0. \tag{26.15}$$

The matrix elements obey the triangle conditions $J_f = J_i$ ($\Delta J = 0$). The Fermi operator has $\pi_O = +1$, and thus the initial and final nuclear states must have $\pi_i \pi_f = +1$ for the matrix element to be nonzero under the parity transform.

When isospin is conserved the Fermi matrix element must obey the isospin triangle condition $T_f - T_i$ ($\Delta T = 0$), and the Fermi operator can only connect isobaric analogue states. For β_- decay

$$\begin{aligned} & T_- \mid \omega_i, J_i, M_i, T_i, T_{zi} > \\ & = \sqrt{(T_i(T_i+1) - T_{zi}(T_{zi}-1)} \mid \omega_i, J_i, M_i, T_i, T_{zi} - 1 >, \end{aligned} \tag{26.16}$$

and

$$\begin{aligned} B(F_-) &= |< \omega_f, J_f, M_f, T_f, T_{zi} - 1 \mid T_- \mid \omega_i, J_i, M_i, T_i, T_{zi} >|^2 \\ &= [T_i(T_i+1) - T_{zi}(T_{zi}-1)] \delta_{\omega_f,\omega} \, \delta_{J_i,J_f} \, \delta_{M_i,M_f} \, \delta_{T_i,T_f}. \end{aligned} \tag{26.17}$$

For β_+ we have

$$\begin{aligned} B(F_+) &= |< \omega_f, J_f, M_f, T_f, T_{zi} + 1 \mid T_+ \mid \omega_i, J_i, M_i, T_i, T_{zi} >|^2 \\ &= [T_i(T_i+1) - T_{zi}(T_{zi}+1)] \delta_{\omega_f,\omega} \, \delta_{J_i,J_f} \, \delta_{M_i,M_f} \, \delta_{T_i,T_f}. \end{aligned} \tag{26.18}$$

For neutron-rich nuclei ($N_i > Z_i$) we have $T_i = T_{zi}$ and thus

$$B(F_-)(N_i > Z_i) = 2T_{zi} = (N_i - Z_i) \, \delta_{\omega_f,\omega} \, \delta_{J_i,J_f} \, \delta_{M_i,M_f} \, \delta_{T_i,T_f}, \tag{26.19}$$

and

$$B(F_+)(N_i > Z_i) = 0. \tag{26.20}$$

For proton-rich nuclei ($Z_i > N_i$) we have $T_{zi} = -T_i$ and thus

$$B(F_+)(Z_i > N_i) = -2T_{zi} = (Z_i - N_i) \, \delta_{\omega_f,\omega} \, \delta_{J_i,J_f} \, \delta_{M_i,M_f} \, \delta_{T_i,T_f}, \tag{26.21}$$

and

$$B(F_-)(Z_i > N_i) = 0. \tag{26.22}$$

26.2.2 Gamow-Teller decay

The operator for Gamow-Teller beta decay in terms of sums over the nucleons is

$$\mathcal{O}(GT_{\pm}) = \sum_k \sigma_k t_{k\pm}. \tag{26.23}$$

The reduced matrix elements is

$$B_{i,f}(GT_{\pm}) = \frac{|< f||\mathcal{O}(GT_{\pm})||i >|^2}{(2J_i+1)} = \frac{[M_{i,f}(GT_{\pm})]^2}{(2J_i+1)}, \tag{26.24}$$

where

$$M_{i,f}(GT_{\pm}) =< f||\mathcal{O}(GT_{\pm})||i > \tag{26.25}$$

The matrix elements are reduced in orbital space and the $(2J_i+1)$ factor comes from the average over initial M_i states. The magnitude of reduced matrix element $M(GT)$ does not depend on the direction of the transition, i.e.,

$$\mid M(GT, a \rightarrow b) \mid = \mid M(GT, b \rightarrow a) \mid \tag{26.26}$$

whereas

$$B(GT, a \rightarrow b) = \frac{(2J_b+1)}{(2J_a+1)} B(GT, b \rightarrow a). \tag{26.27}$$

The matrix elements obey the triangle $\Delta(J_i, j_i, \Delta J = 1)$. The Gamow-Teller operator has $\pi_O = +1$, and thus the initial and final nuclear states must have $\pi_i \pi_f = +1$ for the matrix element to be nonzero under the parity transform. When isospin is conserved the Gamow-Teller matrix elements obey the isospin triangle condition $\Delta(T_f, T_i, \Delta T = 1)$.

In second-quantized form the GT_- operator has the form

$$O(GT_-) = \sum_{\alpha\beta} < \alpha \mid \sigma t_- \mid \beta > a^+_{\alpha,p} a_{\beta,n}, \tag{26.28}$$

where $a_{\beta,n}$ destroys a neutron in state β and $a^+_{\alpha,p}$ creates a proton in state α. The J-coupled form is

$$O(GT_-) = \sum_{k_a k_b} < k_a, p||\sigma t_-||k_b, n > \frac{[a^+_{k_a,p} \otimes \tilde{a}_{k_b,n}]^\lambda}{\sqrt{(2\lambda+1)},} \tag{26.29}$$

where λ=1 for the GT operator. The reduced transition probability for the transition from an initial state i to a final state f is given by

$$B(GT_-) = \sum_{k_a k_b} < k_a, p||\sigma t_-||k_b, n > \mathrm{OBTD}(k_a, k_b, f, i), \tag{26.30}$$

where

$$\mathrm{OBTD}(k_a,k_b,f,i) = \frac{< f|||[a^+_{k_a,p}\otimes \tilde{a}_{k_b,n}]^\lambda|||i>}{\sqrt{(2\lambda+1)}} \tag{26.31}$$

The analogous equations for GT_+ are

$$O(GT_+) = \sum_{\alpha\beta} < \alpha \mid \sigma t_+ \mid \beta > a^+_{\alpha,n}a_{\beta,p}, \tag{26.32}$$

where $a_{\beta,p}$ destroys a proton in state β and $a^+_{\alpha,n}$ creates a neutron in state α. The J-coupled form is

$$O(GT_+) = \sum_{k_ak_b} < k_a,n||\sigma t_+||k_b,p > \frac{[a^+_{k_a,n}\otimes \tilde{a}_{k_b,p}]^\lambda}{\sqrt{(2\lambda+1),}} \tag{26.33}$$

and the reduced transition probability is

$$B(GT_+) = \sum_{k_ak_b} < k_a,n||\sigma t_+||k_b,p > \mathrm{OBTD}(k_a,k_b,f,i), \tag{26.34}$$

where

$$\mathrm{OBTD}(k_a,k_b,f,i) = \frac{< f|||[a^+_{k_a,n}\otimes \tilde{a}_{k_b,p}]^\lambda|||i>}{\sqrt{(2\lambda+1)}} \tag{26.35}$$

The reduced single-particle matrix elements are given by

$$< k_a,p||\sigma t_-||k_b,n > = < k_a,n||\sigma t_+||k_b,p > = 2 < k_a||\vec{s}\,||k_b >, \tag{26.36}$$

where the matrix elements of $\vec{s}$ are given by

$$< k_a||\vec{s}\,||k_b > = < j_a||\vec{s}||j_b > \delta_{n_a,n_b}$$

$$= (-1)^{\ell_a+j_a+3/2}\sqrt{(2j_a+1)(2j_b+1)}\begin{Bmatrix} 1/2 & 1/2 & 1 \\ j_b & j_a & \ell_a \end{Bmatrix} < s||\vec{s}||s > \delta_{\ell_a,\ell_b}\delta_{n_a,n_b}, \tag{26.37}$$

with

$$< s||\vec{s}||s > = \sqrt{3/2}\,,$$

The matrix elements of $\vec{s}$ has the selection rules δ_{ℓ_a,ℓ_b} and δ_{n_a,n_b}. Thus the orbits which are connect by the GT operator are very selective; they are those in the same major oscillator shell with the same ℓ value. The matrix elements such as $1s_{1/2}-0d_{3/2}$ which have the allowed Δj coupling but are zero due to the $\Delta\ell$ coupling are called "ℓ-forbidden" matrix elements.

26.3 Sum rules

Sum rules for Fermi and Gamow-Teller matrix elements can be obtained. The sum rule for Fermi is obtained from the sum

$$\sum_f [B_{i,f}(F_-) - B_{i,f}(F_+)] = \sum_f \left[|< f \mid T_- \mid i >|^2 - |< f \mid T_+ \mid i >|^2 \right]$$

The final states f in the T_- matrix element go with the $Z_f = Z_i + 1$ nucleus and those in the T_+ matrix element to with the $Z_f = Z_i - 1$ nucleus. One can explicitly sum over the final states to obtain

$$\sum_f [< i \mid T_+ \mid f >< f \mid T_- \mid i > - < i \mid T_- \mid f >< f \mid T_+ \mid i >]$$

$$=< i \mid T_+T_- - T_-T_+ \mid i >=< i \mid 2T_z \mid i >= (N_i - Z_i). \tag{26.38}$$

The sum rule for Gamow-Teller is obtained as follows.

$$\sum_{f,\mu} |< f \mid \sum_k \sigma_{k,\mu} t_{k-} \mid i >|^2 - \sum_{f,\mu} |< f \mid \sum_k \sigma_{k,\mu} t_{k+} \mid i >|^2$$

$$= \sum_{f,\mu} < i \mid \sum_k \sigma_{k,\mu} t_{k+} \mid f >< f \mid \sum_{k'} \sigma_{k',\mu} t_{k'-} \mid i >$$

$$- \sum_{f,\mu} < i \mid \sum_k \sigma_{k,\mu} t_{k-} \mid f >< f \mid \sum_k{}' \sigma_{k',\mu} t_{k'+} \mid i >$$

$$= \sum_\mu \left[< i \mid \left(\sum_k \sigma_{k,\mu} t_{k+} \right) \left(\sum_{k'} \sigma_{k',\mu} t_{k'-} \right) - \left(\sum_k \sigma_{k,\mu} t_{k-} \right) \left(\sum_{k'} \sigma_{k',\mu} t_{k'+} \right) \mid i > \right]$$

$$= \sum_\mu < i \mid \sum_k \sigma_{k,\mu}^2 \left[t_{k+} t_{k-} - t_{k-} t_{k+} \right] \mid i >= 3 < i \mid \sum_k \left[t_{k+} t_{k-} - t_{k-} t_{k+} \right] \mid i >$$

$$= 3 < i \mid T_+T_- - T_-T_+ \mid i >= 3 < i \mid 2T_z \mid i >= 3(N_i - Z_i). \tag{26.39}$$

We have used the fact that $\sigma_x^2 = \sigma_y^2 = \sigma_z^2 = 1$. When $k \neq k'$ the operators commute and cancel. These sum rules hold for each M_i value and thus also hold for $B(F)$ and $B(GT)$ when we take an average over the M_i values. Thus

$$\sum_f [B_{i,f}(F_-) - B_{i,f}(F_+)] = (N_i - Z_i), \tag{26.40}$$

and

$$\sum_f [B_{i,f}(GT_-) - B_{i,f}(GT_+)] = 3(N_i - Z_i). \tag{26.41}$$

The sum-rule for the Fermi matrix elements applies even when isospin is not conserved. When isospin is conserved we recover the results given by Eqs. (26.17)

and (26.18). For and $N > Z$ we usually have $T_i = T_{zi}$ which means that $B(F_+) = 0$ and we can use Eq. (26.40) to obtain $B(F_-) = (N_i - Z_i)$ (the same as Eq. (26.19)) for the transition to the isobaric analogue state. For $N = Z(T_{zi} = 0)$ and $T_i = 0$ we have from Eqs. (26.17) and (26.18) $B(F_+) = B(F_-) = 0$, and for $T_i = 1$ we have $B(F_+) = B(F_-) = 2$. Fermi transitions which would be zero if isospin is conserved are called isospin-forbidden Fermi transitions.

When $N > Z$ there are some situations where one has $B(GT_+) = 0$, and then from (26.41) we have $B(GT_-) = 3(N_i - Z_i)$. In particular for the β_- decay of the neutron we have $B(F_-) = 1$ and $B(GT_-) = 3$.

26.4 Effective operators for Gamow-Teller matrix elements

There are several reasons why the "free-nucleon" calculations may differ from experiment. In reality the nuclear wave functions are more complicated than the theoretical model we use in that they incorporate nucleon degrees of freedom beyond the sd-shell space. In addition, non-nucleonic degrees of freedom involving the delta isobars and mesons in the nucleus may be important in the observed rates. The calculation of the corrections corresponding to these processes have been the subject of many theoretical investigations. Most recently these were carried out by Towner and Khanna [3]. For references and comparisons to the earlier works, see [3] and [4]

Since the factor g_A^2 appears in front of $B(GT)$ one might parameterize the effective matrix in terms of an effective g_A value − one speaks of a renomalization of the axial vector current in the nuclear medium. Equivalently one can express the renormalization in terms of corrections to the GT operator. It is convenient to express the effective GT operator as:

$$O(GT_\pm)^{eff} = (\vec{s} + \delta O_{GT})t_\pm, \tag{26.42}$$

where

$$\delta O_{GT} = \delta_s \vec{s} + \delta_\ell \vec{\ell} + \delta_p \vec{p}(s - d), \tag{26.43}$$

and where

$$\vec{p} = (8\pi)^{1/2}[Y^{(2)}(\vec{r}) \otimes \vec{s}]^{(1)}. \tag{26.44}$$

The δ coefficients characterize the renormalizations which are needed when working within the sd-shell model space. The reduced single-particle matrix elements for the individual operator components $\vec{s}$, $\vec{\ell}$ and $\vec{p}$ are given in [4].

δ_ℓ and δ_p turn out to be relatively small compared to δ_s. Thus to a good approximation we may take the effective operator as just:

$$O(GT_\pm)^{eff} = (1 + \delta_s)\vec{s}t_\pm, \tag{26.45}$$

A small δ_p value means that the ℓ-forbidden $0d_{3/2} \rightarrow 1s_{1/2}$ single-particle matrix element is not zero but is relatively small.The weak branch for the beta decay of the ^{39}Ca $3/2^+$ state to the $1/2^+$ state in ^{39}K has been measured [5]. In the sd shell model these levels are just the $0d_{3/2}$ and $1s_{1/2}$ single-particle states and the ft value for this transition thus directly provides a value for the ℓ-forbidden matrix element or for the parameter δ_p(s-d). From the $A = 39$ datum a value of $\mid \delta_p(s-d) \mid = 0.017 \pm 0.003$ is obtained. The δ_p value extracted from a fit to many sd-shell GT decays [6] is $\delta_p = +0.021(8)$. The value of δ_p is positive as expected theoretically [3].

References

[1] D. H. Wilkinson, A. Gallman and D. E. Alburger, Phys. Rev. C18, 401 (1978)

[2] D. H. Wilkinson, Nucl. Phys. A377, 474 (1982)

[3] I. S. Towner and F. C. Khanna, Nucl. Phys. A399, 334 (1983).

[4] B. A. Brown and B. H. Wildenthal, Phys. Rev. C28, 2397 (1983).

[5] E. C. Adelberger, J. L. Osborne, H. E. Swanson and B. A. Brown, Nucl. Phys. A **417**, 269 (1984).

[6] B. A. Brown and B. H. Wildenthal, Atomic Data Nucl. Data Tables **33**, 347 (1985). The $B(GT)$ as defined in the present work is related to the $M(GT)$ of this references by $B(GT) = [M(GT)/1.251]^2/(2J_i + 1)$.